



UNIL | Université de Lausanne

Unicentre

CH-1015 Lausanne

<http://serval.unil.ch>

Year : 2023

The conjugative system encoded by the integrative conjugative element ICE_{clc} in *Pseudomonas putida*

Daveri Andrea

Daveri Andrea, 2023, The conjugative system encoded by the integrative conjugative element ICE_{clc} in *Pseudomonas putida*

Originally published at : Thesis, University of Lausanne

Posted at the University of Lausanne Open Archive <http://serval.unil.ch>

Document URN : urn:nbn:ch:serval-BIB_7BA27E901BC93

Droits d'auteur

L'Université de Lausanne attire expressément l'attention des utilisateurs sur le fait que tous les documents publiés dans l'Archive SERVAL sont protégés par le droit d'auteur, conformément à la loi fédérale sur le droit d'auteur et les droits voisins (LDA). A ce titre, il est indispensable d'obtenir le consentement préalable de l'auteur et/ou de l'éditeur avant toute utilisation d'une oeuvre ou d'une partie d'une oeuvre ne relevant pas d'une utilisation à des fins personnelles au sens de la LDA (art. 19, al. 1 lettre a). A défaut, tout contrevenant s'expose aux sanctions prévues par cette loi. Nous déclinons toute responsabilité en la matière.

Copyright

The University of Lausanne expressly draws the attention of users to the fact that all documents published in the SERVAL Archive are protected by copyright in accordance with federal law on copyright and similar rights (LDA). Accordingly it is indispensable to obtain prior consent from the author and/or publisher before any use of a work or part of a work for purposes other than personal use within the meaning of LDA (art. 19, para. 1 letter a). Failure to do so will expose offenders to the sanctions laid down by this law. We accept no liability in this respect.



UNIL | Université de Lausanne

Faculté de biologie
et de médecine

Département de Microbiologie Fondamentale

**The conjugative system encoded by the integrative
conjugative element ICE_{clc} in *Pseudomonas putida***

Thèse de doctorat ès sciences de la vie (PhD)

présentée à la

Faculté de biologie et de médecine
de l'Université de Lausanne

par

Andrea Daveri

Master en Biotechnologie Cellulaire et Moléculaire
de l'Université de Wageningen

Jury

Prof. Claus Wedekind, Président

Prof. Jan Roelof van der Meer, Directeur de thèse

Prof. Melanie Blokesch, Experte

Prof. Stephan Gruber, Expert

Prof. Manuela Hospenthal, Experte

Lausanne

2023



UNIL | Université de Lausanne

Faculté de biologie
et de médecine

Ecole Doctorale

Doctorat ès sciences de la vie

Imprimatur

Vu le rapport présenté par le jury d'examen, composé de

Président·e	Monsieur	Prof.	Claus	Wedekind
Directeur·trice de thèse	Monsieur	Prof.	Jan Roelof	van der Meer
Expert·e-s	Madame	Prof.	Melanie	Blokesch
	Monsieur	Prof.	Stephan	Gruber
	Madame	Prof.	Manuela	Hospenthal

le Conseil de Faculté autorise l'impression de la thèse de

Andrea Daveri

Master Degree in Cellular and molecular biotechnology, Wageningen University and Research,
Pays-Bas

intitulée

**The conjugative system encoded by the integrative
conjugative element ICE*clc* in *Pseudomonas putida***

Lausanne, le 13 mars 2024

pour le Doyen
de la Faculté de biologie et de médecine

Prof. Claus Wedekind

Table of Content

Summary (English) p. 2

Resumé (French) p. 4

Chapter 1: p. 6

General Introduction

Chapter 2: p. 36

Characterization of an atypical but widespread type IV secretion system for transfer of the integrative and conjugative element (ICE_{clc}) in *Pseudomonas putida*

Chapter 3: p. 107

Identification of the ICE_{clc} conjugative pilus and in vivo visualization

Chapter 4: p. 140

Dynamic behaviour of an inner and outer membrane subunit of the T4SS encoded by ICE_{clc} in *Pseudomonas putida*

Chapter 5: p. 165

General Discussion and Outlook

Acknowledgements p. 176

Curriculum Vitae p. 177

Summary

Integrative and conjugative elements (ICE) are a widespread class of mobile genetic elements, which play an important role for bacterial evolution and adaptation to new niches. ICE transfer between cells requires a multi-subunit protein complex known as type IV secretion system (T4SS) which is usually self-encoded. Although several T4SS have been discovered and characterized in the years, they mostly belong to mobile plasmids and ICE-encoded T4SS remain severely understudied. Here we focused on the T4SS encoded by the ICE*clc* element first found in *Pseudomonas knackmussii* B13 in two identical copies. The core region of ICE*clc*, which includes the genetic locus encoding for the T4SS, is conserved among several β - and γ -proteobacteria, thus understanding peculiarities about this conjugation system would be representative for a large number of mobile elements. In this work we mainly focused on the extensive characterization of the ICE*clc* T4SS genetic locus with a combination of 'in silico', molecular biology and microscopy approaches.

The first chapter introduces the theme of horizontal gene transfer with a closer look at integrative and conjugative elements characteristics, evolutionary importance and DNA conjugation mechanism with in depth description of the up to date knowledge in T4SS classification and structural composition.

In the second chapter we present the general characterization of the 24 genes of the ICE*clc* T4SS locus. With bioinformatics analysis we inferred homologies between ICE encoded and known T4SS components. Single gene knockouts of 22 out of the 24 open reading frames were used to understand their essentiality for ICE transfer. To better understand T4SS localization at single cell level, we fused nine predicted T4SS subunits to fluorescent proteins and studied their cellular localization. By coupling fluorescent labelling and gene deletions we showed possible interactions between several T4SS subunits and we proposed a dynamic model of T4SS assembly.

The third chapter focuses on the characterization of the conjugative pilus, one of the four major protein subassemblies of T4SS. With protein 3D structure prediction, we identified the gene encoding the pilin in ICE*clc*, being *orf66625*. With a microscopy technique based on chemical labelling of cysteine residues we could observe the conjugative pilus in vivo. In addition, we used cryo-CLEM to gain detailed morphological information on this cellular appendage.

The fourth chapter presents a study on the dynamic behaviour of two ICE*clc* T4SS subunits. Here we focused on IceB7 and IceB4 located in the outer and inner-membrane respectively. With high

resolution confocal microscopy we followed the localization of the two labelled subunits overtime both in presence and absence of recipient cells and we inferred their dynamics with custom made image analysis pipelines. Our results suggest a highly stable IceB7, which is one of the core members of the outer membrane assembly and a highly dynamic IceB4, suggesting that the ATPase of the T4SS are not constitutively docked to the conjugative machinery and that they might do so only when ICE DNA is about to be transferred.

Finally, we conclude with a general discussion on the outcomes and relevance of this work and the perspective for future studies.

Resumé

Les éléments intégratifs et conjugatifs (ICE) constituent une classe répandue d'éléments génétiques mobiles qui jouent un rôle important dans l'évolution bactérienne et l'adaptation à de nouvelles niches. Le transfert des ICE nécessite le contact entre deux bactéries et la mise en place d'un complexe protéique reliant les deux cellules appelé système de sécrétion de type IV (T4SS). Bien que plusieurs T4SS appartenant à des familles distinctes aient été découverts et caractérisés au cours des dernières décennies, la plupart appartiennent à des plasmides mobiles et les T4SS codés par les ICE restent gravement sous-étudiés. Dans cette étude, nous nous sommes concentrés sur le T4SS codé par l'élément *ICE_{clc}*, initialement découvert en deux copies identiques intégrées dans le chromosome de *Pseudomonas knackmussii* B13. La région centrale d'*ICE_{clc}*, qui inclut le locus génétique codant le T4SS, est conservée chez plusieurs éléments apparentés présents dans le génome de protéobactéries des groupes β et γ . Ainsi, la compréhension des particularités de ce système de conjugaison serait représentatif d'un grand nombre d'éléments mobiles. Dans ce travail, nous avons focalisé notre attention sur la caractérisation approfondie du locus génétique du T4SS d'*ICE_{clc}* en utilisant une combinaison d'approches bioinformatiques, génétiques, et microscopiques.

Le premier chapitre introduit le thème du transfert horizontal de gènes en se penchant sur les caractéristiques des éléments intégratifs et conjugatifs, leur importance évolutive et le mécanisme de transfert d'ADN par conjugaison, avec une description approfondie des connaissances actuelles sur la classification et la composition structurelle du T4SS.

Dans le deuxième chapitre, nous présentons la caractérisation générale des 24 gènes du locus T4SS d'*ICE_{clc}*. Grâce à une analyse bioinformatique des homologies entre les composants du T4SS codés par *ICE_{clc}* et d'autres déjà connus, nous avons inféré des fonctions aux produits de la majorité des gènes du locus T4SS. 22 variants d'*ICE_{clc}* délétés pour 1 des 24 gènes codant des sous-unités putatives du T4SS ont été utilisés pour comprendre la nécessité de chaque sous-unité pour le transfert de l'ICE. Afin de mieux comprendre la dynamique de mise en place et la localisation des différentes parties du T4SS au niveau de la cellule individuelle, nous avons fusionné neuf sous-unités prédites du T4SS à des protéines fluorescentes, et étudié leur localisation cellulaire par microscopie à épifluorescence. En associant le marquage fluorescent et les délétions géniques, nous avons montré des interactions possibles entre plusieurs sous-unités du T4SS et avons proposé un modèle dynamique de l'assemblage du T4SS.

Le troisième chapitre se concentre sur la caractérisation du pilus de conjugaison, l'un des quatre sous-ensembles protéiques du T4SS. Une analyse bioinformatique reposant sur la prédiction de la structure tridimensionnelle des protéines a permis d'identifier le gène *orf66625* codant la piline (sous-unité protéique majeure du pilus) chez *ICEclc*. Grâce à une technique de microscopie basée sur le marquage chimique des cystéine, nous avons pu observer le pilus conjugatif *in vivo*. De plus, nous avons obtenu des informations morphologiques détaillées sur cet appendice cellulaire grâce à une technique spécifique de microscopie électronique, appelée cryo-CLEM.

Le quatrième chapitre présente une étude sur la dynamique d'IceB7 et IceB4, deux sous-unités du T4SS d'*ICEclc* situées dans la membrane externe et la membrane interne respectivement. Grâce à la microscopie confocale à haute résolution, nous avons suivi la localisation des deux sous-unités au fil du temps, en présence et en absence de cellules receveuses, et analysé leur dynamique à l'aide de « pipelines » d'analyse d'images développés par nos soins. D'une part, nos résultats suggèrent qu'IceB7 est hautement stable, et est l'un des membres centraux de l'assemblage du complexe dans la membrane externe. D'autre part, IceB4 est hautement dynamique, ce qui suggère que cette protéine n'est pas constitutivement ancrée à la machinerie de transfert, et pourrait l'être uniquement lorsque l'ADN de l'ICE est sur le point d'être transféré.

Enfin, ce manuscrit se termine par une discussion générale sur les résultats et la pertinence de ce travail, ainsi que les perspectives pour des études futures.

Chapter 1

General introduction

Horizontal gene transfer: a focus on integrative and conjugative elements and their conjugative systems

Horizontal gene transfer and microbial diversity in the environment

Bacteria in the environment self-organize in highly complex communities. Microbial communities are essential for global biogeochemical processes, conducting organic matter and nutrient cycling (1,2). Communities are also a crucial aspect of plant (3), human (4) and animal health (5). The wide taxonomic diversity of most communities helps to adapt to changing environmental conditions, which is favored by horizontal gene transfer between species (HGT). Indeed, it has been estimated that $81 \pm 15\%$ of bacterial genes have been acquired by HGT at some point during evolution (6). Acquisition of exogenous DNA can provide bacterial cells with competitive advantages, which can help them to expand in their environmental niche and/or change the sign or extent of host- or interspecific interactions (7).

There are three known main mechanisms of HGT, which are described as transformation, conjugation and transduction. Transformation consists in the ability of an organism to uptake free DNA from the extracellular space (8). Transduction is known as the delivery of exogenous DNA via phages and their subsequent integration in the genome (9). Conjugation, in contrast, requires contact between the donor and recipient cell membranes, and once contact is established, DNA transfer takes place through a so-called mating pore (10). Conjugation is mediated by a protein complex known as the Type IV Secretion System (T4SS) (11), which can transfer plasmid DNA, or chromosomally excised DNA, like Integrative and Conjugative Elements (ICEs), and even entire chromosomes (12). Usually the conjugative machinery is encoded by the mobile element, however transfer of elements by non-self encoded T4SS ('mobilization') has been documented (13).

If conjugated DNA cannot replicate in the new cell, it must integrate in the host chromosome in order to be propagated in the bacterial population. The mechanism of integration may differ depending mainly on how the DNA is acquired (14). For example, integration may be achieved with homologous recombination mediated by RecA (15), or via site-specific recombination, as is the case for ICEs and phages (16,17). Site-specific recombination is facilitated by an integrase enzyme (recombinase), which recognizes an attachment site on the DNA that consists of a short repeat sequence that can range from 4 to 18 bp (18,19). Integrases can mediate both integration and excision through the same mechanism, although excision is further assisted by an excisionases.

Selection and adaptation in HGT

Intuitively one might think that incorporation and maintenance of heterologous DNA always gives an evolutionary advantage for the recipient cell. However, multiple studies have demonstrated that this is not necessarily true, and acquisition of mobile genetic elements (MGEs) may pose a variety of burdens on the new host (20,21). This is illustrated by the work of Maddamsetti et al. (21), who showed that the efficiency of plasmid transmission from a donor into twelve different laboratory evolved *E. coli* populations was highly variable. In some of the 12 *E. coli* populations the plasmid transfer rate was very low, while in others much higher and caused a significant genomic restructuring which included loss of beneficial alleles, implying an overall fitness loss for the host (21). Based on this evidence, there must be another underlying reason behind the evolutionary success of horizontal gene transfer, one hypothesis is that the newly acquired DNA does not lead to severe fitness losses. Here we must distinguish between ICEs which co-replicate with and plasmids which replicate independently from the host chromosome. Several examples exist where plasmid maintenance causes significant fitness losses for the host and results in reduced growth and loss of competitiveness within the population (22). Fitness loss would thus present a counterselection for maintaining the plasmid, unless the plasmid itself has an addiction program that kills plasmid-free hosts (23). Plasmids have evolved different maintenance mechanisms which can be grouped into two categories: post-segregational killing systems (PSK) and partition systems (24). PSK are better known as toxin-antitoxin systems. These plasmid loci have a gene for an antibacterial toxin that either kills or stops cell growth when expressed and a less stable product that acts as an antidote to the toxin. If the plasmid is lost the antidote is quickly degraded and the toxin acts to stop cellular functions (25). Partition systems are a set of proteins encoded on the plasmid that help to segregate the element between mother and daughter cell during division to avoid loss (26). Plasmid genes, however, can also provide selective benefits for the host. However, there are known cases where the beneficial genes carried by plasmids were integrated into the chromosome (27), suggesting that the presence of host-beneficial genes is not sufficient to maintain plasmids in the cell, and therefore not per se an argument as to why generally speaking plasmids persist in microbial communities. An alternative hypothesis explaining plasmid maintenance is the one that posits compensatory evolution (28). The hypothesis here is that the initial fitness cost caused by acquisition and replication of hexogenous DNA is rapidly alleviated by compensatory mutations either in the plasmid or in host chromosome. Indeed, a number of studies have analysed the molecular basis of plasmid cost-compensation and found evidence for positively selected mutations (29-32). ICEs, on

the other hand, mostly stay integrated in the host chromosome, and do not need to maintain an independent replication program, which could pose a fitness burden to the host. Furthermore, ICE 'activation' functions remain mostly silent, and without measurable fitness costs, which we demonstrated for integrated ICE*clc* in *P. aeruginosa* PAO1 (33). Surprisingly, the acquisition of ICE*clc* did not significantly change the genome-wide expression (<1%), suggesting that overexpression of horizontally acquired genes may be deleterious for the maintenance of the element (33). Therefore, one could argue that ICE conjugal transfer leads to the exchange (and selection) of two distinct entities: the element itself and the auxiliary genes which may be giving adaptive benefits. That probably means that core functions of MGEs have evolved mechanisms to control efficient transfer and maintenance without disturbing host metabolism, which is independent from the regulatory controls of the auxiliary genes (33). Not to forget is also the genomic context in which the newly acquired element enters, indeed the same genes are expressed differently depending on the host's GC content and sigma factors (34). Ultimately, however, positive selection dictates which transferred genes are maintained within a species over evolutionary timescales, but genes that do not provide a benefit to a species may still persist over short timescales according to simulation studies (35). These patterns do not rule out the role in microbial adaptation of HGT, but rather imply that many transfer events, like many mutations, may not be directly proportional to individual fitness gain or loss.

The study of HGT is thus highly fascinating and relevant. First, to understand its role in bacterial adaptation and persistence in selective environmental niches. Second, better understanding of HGT can provide clues to avoid or limit it, which may help to reduce the rates or possibilities of antibiotic resistance gene transmission or virulence factors into pathogenic bacteria (36). HGT may also be exploited for engineering of microbial communities. For example, DNA can be transferred from specific bacterial donors into a wider range of recipients in a community, with the aim to enhance pollutant degradation, or to target specific pathogens for killing (37). ICEs may have some advantages in such engineering concepts as opposed to plasmids. First, they may be more stably maintained in both host and recipient, because of their inherent integration into the host chromosome. Secondly, they have various admissible sites for new gene insertions, giving them a wider range for inclusion of new genetic material that may serve engineering purposes (38).

Genomic Islands: focus on Integrative and Conjugative Elements

Mobile genetic elements can be distinguished in three main classes, mobile plasmids, bacteriophages and genomic islands (GIs) (39). The latter are defined as segments of DNA in a host chromosome with evidence of present or past mobility. The GI concept was first developed in the 1980s when Hacker and collaborators studied the genetic basis of pathogenesis in *Escherichia coli* isolates. They discovered unstable genomic regions with variable virulence-associated characteristics and phenotypes, which they named as pathogenicity islands (PAIs) (40). Nowadays, it is recognized that GIs encompass a much wider group of mobile elements than PAIs, with variable sizes and carrying very diverse functional properties (41), that may include: symbiosis (42,43), antimicrobial resistance (44), aromatic compound degradation (45,46), heavy metal resistance (47), siderophore production (48) and many others. It is widely assumed that those functions on GIs have been selected to provide adaptive benefit to their host.

GIs can be highly diverse in their genetic content. Therefore, it may be difficult to define them clearly. However, there are some characteristics that are shared: GIs consist of relatively long DNA regions, spanning between 10 and 200 kb (49). Their GC content is usually different from the rest of the genome, and their extremities are usually characterized by the presence of directed repeats, which may represent the site-specific recombination site (50). GIs frequently locate in or next to a gene for tRNA (51,52). They often carry genes coding for integrases, as well as genes encoding a conjugative machinery, or parts thereof. Based on these characteristics, several bioinformatics tools have been developed to detect the presence of GIs in bacterial genomes (53). Nonetheless, their precise classification remains difficult, because not all GIs have the above described characteristics. Secondly, phylogenetic and sequence comparisons revealed that gene similarity and synteny is found mostly among GIs found in the same bacterial genus (49). These data suggest that different GI groups exist with distinct evolutionary origin, which may have arisen independently over time and evolved in parallel. Some GIs contain genes of phage origin, while others show plasmid inheritance, for example, in their conjugative transfer modules, suggesting modular evolution (49). It is very common to find defect prophages in bacterial genomes, which, plausibly, have lost functional genes after integration and acquired genes of non-phage origin, forming a GI (54). Also plasmids may have recombined into the genome, lost functional genes and acquired new genes turning them into GI. Indeed, some GIs encode a conjugative transfer system with high similarity to self-transmissible plasmids, such as ICESXT of *Vibrio cholerae* (55) or ICE_{KKS1024677} found in

Acidovorax sp. Strain KKS102 (56). In conclusion, GIs encompass a wide variety of mobile DNA elements of modular origin, such as ICEs or conjugative transposons, defect prophages, Integrative and Mobilizable Elements (IMEs) (13), or phage-Inducible Chromosomal islands (PICIs) (57). For the interest of this introduction, we will continue with a specific focus on integrative and conjugative elements (ICEs).

ICEs or conjugative transposons (CTNs) are, as their name implies, DNA fragments integrated in the host chromosome, which coreplicate with the genome, but can excise from the chromosome and conjugate to another bacterial cell (58). Also ICEs and CTNs can accumulate changes over time, which can lead to inactivation of their self-transmissibility. However, even non-self-transmissible elements can be mobilized by the conjugative system of another ICE or plasmid, residing in the same cell (59,60). Non self-transmissible integrated elements are called integrative and mobilizable elements (IMEs) (13). ICEs and IMEs are characterized by two distinct DNA molecular states: an integrated and an excised state (Fig 1A-D). Both states rely on the process of site-specific recombination (Fig. 1A), which for ICEs is mediated between two direct repeats, either between the repeat copies on either side of the ICE when residing in the chromosome (resulting in excision), or between a single repeat copy on the ICE and the other on the chromosome (resulting in integration). The recombination sequences are enclosed within regions called the attachment sites (*att*) that may carry additional binding sites for proteins involved in the recombination process (16). Both are catalyzed by an integrase, with additional help of an excisionase. Most of the integrases found in ICEs belong to the family of the tyrosine recombinases, for example: ICESXT-R391, ICE*clc*, ICE*Hin1056*, or PAPI-1. Apart from ICESXT, which integrates in the 3' end of the *prfC* gene, most ICEs integrate at the 3' end of tRNA genes (61-64).

ICE excision leads to the formation of a closed circular DNA molecule (Fig. 1B). Most often, ICE excision is facilitated by an excisionase (Xis) in addition to the integrase. For example, the Xis excisionase physically bends the DNA close to the ends of the integrated form, near the integrase binding sites, and helps the correct formation of the nucleoprotein complex (65).

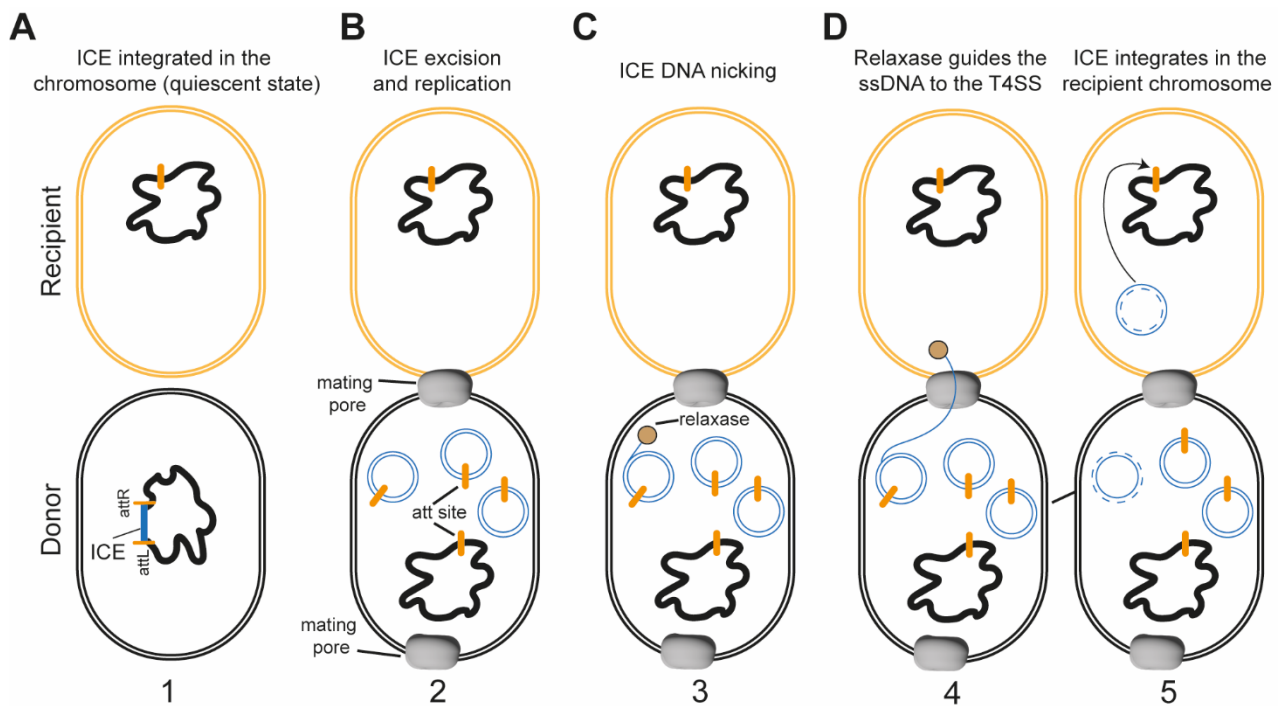


Figure 1 ICE life cycle. **A)** ICEs normally remain integrated in the host chromosome, in a so called quiescent state. **B)** Depending on the element, under specific conditions the ICE excises from the chromosome to form a circular DNA molecule, which in addition can self-replicate. **C)** Upon excision the relaxase nicks the circular ICE molecule at the origin of transfer *oriT* and **D)** guides the ssDNA to the mating pore. Here with the help of ATP hydrolysis ICE DNA and relaxosome are transferred to the recipient cell. The second strand is reconstituted via replication and finally integrates in the chromosome.

Depending on the binding site, Xis can either increase or decrease the excision rate. For example, in Tn916, *attL*-bound Xis increases the excision rate, while binding to the right end of the element (*attR*) decreases it (66). This hints to a regulatory role of this protein in the excision reaction. The dynamics of integration and excision are most likely characteristic for each individual ICE, and may depend on the ratio of expressed integrase and excisionase. Nevertheless, the rate of excision is not directly proportional to the transfer rate of the element indicating that excision is not always the limiting step for ICE propagation (67).

Excision of an ICE or IME leads to a physical separation of the ICE- (IME-) DNA from the chromosome. Therefore, the ICE would be lost from a daughter cell if chromosomal DNA is replicated but ICE-DNA is not, and cells divide. Different mechanisms have been described which seem to prevent ICE loss upon excision. Some ICEs can replicate the excised form, with a mechanism similar to rolling-circle replication of plasmids (Fig. 1B). Replication of excised ICE is an important feature for their stability and propagation, as was shown for ICEBs1 (68), SXT/R391 (69), and ICE*clc* (70). Other systems that may ensure ICE maintenance after excision include active DNA partitioning, a process thought to be similar to plasmid partitioning. Indeed ICEsXT and ICE*clc* encode the ParMRC and ParABS proteins,

respectively (71,72), which are analogous to the chromosomal ParABC system. Expression of the ICE *par* genes is upregulated during excision, which is in agreement with the idea that their Par-systems ensure partitioning of the element to daughter cells at the time when it is excised. The second mechanism to ensure ICE stability relies on a toxin-antitoxin system, which would actively stall division of ICE-free daughter cells, or kill them (73,74). Evidence for toxin-antitoxin involvement came from deletion studies with the SXT system, which highly increased ICE loss in the population (74).

The next step in ICE-DNA life cycle is its conjugative transfer to a recipient cell. This process starts with a nick at the ICE origin of transfer (*oriT*), exerted by the relaxase (Fig. 1C). A single-stranded DNA nucleoprotein complex is formed, which is thought to translocate from the donor to a recipient cell via a T4SS. Once in the recipient cell the second strand of ICE is reconstituted via replication, the relaxase closes the nick by reverse transesterification, and the double-stranded DNA molecule integrates in the recipient genome (Fig. 1D).

ICE*clc* organization and activation.

The model ICE for my study is the ICE*clc* element. ICE*clc* was discovered in *Pseudomonas knackmussii* B13, where it occurs in two identical copies, each integrated in a different tRNA-Gly locus (75). The element carries the genes for the degradation of 3-chlorocatechol, an intermediate of 3-chlorobenzoate metabolism (3-CBA). It further carries a gene cluster for 2-aminophenol degradation (*amn*), although *amn* expression does not lead to functional 2-aminophenol metabolism in strain B13 itself (75). ICE*clc* makes a good model, because of its higher transfer frequency compared to other ICEs, which enables individual cell-based microscopy studies. In addition, transfer can be easily selected for by growing recipients on 3-CBA as the sole carbon source (76). ICE*clc* has been transferred from B13 to other species of β - and γ -proteobacteria (46), where it integrates at the 3' end of tRNA^{gly} gene (19). GIs similar to ICE*clc* can be found in many different genera, which all have a characteristic modular core region of some 50 kb (Fig. 2), containing the regulatory genes controlling ICE*clc* 'activation', the genes for a T4SS conjugative transfer system, and others of unknown function. In addition, the localization of the integrase gene closed to the tRNA-Gly insertion site is typical. Depending on the degree of imposed similarity threshold, many elements with the same genetic make-up can be found, suggesting they are functional ICEs. For example, a recent survey among *Pseudomonas aeruginosa* isolates found hundreds of elements related to ICE*clc*, broadly falling in three major clades (47,75,77). A further characteristic of ICE*clc*-like

elements is their variable region, located in between the integrase gene and the core region (Fig. 2A). ICE clc itself carries here the genes for the degradation of 3-chlorocatechol and 2-aminophenol (75), plus a variety of others. Typical for ICE clc itself is an operon of three regulatory genes *mfsR*, *marR*, and *tcIR* that control its activation (76), but which are not universally conserved among the ICE clc family (Fig. 2).

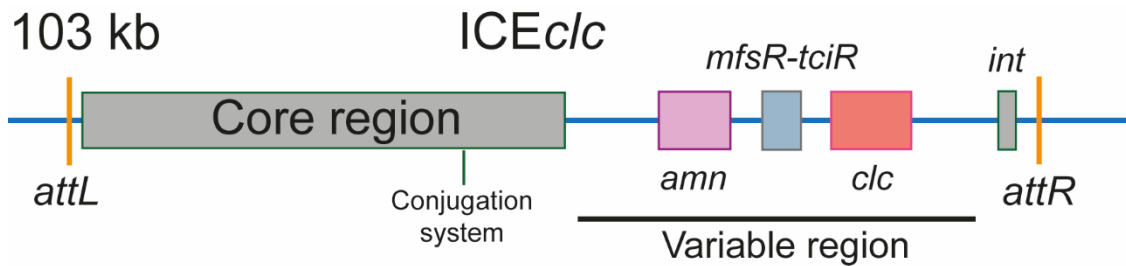


Figure 2 ICE clc organization. Schematic organization of ICE clc in the integrated form. The core region encompasses its conjugation system locus, regulatory gene loci and the *par* system. Other key features of ICE clc (*int*, integrase gene, *mfsR-tciR*: regulatory genes, *amn*, *clc*: metabolic pathway gene clusters, *attL-R*, recombination sites) are indicated.

Studies using ICE clc established that global regulation of its core genes is characterised by two states: an *off*-state (integrated ICE) (Fig. 3A), and an *on*-state (leading to excision and transfer). The *on*-state can be observed with the help of single-copy transcriptional fluorescent reporter gene fusions to ICE-core promoters, such as P_{int} (integrase promoter) or P_{inR} (upstream of a gene named *inrR*). Fluorescent cells are then typically observed in a very small part of the cell population, between 3% and 6%, and exclusively under stationary phase conditions (Fig. 3B). Growth on 3-CBA leads to the highest frequency of activation (78). Microscopy imaging in individual cells showed that ICE transfer itself does not take place in stationary phase, but rather when such cells are again stimulated with fresh nutrients and resume growth (79) (Fig. 3C). The cells that undergo activation of ICE promoters have been named ‘transfer competent’ cells (or tc-cells). Transfer competence is controlled by a cascade of regulatory genes, which starts with MfsR – inhibiting TciR, which then activates BisR; whereas BisR stimulates a promoter upstream of *alpA*, kicking in expression of BisDC that further activate the same *alpA* promoter. A positive feedback loop is formed, which effectively maintains bistability and coordinates expression of some 7 other promoters on the ICE (71). tc Cells don’t seem to ‘return’ to an inactive state, but maintain a different physiology compared to non-tc cells. Their division rate is considerably lower and stalls after a few divisions (80). Cell morphology of tc cells is different, and they have high reactive oxygen species levels and frequently lyse (81).

Several key aspects of the regulatory mechanisms controlling ICE activation and formation of the bistable state have been uncovered. Yet, how environmental factors influence the frequency of

activation is not well understood. One hypothesis is that growth on 3-CBA induces formation of more reactive oxygen species in cells, which increases the probability to induce transfer competence.

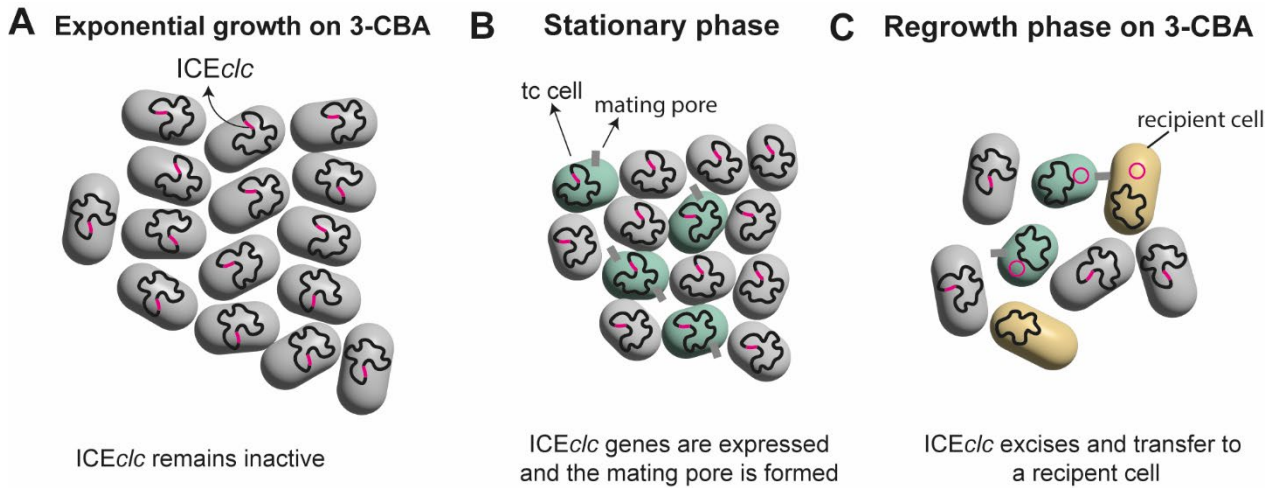


Figure 3 ICElc bistability. **A)** *P. putida* cells grown on 3-CBA during exponential phase. ICElc remains silent. **B)** During stationary phase a small proportion of cells (3-6%) starts to express core ICElc genes like the integrase and the mating pore subunits. **C)** ICE excision takes place in presence of fresh nutrients, the element can then be transferred among contact with a recipient cell.

Type IV Secretion System structural organization.

The DNA conjugative process is typically carried out by a type IV secretion system (T4SS), a multiprotein multicomponent structure assembled in the cell envelope. T4SSs are ubiquitous among gram-negative and -positive bacteria, as well as some archeal species. They are not only involved in DNA transfer by conjugation, but some T4SS catalyze the reverse process of DNA uptake, whereas others function as secretion systems for effector proteins only. Effector protein secretory systems can target both prokaryotic or eukaryotic cells. T4SSs have been well characterized for a number of human and plant pathogens, such as the Dot/Icm system of *Legionella pneumophila* (82), the Cag system of *Helicobacter pylori* (83), or the bacterial killing system of *Xanthomonas citri* (84). Well-known examples of T4SS involved in DNA conjugation come from the F and R388 plasmids of *Escherichia coli* (85,86), the Ti plasmid of *Agrobacterium tumefaciens* (87), and from other mobile genetic elements like ICEBs1 of *Bacillus subtilis* (88), ICElc of *Pseudomonas* sp. (89), or ICEHin1065 of *Hemophilus influenzae* (90). The best studied example of a DNA uptake T4SS is the ComB machinery of *Helicobacter pylori* (91), which is responsible for the high strain to strain variability within the species (92).

The structural organization of the different types of T4SSs in gram-negative bacteria is similar, being composed of four main protein subassemblies: (I) the cytoplasmic ATPases; (II) an inner membrane complex (IMC); (III) an outer membrane complex; (IV) and a conjugative pilus (11) (Fig. 4). In addition to the above mentioned assemblies some accessory proteins are commonly found, but which have no clear 'structural' role (yet). Examples include genes encoding lytic transglycosylase or disulphide-isomerases (93,94) (Fig. 4).

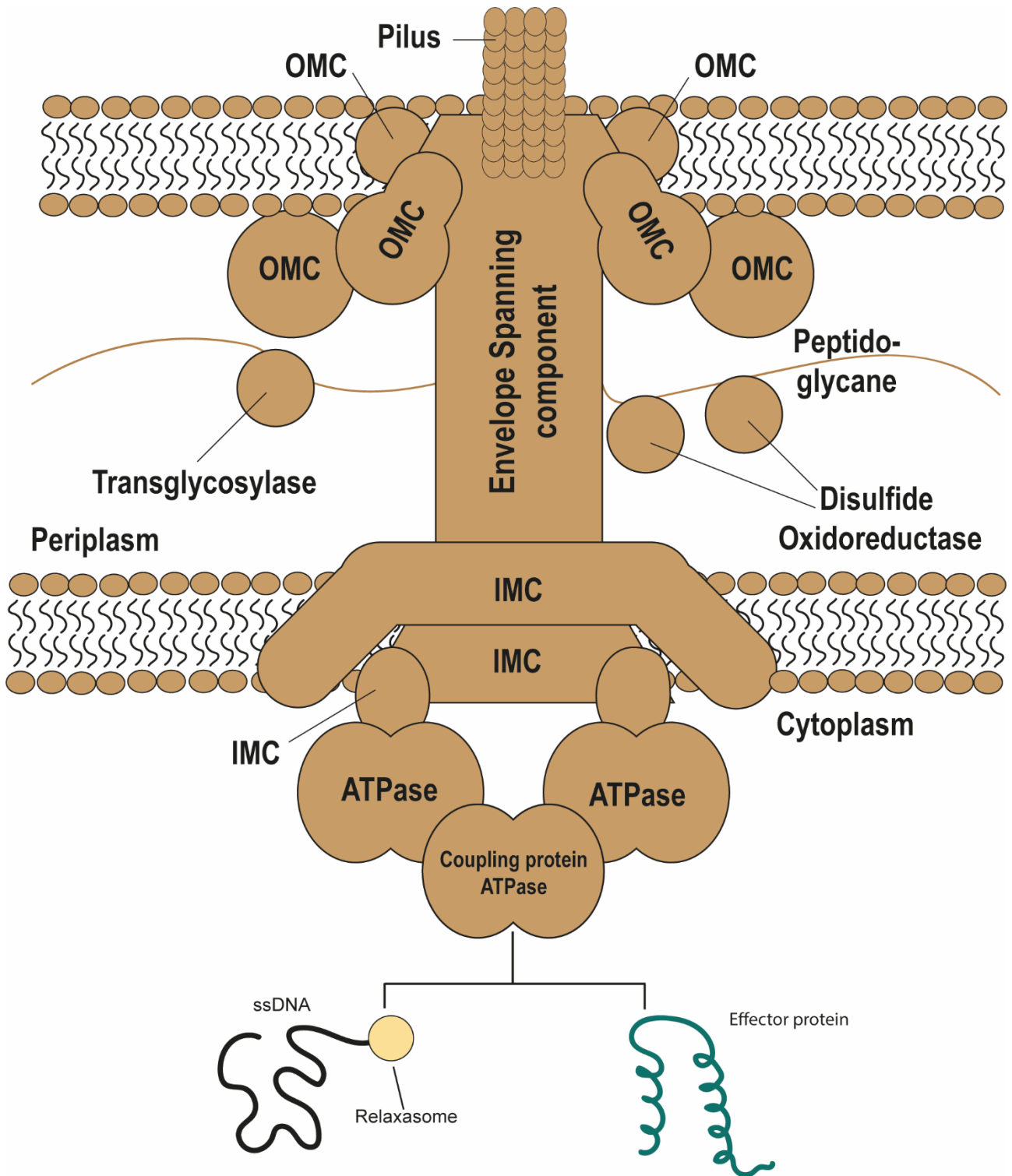


Figure 4 Schematic representation of a T4SS in gram-negative bacteria. All the four characteristic protein subassemblies are represented in addition to other periplasmic proteins often present in T4SS, which co-adjuvate conjugation. The inner and outer membranes are represented together with the peptidoglycane layer in the periplasm. Subunits forming the inner membrane channel are named IMC, the ones forming the outer membrane channel OMC. The two potential substrate of conjugation are depicted at the bottom (ssDNA and Effector protein).

All T4SS involved in DNA conjugation include an essential set of ATPases. Commonly these are three, but in some cases, like for the F plasmid, only two ATPases (95). One of them is known as the coupling protein, and was named VirD4 for the *A. tumefaciens* T4SS. The VirD4 ATPase is responsible for the recognition of the 'substrate' (DNA and/or protein), and initiation of transfer through the mating channel (96). VirD4 is characterized by two trans-membrane α -helices at the N-terminal and a globular cytoplasmic moiety at the C-terminal. *In vitro* experiments showed that it adopts a hexameric stoichiometry (97). The globular moiety is characterized by a nucleotide binding domain (NBD) and an all alpha-helix domain (AAD). The AAD domain is crucial for the docking of the relaxase in case of DNA transfer or the effector protein in case of protein secretion (98,99). Some coupling proteins present an additional stretch of charged amino acids at the C-terminal extremity, which is thought to be necessary for the secretion process by interacting with other proteins that form the 'coupling complex' (100-102). VirD4-substrate binding is dynamic, and in that sense it is not an integral component of the T4SS complex. The coupling protein itself is also not necessary for the assembly of the T4SS complex, although cryo-EM structures showed VirD4 in *A. tumefaciens* to associate to the mating pore in close proximity to the VirB4 ATPase and the IMC, suggesting a variety of molecular interactions (103).

The second conserved ATPase of the conjugative T4SS is VirB4 (*A. tumefaciens* T4SS nomenclature). Its conservation has been frequently used to infer T4SS phylogenetic relationships (104). VirB4 is one of the biggest proteins in the T4SS (>70 kDa) (105), and presents a hexameric symmetry within structurally solved systems (95,103,106,107). VirB4 is located in the cytoplasm, where it interacts with other proteins forming the IMC structure (107-110). The third ATPase is known as VirB11 (*A. tumefaciens* T4SS nomenclature), which, similarly to VirB4, adopts a hexameric organization in the T4SS complex (111). Both VirB4 and VirB11 ATPases are known to interact, from studies of the Dot/Icm of *L. pneumophila* and Cag systems of *H. pylori* (106,107). DotB (the equivalent of VirB11) binds to the IMC and induces a conformational change in the neighbouring proteins, which is essential for the opening of the channel at the inner membrane allowing the passage of the effector protein/DNA (112). Not all T4SS possess a VirB11 homolog, most notably the F plasmid machinery (95). Therefore, there must be different mechanisms of substrate transfer, which are still not understood, and which may depend on the organism or the type of conjugative DNA.

The second major protein subassembly of a T4SS is the IMC, which is composed of a set of lipophilic proteins with one or more trans-membrane domains, which form a pore in the inner membrane

and connect the cytoplasmic ATPases to the OMC, building the 'complete' T4SS (as in Fig. 4). The minimal composition of the IMC was deduced from the solved macromolecular structure of the T4SS encoded by the R388 plasmid of *E. coli*. It includes three different multimeric subunits, composed of VirB3, VirB6, and VirB8 (113). VirB3 is a small protein usually made of 2-3 α -helices, which is known to directly interact with VirB4 and is present in six units (113). VirB6 is a large protein (> 300 residues) with 5 or more trans-membrane helices and two long periplasmic loops (114), which presents a pentameric symmetry (113). VirB6 is thought to be an interaction hub crucial for substrate transfer and incorporation of pilin subunits into the conjugative pilus. Reported interacting partners of VirB6 are VirB10, VirB7, VirB8 and VirB9 (115-118). VirB8 is a two-domain protein, with a long N-terminal α -helix that spans the inner membrane and a globular periplasmic domain (119). Together with VirB6, it is thought to form the inner membrane channel, and connecting the IMC to the OMC. Both VirB6 and VirB8 are conserved in conjugative T4SS (120). This is obviously a very rough general model of a T4SS IMC, which may be realistic for the R388 T4SS, or the F-plasmid T4SS. However, we know that in many cases several other proteins are participating to the formation of the IMC of the respective T4SS.

The third major protein subassembly of the T4SS is the OMC, which is located in the outer membrane and forms a channel through which the substrate is transferred to the recipient cell. According to recently solved structures of the R388 plasmid T4SS (113), the OMC is composed of three subunits, formed by multimers of VirB7, VirB9, and VirB10. The ensemble of VirB7, VirB9 and VirB10 is known as T4SS core complex and is structurally characterized by a two layered ring-like architecture, made of an outer-(O) and inner-(I) layer (not to confuse with the IMC) (121). VirB10-like proteins among different T4SS are highly variable in structure, but in all cases due to reported interactions with IMC components and cytoplasmic ATPases is thought to be the only subunit that spans both inner and outer membrane (11). This is confirmed by recent structural studies showing the two-helix bundle at the C-terminal end of VirB10 forming the channel in the outer membrane O-layer, and its N-terminal part (I-layer) connecting to the IMC (122,123). VirB10 (at least for the *A. tumefaciens* system) is also sensitive to ATP hydrolysis of VirD4 and VirB11, leading to a conformational change that opens the channel for DNA transfer (124). The multimeric assembly of VirB10 C-terminal end(s) is surrounded by VirB7 protomers and (the C-terminal end) of VirB9 protomers, which form a sort of dome-like shape in the O-layer. The I-layer is then formed by the N-terminal parts of both VirB9 and VirB10 protomers (125). The *H. pylori* Cag and the *L. pneumophila* Dot/Icm systems showed similar global architecture of the two layers of the OMC, even though the

number of protomers and their dimensions are different (121). For example, it seems the Cag core complex is formed by five distinct proteins, two of which are strain specific and the other three are homologs to VirB7, VirB9 and VirB10 (126). In contrast, the Dot/Icm OMC structure shows nine different proteins in Cryo-EM complexes, six of which are unique and the other three are homologs of VirB7, VirB9 and VirB10 (127).

The final protein subassembly of the T4SS is the conjugative pilus, which is formed by the polymerization of thousands of pilin subunits, resulting in an extracellular protrusion. The pilus is thought to exert an important role in conjugation by connecting donor and recipient cells and signalling established contacts. The best characterized example is the F-pilus from the F plasmid. The F-pilus is long and flexible (128), and randomly extends and retracts, which can be interpreted as an attempt to scan the environment for the recognition of recipient cells (129). Interestingly, already in the 1970's, experimental evidence showed that F-pilus contact with a recipient initiates DNA transfer (130). More recent studies have shown that F-pili are important to establish contact with recipient cells, which provokes a signal transduction cascade that is linked to plasmid DNA processing in the donor cell (131,132). Cryo-EM solved structures showed that pili are not only composed of pilin subunits, but contain an equimolar number of phospholipid molecules (133,134). The exact role of phospholipids in pili is not completely understood, however, a recent computational model simulating molecular pili dynamics showed morphological defects in pili without phospholipids. Furthermore, the polymerization process and biochemical properties of phospholipid-deficient pili are different compared to wild-type pili, suggesting their importance for structural stability (131). Another unclear aspect of conjugative pili is the mechanism of their biogenesis. It is assumed that pilin subunits exist in a so-called pre-pilin state and are inserted into the growing pilus at the level of the inner membrane (135). The action of both VirB4 and VirB11 is thought to initiate this incorporation and assembly (136,137). A recent computational model based on protein structure predictions of the R388 T4SS suggested that the conjugative pilus is using the VirB6 pentamer in the periplasm as a basis for polymerization. This was deduced from their matching macromolecular symmetries, since both pilus 'rings' and VirB6 consist of five units (113). Different T4SS likely have very different associated pili types, with specific biomechanical characteristic and functions (138). Therefore, a lot remains to be understood from the dynamic play of the T4SS conjugation and its cellular appendages.

T4SS diversity

Despite an evolutionary conserved core structure, predicted T4SS for DNA conjugation show a wide diversity. First of all, the number of subunits may differ, leading to altered molecular machineries (139,140), with potentially different mechanistic properties in the DNA/protein translocation process. Secondly, T4SSs have different evolutionary origins. How to characterize T4SS diversity? One of the first classifications was based on the plasmid incompatibility group distinction (Incl, IncF, IncP), resulting in the F-, P- and I-type classification (11,141). This classification was too restrictive, because it does not include mobile elements that do not fall under the Inc classification. A more comprehensive phylogenetic classification was then proposed based on the DNA relaxase, which yielded six different clades of conjugative systems (142). However, even though the relaxase is an essential protein for DNA conjugation, it is not part of the actual conjugative machinery. In fact, some non-self transmissible mobile genetic elements that are mobilizable by others, possess both relaxase and coupling proteins, but not a corresponding T4SS. Furthermore, non-conjugative T4SSs specialized in protein secretion, such as the Dot/Icm system of *L. pneumophila* and the bactericidal T4SS of *X. citri*, lack relaxase components (MOBless T4SS) (120).

To overcome these shortcomings, other classification strategies were proposed. Given the high versatility of T4SSs, of which a high number is not yet well characterized, the best phylogenetic marker would be a ubiquitously conserved protein with the same functional characteristics. The only such example known so far is the VirB4 ATPase. Guglielmini and co-workers were the first to base T4SS classification on VirB4 comparisons. This yielded eight different clades, which were called Mating-Pair-Formation (MPF) complex (93). The classes MPF_B and MPF_C are poorly characterized and include T4SSs from Bacteroidetes and Cyanobacteria groups, respectively. The model for the **MPF_B** class is CTnDOT of *Bacteroides thetaiotaomicron* (143). The corresponding T4SS is encoded by a 17-gene operon, which comprises VirB4, but also VirB9 (two separate genes), VirB10 homologs, and the three main components of the inner membrane channel, VirB3, VirB6 and VirB8. Three different genes in CTnDOT show homology to conjugative pili.

The **MPF_C** class is exclusively present in Cyanobacteria. Although conjugation events between different cyanobacteria strain have been documented (144), the types of elements and corresponding MPF_C system(s) remain unclear. More recently, whole genome sequencing detected several Cyanobacterial mobilizable plasmids; with relaxase and coupling protein, but lacking a T4SS (145). HMMER sequence searches identified other distant homologs of VirB4 in cyanobacterial

genomes (104). Further computational prediction reconstructed eight T4SS protein profiles from the alpha plasmid of *Nostoc sp.* PCC 7120, which apart from VirB4, identified distant homologs of VirB9, VirB10 and of the inner membrane subunits VirB3, VirB6 and VirB8 (93).

Two other MPF clades include only monoderm bacteria and/or archaea. The first is named MPF_{FA} and is found in Firmicutes (F) and Actinobacteria (A), the second was named MPF_{FATA}, and in addition to Firmicutes (F) and Actinobacteria (A) is also found in Tenericutes (T) and Archaea (A). The **MPF_{FA}** class is encoded on mobile elements such as Tn916, ICEBs1 of *Bacillus subtilis*, and the plasmid pCW3, which is found in several Clostridia. The Tn916 system has been well characterized. In addition to carrying a distant homolog of VirB4, the Tn916-T4SS contains an FtsK-like coupling protein, analogous to VirD4. Tn916 lacks homologs of the archetype OMC subunits (VirB7, VirB9, VirB10), which makes sense considering it is present in monoderm bacteria that have no outer membrane. MPF_{FA}-types do have VirB6- and VirB8-homologs, suggesting a similar organization of the IMC among mono- and diderm cell types, which both were essential for conjugation (146-149). The MPF_{FA} type further has two specific inner membrane proteins, called TcpD and TcpE (for the pCW3 plasmid), which contain two or more transmembrane moieties and are essential for plasmid transfer (150). Immunofluorescent labelling of TcpD and TcpE showed a preferred localization at the cell pole, which coincided with that of the pCW3-VirB6 homolog, suggesting they are part of the same macromolecular assembly. Their exact role in conjugation, however, remains unclear (149,150). MPF_{FA} also have a VirB1-homolog, which encodes the lytic transglycosylase. Surprisingly, however, VirB1 was not essential for transfer, although one would think that the thick peptidoglycan layer characterising monoderm cells would require a specific lytic transglycosylase (151).

The **MPF_{FATA}** class includes systems from diverse prokaryote groups, mostly Firmicutes, Actinobacteria, Tenericutes and Archaea. The first two phyla are characterized by a very thick cell wall, while Tenericutes are completely devoid of it and Archaea have a different lipid composition of the membrane and no peptidoglycan. This clade was reconstructed from the pGO1 plasmid of *Staphylococcus aureus* (152), the pCF10 plasmid of *Enterococcus faecalis* (153), the ICECtn2 of *Clostridium difficile* (154) and the ICESaNEM316 of *Streptococcus agalactiae* (155). Similarly to MPF_{FA}, homologs of VirB3, VirB6, and VirB8 were found, in addition to a lytic-transglycosylase.

The remaining four clades encompass T4SSs found in Proteobacteria and closely related taxa, and have been named MPF_T, MPF_F, MPF_I and MPF_G. The **MPF_T** clade includes the VirB system of *A.*

tumefaciens, whereas the **MPF_F** clade takes his name from the *E. coli* F-plasmid. Both classes have been extensively studied and described above; therefore, we will not discuss them further.

The **MPF_I** systems are exemplified by the IncI plasmid R64 (156). The MPF_I system has clear VirB8 (inner membrane), VirB10 (core component) and VirB11 (ATPase) homologs. Interestingly, R64 carries two *virB2* genes encoding for putative pilins. Experimental evidence showed that both *virB2* genes on R64 are essential, but exclusive for conjugation under different conditions, one in liquid and the other on solid media. The pilus used in liquid conjugation is thinner and shows homology to type IV pili (157). Several other proteins essential for R64 transfer have no homologs to known T4SS components from the MPF_T- and F-classes.

The last clade recognized by the Guglielmini classification is **MPF_G**, which almost exclusively comprises conjugative systems encoded by ICEs of β - and γ -proteobacteria. T4SS of this class have been widely understudied, with only one secretion system having been partially characterized (at the start of the thesis); the one encoded by ICE*Hin1056* of *H. influenzae* (90). A group of 24 genes of ICE*Hin1056* was suggested as candidates for the conjugative system (*tfc1-tfc24*). Homologs of the two quintessential T4SS proteins were found: Tfc6 (the VirD4 coupling protein ATPase) and Tfc16 (the VirB4 ATPase). In addition, a homolog to TraB of the F-plasmid was detected (Tfc14), and a set of seven genes involved in conjugative pilus formation, which included *tfc14* and *tfc16*. With a more refined bioinformatics analysis Guglielmini et al. (93) identified several other homologies between the ICE*Hin1056* and other T4SSs, such as the proteins forming the suspected OMC and IMC complexes. Interestingly, as in other MPF classes, two genes on ICE*Hin1056* are predicted to encode for pilins: *tfc9* and *tfc10*.

State of the art of ICE-encoded T4SSs

With the development of increasingly cheap and efficient sequencing techniques, the number of available bacterial genome sequences is constantly growing and with it the amount of mobile elements discovered. By comparing genomes of closely related strains, new ICEs are constantly being detected. This includes human or animal pathogens (47,77,158,159), soil bacteria (160-162), or marine species (163,164). Despite this bioinformatic characterization, the actual genetic and biochemical evidence is actually very limited, one of the reasons probably being the lack of host genetic accessibility. At the onset of my thesis, the two best characterized ICE-encoded T4SS were the ones of ICE*Bs1* (*B. subtilis*) and ICE*Hin1056* (*H. influenzae*). Two studies on ICE*Bs1* had mainly

focused on the characterization of the *virB4*-homolog named *conE*. The essentiality of ConE for ICEBs1 transfer was demonstrated by genetic studies, with point mutations in the Walker A and B motifs showing that its enzyme functionality is necessary for conjugation. ConE-GFP in *B. subtilis* was preferentially located at the cell poles, suggesting that DNA conjugation starts from the cell extremity (88). ConE itself was purified and biochemically characterized. It has a monomeric state in solution (165), and can bind to ConB and ConQ. ConB is a homolog of VirB8 and ConQ of VirD4, and both are located in the inner membrane of *B. subtilis*. A third study focused on ConB (VirB8), ConC, ConD (VirB3) and ConG (VirB6), which were all found to be necessary for ICEBs1 conjugative transfer. In addition, ConB and ConD were required for proper localization of ConE-GFP at the cell poles (166). More recently, a T4SS encoded by the *CTn4* element in *C. difficile* was partially characterized, which detected homologs of VirB4 and VirD4, and investigated their enzymatic properties and oligomerization *in vitro* (167). Overall, it was (and is) clear that there is a great lack of in depth knowledge on the conjugation systems of ICEs, in particular, of the MPF_G clade.

Aim of the project and approaches

The main aim of my thesis project was thus to better characterize the conjugative system encoded by ICE*clc* as example of a MPF_G clade-member, and uncover features that would make it distinct from other MPF-types. Given that the ICE*clc* core region, which includes the genetic locus encoding for the T4SS (Fig. 2), is highly conserved among a wide range of β - and γ -proteobacteria, we also envisioned that discovering particularities about ICE*clc* conjugation would be representative for HGT of a large number of mobile elements. In practice, my work still forms the first extensive study of an ICE-encoded T4SS, which I hope will pave the way for more in depth studies in the future.

1. In the first part of my work I focused on the molecular and genetic characterization of the T4SS genetic locus of ICE*clc*. With the help of different bioinformatic tools I inferred homologies to known T4SS subunits. I constructed single deletion mutants for 22 out of the 24 genes in the predicted T4SS locus to demonstrate their importance for ICE*clc* transfer. To gain more knowledge on T4SS assembly at single cell level, I fluorescently labelled nine different ICE*clc*-T4SS components with predicted location in the inner-membrane, outer-membrane and periplasm, and studied their subcellular localization in tc cells. Notably, I found that tc cells have multiple T4SS around the cell, with potential different 'states' of their full assembly. By combinations of fluorescently tagged T4SS subunits and deletion mutants

I could infer interactions between inner- outer-membrane subunits and proposed a dynamic process of IMC- and OMC formation.

2. In the second part I focused on the identification and visualization of the ICE*clc* conjugative pilus. Previous sequence homology searches did not conclusively detect any pilin candidates within the ICE*clc* T4SS locus, but older literature evidence suggested two open reading frames: *orf67231* and *orf66625*. By using AlphaFold2 protein 3D structure prediction I identified the most likely gene candidate for the major pilin as *orf66625*. I visualized the conjugative pilus in live cells by using chemical labelling of exposed (mutated) cysteine residues, and used different EM techniques (cryo-CLEM) to propose that the observed structures exclusively originate from tc cells.
3. In the third part of my thesis I focused on the dynamics of the ICE*clc* T4SS macromolecular structures. From my previous results I developed two working hypotheses, which I wanted to test in subsequent experiments. First, I imagined that IMC- and OMC-parts of the T4SS could be present independently in the cell envelope of tc cells, but would only 'dock' together to a full structure upon actual DNA conjugation. Secondly, I wondered whether ICE conjugation would be 'blind' or could somehow detect the presence of recipient cells, which would then 'direct' IMC- and OMC-complexes to the appropriate localization to start conjugation. The interactions between donor and recipient cells during conjugation in general are not well understood. I conducted experiments with or without recipient cells and monitored the number and dynamics of labeled T4SS complexes. I mainly focused on two labeled subunits, IceB4 of the IMC and IceB7 of the OMC, which were fused to sfGFP and mCherry, respectively, and which had been shown to be still permissive for conjugation. Fluorescently labelled *P. putida* ICE*clc* donor strains were monitored with time-lapse microscopy alone or with recipients, and the dynamic positioning of IceB4 and IceB7 fluorescent foci localization were inferred. Our results show that IceB7 forms stable foci at the cell membrane, while IceB4 is highly dynamic, which suggests the existence of OMC and IMC as independent complexes that come together only under certain conditions. Adding a recipient to the mixture had slight but significant effect in the movement of IceB7 foci, which was reduced, on the other hand IceB4 dynamics was not reduced compared to what we observed with donors alone. This result clearly demonstrate that T4SS machineries are not static entities but rather dynamic molecular assembly that undergo a series of structural and conformational changes in the different stages of conjugation. The data that we acquired on

the recipient prove that their presence can influence T4SS subunit stability in the donor, however more experiments and data need to be acquired to fully comprehend donor-recipient interaction in conjugative transfer.

References

1. Tecon, R. and Or, D. (2017) Biophysical processes supporting the diversity of microbial life in soil. *FEMS Microbiol Rev*, **41**, 599-623.
2. Moran, M.A. (2015) The global ocean microbiome. *Science*, **350**, aac8455.
3. Trivedi, P., Leach, J.E., Tringe, S.G., Sa, T. and Singh, B.K. (2020) Plant-microbiome interactions: from community assembly to plant health. *Nat Rev Microbiol*, **18**, 607-621.
4. Gilbert, J.A., Blaser, M.J., Caporaso, J.G., Jansson, J.K., Lynch, S.V. and Knight, R. (2018) Current understanding of the human microbiome. *Nat Med*, **24**, 392-400.
5. Raymann, K. and Moran, N.A. (2018) The role of the gut microbiome in health and disease of adult honey bee workers. *Curr Opin Insect Sci*, **26**, 97-104.
6. Dagan, T., Artzy-Randrup, Y. and Martin, W. (2008) Modular networks and cumulative impact of lateral transfer in prokaryote genome evolution. *Proc Natl Acad Sci U S A*, **105**, 10039-10044.
7. Brito, I.L. (2021) Examining horizontal gene transfer in microbial communities. *Nat Rev Microbiol*, **19**, 442-453.
8. Lorenz, M.G. and Wackernagel, W. (1994) Bacterial gene transfer by natural genetic transformation in the environment. *Microbiol Rev*, **58**, 563-602.
9. Lang, A.S., Zhaxybayeva, O. and Beatty, J.T. (2012) Gene transfer agents: phage-like elements of genetic exchange. *Nat Rev Microbiol*, **10**, 472-482.
10. Cabezón, E., Ripoll-Rozada, J., Pena, A., de la Cruz, F. and Arechaga, I. (2015) Towards an integrated model of bacterial conjugation. *FEMS Microbiol Rev*, **39**, 81-95.
11. Christie, P.J. (2016) The Mosaic Type IV Secretion Systems. *EcoSal Plus*, **7**.
12. Schneider, H. and Falkow, S. (1964) Characterization of an Hfr Strain of *Shigella Flexneri*. *J Bacteriol*, **88**, 682-689.
13. Guedon, G., Libante, V., Coluzzi, C., Payot, S. and Leblond-Bourget, N. (2017) The Obscure World of Integrative and Mobilizable Elements, Highly Widespread Elements that Pirate Bacterial Conjugative Systems. *Genes (Basel)*, **8**.
14. Arnold, B.J., Huang, I.T. and Hanage, W.P. (2022) Horizontal gene transfer and adaptive evolution in bacteria. *Nat Rev Microbiol*, **20**, 206-218.
15. Michel, B. and Leach, D. (2012) Homologous Recombination-Enzymes and Pathways. *EcoSal Plus*, **5**.
16. Delavat, F., Miyazaki, R., Carraro, N., Pradervand, N. and van der Meer, J.R. (2017) The hidden life of integrative and conjugative elements. *FEMS Microbiol Rev*, **41**, 512-537.
17. Bobay, L.M., Rocha, E.P. and Touchon, M. (2013) The adaptation of temperate bacteriophages to their host genomes. *Mol Biol Evol*, **30**, 737-751.
18. Durrant, M.G., Li, M.M., Siranosian, B.A., Montgomery, S.B. and Bhatt, A.S. (2020) A Bioinformatic Analysis of Integrative Mobile Genetic Elements Highlights Their Role in Bacterial Adaptation. *Cell Host Microbe*, **27**, 140-153 e149.
19. Sentchilo, V., Czechowska, K., Pradervand, N., Minoia, M., Miyazaki, R. and van der Meer, J.R. (2009) Intracellular excision and reintegration dynamics of the ICE_{clc} genomic island of *Pseudomonas knackmussii* sp. strain B13. *Mol Microbiol*, **72**, 1293-1306.
20. Slomka, S., Françoise, I., Hornung, G., Asraf, O., Biniashvili, T., Pilpel, Y. and Dahan, O. (2020) Experimental Evolution of *Bacillus subtilis* Reveals the Evolutionary Dynamics of Horizontal Gene Transfer and Suggests Adaptive and Neutral Effects. *Genetics*, **216**, 543-558.
21. Maddamsetti, R. and Lenski, R.E. (2018) Analysis of bacterial genomes from an evolution experiment with horizontal gene transfer shows that recombination can sometimes overwhelm selection. *PLoS Genet*, **14**, e1007199.
22. San Millan, A. and MacLean, R.C. (2017) Fitness Costs of Plasmids: a Limit to Plasmid Transmission. *Microbiol Spectr*, **5**.
23. Ni, S., Li, B., Tang, K., Yao, J., Wood, T.K., Wang, P. and Wang, X. (2021) Conjugative plasmid-encoded toxin-antitoxin system PrpT/PrpA directly controls plasmid copy number. *Proc Natl Acad Sci U S A*, **118**.

24. Sengupta, M. and Austin, S. (2011) Prevalence and significance of plasmid maintenance functions in the virulence plasmids of pathogenic bacteria. *Infect Immun*, **79**, 2502-2509.
25. Jurenas, D., Fraikin, N., Goormaghtigh, F. and Van Melderen, L. (2022) Biology and evolution of bacterial toxin-antitoxin systems. *Nat Rev Microbiol*, **20**, 335-350.
26. Baxter, J.C. and Funnell, B.E. (2014) Plasmid Partition Mechanisms. *Microbiol Spectr*, **2**.
27. Hall, J.P., Wood, A.J., Harrison, E. and Brockhurst, M.A. (2016) Source-sink plasmid transfer dynamics maintain gene mobility in soil bacterial communities. *Proc Natl Acad Sci U S A*, **113**, 8260-8265.
28. Bouma, J.E. and Lenski, R.E. (1988) Evolution of a bacteria/plasmid association. *Nature*, **335**, 351-352.
29. San Millan, A., Pena-Miller, R., Toll-Riera, M., Halbert, Z.V., McLean, A.R., Cooper, B.S. and MacLean, R.C. (2014) Positive selection and compensatory adaptation interact to stabilize non-transmissible plasmids. *Nat Commun*, **5**, 5208.
30. Zwanzig, M., Harrison, E., Brockhurst, M.A., Hall, J.P.J., Berendonk, T.U. and Berger, U. (2019) Mobile Compensatory Mutations Promote Plasmid Survival. *mSystems*, **4**.
31. Porse, A., Schonning, K., Munck, C. and Sommer, M.O. (2016) Survival and Evolution of a Large Multidrug Resistance Plasmid in New Clinical Bacterial Hosts. *Mol Biol Evol*, **33**, 2860-2873.
32. Yano, H., Wegrzyn, K., Loftie-Eaton, W., Johnson, J., Deckert, G.E., Rogers, L.M., Konieczny, I. and Top, E.M. (2016) Evolved plasmid-host interactions reduce plasmid interference cost. *Mol Microbiol*, **101**, 743-756.
33. Gaillard, M., Pernet, N., Vogne, C., Hagenbuchle, O. and van der Meer, J.R. (2008) Host and invader impact of transfer of the *clc* genomic island into *Pseudomonas aeruginosa* PAO1. *Proc Natl Acad Sci U S A*, **105**, 7058-7063.
34. Gomes, A.L.C., Johns, N.I., Yang, A., Velez-Cortes, F., Smillie, C.S., Smith, M.B., Alm, E.J. and Wang, H.H. (2020) Genome and sequence determinants governing the expression of horizontally acquired DNA in bacteria. *ISME J*, **14**, 2347-2357.
35. Hughes, A.L. (2005) Evidence for abundant slightly deleterious polymorphisms in bacterial populations. *Genetics*, **169**, 533-538.
36. Cabezon, E., de la Cruz, F. and Arechaga, I. (2017) Conjugation Inhibitors and Their Potential Use to Prevent Dissemination of Antibiotic Resistance Genes in Bacteria. *Front Microbiol*, **8**, 2329.
37. Top, E.M., Springael, D. and Boon, N. (2002) Catabolic mobile genetic elements and their potential use in bioaugmentation of polluted soils and waters. *FEMS Microbiol Ecol*, **42**, 199-208.
38. Peters, J.M., Koo, B.M., Patino, R., Heussler, G.E., Hearne, C.C., Qu, J., Inclan, Y.F., Hawkins, J.S., Lu, C.H.S., Silvis, M.R. *et al.* (2019) Enabling genetic analysis of diverse bacteria with Mobile-CRISPRi. *Nat Microbiol*, **4**, 244-250.
39. Frost, L.S., Leplae, R., Summers, A.O. and Toussaint, A. (2005) Mobile genetic elements: the agents of open source evolution. *Nat Rev Microbiol*, **3**, 722-732.
40. Hacker, J., Bender, L., Ott, M., Wingender, J., Lund, B., Marre, R. and Goebel, W. (1990) Deletions of chromosomal regions coding for fimbriae and hemolysins occur in vitro and in vivo in various extraintestinal *Escherichia coli* isolates. *Microb Pathog*, **8**, 213-225.
41. Dobrindt, U., Hochhut, B., Hentschel, U. and Hacker, J. (2004) Genomic islands in pathogenic and environmental microorganisms. *Nat Rev Microbiol*, **2**, 414-424.
42. Arashida, H., Otake, H., Sugawara, M., Noda, R., Kakizaki, K., Ohkubo, S., Mitsui, H., Sato, S. and Minamisawa, K. (2022) Evolution of rhizobial symbiosis islands through insertion sequence-mediated deletion and duplication. *ISME J*, **16**, 112-121.
43. Zhu, D., He, J., Yang, Z., Wang, M., Jia, R., Chen, S., Liu, M., Zhao, X., Yang, Q., Wu, Y. *et al.* (2019) Comparative analysis reveals the Genomic Islands in *Pasteurella multocida* population genetics: on Symbiosis and adaptability. *BMC Genomics*, **20**, 63.
44. Roy Chowdhury, P., Scott, M., Worden, P., Huntington, P., Hudson, B., Karagiannis, T., Charles, I.G. and Djordjevic, S.P. (2016) Genomic islands 1 and 2 play key roles in the evolution of extensively drug-resistant ST235 isolates of *Pseudomonas aeruginosa*. *Open Biol*, **6**.
45. Carraro, N., Sentchilo, V., Polak, L., Bertelli, C. and van der Meer, J.R. (2020) Insights into Mobile Genetic Elements of the Biocide-Degrading Bacterium *Pseudomonas nitroreducens* HBP-1. *Genes (Basel)*, **11**.

46. Gaillard, M., Vallaey, T., Vorholter, F.J., Minoia, M., Werlen, C., Sentchilo, V., Puhler, A. and van der Meer, J.R. (2006) The *clc* element of *Pseudomonas* sp. strain B13, a genomic island with various catabolic properties. *J Bacteriol*, **188**, 1999-2013.
47. Benigno, V., Carraro, N., Sarton-Loheac, G., Romano-Bertrand, S., Blanc, D.S. and van der Meer, J.R. (2023) Diversity and evolution of an abundant ICE_{clc} family of integrative and conjugative elements in *Pseudomonas aeruginosa*. *mSphere*, e0051723.
48. Duquesne, S., Destoumieux-Garzon, D., Peduzzi, J. and Rebuffat, S. (2007) Microcins, gene-encoded antibacterial peptides from enterobacteria. *Nat Prod Rep*, **24**, 708-734.
49. Juhas, M., van der Meer, J.R., Gaillard, M., Harding, R.M., Hood, D.W. and Crook, D.W. (2009) Genomic islands: tools of bacterial horizontal gene transfer and evolution. *FEMS Microbiol Rev*, **33**, 376-393.
50. Schmidt, H. and Hensel, M. (2004) Pathogenicity islands in bacterial pathogenesis. *Clin Microbiol Rev*, **17**, 14-56.
51. Larbig, K.D., Christmann, A., Johann, A., Klockgether, J., Hartsch, T., Merkl, R., Wiehlmann, L., Fritz, H.J. and Tummeler, B. (2002) Gene islands integrated into tRNA(Gly) genes confer genome diversity on a *Pseudomonas aeruginosa* clone. *J Bacteriol*, **184**, 6665-6680.
52. Ravatn, R., Studer, S., Springael, D., Zehnder, A.J. and van der Meer, J.R. (1998) Chromosomal integration, tandem amplification, and deamplification in *Pseudomonas putida* F1 of a 105-kilobase genetic element containing the chlorocatechol degradative genes from *Pseudomonas* sp. Strain B13. *J Bacteriol*, **180**, 4360-4369.
53. Langille, M.G., Hsiao, W.W. and Brinkman, F.S. (2010) Detecting genomic islands using bioinformatics approaches. *Nat Rev Microbiol*, **8**, 373-382.
54. Magaziner, S.J., Zeng, Z., Chen, B. and Salmond, G.P.C. (2019) The Prophages of *Citrobacter rodentium* Represent a Conserved Family of Horizontally Acquired Mobile Genetic Elements Associated with Enteric Evolution towards Pathogenicity. *J Bacteriol*, **201**.
55. Carraro, N. and Burrus, V. (2014) Biology of Three ICE Families: SXT/R391, ICEBs1, and ICESt1/ICESt3. *Microbiol Spectr*, **2**.
56. Ohtsubo, Y., Ishibashi, Y., Naganawa, H., Hirokawa, S., Atobe, S., Nagata, Y. and Tsuda, M. (2012) Conjugal transfer of polychlorinated biphenyl/biphenyl degradation genes in *Acidovorax* sp. strain KKS102, which are located on an integrative and conjugative element. *J Bacteriol*, **194**, 4237-4248.
57. Fillol-Salom, A., Martinez-Rubio, R., Abdulrahman, R.F., Chen, J., Davies, R. and Penades, J.R. (2018) Phage-inducible chromosomal islands are ubiquitous within the bacterial universe. *ISME J*, **12**, 2114-2128.
58. Burrus, V., Pavlovic, G., Decaris, B. and Guedon, G. (2002) Conjugative transposons: the tip of the iceberg. *Mol Microbiol*, **46**, 601-610.
59. Carraro, N., Rivard, N., Ceccarelli, D., Colwell, R.R. and Burrus, V. (2016) IncA/C Conjugative Plasmids Mobilize a New Family of Multidrug Resistance Islands in Clinical *Vibrio cholerae* Non-O1/Non-O139 Isolates from Haiti. *mBio*, **7**.
60. Daccord, A., Ceccarelli, D. and Burrus, V. (2010) Integrating conjugative elements of the SXT/R391 family trigger the excision and drive the mobilization of a new class of *Vibrio* genomic islands. *Mol Microbiol*, **78**, 576-588.
61. Qiu, X., Gurkar, A.U. and Lory, S. (2006) Interstrain transfer of the large pathogenicity island (PAPI-1) of *Pseudomonas aeruginosa*. *Proc Natl Acad Sci U S A*, **103**, 19830-19835.
62. Mohd-Zain, Z., Turner, S.L., Cerdano-Tarraga, A.M., Lilley, A.K., Inzana, T.J., Duncan, A.J., Harding, R.M., Hood, D.W., Peto, T.E. and Crook, D.W. (2004) Transferable antibiotic resistance elements in *Haemophilus influenzae* share a common evolutionary origin with a diverse family of syntenic genomic islands. *J Bacteriol*, **186**, 8114-8122.
63. Hochhut, B. and Waldor, M.K. (1999) Site-specific integration of the conjugal *Vibrio cholerae* SXT element into *prfC*. *Mol Microbiol*, **32**, 99-110.
64. Ravatn, R., Studer, S., Zehnder, A.J. and van der Meer, J.R. (1998) Int-B13, an unusual site-specific recombinase of the bacteriophage P4 integrase family, is responsible for chromosomal insertion of the 105-kilobase *clc* element of *Pseudomonas* sp. Strain B13. *J Bacteriol*, **180**, 5505-5514.

65. Cho, E.H., Gumport, R.I. and Gardner, J.F. (2002) Interactions between integrase and excisionase in the phage lambda excisive nucleoprotein complex. *J Bacteriol*, **184**, 5200-5203.
66. Hinerfeld, D. and Churchward, G. (2001) Xis protein of the conjugative transposon Tn916 plays dual opposing roles in transposon excision. *Mol Microbiol*, **41**, 1459-1467.
67. Burrus, V. and Waldor, M.K. (2003) Control of SXT integration and excision. *J Bacteriol*, **185**, 5045-5054.
68. Auchtung, J.M., Aleksanyan, N., Bulku, A. and Berkmen, M.B. (2016) Biology of ICEBs1, an integrative and conjugative element in *Bacillus subtilis*. *Plasmid*, **86**, 14-25.
69. Yin, J., Collier, A.C., Barr, A.M., Honer, W.G. and Procyshyn, R.M. (2015) Paliperidone Palmitate Long-Acting Injectable Given Intramuscularly in the Deltoid Versus the Gluteal Muscle: Are They Therapeutically Equivalent? *J Clin Psychopharmacol*, **35**, 447-449.
70. Delavat, F., Moritz, R. and van der Meer, J.R. (2019) Transient Replication in Specialized Cells Favors Transfer of an Integrative and Conjugative Element. *mBio*, **10**.
71. Carraro, N., Richard, X., Sulser, S., Delavat, F., Mazza, C. and van der Meer, J.R. (2020) An analog to digital converter controls bistable transfer competence development of a widespread bacterial integrative and conjugative element. *Elife*, **9**.
72. Carraro, N., Poulin, D. and Burrus, V. (2015) Replication and Active Partition of Integrative and Conjugative Elements (ICEs) of the SXT/R391 Family: The Line between ICEs and Conjugative Plasmids Is Getting Thinner. *PLoS Genet*, **11**, e1005298.
73. Huguet, K.T., Gonnet, M., Doublet, B. and Cloeckaert, A. (2016) A toxin antitoxin system promotes the maintenance of the IncA/C-mobilizable *Salmonella* Genomic Island 1. *Sci Rep*, **6**, 32285.
74. Wozniak, R.A. and Waldor, M.K. (2009) A toxin-antitoxin system promotes the maintenance of an integrative conjugative element. *PLoS Genet*, **5**, e1000439.
75. Miyazaki, R., Bertelli, C., Benaglio, P., Canton, J., De Coi, N., Gharib, W.H., Gjoksi, B., Goesmann, A., Greub, G., Harshman, K. *et al.* (2015) Comparative genome analysis of *Pseudomonas knackmussii* B13, the first bacterium known to degrade chloroaromatic compounds. *Environ Microbiol*, **17**, 91-104.
76. Pradervand, N., Sulser, S., Delavat, F., Miyazaki, R., Lamas, I. and van der Meer, J.R. (2014) An operon of three transcriptional regulators controls horizontal gene transfer of the integrative and conjugative element ICElc in *Pseudomonas knackmussii* B13. *PLoS Genet*, **10**, e1004441.
77. Benigno, V., Carraro, N., Sarton-Lohéac, G., Romano-Bertrand, S., Blanc, D.S. and van der Meer, J.R. (2023).
78. Minoia, M., Gaillard, M., Reinhard, F., Stojanov, M., Sentchilo, V. and van der Meer, J.R. (2008) Stochasticity and bistability in horizontal transfer control of a genomic island in *Pseudomonas*. *Proc Natl Acad Sci U S A*, **105**, 20792-20797.
79. Delavat, F., Mitri, S., Pelet, S. and van der Meer, J.R. (2016) Highly variable individual donor cell fates characterize robust horizontal gene transfer of an integrative and conjugative element. *Proc Natl Acad Sci U S A*, **113**, E3375-3383.
80. Takano, S., Fukuda, K., Koto, A. and Miyazaki, R. (2019) A novel system of bacterial cell division arrest implicated in horizontal transmission of an integrative and conjugative element. *PLoS Genet*, **15**, e1008445.
81. Reinhard, F., Miyazaki, R., Pradervand, N. and van der Meer, J.R. (2013) Cell differentiation to "mating bodies" induced by an integrating and conjugative element in free-living bacteria. *Curr Biol*, **23**, 255-259.
82. Zink, S.D., Pedersen, L., Cianciotto, N.P. and Abu-Kwaik, Y. (2002) The Dot/Icm type IV secretion system of *Legionella pneumophila* is essential for the induction of apoptosis in human macrophages. *Infect Immun*, **70**, 1657-1663.
83. Censini, S., Lange, C., Xiang, Z., Crabtree, J.E., Ghiara, P., Borodovsky, M., Rappuoli, R. and Covacci, A. (1996) *cag*, a pathogenicity island of *Helicobacter pylori*, encodes type I-specific and disease-associated virulence factors. *Proc Natl Acad Sci U S A*, **93**, 14648-14653.
84. Cenens, W., Andrade, M.O., Llontop, E., Alvarez-Martinez, C.E., Sgro, G.G. and Farah, C.S. (2020) Bactericidal type IV secretion system homeostasis in *Xanthomonas citri*. *PLoS Pathog*, **16**, e1008561.

85. Low, H.H., Gubellini, F., Rivera-Calzada, A., Braun, N., Connery, S., Dujeancourt, A., Lu, F., Redzej, A., Fronzes, R., Orlova, E.V. *et al.* (2014) Structure of a type IV secretion system. *Nature*, **508**, 550-553.
86. Lederberg, J. and Tatum, E.L. (1946) Gene recombination in *Escherichia coli*. *Nature*, **158**, 558.
87. Zupan, J.R., Ward, D. and Zambryski, P. (1998) Assembly of the VirB transport complex for DNA transfer from *Agrobacterium tumefaciens* to plant cells. *Curr Opin Microbiol*, **1**, 649-655.
88. Berkmen, M.B., Lee, C.A., Loveday, E.K. and Grossman, A.D. (2010) Polar positioning of a conjugation protein from the integrative and conjugative element ICEBs1 of *Bacillus subtilis*. *J Bacteriol*, **192**, 38-45.
89. Gaillard, M., Pradervand, N., Minoia, M., Sentchilo, V., Johnson, D.R. and van der Meer, J.R. (2010) Transcriptome analysis of the mobile genome ICEclc in *Pseudomonas knackmussii* B13. *BMC Microbiol*, **10**, 153.
90. Juhas, M., Crook, D.W., Dimopoulou, I.D., Lunter, G., Harding, R.M., Ferguson, D.J. and Hood, D.W. (2007) Novel type IV secretion system involved in propagation of genomic islands. *J Bacteriol*, **189**, 761-771.
91. Hofreuter, D., Odenbreit, S. and Haas, R. (2001) Natural transformation competence in *Helicobacter pylori* is mediated by the basic components of a type IV secretion system. *Mol Microbiol*, **41**, 379-391.
92. Kersulyte, D., Chalkauskas, H. and Berg, D.E. (1999) Emergence of recombinant strains of *Helicobacter pylori* during human infection. *Mol Microbiol*, **31**, 31-43.
93. Guglielmini, J., Neron, B., Abby, S.S., Garcillan-Barcia, M.P., de la Cruz, F. and Rocha, E.P. (2014) Key components of the eight classes of type IV secretion systems involved in bacterial conjugation or protein secretion. *Nucleic Acids Res*, **42**, 5715-5727.
94. Elton, T.C., Holland, S.J., Frost, L.S. and Hazes, B. (2005) F-like type IV secretion systems encode proteins with thioredoxin folds that are putative DsbC homologues. *J Bacteriol*, **187**, 8267-8277.
95. Hu, B., Khara, P. and Christie, P.J. (2019) Structural bases for F plasmid conjugation and F pilus biogenesis in *Escherichia coli*. *Proc Natl Acad Sci U S A*, **116**, 14222-14227.
96. Costa, T.R.D., Harb, L., Khara, P., Zeng, L., Hu, B. and Christie, P.J. (2021) Type IV secretion systems: Advances in structure, function, and activation. *Mol Microbiol*, **115**, 436-452.
97. Gomis-Ruth, F.X. and Coll, M. (2001) Structure of TrwB, a gatekeeper in bacterial conjugation. *Int J Biochem Cell Biol*, **33**, 839-843.
98. Llosa, M. and Alkorta, I. (2017) Coupling Proteins in Type IV Secretion. *Curr Top Microbiol Immunol*, **413**, 143-168.
99. Whitaker, N., Chen, Y., Jakubowski, S.J., Sarkar, M.K., Li, F. and Christie, P.J. (2015) The All-Alpha Domains of Coupling Proteins from the *Agrobacterium tumefaciens* VirB/VirD4 and *Enterococcus faecalis* pCF10-Encoded Type IV Secretion Systems Confer Specificity to Binding of Cognate DNA Substrates. *J Bacteriol*, **197**, 2335-2349.
100. Oka, G.U., Souza, D.P., Cenens, W., Matsuyama, B.Y., Cardoso, M.V.C., Oliveira, L.C., da Silva Lima, F., Cuccovia, I.M., Guzzo, C.R., Salinas, R.K. *et al.* (2022) Structural basis for effector recognition by an antibacterial type IV secretion system. *Proc Natl Acad Sci U S A*, **119**.
101. Kwak, M.J., Kim, J.D., Kim, H., Kim, C., Bowman, J.W., Kim, S., Joo, K., Lee, J., Jin, K.S., Kim, Y.G. *et al.* (2017) Architecture of the type IV coupling protein complex of *Legionella pneumophila*. *Nat Microbiol*, **2**, 17114.
102. Lu, J., Wong, J.J., Edwards, R.A., Manchak, J., Frost, L.S. and Glover, J.N. (2008) Structural basis of specific TraD-TraM recognition during F plasmid-mediated bacterial conjugation. *Mol Microbiol*, **70**, 89-99.
103. Redzej, A., Ukleja, M., Connery, S., Trokter, M., Felisberto-Rodrigues, C., Cryar, A., Thalassinou, K., Hayward, R.D., Orlova, E.V. and Waksman, G. (2017) Structure of a VirD4 coupling protein bound to a VirB type IV secretion machinery. *EMBO J*, **36**, 3080-3095.
104. Guglielmini, J., de la Cruz, F. and Rocha, E.P. (2013) Evolution of conjugation and type IV secretion systems. *Mol Biol Evol*, **30**, 315-331.
105. Dang, T.A. and Christie, P.J. (1997) The VirB4 ATPase of *Agrobacterium tumefaciens* is a cytoplasmic membrane protein exposed at the periplasmic surface. *J Bacteriol*, **179**, 453-462.

106. Hu, B., Khara, P., Song, L., Lin, A.S., Frick-Cheng, A.E., Harvey, M.L., Cover, T.L. and Christie, P.J. (2019) In Situ Molecular Architecture of the Helicobacter pylori Cag Type IV Secretion System. *mBio*, **10**.
107. Chetrit, D., Hu, B., Christie, P.J., Roy, C.R. and Liu, J. (2018) A unique cytoplasmic ATPase complex defines the Legionella pneumophila type IV secretion channel. *Nat Microbiol*, **3**, 678-686.
108. Mossey, P., Hudacek, A. and Das, A. (2010) Agrobacterium tumefaciens type IV secretion protein VirB3 is an inner membrane protein and requires VirB4, VirB7, and VirB8 for stabilization. *J Bacteriol*, **192**, 2830-2838.
109. Yuan, Q., Carle, A., Gao, C., Sivanesan, D., Aly, K.A., Hoppner, C., Krall, L., Domke, N. and Baron, C. (2005) Identification of the VirB4-VirB8-VirB5-VirB2 pilus assembly sequence of type IV secretion systems. *J Biol Chem*, **280**, 26349-26359.
110. Ward, D.V., Draper, O., Zupan, J.R. and Zambryski, P.C. (2002) Peptide linkage mapping of the Agrobacterium tumefaciens vir-encoded type IV secretion system reveals protein subassemblies. *Proc Natl Acad Sci U S A*, **99**, 11493-11500.
111. Savvides, S.N., Yeo, H.J., Beck, M.R., Blaesing, F., Lurz, R., Lanka, E., Buhrdorf, R., Fischer, W., Haas, R. and Waksman, G. (2003) VirB11 ATPases are dynamic hexameric assemblies: new insights into bacterial type IV secretion. *EMBO J*, **22**, 1969-1980.
112. Park, D., Chetrit, D., Hu, B., Roy, C.R. and Liu, J. (2020) Analysis of Dot/Icm Type IVB Secretion System Subassemblies by Cryoelectron Tomography Reveals Conformational Changes Induced by DotB Binding. *mBio*, **11**.
113. Mace, K., Vadakkepat, A.K., Redzej, A., Lukoyanova, N., Oomen, C., Braun, N., Ukleja, M., Lu, F., Costa, T.R.D., Orlova, E.V. et al. (2022) Cryo-EM structure of a type IV secretion system. *Nature*, **607**, 191-196.
114. Jakubowski, S.J., Krishnamoorthy, V., Cascales, E. and Christie, P.J. (2004) Agrobacterium tumefaciens VirB6 domains direct the ordered export of a DNA substrate through a type IV secretion System. *J Mol Biol*, **341**, 961-977.
115. Mary, C., Fouillen, A., Bessette, B., Nanci, A. and Baron, C. (2018) Interaction via the N terminus of the type IV secretion system (T4SS) protein VirB6 with VirB10 is required for VirB2 and VirB5 incorporation into T-pili and for T4SS function. *J Biol Chem*, **293**, 13415-13426.
116. Casu, B., Mary, C., Sverzhinsky, A., Fouillen, A., Nanci, A. and Baron, C. (2018) VirB8 homolog TraE from plasmid pKM101 forms a hexameric ring structure and interacts with the VirB6 homolog TraD. *Proc Natl Acad Sci U S A*, **115**, 5950-5955.
117. Bao, W., Kumagai, Y., Niu, H., Yamaguchi, M., Miura, K. and Rikihisa, Y. (2009) Four VirB6 paralogs and VirB9 are expressed and interact in Ehrlichia chaffeensis-containing vacuoles. *J Bacteriol*, **191**, 278-286.
118. Hapfelmeier, S., Domke, N., Zambryski, P.C. and Baron, C. (2000) VirB6 is required for stabilization of VirB5 and VirB3 and formation of VirB7 homodimers in Agrobacterium tumefaciens. *J Bacteriol*, **182**, 4505-4511.
119. Kumar, R.B. and Das, A. (2001) Functional analysis of the Agrobacterium tumefaciens T-DNA transport pore protein VirB8. *J Bacteriol*, **183**, 3636-3641.
120. Alvarez-Martinez, C.E. and Christie, P.J. (2009) Biological diversity of prokaryotic type IV secretion systems. *Microbiol Mol Biol Rev*, **73**, 775-808.
121. Sheedlo, M.J., Ohi, M.D., Lacy, D.B. and Cover, T.L. (2022) Molecular architecture of bacterial type IV secretion systems. *PLoS Pathog*, **18**, e1010720.
122. Liu, X., Khara, P., Baker, M.L., Christie, P.J. and Hu, B. (2022) Structure of a type IV secretion system core complex encoded by multi-drug resistance F plasmids. *Nat Commun*, **13**, 379.
123. Sheedlo, M.J., Durie, C.L., Chung, J.M., Chang, L., Roberts, J., Swanson, M., Lacy, D.B. and Ohi, M.D. (2021) Cryo-EM reveals new species-specific proteins and symmetry elements in the Legionella pneumophila Dot/Icm T4SS. *Elife*, **10**.
124. Cascales, E. and Christie, P.J. (2004) Agrobacterium VirB10, an ATP energy sensor required for type IV secretion. *Proc Natl Acad Sci U S A*, **101**, 17228-17233.

125. Rivera-Calzada, A., Fronzes, R., Savva, C.G., Chandran, V., Lian, P.W., Laeremans, T., Pardon, E., Steyaert, J., Remaut, H., Waksman, G. *et al.* (2013) Structure of a bacterial type IV secretion core complex at subnanometre resolution. *EMBO J*, **32**, 1195-1204.
126. Sheedlo, M.J., Chung, J.M., Sawhney, N., Durie, C.L., Cover, T.L., Ohi, M.D. and Lacy, D.B. (2020) Cryo-EM reveals species-specific components within the *Helicobacter pylori* Cag type IV secretion system core complex. *Elife*, **9**.
127. Durie, C.L., Sheedlo, M.J., Chung, J.M., Byrne, B.G., Su, M., Knight, T., Swanson, M., Lacy, D.B. and Ohi, M.D. (2020) Structural analysis of the *Legionella pneumophila* Dot/Icm type IV secretion system core complex. *Elife*, **9**.
128. Arutyunov, D. and Frost, L.S. (2013) F conjugation: back to the beginning. *Plasmid*, **70**, 18-32.
129. Clarke, M., Maddera, L., Harris, R.L. and Silverman, P.M. (2008) F-pili dynamics by live-cell imaging. *Proc Natl Acad Sci U S A*, **105**, 17978-17981.
130. Ou, J.T. (1975) Mating signal and DNA penetration deficiency in conjugation between male *Escherichia coli* and minicells. *Proc Natl Acad Sci U S A*, **72**, 3721-3725.
131. Patkowski, J.B., Dahlberg, T., Amin, H., Gahlot, D.K., Vijayrajratnam, S., Vogel, J.P., Francis, M.S., Baker, J.L., Andersson, M. and Costa, T.R.D. (2023) The F-pilus biomechanical adaptability accelerates conjugative dissemination of antimicrobial resistance and biofilm formation. *Nat Commun*, **14**, 1879.
132. Lang, S., Kirchberger, P.C., Gruber, C.J., Redzej, A., Raffl, S., Zellnig, G., Zangger, K. and Zechner, E.L. (2011) An activation domain of plasmid R1 Tral protein delineates stages of gene transfer initiation. *Mol Microbiol*, **82**, 1071-1085.
133. Zheng, W., Pena, A., Low, W.W., Wong, J.L.C., Frankel, G. and Egelman, E.H. (2020) Cryoelectron-Microscopic Structure of the pKpQIL Conjugative Pili from Carbapenem-Resistant *Klebsiella pneumoniae*. *Structure*, **28**, 1321-1328 e1322.
134. Costa, T.R.D., Ilangovan, A., Ukleja, M., Redzej, A., Santini, J.M., Smith, T.K., Egelman, E.H. and Waksman, G. (2016) Structure of the Bacterial Sex F Pilus Reveals an Assembly of a Stoichiometric Protein-Phospholipid Complex. *Cell*, **166**, 1436-1444 e1410.
135. Paiva, W.D., Grossman, T. and Silverman, P.M. (1992) Characterization of F-pilin as an inner membrane component of *Escherichia coli* K12. *J Biol Chem*, **267**, 26191-26197.
136. Kerr, J.E. and Christie, P.J. (2010) Evidence for VirB4-mediated dislocation of membrane-integrated VirB2 pilin during biogenesis of the *Agrobacterium* VirB/VirD4 type IV secretion system. *J Bacteriol*, **192**, 4923-4934.
137. Sagulenko, E., Sagulenko, V., Chen, J. and Christie, P.J. (2001) Role of *Agrobacterium* VirB11 ATPase in T-pilus assembly and substrate selection. *J Bacteriol*, **183**, 5813-5825.
138. Beltran, L.C., Cvirkaite-Krupovic, V., Miller, J., Wang, F., Kreutzberger, M.A.B., Patkowski, J.B., Costa, T.R.D., Schouten, S., Levental, I., Conticello, V.P. *et al.* (2023) Archaeal DNA-import apparatus is homologous to bacterial conjugation machinery. *Nat Commun*, **14**, 666.
139. Kubori, T. and Nagai, H. (2016) The Type IVB secretion system: an enigmatic chimera. *Curr Opin Microbiol*, **29**, 22-29.
140. Christie, P.J., Atmakuri, K., Krishnamoorthy, V., Jakubowski, S. and Cascales, E. (2005) Biogenesis, architecture, and function of bacterial type IV secretion systems. *Annu Rev Microbiol*, **59**, 451-485.
141. Lawley, T.D., Klimke, W.A., Gubbins, M.J. and Frost, L.S. (2003) F factor conjugation is a true type IV secretion system. *FEMS Microbiol Lett*, **224**, 1-15.
142. Garcillan-Barcia, M.P., Francia, M.V. and de la Cruz, F. (2009) The diversity of conjugative relaxases and its application in plasmid classification. *FEMS Microbiol Rev*, **33**, 657-687.
143. Cheng, Q., Paszkiet, B.J., Shoemaker, N.B., Gardner, J.F. and Salyers, A.A. (2000) Integration and excision of a *Bacteroides* conjugative transposon, CTnDOT. *J Bacteriol*, **182**, 4035-4043.
144. Muro-Pastor, A.M., Kuritz, T., Flores, E., Herrero, A. and Wolk, C.P. (1994) Transfer of a genetic marker from a megaplasmid of *Anabaena* sp. strain PCC 7120 to a megaplasmid of a different *Anabaena* strain. *J Bacteriol*, **176**, 1093-1098.
145. Smillie, C., Garcillan-Barcia, M.P., Francia, M.V., Rocha, E.P. and de la Cruz, F. (2010) Mobility of plasmids. *Microbiol Mol Biol Rev*, **74**, 434-452.

146. Goessweiner-Mohr, N., Arends, K., Keller, W. and Grohmann, E. (2014) Conjugation in Gram-Positive Bacteria. *Microbiol Spectr*, **2**, PLAS-0004-2013.
147. Goessweiner-Mohr, N., Grumet, L., Arends, K., Pavkov-Keller, T., Gruber, C.C., Gruber, K., Birner-Gruenberger, R., Kropec-Huebner, A., Huebner, J., Grohmann, E. *et al.* (2013) The 2.5 Å structure of the enterococcus conjugation protein TraM resembles VirB8 type IV secretion proteins. *J Biol Chem*, **288**, 2018-2028.
148. Porter, C.J., Bantwal, R., Bannam, T.L., Rosado, C.J., Pearce, M.C., Adams, V., Lyras, D., Whistock, J.C. and Rood, J.I. (2012) The conjugation protein TcpC from *Clostridium perfringens* is structurally related to the type IV secretion system protein VirB8 from Gram-negative bacteria. *Mol Microbiol*, **83**, 275-288.
149. Teng, W.L., Bannam, T.L., Parsons, J.A. and Rood, J.I. (2008) Functional characterization and localization of the TcpH conjugation protein from *Clostridium perfringens*. *J Bacteriol*, **190**, 5075-5086.
150. Wisniewski, J.A., Teng, W.L., Bannam, T.L. and Rood, J.I. (2015) Two novel membrane proteins, TcpD and TcpE, are essential for conjugative transfer of pCW3 in *Clostridium perfringens*. *J Bacteriol*, **197**, 774-781.
151. Bantwal, R., Bannam, T.L., Porter, C.J., Quinsey, N.S., Lyras, D., Adams, V. and Rood, J.I. (2012) The peptidoglycan hydrolase TcpG is required for efficient conjugative transfer of pCW3 in *Clostridium perfringens*. *Plasmid*, **67**, 139-147.
152. Caryl, J.A. and O'Neill, A.J. (2009) Complete nucleotide sequence of pG01, the prototype conjugative plasmid from the Staphylococci. *Plasmid*, **62**, 35-38.
153. Chen, Y., Zhang, X., Manias, D., Yeo, H.J., Dunny, G.M. and Christie, P.J. (2008) *Enterococcus faecalis* PcfC, a spatially localized substrate receptor for type IV secretion of the pCF10 transfer intermediate. *J Bacteriol*, **190**, 3632-3645.
154. Brouwer, M.S., Warburton, P.J., Roberts, A.P., Mullany, P. and Allan, E. (2011) Genetic organisation, mobility and predicted functions of genes on integrated, mobile genetic elements in sequenced strains of *Clostridium difficile*. *PLoS One*, **6**, e23014.
155. Davies, M.R., Shera, J., Van Domselaar, G.H., Sriprakash, K.S. and McMillan, D.J. (2009) A novel integrative conjugative element mediates genetic transfer from group G *Streptococcus* to other beta-hemolytic *Streptococci*. *J Bacteriol*, **191**, 2257-2265.
156. Sampei, G., Furuya, N., Tachibana, K., Saitou, Y., Suzuki, T., Mizobuchi, K. and Komano, T. (2010) Complete genome sequence of the incompatibility group I1 plasmid R64. *Plasmid*, **64**, 92-103.
157. Kim, S.R. and Komano, T. (1997) The plasmid R64 thin pilus identified as a type IV pilus. *J Bacteriol*, **179**, 3594-3603.
158. Sun, H.R., Cui, X.D., Liu, X.K., Li, S.H., Yi, K.F., Pan, Y.S., Wu, H., Yuan, L., Hu, G.Z. and He, D.D. (2020) Molecular Characterization of a Novel Integrative Conjugative Element ICEHp1 in *Haemophilus parasuis*. *Front Microbiol*, **11**, 1884.
159. Baranowski, E., Dordet-Frisoni, E., Sagne, E., Hygonenq, M.C., Pretre, G., Claverol, S., Fernandez, L., Nouvel, L.X. and Citti, C. (2018) The Integrative Conjugative Element (ICE) of *Mycoplasma agalactiae*: Key Elements Involved in Horizontal Dissemination and Influence of Coresident ICEs. *mBio*, **9**.
160. Colombi, E., Hill, Y., Lines, R., Sullivan, J.T., Kohlmeier, M.G., Christophersen, C.T., Ronson, C.W., Terpolilli, J.J. and Ramsay, J.P. (2023) Population genomics of Australian indigenous *Mesorhizobium* reveals diverse nonsymbiotic genospecies capable of nitrogen-fixing symbioses following horizontal gene transfer. *Microb Genom*, **9**.
161. Mohapatra, B., Malhotra, H. and Phale, P.S. (2022) Life Within a Contaminated Niche: Comparative Genomic Analyses of an Integrative Conjugative Element ICEnahCSV86 and Two Genomic Islands From *Pseudomonas bharatica* CSV86(T) Suggest Probable Role in Colonization and Adaptation. *Front Microbiol*, **13**, 928848.
162. Bustamante, P., Covarrubias, P.C., Levican, G., Katz, A., Tapia, P., Holmes, D., Quatrini, R. and Orellana, O. (2012) ICE Afe 1, an actively excising genetic element from the biomining bacterium *Acidithiobacillus ferrooxidans*. *J Mol Microbiol Biotechnol*, **22**, 399-407.

163. Wang, P., Zeng, Z., Wang, W., Wen, Z., Li, J. and Wang, X. (2017) Dissemination and loss of a biofilm-related genomic island in marine *Pseudoalteromonas* mediated by integrative and conjugative elements. *Environ Microbiol*, **19**, 4620-4637.
164. Badhai, J. and Das, S.K. (2016) Characterization of Three Novel SXT/R391 Integrating Conjugative Elements ICEMfulnd1a and ICEMfulnd1b, and ICEMprChn1 Identified in the Genomes of *Marinomonas fungiae* JCM 18476(T) and *Marinomonas profundimaris* Strain D104. *Front Microbiol*, **7**, 1896.
165. Murthy, A.C., Aleksanyan, N., Morton, G.M., Toyoda, H.C., Kalashyan, M., Chen, S., Ragucci, A.E., Broulidakis, M.P., Swerdlow, K.J., Bui, M.N.N. *et al.* (2023) Characterization of ConE, the VirB4 Homolog of the Integrative and Conjugative Element ICEBs1 of *Bacillus subtilis*. *J Bacteriol*, **205**, e0003323.
166. Leonetti, C.T., Hamada, M.A., Laurer, S.J., Broulidakis, M.P., Swerdlow, K.J., Lee, C.A., Grossman, A.D. and Berkmen, M.B. (2015) Critical Components of the Conjugation Machinery of the Integrative and Conjugative Element ICEBs1 of *Bacillus subtilis*. *J Bacteriol*, **197**, 2558-2567.
167. Sorokina, J., Sokolova, I., Rybolovlev, I., Shevlyagina, N., Troitskiy, V., Zhukhovitsky, V. and Belyi, Y. (2021) VirB4- and VirD4-Like ATPases, Components of a Putative Type 4C Secretion System in *Clostridioides difficile*. *J Bacteriol*, **203**, e0035921.

Chapter 2

Characterization of an atypical but widespread type IV secretion system for transfer of the integrative and conjugative element (ICE clc) in *Pseudomonas putida*

Andrea Daveri, Valentina Benigno, Jan Roelof van der Meer

Published as: **Andrea Daveri**, Valentina Benigno, Jan Roelof van der Meer (2023). “Characterization of an atypical but widespread type IV secretion system for transfer of the integrative and conjugative element (ICE clc) in *Pseudomonas putida*”. Daveri, A., Benigno, V., & van der Meer, J. R. (2023). *Nucleic Acids Research*, 51(5), 2345-2362.

Abstract

Conjugation of DNA relies on multicomponent protein complexes bridging two bacterial cytoplasmic compartments. Whereas plasmid conjugation systems have been well documented, those of integrative and conjugative elements (ICEs) have remained poorly studied. We characterize here the conjugation system of the ICE*clc* element in *Pseudomonas putida* UWC1 that is a model for a widely distributed family of ICEs. By in frame deletion and complementation, we show the importance on ICE transfer of 22 genes in a 20-kb conserved ICE region. Protein comparisons recognized seven homologs to plasmid type IV secretion system components, another six homologs to frequent accessory proteins, and the rest without detectable counterparts. Stationary phase imaging of *P. putida* ICE*clc* with in-frame fluorescent protein fusions to predicted type IV components showed transfer-competent cell subpopulations with multiple fluorescent foci, largely overlapping in dual-labeled subcomponents, which is suggestive for multiple conjugation complexes per cell. Cross-dependencies between subcomponents in ICE-type IV secretion system assembly were revealed by quantitative foci image analysis in a variety of ICE*clc* mutant backgrounds. In conclusion, the ICE*clc* family presents an evolutionary distinct type IV conjugative system with transfer competent cells specialized in efficient transfer.

Introduction

Bacterial conjugation is widely appreciated for its importance to horizontal gene distribution and consequent facilitation of adaptation to new selective conditions. Conjugation is mostly attributed to plasmid DNA, but more recently, integrative and conjugative elements (ICEs) have been recognized as additional widespread conjugative vehicles, which, however, are mostly 'hidden' (inserted) within the bacterial genome (1–5). ICEs combine both phage-like and plasmid properties. Like temperate phages, they remain mostly integrated in their host genome, and occasionally excise. In contrast to lysogenic phages, excised ICEs spread by conjugation to a new cell, where they re-integrate in the host's chromosome (Figure 1A). Expression of the ICE excision and conjugation functions is silent in the integrated state, being subject to complex, multi-layered regulatory control that varies across different ICEs (6–8). Various physiological and external cues can lead to activation of ICE transfer (6,8,9). Particularly for the model ICE*clc* of *Pseudomonas knackmussii* B13 (see below), activation only occurs in a subpopulation of transfer competent (tc) cells, and only these cells are the ones that can excise, replicate and conjugate the ICE (9–11). Most known ICEs have a mosaic 'modular' genetic structure, being composed of syntenic conserved gene regions coding for core mobility functions, interspersed with highly variable gene content that can provide adaptive benefits to the host (1,3,5). Different ICE families have been recognized, based on their evolutionary history and relatedness of the different conserved modules (2). Particularly, conserved components of the conjugation machinery, such as the VirB4 and VirD4 ATPases of the Type IV secretion system (T4SS) have been used for the classification (12,13). Based on this, Guglielmini and coworkers proposed eight phylogenetic clades, covering mating pair formation (MPF) systems from both ICEs and plasmids (14). In particular, the MPFG clade is unique for conjugative systems of ICEs, and has so far not been well-characterized (14). The only studied MPFG-class member is ICEHin1056 of *Haemophilus influenzae*, which non-exhaustively identified a number of T4SS components important for pilus biogenesis (15).

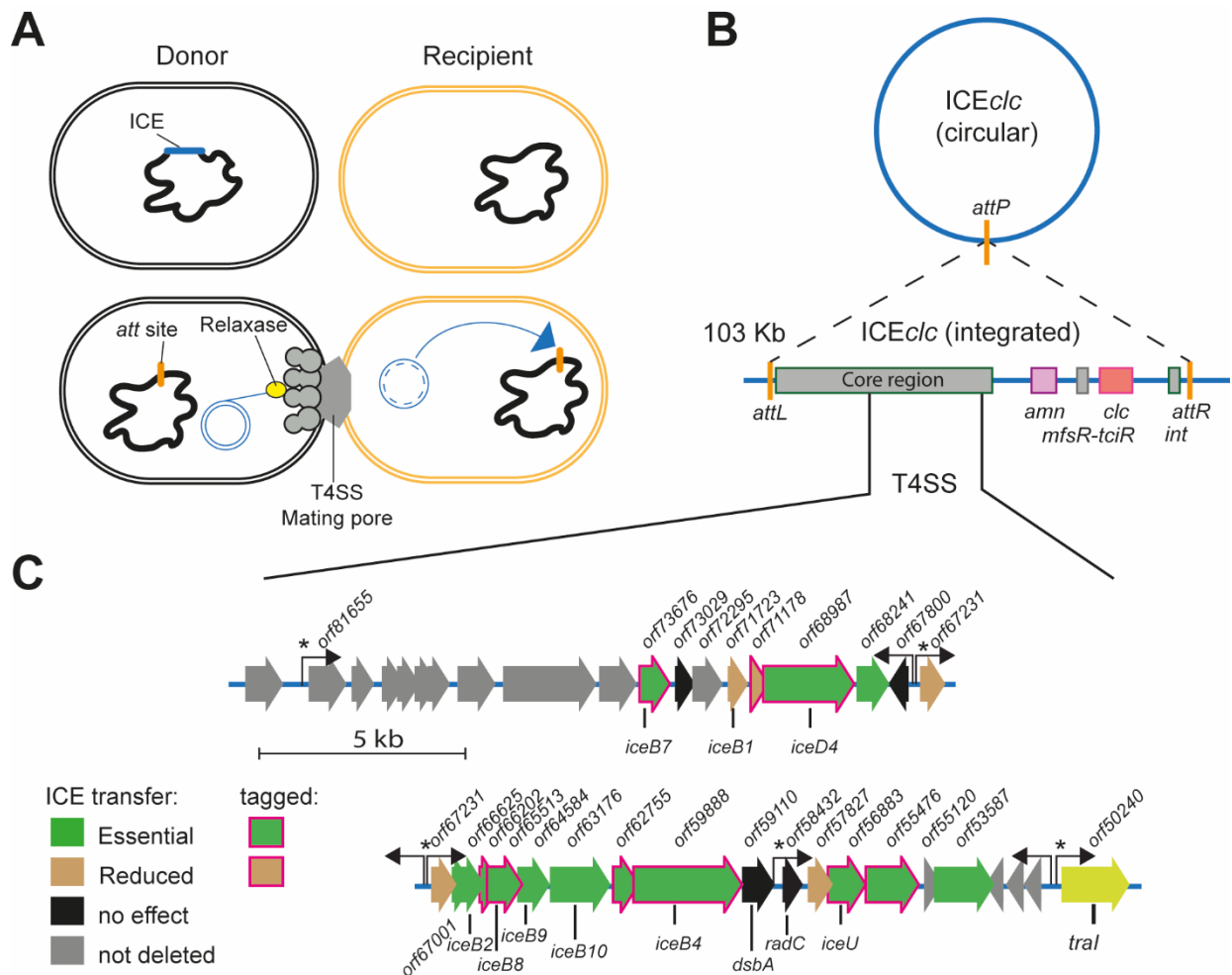


Figure 1 The ICE*clc* lifestyle. **A)** Schematic representation of ICE*clc* transfer from an integrated state (dark blue) to the excised form (double blue circle) that is conjugated through a type IV secretion system (T4SS) mating pore into a recipient cell (yellow), where integration can occur (blue arrow). **B)** Schematic structure of ICE*clc* with its excised circular form recombined at the attP site and the integrated state between attL and attR. Conserved core region shared with other ICE*clc* family members is schematically indicated, as well as are key features of ICE*clc* (int, integrase gene; mfsR-tciR, regulators; amn and clc, metabolic pathway gene clusters). **C)** Detailed map of the conjugative gene region of ICE*clc*. Genes and their orientation are represented by colored arrows, with their original orf designation (as in GenBank AJ617740.2) described above and the deduced relevant gene names below (gene names follow analogous designation as in the vir system). Filled colors correspond to transfer effects as in the colored legend (see Figure 2), whereas magenta arrow outlines point to those components tagged with translational fusions for epifluorescence microscopy. Hooked arrows indicate known promoters; an asterisk pointing to those being active only in transfer competent cells as shown in Ref. (21).

The aim of the current work was to better characterize the MPFG clade conjugative system from the ICE*clc* element and to uncover features distinct from other (plasmid) MPF systems that might point to specific transfer selection. ICE*clc* is 103 kb long and contains genes encoding for metabolism of 3-chlorocatechol and 2-aminophenol (Figure 1B). It is present in two identical copies in the *P. knackmussii* B13 genome at the 3' end of tRNAGly genes (16,17) and can be conjugated to *Pseudomonas putida* where it maintains a single integrated copy. The ICE*clc* core region is highly

conserved among a wide range of putative ICEs detected in genomes of Beta- and Gammaproteobacteria (7,17). Transfer only occurs from tc cells, that appear in 3–5% of the stationary phase population, notably after growth on 3-chlorobenzoate (9,18). After its excision, the ICE*clc* molecule can replicate to up to 7 copies in its host tc cell, which may contribute to more effective and multi-recipient transfer (11). Transfer of ICE*clc* is dependent on the Tral relaxase (Figure 1C), which nicks the DNA at either one of two origins of transfer (*oriT*) (19), and is assumed to guide the single-stranded ICE-DNA molecule to the mating pore.

In order to characterize the components of the ICE*clc* conjugative system, we deployed a combination of genetic dissection, regular and high resolution epifluorescence microscopy and bioinformatics. We focused on a region on ICE*clc* that was previously suggested to locate the genes for its conjugative system (Figure 1C) (20). Out of the 24 genes present in the locus, we seamlessly deleted 22 by double recombination in a *P. putida* ICE*clc* host background, and complemented each deletion individually in trans by a mini-Tn5 delivered single copy wild-type gene, expressed under control of the native ICE promoter upstream of the *orf67231* gene (Figure 1C), which is active only in tc cells (21). The effects of gene deletion and complementation on ICE transfer were quantified from isogenic *P. putida* ICE*clc* donor-recipient matings. Protein structures were predicted from the genes in this ICE region using AlphaFold2 (22) and Phyre2 (23), and compared to the known protein structure databases to find potential homologs. This analysis was complemented by amino acid similarity searches to archetype T4SS components. Finally, a subset of nine identified components of the ICE*clc* conjugative machinery was expressed as in-frame fluorescent protein fusions from their native location to study their cellular localization in *P. putida* ICE*clc* wild-type or mutant backgrounds, and all fusion proteins were verified for functional ICE transfer. Our results indicate that the ICE*clc* conjugation machinery is a very distant T4SS, with several functionally analogous components to the F-plasmid system of *Escherichia coli* (24), the *Agrobacterium tumefaciens* Vir system (25) or the Dot/Icm system of *Legionella pneumophila* (26,27), but with a number of unique other components important for its transfer.

MATERIALS AND METHODS

Biological resources, reagents and growth conditions

Escherichia coli DH5 α λ pir was used for cloning of ICE*clc* genes and plasmid amplification, and was grown at 37°C on Luria-Bertani (LB) liquid or agar-solidified broth. *P. putida* UWC1-ICE*clc*::*lacO*array

was used as host of the ICE, carrying a single copy ICE*clc* integrated at the tRNAGly-5 gene (11). The *lacO* array modification was introduced in the *amnB* gene of the ICE with the purpose to follow single-copy ICE-DNA transfer, if needed (11). *P. putida* UWC1 Tn7 *P_{BAD}-lacI-cfp* or UWC1 Tn7 *P_{tac}-mcherry* were used as recipient strains for mating experiments. *P. putida* was cultured at 30°C either on LB, on nutrient agar (Oxoid) or on minimal medium (MM, type 21C (28)). MM was supplemented with either 5 mM succinate or 3 mM 3-chlorobenzoate (3-CBA) as sole carbon source. Both *E. coli* and *P. putida* were cultured aerobically in shaking flasks. Where necessary for plasmid maintenance or for selection of genomic constructs, antibiotics were added at the following concentrations: kanamycin (Km, 50 µg ml⁻¹), ampicillin (Amp, 100 µg ml⁻¹ for *E. coli*, 500 µg ml⁻¹ for *P. putida*), tetracycline (Tc, 20 µg ml⁻¹ for *E. coli*, 50 µg ml⁻¹ for *P. putida*), or gentamycin (Gm, 20 µg ml⁻¹, 10 µg ml⁻¹ in MM). The following supplements were added for screening or promoter induction (see below): 5-bromo-4-chloro-3-indolyl-β-D-galactopyranoside (X-Gal; 20 µg ml⁻¹), isopropyl-β-D-1-thiogalactopyranoside (IPTG, 0.5 mM), or m-toluate (15 mM). All produced strains are listed in Supplementary table S1.

DNA manipulations

DNA manipulations followed standard procedures or as indicated by the reagent supplier. Plasmids were purified from *E. coli* DH5α *λpir* using NucleoSpin Plasmid kits (Macherey-Nagel, Duren, Germany). Oligonucleotide primers were purchased from SigmaAldrich. PCR amplicons and digested fragments were purified using NucleoSpin Gel and PCR Clean-up kits (Macherey-Nagel). Clones were initially screened by PCR on resuspended individual colonies in a GoTaq® G2 green master mix (20 µl, Promega, Madison, United States). Plasmid fragments were assembled using the ClonExpress II One Step Cloning Kit (Vazyme, Nanjing, China), digesting the plasmid backbone with appropriate restriction enzymes (New England Biolabs, Ipswich, United States), and mixing with insert-DNA. All of the constructed plasmid inserts were sequenced prior to further use in *P. putida*, to verify their correctness, using the ICE*clc* sequence as a reference (29) (GenBank AJ617740.2). Plasmids are listed in Supplementary table S2.

Chromosomal gene knockouts and complementations

Seamless in-frame deletions of ICE*clc* genes were created using double recombination with marker counterselection (30). Up- and downstream regions (~800 bp) of the target gene were PCR amplified using Q5 high fidelity polymerase (New England BioLabs) and primers as detailed in Supplementary table S3, and subsequently cloned into the suicide vector pEMG (30). Purified

plasmids (300–500 ng) were electroporated into *P. putida* UWC1-ICE*clc*::*lacO*array as described previously (19). Single recombinants were selected on plates with Km, and colonies were verified by PCR for integration of the suicide vector. Single recombinants were then cultured and transformed with 50 ng of purified plasmid pSW (30). Transformants were cultured and induced by addition of 15 mM m-toluate (Honeywell Fluka™) for 16 h, to express the I-SceI nuclease and force chromosomal repair, after which culture dilutions were spread on LB plates. Candidate colonies were again verified by PCR for the success of the double recombination and the deletion genotype. Successful clones were then cultured in absence of antibiotics to segregate out pSW, and stored at –80°C with 15% v/v glycerol. Deleted genes on ICE*clc* were complemented by individual or combinations of the cognate gene(s), placed in trans in single-copy on the *P. putida* chromosome using mini-Tn5 delivery (31). ICE*clc* genes for complementation were amplified using Q5 high-fidelity DNA polymerase (New England BioLabs) and primers as in Supplementary table S3, and then brought under control of the native wild-type ICE*clc* promoter P₆₇₂₃₁ that is active only in tc cells (21). The 360-bp P₆₇₂₃₁-promoter region was amplified with primers containing appropriate restriction sites for cloning into the mini-Tn5 delivery vector pBAM (31) and overhangs to allow assembly. Assembled DNA mixtures were transformed by heat-shock into *E. coli* DH5α λpir for propagation and plasmid DNA purification. Purified plasmids were sequenced to verify the cloned insert, and electroporated into the corresponding *P. putida* ICE*clc* gene deletion strain. Integrants were selected for antibiotic resistance from the mini-Tn5 delivered construct and verified by PCR, after which three clones with potentially different integration positions of the complementation insert were frozen at –80°C for further analysis.

Fluorescent protein fusions

The same strategy used to produce gene deletions was employed for translationally fusing fluorescent protein tags (mCherry or sfGFP) at the N- or C-terminal end of target ICE*clc* conjugative system proteins. In case of N-terminal fusion the open reading frame of the fluorescent protein was inserted after the signal sequence if present (e.g. *orf62755*), otherwise following the start codon (e.g. *iceB8*), followed by a short linker peptide as in (32). In case of C-terminal fusion the linker and the fluorescent protein were inserted before the stop codon of the target gene. In the eventuality of overlap between the translation stop and start of two consecutive genes, the insertion was performed in such a way that the ribosome binding site of the following gene remained intact. Primers used for the amplification of the homology regions and fluorescent proteins are listed in

Supplementary table S3. Cognate ICE-genes were replaced with the fluorescently-tagged version directly on wild-type integrated ICE*clc* in *P. putida* or on ICE*clc* carrying additional deletions for conjugative components. *P. putida* without ICE*clc* was used as control for fluorescent protein auto-aggregation, and transformed with relevant mini-Tn5 constructs and plasmids pME-bisR or pME-bisDC expressing two known transcriptional regulators involved in ICE*clc* activation to induce the P67231-promoter in all cells (7). *P. putida* codon-optimized coding sequences (JCat tool (33)) for mCherry and sfGFP were synthesized by ThermoFisher (Waltham, USA).

Protein homology assignments

Homology and functional predictions focused on ICE*clc* genes in the conserved presumed conjugative gene region (gene designations *orf53587–orf73676*, as defined in AJ617740.2, Figure 1C). To avoid finding numerous spurious hits to highly homologous ICE genes in other bacterial genomes, we first compared the translated amino acid sequences from individual ICE*clc* genes to each of the known components of the classical ‘Vir’ T4SS from *A. tumefaciens* (NZ_CP029048.1) by EMBOSS needle alignment across the full protein length. Next, we identified any conserved domains by BLASTp (34), Phyre2 (23), pfam (35), or Dali (36), and used TMHMM (37) and SignalP (38) to predict the presence of transmembrane domains and signal peptides. Finally, we used AlphaFold2 (22) to predict structures for each of the presumed ICE*clc* conjugative components (using standard settings on the web server platform https://colab.research.google.com/github/sokrypton/ColabFold/blob/main/beta/AlphaFold2_advanced.ipynb), and then compared the highest ranked derived .pdb structure prediction in PDBeFold (39) with the PDB database to find potential structural analogs. PDBeFold analyses were carried out with default parameter settings.

ICE*clc* transfer experiments

ICE*clc* transfer was quantified from binary mating experiments. As donors we tested *P. putida* carrying ICE*clc* wild-type, or ICE*clc* with an inserted lacOarray (11), ICE*clc* gene deletion variants and the various complemented strains, as well as fluorescent protein fusion variants. As recipient we used isogenic but ICE*clc*-free *P. putida* UWC1 carrying a chromosomally integrated Gm resistance (Supplementary table S1). Donors and recipient were freshly plated from –80°C stocks on LB agar plates with appropriate antibiotics and grown for 16 h. Three separate clones (donors) and a single colony (recipient) were picked and inoculated each in 10 ml LB with antibiotics. These individual pre-cultures were grown for 24 h, after which a volume of 40 µl was transferred into 8 ml MM with

3 mM 3-CBA (donors) or 5 mM succinate (recipient) as the sole carbon sources, without antibiotics. After 48 h (donor) and 24 h (recipient) of growth the culture turbidities were measured (OD₆₀₀), and recipient and donor cultures were mixed together in new vials in a 2:1 ratio (OD/OD), respectively, and to a final volume of 1 ml. Donor and recipient cultures alone served as controls for the appearance of background growth on selective plates.

Donor-recipient cell mixtures were centrifuged at 13 000 rpm (Thermo Scientific Fresco™ 21 Microcentrifuge) for 2 min, after which the supernatant was discarded and the cell pellet was resuspended in 1 ml of sterile MM (without carbon source). The suspension was centrifuged as before and cell pellets were now resuspended in 20 µl of MM. The suspension was transferred on top of a 0.2-µm, 25 mm ø cellulose acetate filter (Huberlab, Aesch, Switzerland), that had been placed on a MM agar plate with 0.5 mM 3-CBA. Matings were incubated at 30°C for 48 h, after which cells were washed from the filters with 1 ml MM. Cell suspensions were tenfold serially diluted and 5 µl aliquots of every dilution were dropped and dried on MM-agar with 3 mM 3-CBA to select for the donor alone, on MM-agar with 5 mM succinate and Gm to select for the recipient, and on MM-agar with 3 mM 3-CBA and Gm to select for the transconjugants. Plates were incubated at 30°C until colonies appeared. ICE clc transfer rates were then calculated as the ratio of the number of transconjugant colonies per filter and that of the donor. Transfer rates were normalized across different experiments to that of *P. putida* ICE $clc::lacO$ array, which was used as positive control in all experiments.

Epifluorescence microscopy

Fluorescently labelled *P. putida* ICE clc strains were grown for 96 h in liquid MM supplemented with 3 mM 3-CBA to induce the ICE clc transfer competence pathway (7). Cells were then transferred on the surface of 1-mm thick 1% MM-agarose patches (ø1 cm) placed upside down on a round microscope slide and enclosed in an imaging chamber (Perfusion Chamber, H. Saur Laborbedarf, Germany) as described (9). Cells were imaged with a Nikon Eclipse Ti-E inverted microscope with a perfect focus system (PFS), pE-100 CoolLED, a Plan Apo λ 100 × 1.45 oil objective (Nikon) and a Hamamatsu ORCA-Flash4.0 V2 C11440-22CU camera (Hamamatsu, Hamamatsu City, Japan) installed in a controlled temperature room (22°C). sfGFP and mCherry fluorescence were imaged with exposure times of 500 ms and exported as 16-bit .TIF files. Images for display were adjusted to the same level in Adobe Photoshop (v. 2020, Adobe Inc.), downsampled to 8-bit, cropped and saved as 300 dpi.

For improved resolution, samples of the same cell cultures were additionally imaged with a ZEISS LSM 980 Airyscan 2 microscope equipped with ZEN 3.3 software, installed in a controlled temperature room (22°C). Bacterial cells were located on the agarose patches using phase-contrast, after which Z-stacks ($Z = 0.17 \mu\text{m}$, 14 layers) of individual cells were acquired in the GFP and/or mCherry channels with an exposure time of 314 ms per layer. Images were processed with the Zeiss Deconvolution algorithm with default settings. Images show a single representative deconvoluted 170-nm Z-slice saved as .TIF file, 'auto-toned' in Adobe Photoshop (v. 2020), cropped to the final size and saved as 300 dpi.

Image analysis

Individual *P. putida* cells were segmented on the Nikon 16-bit .TIF phase-contrast images using SuperSegger (40), and the fluorescence intensities, scores, and positions of up to 5 foci in individual cells were extracted. SuperSegger uses 1D-Gaussian fitting on background-normalized and watershed fluorescence cell images to detect foci, as illustrated in Supplementary Figure S1. Subpopulations of tc cells were identified from quantile-quantile plot analysis (41) of the median cell sfGFP or mCherry fluorescent signals. 'Real' and spurious fluorescent foci were distinguished by plotting distributions of the normalized foci intensities among tc and non-tc cell populations, and setting a threshold at which the probability for foci detection in non-tc cells was <1%. Custom made MATLAB scripts were used to extract the following parameters: number of foci per cell, median fluorescence intensity per cell, median top 5% pixel intensity per cell (as proxy for foci intensity), distributions of SuperSegger foci scores (quality of the Gaussian fit) and of Gaussian fit sigma values (as proxy for the apparent foci peak-to-size aspect).

Linear fluorescence profiles were derived from the outer 2-pixel (px) perimeter ('cell envelope') of each identified tc cell using its phase-contrast logical mask, and a further 1-px dilated mask. Profiles were scaled to a median cell perimeter of 50 px for plotting. The 20th percentile fluorescence value was taken as proxy for the cell 'membrane' fluorescence background, from which we calculated the median across all tc cells per replicate ($n = 142\text{--}1996$ cells); which were compared between wild-type fluorescent protein labeled strains and those with gene deletions in *ICEc/c*. The standard deviation of the pixel fluorescence values in the two cell perimeters was calculated as second proxy for potential relocalization of fluorescent protein from foci to the cell envelope.

Statistical comparisons

ICE*clc* transfer rates were normalized across all experiments to that of *P. putida* ICE*clc*::*lacO*array, which was taken as a control in all individual mating series. Significance of transfer rate decrease was then calculated by pair-wise two-tailed t-test comparison of independent biological triplicate matings to that of the wild-type. Subpopulations of tc cells were estimated from quantile-quantile plotting of sfGFP or mCherry fluorescence values with a 95% confidence assumption (41). Differences in foci intensities were tested from pair-wise comparison to their wild-type ICE protein fusion of the median top 5% fluorescence pixel value in biological triplicates (as proxy for the foci intensity), and of the proportion of tc cells without detectable foci (above a normalized foci intensity threshold of 6 for –sfGFP, -mCherry fusions, and 3 for Orf55476-mCherry fusions due to lower background). Median 20th percentiles and median standard deviations of cell envelope pixel fluorescence values were compared between wild-type and mutants in a two-sample equal variance t-test.

Results

Function prediction of the genes in the conjugative region of ICE*clc*

In order to better delineate the genes on ICE*clc* important for conjugative transfer and to define their potential functional roles, we focused on the region in between *orf53587* and *orf73676* (Fig. 1C) with previously shown low homology to *H. influenzae* ICE*Hin1056* (20). Low amino acid similarities (23-30%) were found in full-length alignments of some ICE*clc* genes and VirB-T4SS components encoded by the Ti plasmid of *A. tumefaciens*, notably, VirD4, VirB1, VirB2, VirB4, VirB8, VirB9, and VirB10 (Table 1). Further structure prediction using AlphaFold2 and comparison with the PDB database suggested that these may be *bona fide* T4SS functional homologs (Table 1, Supplementary figure S2). An additional ICE gene product (Orf73676) showed structural homology to DotD of the Dot/Icm system of *L. pneumophila* and contained a lipoprotein signal peptide (Table 1). DotD is a component of the T4SS outer membrane complex (42) and an analog of VirB7 of the *Xanthomonas citri* T4SS (43). Another gene (*orf56883*) showed domain similarity to TraU (Table 1) of the F-plasmid in *E. coli* (44). In contrast, the products of the ICE*clc* genes *orf53587*, *orf55476*, *orf62755*, *orf66202* and *orf68241* displayed conserved domains to other hypothetical proteins without function prediction, nor structural overlap to other known proteins, although with predicted transmembrane helices and/or translocation signals (Table 1). A lipoprotein signal

sequence was further predicted for the *orf62755* gene product, suggesting it may be localized in the outer membrane. A further number of genes in this ICE*clc* region code for proteins with detectable functional domains, but unrelated to the T4SS per se (for example, a RadC DNA repair domain in Orf58432, Table 1). Several proteins have predicted functional domains related to cysteine modifications (i.e., *orf57827* disulfide oxidoreductase, *orf59110* protein disulphide isomerase, *orf71178* thioredoxin oxidoreductase, *orf72295* disulfide oxidoreductase), suggesting their implication in post-translational protein modifications. The two proteins encoded by *orf67001* and *orf67231* showed structural similarities with multicomponent ring-like membrane complexes (Table 1, Supplementary figure S2), suggesting they may be forming multi-subunit structures in the inner (*orf67001*) or outer (*orf67231*) membrane. Finally, the *orf73029* gene product showed structural similarity to a protein involved in pilus biogenesis (Table 1). Although none of the software used showed any significant similarities for the *orf55476* gene product, previous alignments (20) had pointed to low amino acid similarity (41%) with a proposed PilT homolog of ICE*Hin1056* (15). The *orf55476* protein was further predicted to carry a translocation signal peptide (Table 1). Therefore, it may encode a PilT-like ATPase of the ICE*clc* conjugative machinery, involved in pilus depolymerization (45). The sequence and structural homology searches thus suggested the following protein subassemblies for the ICE*clc* T4SS (Supplementary figure S2), which, whenever possible, we propose to rename analogous to the Vir-nomenclature (e.g., *orf59888* becomes *iceB4* in analogy to *virB4*, Table 1). Two ATPases, *iceB4* and *iceD4*, may associate on the cytoplasmic side of the inner membrane. A third ATPase and PilT analog, encoded by *orf55476*, may be located in the periplasm. An inner membrane complex (IMC) of the T4SS likely constituted of Orf53587, *iceB8*, Orf66202, Orf68241 and Orf67001 (Supplementary figure S2). *iceB10* would contact and span from the inner to the outer membrane complex (OMC), further composed of *iceB9* and *iceB7*, and possibly Orf62755. Finally, structural analysis suggested that the conjugative pilus might be formed from *iceB2* (Orf66625) subunits (Supplementary figure S2). In absence of Vir-homolog, we renamed Orf56883 to *iceU*, following the Tra-nomenclature. A set of periplasmic proteins may complete or associate with the ICE-T4SS complex, including *iceU*, *iceB1* and Orf67231, and the putative post-translational modifier proteins Orf57827, Orf59110, Orf71178, Orf72295 and Orf73029 (Supplementary figure S2).

Table 1 Sequence and structural homology predictions of genes in the ICEclc conjugative transfer region

ICEclc gene designation ^a	Length (aa)	Archetype T4SS ^b	Similarity %/gaps/overlap length	NCBI conserved domains/pfam	E-value	AlphaFold2/PDBeFOLD prediction	Signal Peptide	Trans-membrane helices	Suggested gene function	Essential for transfer ^d
<i>orf53587</i> (CAE92904.1)	505	VirB6 (WP_010974917.1)	11.9/482/641	TraG_N/07916	2.29e-71	No structural overlap ^c	–	5	Inner membrane protein	+
<i>orf55120</i> (CAE92905.1)	119	-	-	None	-	FrmR formaldehyde transcriptional repressor	–	3	Transcription regulator	ND
<i>orf55476</i> (CAE92906.1)	465	VirB11 (WP_010974918.1)	3.7/695/752	Conjugal TIGR03755	0e+00	No structural overlap	SPI	1	<i>pilT</i>	+
<i>orf56883</i> (CAE92907.1)	315	-	-	TraU superfamily	0e+00	No structural overlap	SPI	–	<i>traU/iceU</i>	+
<i>orf57827</i> (CAE92908.1)	148	-	-	DURF1525/pfam07511	2.07e-55	Thioredoxin-like protein	SPI	1	Disulfide oxidoreductase	–
<i>orf58432</i> (CAE92909.1)	164	-	-	PRK00024 super family	1.31e-62	DNA repair protein RadC	–	–	Putative DNA repair protein	–
<i>orf59110</i> (CAE92910.1)	254	-	-	DsbA family motif/Thioredoxin-like superfamily	5.78e-13	Protein disulfide isomerase	–	1	<i>dsbA</i>	–
<i>orf59888</i> (CAE92911.1)	955	VirB4 (WP_010974916.1)	29.4/362/1053	TraC_PFL_4706	0e00	Type VII Secretion ATPase EccC	–	–	Conjugative transfer ATPase (<i>virB4</i>)/ <i>iceB4</i>	+
<i>orf62755</i> (CAE92912.1)	146	-	-	conj_TIGR03751	5.9e-61	No structural overlap	SPII	–	Outer membrane protein	+
<i>orf63176</i> (CAE92913.1)	472	VirB10 (WP_010891494.1)	23.2/289/569	conj_TIGR03752	0e00	COMB10 of a COM-type IV secretion system	–	1	<i>virB10/iceB10</i>	+

<i>orf64584</i> (CAE92914.1)	310	VirB9 (WP_010891495.1)	29.1/ 145/374	TraK superfamily/ pfam11920	1.67e- 160	No structural overlap	SPI	1	<i>virB9/iceB9</i>	+
<i>orf65513</i> (CAE92915.1)	230	VirB8 (WP_010891496.1)	30.8/ 111/289	conj_TIGR03746	1.02e- 127	Periplasmic domain of DotI/CagV	-	1	<i>virB8/iceB8</i>	+
<i>orf66202</i> (CAE92916.1)	136	VirB3 (WP_010891501.1)	7.5/ 184/213	DUF 3487/ pfam11990	1.35e-48	No structural overlap	-	2	Inner membrane protein	+
<i>orf66625</i> (CAE92917.1)	119	VirB2 (WP_010891502.1)	25.9/ 76/158	conj_TIGR03745/ DUF2976	4.69e-46	Conjugative pili	SPI	3	Candidate major pilin/ <i>iceB2</i>	(+)
<i>orf67001</i> (CAE92918.1)	77	-	-	conj_TIGR03758/ DUF3262	8.62e-21	Membrane anchor protein of succinate DH complex	-	2	Inner membrane protein	(+)
<i>orf67231</i> (CAE92919.1)	127	-	-	ICE_RAQPRD	7.35e-38	Modular repressor recruitment protein	SPI	-	Unknown	(+)
<i>orf67800</i> (CAE92920.1)	134	-	ND	No match	-	No structural overlap	-	-	Unknown	-
<i>orf68241</i> (CAE92921.1)	249	-	-	conj_TIGR03747/ DUF4400	3.54e- 117	No structural overlap	-	4	Inner membrane protein	+
<i>orf68987</i> (CAE92922.1)	728	VirD4 (WP_065698658.1)	28.3/ 366/881	conj_TOL_TraD	0e+00	Coupling protein TrwB	-	2	<i>virD4/iceD4</i>	+
<i>orf71178</i> (CAE92923.1)	182	-	ND	DUF 2859/ pfam11072	1.67e-72	Thiol:disulfide Interchange Protein DsbE	SPI	-	Thioredoxin-like	+/-
<i>orf71723</i> (CAE92924.1)	196	VirB1 (WP_010891503.1)	31.8/ 107/274	Lyz-like super family	2.51e-09	Lytic transglycosylase	SPI	-	<i>virB1/iceB1</i>	+/-
<i>orf72295</i> (CAE92925.1)	239	-	-	conj_TIGR03759	6.73e- 112	Thiol-disulfide oxidoreductase	SPI	-	Thioredoxin-like	ND
<i>orf73029</i> (CAE92926.1)	216	-	ND	No match	-	Membrane anchoring PilP type IV pili protein.	-	-	Unknown	-

<i>orf73676</i> (CAE92927.1)	206	-	ND	conj_PilL	9.91e-51	STN superfamily periplasmic signaling domain/DotD	SPII	-	<i>dotD/iceB7</i>	+
---------------------------------	-----	---	----	-----------	----------	--	------	---	-------------------	---

a) Designation in GeneBank AJ617740.2

b) Archetype Vir-T4SS of *A. tumefaciens*

c) RMSD>3

d) See Figure 2; ND, not determined

Gene deletions implicate ICE*clc* functions in conjugative transfer

To study their potential implication in ICE*clc* transfer, we individually deleted 22 out of the identified 24 open reading frames in the predicted T4SS-encoding region (Figure 1, Table 1). Deletions were created in-frame by leaving a stretch of 6–10 amino acids at the N- and C-terminal of the protein, to avoid polar effects. Neither single nor double deletions could be recovered of *orfs iceB2*, *67001* and *67231*, perhaps because of their small gene size. This was then replaced by a single deletion removing all the three consecutive genes (i.e. Δ *orf67231-iceB2*).

Deletions of 15 of the targeted genes caused a more than 100-fold decrease of ICE*clc* transfer rates in isogenic *P. putida* matings. These comprised both genes analogous to archetype T4SS components (i.e. *iceB4*, *iceB8*, *iceB9*, *iceB10*, *iceD4*, and *iceB7*, Figure 2A; see Figure 1B for original *orf* nomenclature and location, and Table 1), as well as those without clear T4SS counterparts (i.e. *orf53587*, *orf55476*, *iceU*, *orf62755*, *orf66202*, *orf67231-iceB2* and *orf68241*, Figure 2B). Two other deletions significantly affected ICE*clc* transfer, but less severely than the ones mentioned above. ICE transfer decreased by 50-fold in a Δ *iceB1* (*orf71723*) mutant (Figure 2A), and 10-fold in a Δ *orf71178* mutant compared to wild type (Figure 2B). Ectopic complementation with a single-copy wild-type gene under control of the ICE*clc* transfer competence P_{67231} -promoter restored transfer in all cases but one (i.e. *orf53587*, Figure 2A and B), indicating that deletion of *orf53587* might have caused a polar effect. However, for all the other deletions the transfer defect was attributable to the single gene knockout. Several deletions, e.g. of *orf55476*, *orf66202*, *orf67231-iceB2*, *orf71178*, *iceB7* or *iceB10*, were restored partly by ectopic complementation (Figure 2B). This might indicate that ectopic placement resulted in imbalanced expression levels or timing for functional complementation. Since the deletion of Δ *orf67231-iceB2* involved three consecutive genes, we further complemented this with each gene individually or in pairs, ectopically placed in single integrated copy under control of the P_{67231} -promoter (Supplementary figure S3). Only the combination of *orf67001-iceB2* partly restored transfer, suggesting they are the essential genes, whereas *orf67231* is not (Supplementary figure S3). In contrast, a further set of four gene deletions did not cause detectable effects on ICE transfer (*orf58432*, *orf59110*, *orf67800*, and *orf73029*, Figure 2C), whereas deletion of *orf57827* and its complementation reduced transfer by 4-fold (Figure 2C). This suggests them to have minor or no influence on ICE transfer, or to be functionally redundant.

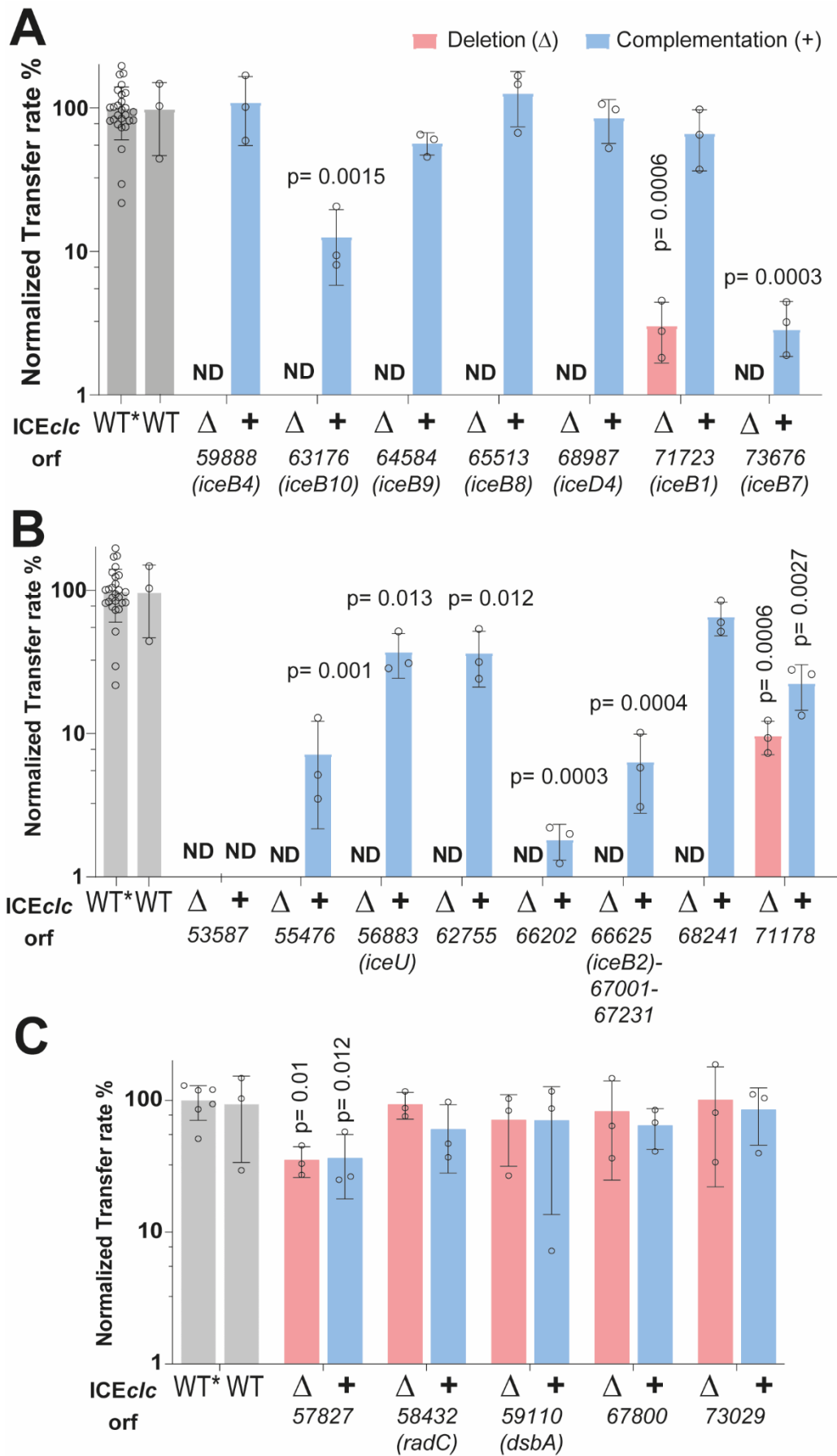


Figure 2 Effects of individual *ICEclc* gene deletion and complementation on transfer. **A)** Deletion effects of *ICEclc* genes with distinct sequence and/or structural similarity to known T4SS components. **B)** *ICEclc* genes without distinct sequence

and structural similarity. **C)** ICE*clc* genes without or with mild effect on transfer. Bars represent the mean normalized transfer rates of ICE with single gene deletions (Δ , salmon), or single copy complementations (+, blue), as percentage of that of wild-type ICE*clc* (grey) in *P. putida* UWC1 isogenic matings, each individually quantified as the frequency of transconjugant colony forming units (CFU) on selective medium per donor CFU. Error bars indicate calculated standard deviations on biological replicates, with open circles showing the individual replicate values. *Orf* and gene names indicated below. ND, below detection limit (< 1%). WT, unmodified ICE*clc* wild-type. WT*, ICE*clc* carrying an integrated *lacO*-array ; used for producing the deletions and complementations. Note that the same WT and WT* rates are reproduced in all panels for ease of comparison. p-Values were calculated with a two-tailed t-test between wild-type (WT*) and mutant replicate rates (as percentages). Only p-values <0.05 are shown.

We concluded from these results that the region in between *orf53587* and *orf73676* on ICE*clc* is indeed essential for its conjugation. The predicted ICE-T4SS is very dissimilar to archetypal plasmid T4SSs, except for a few distantly structurally related components (Supplementary figure S2). In contrast, the ICE-T4SS loci and gene synteny are highly conserved between ICE*clc* and genome regions in other β and γ -proteobacteria, suspected to carry similar ICEs (Figure 3). This strongly suggests functional conservation, even for those genes whose deletion on ICE*clc* did not directly affect isogenic transfer rates. Two sites (nearby *orf67800* and *orf58432* on ICE*clc*) were permissive for gene loss in the other compared genomic regions (Figure 3). Nevertheless, the strong conservation of gene order and overall similarity is an indication that these are parts of mobile elements capable of producing T4SS conjugative systems for which ICE*clc* is a representative model.

Subcellular localization of the ICE*clc* conjugative system proteins

To further corroborate bioinformatic predictions and transfer results, we investigated the subcellular localization of nine of the encoded proteins in the ICE*clc* conjugative system gene region. This choice was not exhaustive, but contained a number of predicted structurally 'known' (e.g. IceB4, IceB7, IceB8) as well as less clear components (e.g. Orf66202, Orf55476, outlined in Figure 1C), and targeting both proteins predicted to be associated to the inner and outer membranes, as well as those with predicted periplasmic localization. In order to visualize protein localization, we translationally fused the target open reading frames within their original ICE*clc* locus with the reading frame of super-folder green fluorescent protein (*sfGFP*) or of *mcherry*, separated by a small linker peptide to avoid folding complications, as in Ref. (32). This approach was expected to best preserve stoichiometry and timing of fusion protein production with respect to the native ICE*clc* counterpart. Our hypothesis here was that if the targeted protein would be part of a multi-component and multi-subunit T4SS complex, expressing the fluorescent protein fusion might

result in a well-defined fluorescent spot, whereas if it would not be part of the T4SS, its fluorescence would be homogenously distributed in the cytoplasm or in the cell envelope.

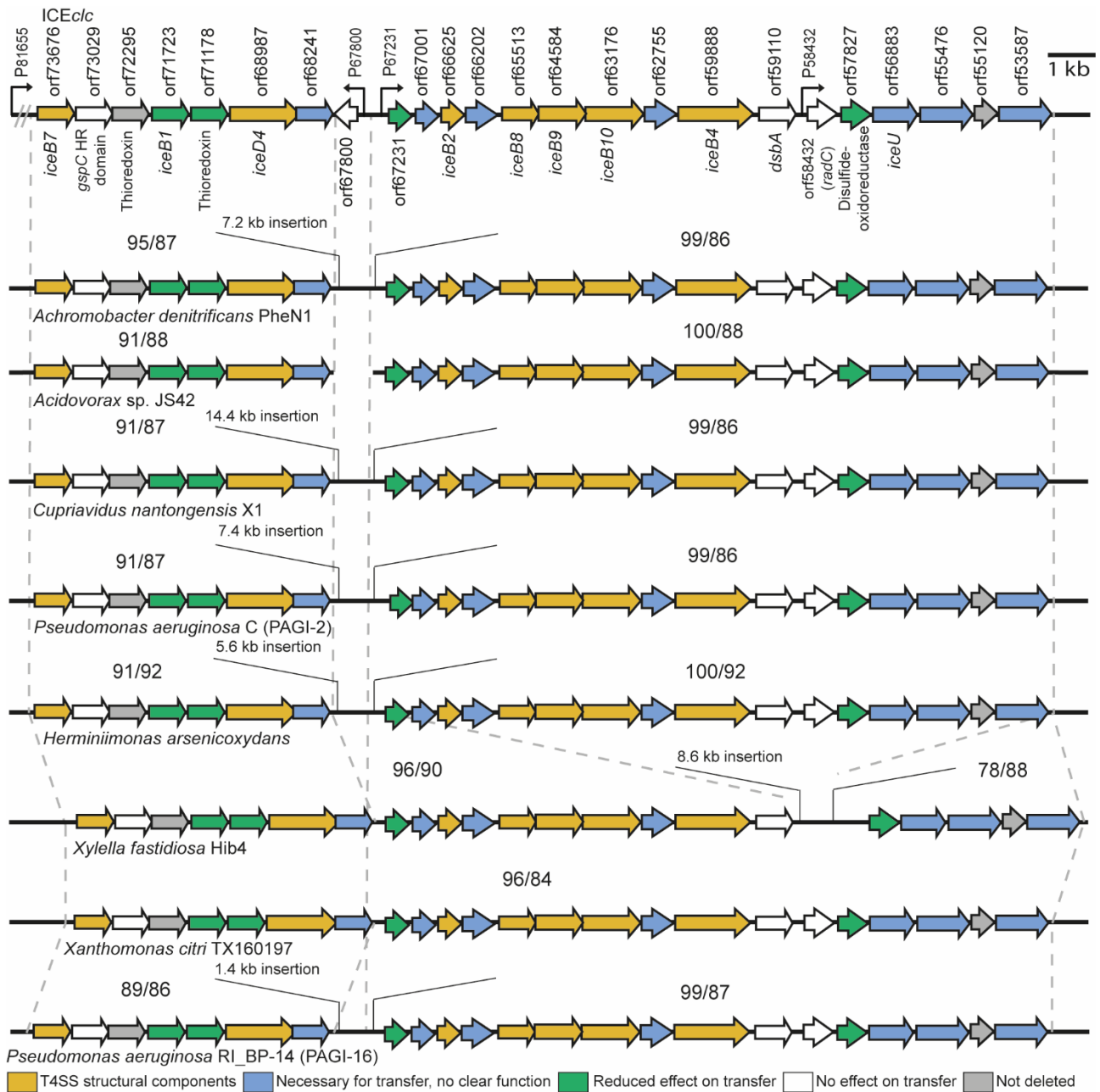


Figure 3 ICE c/c transfer region gene and synteny conservation. Genetic organization of the ICE c/c T4SS locus (top), aligned with corresponding regions within the genomes of 8 other β - and γ -Proteobacteria. The dotted lines delimit the regions of synteny to ICE c/c , with numbers representing the sequence coverage (left) and the percentage of nucleotide identity (right), respectively. Arrows indicate coding frames and their orientations, with filled colors representing transfer effects as in the legend on the bottom of the figure.

We chose a combination of both sfGFP and mCherry in order to test for colocalization of different components (see below). To test for functionality of the expressed fluorescent fusion protein, we quantified ICE transfer from respective *P. putida* donors and compared this to wild-type ICE. We assumed similar transfer rates to be the best indication for proper functionality, in which case we

concluded that the position and/or distribution of the observed fluorescence was representative for the true (non-labeled) protein localization. All tested ICE-fusion proteins produced multiple clear fluorescent foci in stationary phase *P. putida* cells, with in about half of the cases, accentuated fluorescent cell outlines (Figure 4A). As expected from previous studies using transcriptional fusions to key ICE*clc* transfer competence promoters (7, 21), fluorescent fusion protein expression was limited to a subpopulation of cells appearing in stationary phase (Figure 4B). These subpopulations reached similar abundances for the different constructs, as deduced from quantile-quantile plots of observed versus expected normal distribution of fluorescence values (Figure 4B, light brown-shaded regions). A co-expressed cytoplasmic marker for transfer competence (P_{inR} -*echerry*) labeled the same cells as those displaying the fluorescent fusion protein-signal in stationary phase (Supplementary Figure S4A). This would be in agreement with the hypothesis that only tc cells assemble the ICE conjugative machinery. Foci were situated near the cell edge in high-resolution images (Figure 4A, Airyscan), coinciding with stained cell membranes (Supplementary Figure S4B), as expected for a membrane-spanning protein complex such as the T4SS. Because of the limited throughput in high-resolution microscopy (i.e. Figure 4A, Airyscan) we quantified foci numbers from larger numbers of cells (1000–10 000 per replicate per strain) imaged in regular epifluorescence microscopy, and using a threshold for foci detection based on differences in foci scores among non-tc and tc cells (Figure 4B). This confirmed the high-resolution visual aspects; notably, the occurrence of multiple foci per cell in case of fusions to IceD4, IceB4, IceB7, iceB8, Orf55476 and Orf66202 (Figure 4C). In contrast, fusions to IceU, Orf62755 and Orf71178 showed fewer quantifiable foci, also in agreement with the high resolution aspect of the cell envelope outlines (Figure 3, Supplementary Figure S5). ICE transfer rates from *P. putida* donors were unaffected for seven of the nine tested fluorescent protein fusions, suggesting no functional impairments (Figure 4D). In contrast, donors expressing sfGFP-IceB8 or mCherry-Orf62755 reduced ICE transfer by 10- and 50-fold, respectively, compared to wild-type, indicating loss of some aspect of functionality by the fluorescent protein fusion (Figure 4D). To provide further evidence that the observed fluorescent foci were specific for conjugation complexes in *P. putida* ICE*clc* tc cells, and not the result of aberrant or spontaneous fluorescent protein aggregation, we studied control strains of *P. putida* ICE*clc* expressing only sfGFP from the same P_{67231} promoter but artificially induced in all cells by overexpression of the ICE-transcription factor BisR (7). These cells showed no detectable foci but homogenous cytoplasmic fluorescence, indicating that sfGFP does not self-aggregate into fluorescent foci at the cell envelope (Figure 4E and Supplementary Figure S4C).

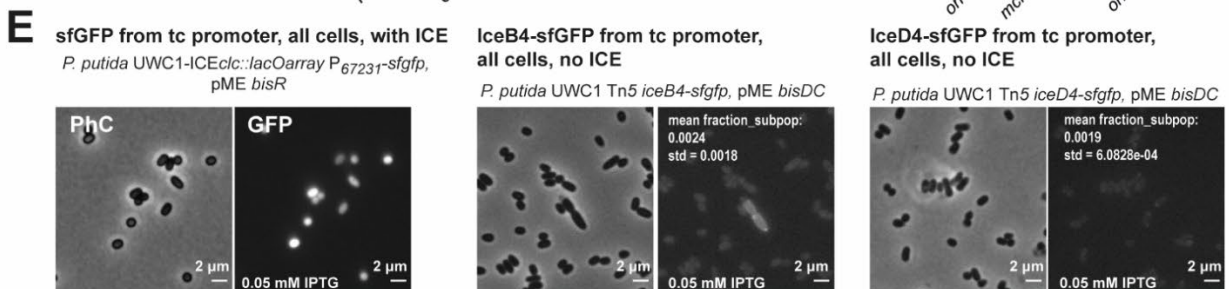
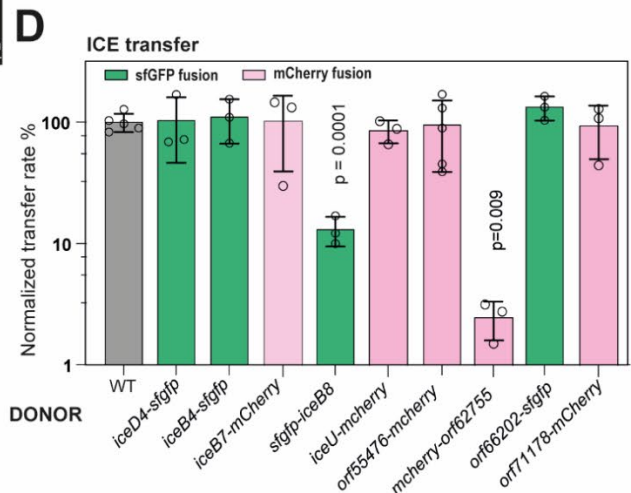
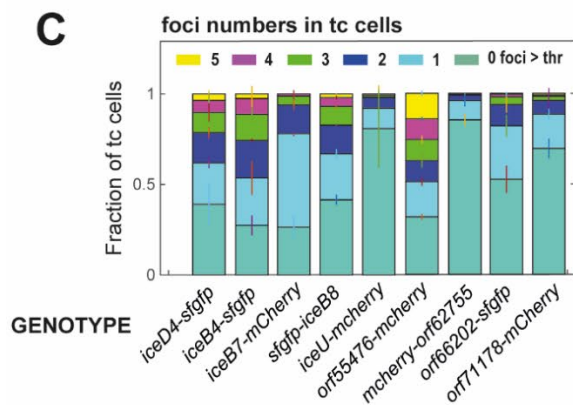
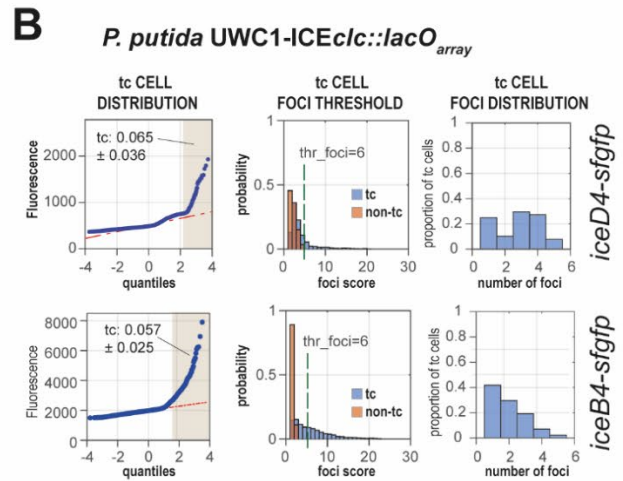
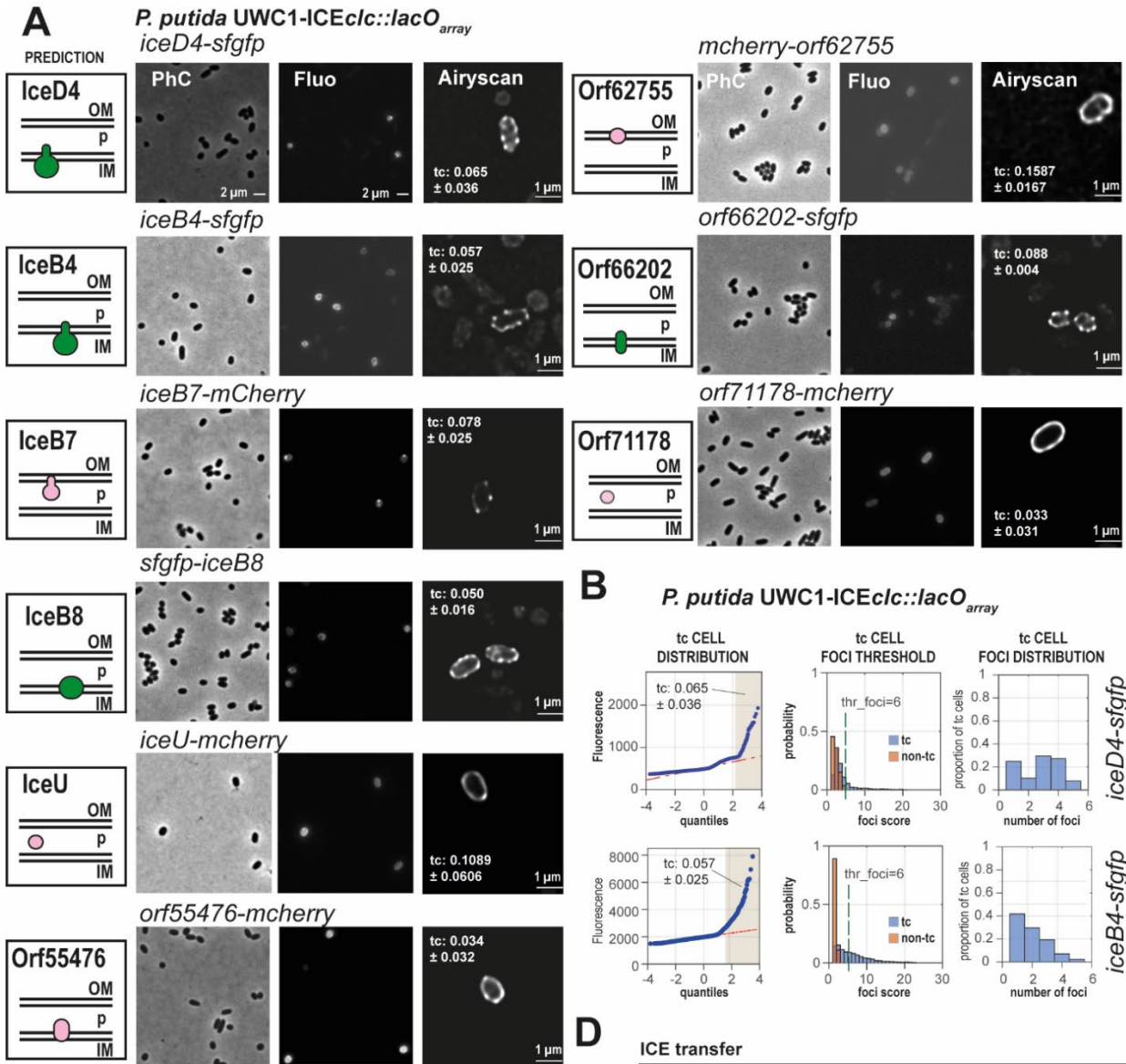


Figure 4 Subcellular localization of predicted ICE $_{cIc}$ conjugative system subcomponents. **A)** Micrographs of *P. putida* strains with indicated fluorescently tagged conjugative system components, imaged in stationary phase cultures after growth on 3-CBA. Panels on the left show the bioinformatic prediction of the protein's localization with respect to inner membrane (IM), periplasmic space (P) or outer membrane (OM); green, sfGFP-tagged protein fusion; pink, mCherry-fusion. PhC, Phase contrast; Fluo, fluorescent channel. Airyscan, high-resolution deconvoluted 170-nm image slice of the respective strain. Proportion of observed tc cells (mean \pm one SD of individual biological triplicates) indicated within the Airyscan panels. **B)** Example of tc cell foci quantification on epifluorescence images of *P. putida* ICE $_{cIc}$ hosts expressing either IceB4- or IceD4-sfGFP; quantile-quantile plot of median fluorescence per cell measured on a single replicate set of images for the different strains and showing the derived tc cell subpopulation (highlighted in light brown and its mean proportion \pm one SD). Thresholds (thr_foci) used for distinguishing foci for the labeled constructs in tc cells (blue bars) from spurious background 'foci' in the majority of non-tc cells (red bars), based on calculated foci intensities from Gaussian fitting. Plots show probability normalized distributions of foci intensities among the two cell groups (differentiated based on quantile-quantile plots). Derived number of foci per tc cell at the indicated threshold (thr_foci) for a single replicate. **C)** Stack plots showing the mean proportions of foci (\pm one SD from biological triplicates) above threshold in tc cells for all constructs shown in panel (A). **D)** Mean normalized ICE $_{cIc}$ transfer rates (\pm one SD from biological triplicates; open circles showing individual data points) of wild-type ICE and the fluorescently tagged donor strains into *P. putida* recipients. Differences compared to wild-type were assessed with a two-tailed t-test on biological triplicate pairs (if not indicated, p-values were > 0.05). **E)** Micrographs of control strains *P. putida* UWC1 ICE $_{cIc}$ -lacO $_{array}$ expressing sfGFP from the P $_{67231}$ -promoter, and of *P. putida* UWC1 devoid of ICE $_{cIc}$ expressing IceB4-sfGFP or IceD4-sfGFP. P $_{67231}$ -promoter activation was induced in all cells by overexpressing the proteins BisR or BisDC with 0.05 mM IPTG, two known regulators of ICE $_{cIc}$ activation cascade [Carraro, 2020]. Numbers indicate the mean proportion of the subpopulation of cells in quantile-quantile plots from biological triplicates (\pm one SD).

Secondly, we expressed the *iceB4-sfgfp* or *iceD4-sfgfp* fusions in all cells of *P. putida* UWC1 devoid of ICE $_{cIc}$, through induction with the ICE-transcription factor complex BisDC (7). These cell populations showed very little fluorescence, with some 0.2% outliers from quantile-plotting (Figure 4E). Sporadic low-intensity foci were observed among this subpopulation of fluorescent cells (Figure 4E, Supplementary figure S4D and E), appearing at polar regions and accompanied by cellular morphological aberrations (Figure 4E). Although there is a tendency of expressed IceB4- or IceD4-sfGFP protein to aggregate into sporadic fluorescent foci, this frequency is 10- to 50-fold lower than appearing clear foci in envelopes of *P. putida* tc cells carrying ICE $_{cIc}$. It is therefore very unlikely that the multiple bright foci detected with six of the fluorescently tagged ICE conjugative proteins (Figure 4C) consist of autoaggregated misfolded proteins.

Colocalization of dual-labeled ICE $_{cIc}$ conjugative system components

In order to determine whether the multiple foci seen in tc cells for different fluorescently-tagged ICE proteins were likely part of the same macromolecular protein complexes, we quantified the colocalization of sfGFP and mCherry signals in *P. putida* ICE $_{cIc}$ hosts expressing double-labeled components. We chose for this a combination of either *iceB4-sfgfp* and *iceB7-mcherry*, or *iceB4-sfgfp* and *orf55476-mCherry*. ICE transfer rates from donors with the double label IceB4-IceB7 combination was again very close to wild-type transfer rates (Figure 5A), suggesting retained

functionality. Double labeling of IceB4 and Orf55476 resulted in a tenfold decrease in mean transfer rate compared to wild-type – although this was not statistically significant (Figure 5A).

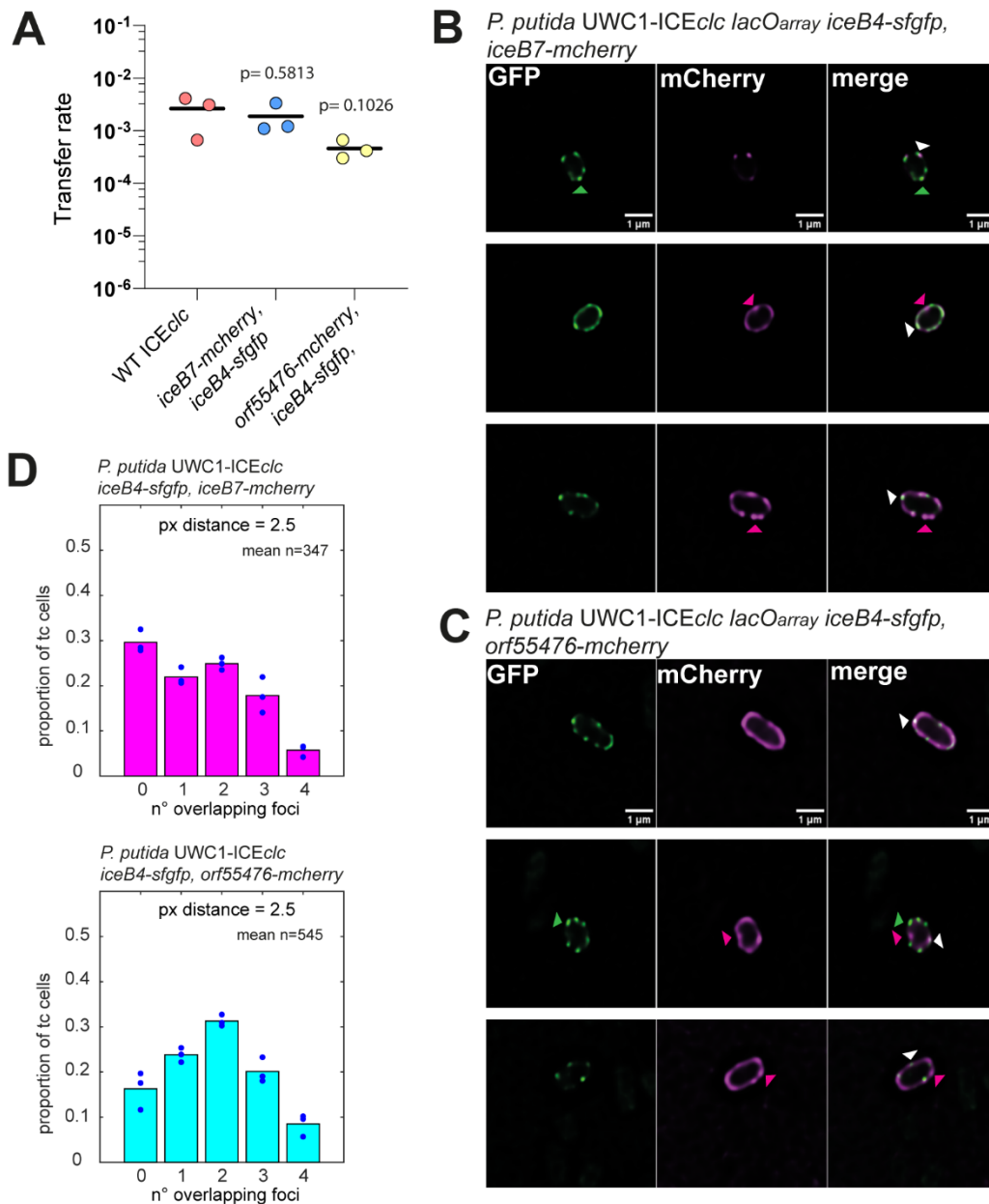


Figure 5 Colocalization of dual-labeled components of the ICEclc conjugative system. A) Mean transfer rates (lines) of ICEclc in isogenic *P. putida* matings from wild-type donors or ICE with dual-labeled fluorescent protein constructs, as indicated. Dots depict individual replicates, p-values show the probability of means being dissimilar in two-tailed t-test comparisons. **B and C)** Micrographs of individual tc cells of *P. putida* ICEclc::lacOarray expressing both IceB4-sfGFP and IceB7-mCherry, or IceB4-sfGFP and Orf55476-mCherry, imaged in stationary phase after growth on 3-CBA in their proper individual fluorescent channel (GFP, mCherry), or presented as overlay (merge, GFP is green; mCherry is magenta). Images composed of a single 170-nm deconvoluted slice in Airyscan microscopy. Colored triangles in B and C point to examples of non-colocalized (green or magenta) or overlapping foci (white). **D)** Measured mean proportions (bars) of the number of overlapping sfGFP and mCherry foci (1–4) in tc cells of both strains (overlap is within a minimum distance of 2.5 pixel or 165 nm of the fitted 2D-Gaussian foci centres). Circles are individual replicate values. *n* = mean number of tc cells per replicate.

We assumed foci overlap at geometric distances within 165 nm (2.5 pixels on the images), and imaged potential colocalization in deconvoluted high-resolution 170-nm cell slices. Visual inspection from high-resolution images of *P. putida* expressing double fusions confirmed that the two proteins are expressed simultaneously in tc cells and suggested mostly overlapping foci, but not exclusively (Figure 5B, C). Quantification of foci distances on larger numbers of tc cells from epifluorescence images, indicated that on average between 1 and 4 foci overlapped in 70% of tc cells with dual IceB4- and IceB7-labeling, and 83% of tc cells in case of strains with both IceB4-sfGFP and Orf55476-mCherry labeling (Figure 5D). In conclusion, the microscopy and transfer experiments indicated that fluorescent foci observed in stationary phase tc cells of *P. putida* ICE*clc* are most likely representative for the formation and positions of multimeric protein complexes such as expected from the T4SS, and not the result of spontaneous aggregation of the fluorescent protein fusions. Obtaining similar foci-per-cell numbers in case of fusions to IceD4, IceB4, IceB7, IceB8 (despite its partial loss of functionality), Orf55476 and Orf66202 is very suggestive for these proteins to be part of the same multiprotein complexes, which was confirmed to some extent by the fluorescent marker overlap in double-labeled strains. The different fluorescence aspect (e.g. stronger cell envelope outlines) of the IceU- and Orf71178- fusions (the Orf62755-fusion being impaired for ICE transfer) may be an indication for them not being integral part of a T4SS and performing a different role in the ICE conjugative process.

Interdependencies among subcomponents of the ICE*clc* conjugative system

Finally, we studied potential dependencies of the observed foci formation on other predicted components of the ICE conjugative system. The same fluorescent protein fusion constructions were reproduced in their native locus in *P. putida* that further carried single copy deletions in ICE*clc* conjugative system genes, and effects of the deletions on fluorescent signals were examined (Figure 6A–C). Apart from direct high-resolution cell images we focused on three aspects of fluorescence measurements that we expected to yield quantifiable differences. First of all, we assumed that observed foci intensities might diminish, for example, if fewer of the tagged protein subunits would assemble into the T4SS structure, or if their turnover would be faster in absence of proper assembly. Secondly, we expected that mutations might lead to fewer fluorescent foci per cell, for example, as a result of T4SS assembly failures. This might then result in enrichment of the fluorescence signal of the tagged protein in, for example, the cell envelope. Finally, we imagined that quantifiable differences in foci ‘aspects’ might occur in mutants (i.e. blurring; visible from fitting

scores and Gaussian sigma values, Supplementary figure S1D and E), due to impaired T4SS assembly or misfolded multimeric structures. We quantified these parameters from epifluorescence imaging of tc cell subpopulations (142–1996 tc cells per replicate) in stationary phase cultures and in comparison to wild-type tagged constructs in biological independent triplicates to calculate statistical significance. We do acknowledge that at the resolution of EFM and the Airyscan, observed differences may have different underlying causes from what we assumed.

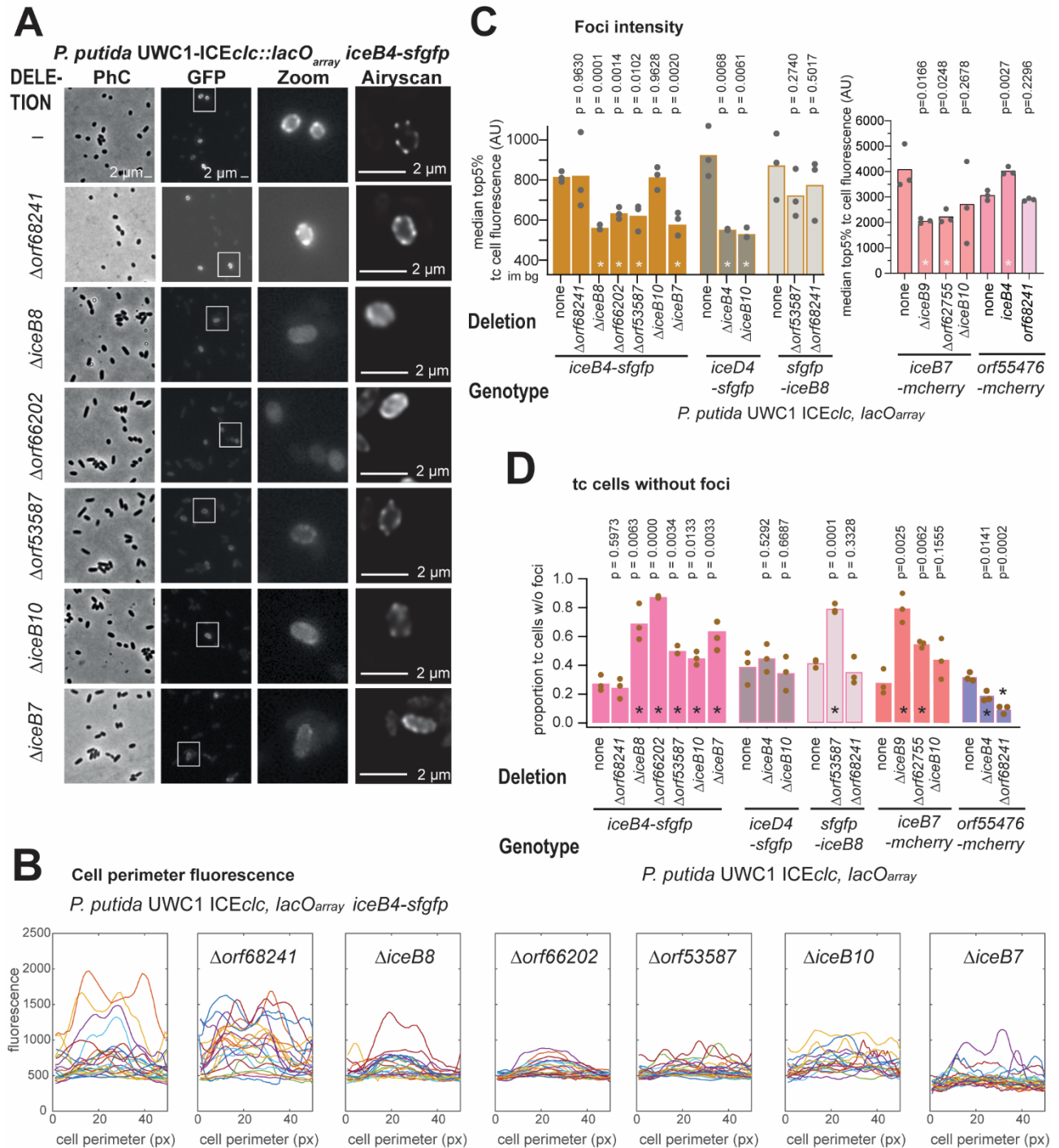


Figure 6 Dependencies among subcomponents of the ICE_{clc} conjugative system. **A)** Microscopy images of IceB4-sfGFP in *P. putida* in stationary phase after growth on 3-CBA with a single integrated copy of (otherwise) wild-type ICE_{clc}::*lacO*_{array}, in comparison to additional deletions of *orf68241*, *iceB8*, *orf66202*, *orf53587*, *iceB10*, or *iceB7*. Micrographs as in Fig. 4 with a highlighted cell area (Zoom) from the GFP image and a high-resolution Airyscan image (single 170-nm slice). Images are scaled to the same maximum and minimum intensities. **B)** sfGFP fluorescence profile of the perimeter of individual tc cells (1-pixel outer ‘shell’) of the indicated constructs in panel (A) on their absolute fluorescent scales. ‘Peaks’ correspond to foci in the cell micrographs. **C)** Mean top 5% median fluorescence among tc cells (bars, indicative for foci intensity) among biological triplicates of the different labeled strains in wild-type or mutant backgrounds (circles showing individual replicate values; im bg, image background fluorescence). P-values result from paired two-tailed t-test comparisons of mutant to wild-type (asterisks indicating significance at 0.05 or below). **D)** As C, but for the mean proportion of tc cells without detectable foci (threshold determination as in Fig. 4). All other individual strain micrographs and foci analysis are presented in Supplementary figures (see main text).

As an example, in case of IceB4-sfGFP background (Figure 6A), all tested deletions except that of *orf68241*, affected some aspect of fluorescent foci formation (Supplementary Table S4). This was mostly quantifiable as generally weaker and more diffuse foci (Figure 6B, C, Supplementary Figure S6), and more cells without any detectable foci (Figure 6D). There was no increase in the median tc-cell cytoplasmic fluorescence intensity as a result of lowered foci intensities in mutants (Supplementary Table S5), but the estimated sizes of the tc population remained the same (Supplementary Table S5). Altogether, this would indicate that IceB4-sfGFP assembly into fluorescent foci is directly or indirectly dependent on IceB7, IceB8, Orf66202, Orf53587 and IceB10, but not on Orf68241. All of these deletions by themselves completely abolish ICE transfer (Figure 2), and, therefore, loss of IceB4-sfGFP foci formation would be in agreement with an impairment of proper multi-component T4SS assembly.

A number of other deletions were tested in the IceB7-mCherry, sfGFP-IceB8, IceD4-sfGFP and Orf55476-mCherry backgrounds, the effects of which are summarized in Figure 7. Deletions of either *iceB9* or *orf62755* in IceB7-mCherry background resulted in weaker and fewer foci in tc cells, whereas effects of an *iceB10* deletion were inconclusive (Figure 6C and D, Supplementary Figure S7). Similar as in case of IceB4-sfGFP background, the deletion of *orf68241* did not measurably change foci numbers of sfGFP-IceB8, whereas deletion of *orf53587* caused foci to become weaker and more blurred (Figure 6C and D, Figure 7, Supplementary Figure S8). Both deletions of *iceB4* or *iceB10* yielded weaker and fewer IceD4-sfGFP foci (Figure 6C and D, Figure 7, Supplementary Figure S9). Finally, deletion of *iceB4* in Orf55476-mCherry background produced more foci variability, whereas deletion of *orf68241* resulted in weaker foci and clearer cell

outlines (Supplementary Figure S10). Since all the deletions individually by themselves abolish ICE*clc* transfer, these different aspects of foci fluorescence in mutant strains (Figure 7) suggest impairments and/or losses of proper assembly of the multimeric multiprotein conjugative complexes, as will be discussed further below.

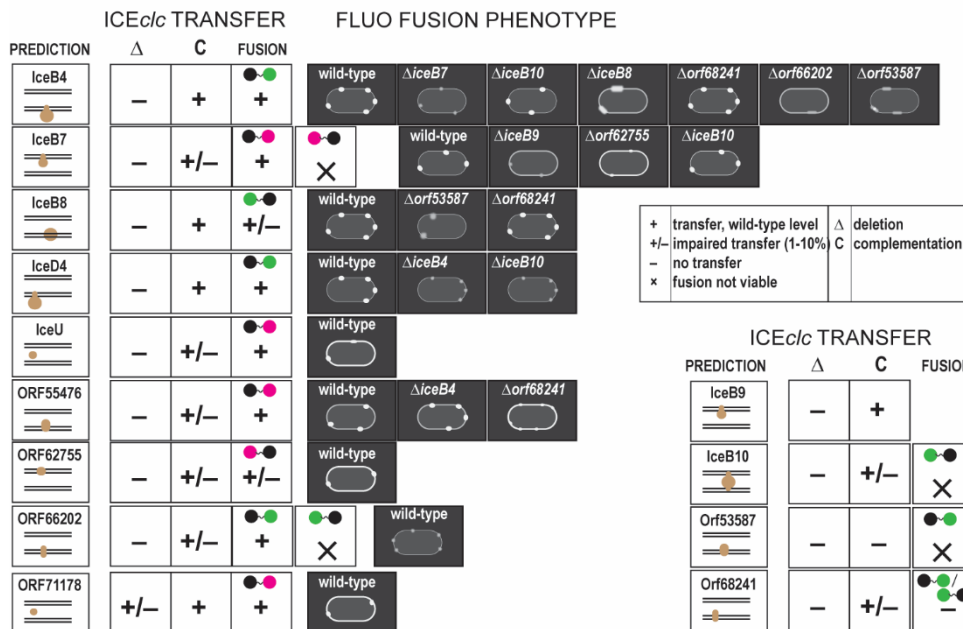


Figure 7 Schematic summary presentation of subcomponent dependencies in the ICE*clc* conjugative system, derived from transfer, mutant and fluorescent protein fusion studies. Panels show for each of the labelled T4SS component the bioinformatic prediction of its localization, the ICE*clc* transfer frequency of its deletion mutant (Δ), the complementation (C), and of the fusion construct (magenta, mCherry fusion; green, sfGFP; black circle, targeted protein). Fluorescent protein fusion phenotypes schematically indicated for the type (crisp, small, fuzzy) and numbers of foci observed, and cell envelope fluorescence characteristic (thick, more pronounced outline). Qualitative indication of transfer rates as in the legend, corresponding to measured values as in Figure 4D.

Discussion

We performed a systematic analysis of the gene functions involved in ICE*clc* conjugation as representative of the poorly studied MPF_G clade of T4SS conjugation systems (14). Our results indicate that ICE*clc* encodes a conjugative system that has both a number of structurally analogous components to known T4SS, as well as several crucial unique and unknown components (Table 1). The unique components are common to a wide class of elements related to ICE*clc*. We further find that formation of the ICE*clc*-T4SS is restricted to transfer competent (tc) cells, which can carry multiple such systems per cell as judged from microscope imaging. The occurrence of multiple T4SS per *P. putida* ICE*clc* tc cell is similar as what was found for labeled Vir-components in case of *Agrobacterium tumefaciens* (25, 46) and from cryo-tomography of *Legionella*

pneumophila Dot/Icm cells (27), and may contribute to the efficiency of the ICE to transfer from specialized cells (11, 47).

Despite representing its rightful separate evolutionary lineage, the T4SS of ICE*clc* has parallel structural and functional analogies to other widespread types such as Mpf_T and Mpf_F. Our functionality analysis was based on detailed bioinformatic structural analysis, individual gene deletion and complementation studies, fluorescent fusion protein analysis, and their effects on ICE transfer. Mating-pair formation complexes can comprise between 12 and more than 20 individual proteins (48, 49). We found 14–15 essential elements within the ICE*clc* conjugative gene region (including *tral*, Figure 1). Weak full length amino acid similarities and predicted structural homologies enabled to classify analogs of archetypal T4SS structural components within the ICE*clc* system, which we named IceB2 (for VirB2 analog, etc.), IceB4, IceB7, IceB8, IceB9, IceB10, and IceD4, as well as unknown components (e.g. Orf55476, Orf53587; Table 1). Indeed, their deletion abolished ICE*clc* transfer, whereas ectopic single copy complementation under control of a transfer competence promoter partly or fully restored it, indicating clear gene-dependent effects. Microscopy imaging of strains expressing translational fluorescent protein fusions from their native ICE*clc* loci showed that IceD4, IceB4, IceB8, and IceB7 fusions form clearly localized fluorescent foci in the cell envelope. Of these, IceD4-, IceB4- and IceB7-fusions retained wild-type transfer rates, confirming their functionality. Mutation studies in backgrounds of fluorescently-tagged ICE proteins, indicated that foci formation of IceB4-sfGFP was impaired by additional deletions of *iceB7*, *iceB8*, *iceB10*, *orf53587* and *orf66202*; of IceD4-sfGFP by deletions of *iceB4* and *iceB10*, and of IceB7-mCherry by *iceB9* or *orf62755* (Figure 7). Since these deletions in wild-type background completely abolish ICE-transfer, this strongly suggests that foci consist of the ICE-T4SS conjugation machines, which cannot correctly assembly in absence of their core components. This is consistent with a hypothesis of IceB4, IceB7, IceB8, IceB9, IceB10 and IceD4 being part of a multicomponent structure similar to known plasmid-type T4SSs (schematically assigned as in Supplementary Figure S2A).

Various analogies can be drawn from other T4SSs and our results on the ICE*clc* system, which support the hypothesis of their overall structural resemblance. For example, the localization of IceB4 (the predicted cytoplasmic ATPase) to the ICE*clc*-T4SS required the presence of Orf66202, IceB8, Orf53587, IceB10 and IceB7 proteins (predicted inner and outer membrane components). This would be in agreement with observed dependencies of the VirB4-analog DotO protein of the

Dot/Icm T4SS in *L. pneumophila* (50), and crucial documented protein-protein interactions between VirB4 and either VirB3 or VirB8, and between VirB3 and VirB8 (51-53). Fluorescent protein fusions to Orf66202 also formed multiple visible foci (albeit weaker than to IceB4) in the cell envelope of tc cells (Figure 7), and remained functionally intact. Orf66202 is a predicted inner membrane protein with two transmembrane helices, and, in that sense, may have a similar role as VirB3 (54), although there was no detectable sequence or structural similarity between Orf66202 and VirB3. Although we did not manage to obtain a viable fluorescent protein fusion to Orf53587 (Figure 7), deletion of its gene disturbed formation of both IceB4-sfGFP and sfGFP-IceB8 foci, suggesting it is involved in T4SS assembly. Orf53587 is also predicted to be an inner membrane protein, with five transmembrane helices, which is analogous to the *A. tumefaciens* VirB6 protein (55). Therefore, Orf53587 of ICE*clc* may have a similar role. VirB6 and VirB8 dependencies have also been described (56), which would then be in agreement with the effects observed here for the *orf53587* deletion on sfGFP-IceB8 foci. We acknowledge that sfGFP-IceB8 labeling caused a tenfold decrease of ICE transfer, indicative for partial functionality, but its foci were crisp and strongly similar in numbers to those of completely functional fusions, e.g. IceB4-sfGFP. We assume, therefore, that sfGFP-IceB8 foci are still representative for the ICE*clc* conjugative systems localization in the cell, which in absence of Orf53587 cannot assemble properly (Figure 7). As far as tested here, IceD4 association to the conjugative systems seemed to be dependent on IceB4 and IceB10, which we concluded from strongly diminished IceD4-sfGFP foci intensity and foci numbers in their absence (Figure 7). IceD4 is the predicted analog of the coupling protein ATPase, which is thought to oligomerize and activate only upon substrate binding (57). IceD4, with its two predicted trans-membrane (TM) helices in the N-terminal region, probably has natural affinity for the cytoplasmic membrane. Weaker IceD4-sfGFP foci intensities in absence of *iceB4* may thus be the consequence of IceD4 missing its molecular interaction partner, leading to destabilization of protein contacts, even though the T4SS core complex itself would be present. Cryo-EM studies on the R388 plasmid system showed that its VirD4 coupling protein indeed locates in close proximity of VirB4 (58). In case of *iceB10* deletion, the IceD4-sfGFP foci are hardly distinguishable from spurious background (Supplementary Figure S9). Unfortunately, IceB10 fluorescent protein fusions were not viable (Figure 7), and the reciprocal localization experiment could not be tested. Therefore, we have to assume that in absence of IceB10, with its predicted core structural role, the ICE conjugative system is not properly assembled; leaving IceD4 without interaction partners. This idea is supported by previous studies of the *A. tumefaciens* T4SS, demonstrating conformational changes in VirB10 upon ATP hydrolysis by

VirD4 (59). We further found that IceB7-mCherry foci formation depended on IceB9 (Figure 7), analogs of which are known to form together the outer membrane channel part of the T4SS (43), which suggests similar protein contacts for the ICE*clc*-system. The dependency of IceB7-mCherry foci formation on Orf62755 has not been previously documented. Orf62755 is a predicted outer membrane protein but without other known structural homology, and its membrane localization was illustrated by the patchy cell envelope fluorescence observed in an mCherry-fusion Orf62755-labeled strain (Figure 7). However, this fusion strain was only partly functional in ICE-transfer, and the localization of its fluorescence may not be completely informative. Orf62755 deletion strongly reduced foci formation of IceB7-mCherry, which would indicate that it is involved in T4SS assembly or a structural component of it.

Finally, one other ICE*clc* essential transfer protein (Orf55476), may be a further structural part of its T4SS. Orf55476-mCherry fusions were functional in ICE transfer and largely colocalized with IceB4-sfGFP foci in individual cells, but formed without strong dependence on *iceB4* (Figure 7). Orf55476 is a distant relative of a proposed PilT-analog in the ICE*Hin1056* element (15), which are more broadly known as ATPases that energize retraction of the Type IV pilus used for twitching motility and natural transformation (60). We hypothesize, therefore, that Orf55476 is an ICE*clc* T4SS-associated protein; possibly implicated in its pilus dynamics. Interestingly, Orf55476-mCherry foci formation was dependent on the presence of Orf68241, itself a transfer-essential protein, but for which neither N- nor C-terminal sfGFP-fused protein was functionally active (Figure 7). As mentioned, deletion of *orf68241* did not influence IceB4-sfGFP foci formation nor that of sfGFP-IceB8 (Figure 7). These results may thus indicate a specific and transient structural linkage between Orf68241 and Orf55476.

Apart from the structural T4SS analog proteins mentioned above, our analysis included predicted proteins without any sequence homology nor structural similarities to other functionally characterized proteins. One of these (IceU, product of *orf56883*) has an analog in TraU. The function of TraU remains unclear, although its absence was shown to reduce pilus formation and decrease transfer rates of the F-plasmid in *E. coli* (44). Our fluorescent reporter fusion to IceU was transfer-functional and localized to the cell envelope, producing occasional foci, in agreement with its predicted periplasmic situation (Figure 7). This suggests its role in transfer to reside in some transient interaction with T4SS complexes.

Deletions of other individual genes in the ICE*clc* T4SS gene region partly inhibited conjugative transfer or were without any noticeable effect altogether. Some of these have clear predicted functions, such as *iceB1* (*orf71723*, lytic transglycosylase), *orf58432* (RadC family), or *orf59110* (thiol disulphide oxidoreductase, DsbA). Lytic transglycosylases are frequently present in T4SS conjugative systems (61). Their assumed role is to locally degrade peptidoglycan and facilitate T4SS complex formation. Despite this, they are not essential for conjugation (62). Indeed, *iceB1* deletion reduced ICE transfer to ~3% compared to the wild type, which is similar to what was observed for deletion of the functional analog VirB1 in the *A. tumefaciens* system (62). Four genes in the ICE*clc* T4SS locus are predicted to encode thioredoxin homologs (Table 1). Similar numbers of thioredoxins have also been documented for other T4SS, such as from the F- and R27-plasmids of *E. coli* (63). These proteins are supposed to facilitate folding or stabilization of the periplasmic, pilin and outer membrane subunits of the T4SS. Their mild (10-fold reduction, for *orf71178*; and 4-fold, for *orf57827*) to no influence on ICE*clc* transfer upon individual deletion can be explained by functional redundancies. The Orf71178-mCherry fusion was functional and localized in the cell envelope with diffuse foci (Figure 4 and 7, and Supplementary figure S5), which might be congruent with a presumed chaperone-like role. Attempts to delete *orf72295* on ICE*clc* were not successful; therefore, it may have some other essential role. Finally, the presence of a well-conserved *radC*-homolog (*orf58432*) on ICE*clc* and its family members remains enigmatic. These widespread proteins were initially thought to have a role in DNA repair at the replication fork (64), and some *radC* are expressed during the competence state in naturally transformable bacteria (65–67). In spite of that, inactivation of *radC* did not influence the efficiency of DNA uptake (68,69) and also deletion of *orf58432* on ICE*clc* had no measurable effect on conjugation rates.

The combination of mutation analysis and foci quantification gives a relatively coherent picture on the ICE*clc* conjugative system, but, evidently, the analysis of fluorescent foci in tc cells comes with uncertainty from limited resolution. Controls in isogenic *P. putida* without ICE*clc* but with overexpressed fluorescent proteins in all cells clearly indicate that the tc cell foci are not the result of unspecific fluorescent protein aggregation, but must be reflections of T4SS subunit multimerization. Furthermore, the combination of higher resolution Airyscan deconvoluted imaging of 170-nm cell slices with epifluorescence foci imaging across large numbers of tc cells provided quantifiable foci features with statistically sound comparisons among the various tagged protein constructs and additional ICE*clc*-gene deletions. Finally, there is precedent for observation of multiple fluorescent foci per cell from tagged T4SS proteins in *A. tumefaciens* (46), which suggested

multiple T4SS units to be formed per cell. This was recently confirmed by cryo-tomography of the Dot/Icm system of *L. pneumophila* showing multiple T4SS complexes in individual cells (27). However, complexes seen in high-resolution microscopy by fluorescence tagging may not be consisting of the same T4SS assembly states, as demonstrated by recent cryo-EM studies of *E. coli* F-plasmid T4SS complexes in mini-cells, which revealed four distinct structural configurations (24).

In conclusion, we provide a detailed characterization of the ICE*clc* conjugative system and its subcellular localization, which is congruent to known plasmid-type T4SSs, but with a number of distinct and unknown structural elements as well as hitherto unreported dependencies. The ICE*clc* gene loci in this region are highly conserved in other Beta- and Gammaproteobacteria, both in sequence and gene synteny. The high conservation of T4SS gene regions in a variety of hosts is supportive for the hypothesis that they are part of other ICE*clc*-family elements, as proposed previously (7,17). Some of those, particularly in *P. aeruginosa* isolates, carry antibiotic resistance cassettes (70,71), suggesting that they encode active conjugative systems and are being selected for their efficient transfer. It is thus important to further unravel the details and potential dynamic steps in T4SS assembly and gene transfer.

References

1. Johnson,C.M. and Grossman,A.D. (2015) Integrative and conjugative elements (ICEs): what they do and how they work. *Annu. Rev. Genet.*, 49, 577–601.
2. Juhas,M., van der Meer,J.R., Gaillard,M., Harding,R.M., Hood,D.W. and Crook,D.W. (2009) Genomic islands: tools of bacterial horizontal gene transfer and evolution. *FEMS Microbiol. Rev.*, 33, 376–393.
3. Delavat,F., Miyazaki,R., Carraro,N., Pradervand,N. and van der Meer,J.R. (2017) The hidden life of integrative and conjugative elements. *FEMS Microbiol. Rev.*, 41, 512–537.
4. Wozniak,R.A. and Waldor,M.K. (2010) Integrative and conjugative elements: mosaic mobile genetic elements enabling dynamic lateral gene flow. *Nat. Rev. Microbiol.*, 8, 552–563.
5. Burrus,V. and Waldor,M.K. (2004) Shaping bacterial genomes with integrative and conjugative elements. *Res. Microbiol.*, 155, 376–386.
6. Beaber,J.W., Hochhut,B. and Waldor,M.K. (2004) SOS response promotes horizontal dissemination of antibiotic resistance genes. *Nature*, 427, 72–74.
7. Carraro,N., Richard,X., Sulser,S., Delavat,F., Mazza,C. and van der Meer,J.R. (2020) An analog to digital converter controls bistable transfer competence development of a widespread bacterial integrative and conjugative element. *Elife*, 9. 10.7554/eLife.57915
8. Auchtung,J.M., Lee,C.A., Monson,R.E., Lehman,A.P. and Grossman,A.D. (2005) Regulation of a *Bacillus subtilis* mobile genetic element by intercellular signaling and the global DNA damage response. *Proc. Natl. Acad. Sci. U.S.A.*, 102, 12554–12559.
9. Reinhard,F., Miyazaki,R., Pradervand,N. and van der Meer,J.R. (2013) Cell differentiation to “mating bodies” induced by an integrating and conjugative element in free-living bacteria. *Curr.Biol.*, 23, 255–259.
10. Minoia,M., Gaillard,M., Reinhard,F., Stojanov,M., Sentchilo,V. and van der Meer,J.R. (2008) Stochasticity and bistability in horizontal transfer control of a genomic island in *Pseudomonas*. *Proc. Natl. Acad. Sci. U.S.A.*, 105, 20792–20797.
11. Delavat,F., Moritz,R. and van der Meer,J.R. (2019) Transient replication in specialized cells favors transfer of an integrative and conjugative element. *Mbio*, 10. 10.1128/mBio.01133-19
12. Fronzes,R., Christie,P.J. and Waksman,G. (2009) The structural biology of type IV secretion systems. *Nat. Rev. Microbiol.*, 7, 703–714.
13. Costa,T.R.D., Harb,L., Khara,P., Zeng,L., Hu,B. and Christie,P.J. (2021) Type IV secretion systems: advances in structure, function, and activation. *Mol. Microbiol.*, 115, 436–452.
14. Guglielmini,J., Neron,B., Abby,S.S., Garcillan-Barcia,M.P., de la Cruz,F. and Rocha,E.P. (2014) Key components of the eight classes of type IV secretion systems involved in bacterial conjugation or protein secretion. *Nucleic Acids Res.*, 42, 5715–5727.
15. Juhas,M., Crook,D.W., Dimopoulou,I.D., Lunter,G., Harding,R.M., Ferguson,D.J. and Hood,D.W. (2007) Novel type IV secretion system involved in propagation of genomic islands. *J. Bacteriol.*, **189**, 761–771.
16. Sentchilo,V., Czechowska,K., Pradervand,N., Minoia,M., Miyazaki,R. and van der Meer,J.R. (2009) Intracellular excision and reintegration dynamics of the ICE_{clc} genomic island of *Pseudomonas knackmussii* sp. Strain B13. *Mol. Microbiol.*, **72**, 1293–1306.
17. Miyazaki,R., Bertelli,C., Benaglio,P., Canton,J., De Coi,N., Gharib,W.H., Gjoksi,B., Goesmann,A., Greub,G., Harshman,K. *et al.* (2015) Comparative genome analysis of *Pseudomonas knackmussii* B13, the first bacterium known to degrade chloroaromatic compounds. *Environ. Microbiol.*, **17**, 91–104.

18. Sentchilo,V., Zehnder,A.J. and van der Meer,J.R. (2003) Characterization of two alternative promoters for integrase expression in the *clc* genomic island of *Pseudomonas* sp. Strain B13. *Mol. Microbiol.*, **49**, 93–104.
19. Miyazaki,R. and van der Meer,J.R. (2011) A dual functional origin of transfer in the ICE*clc* genomic island of *Pseudomonas knackmussii* B13. *Mol. Microbiol.*, **79**, 743–758.
20. Gaillard,M., Pradervand,N., Minoia,M., Sentchilo,V., Johnson,D.R. and van der Meer,J.R. (2010) Transcriptome analysis of the mobile genome analysis of the mobile genome *iceclc* in *Pseudomonas knackmussii* B13. *BMC Microbiol.*, **10**, 153.10.1186/1471-2180-10-153
21. Sulser,S., Vucicevic,A., Bellini,V., Moritz,R., Delavat,F., Sentchilo,V., Carraro,N. and van der Meer,J.R. (2022) A bistable prokaryotic differentiation system underlying development of conjugative transfer competence. *PLoS Genet.*, **18**, e1010286.10.1371/journal.pgen.1010286
22. Jumper,J., Evans,R., Pritzel,A., Green,T., Figurnov,M., Ronneberger,O., Tunyasuvunakool,K., Bates,R., Zidek,A., Potapenko,A. *et al.* (2021) Highly accurate protein structure prediction with AlphaFold. *Nature*, **596**, 583–589.
23. Kelley,L.A., Mezulis,S., Yates,C.M., Wass,M.N. and Sternberg,M.J. (2015) The Phyre2 web portal for protein modeling, prediction and analysis. *Nat. Protoc.*, **10**, 845–858.
24. Hu,B., Khara,P. and Christie,P.J. (2019) Structural bases for F plasmid conjugation and F pilus biogenesis in *Escherichia coli*. *Proc. Natl. Acad. Sci. U.S.A.*, **116**, 14222–14227.
25. Aguilar,J., Zupan,J., Cameron,T.A. and Zambryski,P.C. (2010) *Agrobacterium* type IV secretion system and its substrates form helical arrays around the circumference of virulence-induced cells. *Proc. Natl. Acad. Sci. U.S.A.*, **107**, 3758–3763.
26. Ghosal,D., Jeong,K.C., Chang,Y.W., Gyore,J., Teng,L., Gardner,A., Vogel,J.P. and Jensen,G.J. (2019) Molecular architecture, polar targeting and biogenesis of the *Legionella* Dot/Icm T4SS. *Nat Microbiol*, **4**, 1173–1182.
27. Park,D., Chetrit,D., Hu,B., Roy,C.R. and Liu,J. (2020) Analysis of dot/Icm type IVB secretion system subassemblies by cryoelectron tomography reveals conformational changes induced by DotB binding. *Mbio*, **11**. 10.1128/mBio.03328-19
28. Gerhardt,P., Murray,R.G.E., Costilow,R.N., Nester,E.W., Wood,W.A., Krieg,N.R. and Briggs Phillips,G. (eds.) (1981) *Manual of methods for general bacteriology*. American Society for Microbiology, Washington, D.C.
29. Gaillard,M., Vallaeys,T., Vorhölter,F.J., Minoia,M., Werlen,C., Sentchilo,V., Pühler,A. and van der Meer,J.R. (2006) The *clc* element of *Pseudomonas* sp. strain B13, a genomic island with various catabolic properties. *J. Bacteriol.*, **188**, 1999–2013
30. Martinez-Garcia,E. and de Lorenzo,V. (2011) Engineering multiple genomic deletions in gram-negative bacteria: analysis of the multi-resistant antibiotic profile of *Pseudomonas putida* KT2440. *Environ. Microbiol.*, **13**, 2702–2716.
31. Martinez-Garcia,E., Calles,B., Arevalo-Rodriguez,M. and de Lorenzo,V. (2011) pBAM1: an all-synthetic genetic tool for analysis and construction of complex bacterial phenotypes. *BMC Microbiol.*, **11**, 38. 10.1186/1471-2180-11-38
32. Miyazaki,R., Minoia,M., Pradervand,N., Sulser,S., Reinhard,F. and van der Meer,J.R. (2012) Cellular variability of RpoS expression underlies subpopulation activation of an integrative and conjugative element. *PLoS Genet.*, **8**, e1002818. 10.1371/journal.pgen.1002818
33. Grote,A., Hiller,K., Scheer,M., Munch,R., Nortemann,B., Hempel,D.C. and Jahn,D. (2005) JCat: a novel tool to adapt codon usage of a target gene to its potential expression host. *Nucleic Acids Res.*, **33**, W526–W531.
34. Altschul,S.F., Gish,W., Miller,W., Myers,E.W. and Lipman,D.J. (1990) Basic local alignment search tool. *J. Mol. Biol.*, **215**, 403–410.

35. Mistry,J., Chuguransky,S.,Williams,L., Qureshi,M., Salazar,G.A., Sonnhammer,E.L.L., Tosatto,S.C.E., Paladin,L., Raj,S., Richardson,L.J. *et al.* (2021) Pfam: the protein families database in 2021. *Nucleic Acids Res.*, **49**, D412–D419.
36. Holm,L. (2020) DALI and the persistence of protein shape. *Protein Sci.*, **29**, 128–140.
37. Krogh,A., Larsson,B., von Heijne,G. and Sonnhammer,E.L. (2001) Predicting transmembrane protein topology with a hidden Markov model: application to complete genomes. *J. Mol. Biol.*, **305**, 567–580.
38. Nielsen,H., Engelbrecht,J., Brunak,S. and von Heijne,G. (1997) A neural network method for identification of prokaryotic and eukaryotic signal peptides and prediction of their cleavage sites. *Int. J. Neural Syst.*, **8**, 581–599.
39. Krissinel,E. and Henrick,K. (2004) Secondary-structure matching (SSM), a new tool for fast protein structure alignment in three dimensions. *Acta. Crystallogr. D Biol. Crystallogr.*, **60**, 2256–2268.
40. Stylianidou,S., Brennan,C., Nissen,S.B., Kuwada,N.J. and Wiggins,P.A. (2016) SuperSegger: robust image segmentation, analysis and lineage tracking of bacterial cells. *Mol. Microbiol.*, **102**, 690–700.
41. Reinhard,F. and van der Meer,J.R. (2013) Improved statistical analysis of low abundance phenomena in bimodal bacterial populations. *PLoS One*, **8**, e78288. 10.1371/journal.pone.0078288
42. Nakano,N., Kubori,T., Kinoshita,M., Imada,K. and Nagai,H. (2010) Crystal structure of *Legionella* DotD: insights into the relationship between type IVB and type II/III secretion systems. *PLoS Pathog.*, **6**, e1001129. 10.1371/journal.ppat.1001129
43. Durie,C.L., Sheedlo,M.J., Chung,J.M., Byrne,B.G., Su,M., Knight,T., Swanson,M., Lacy,D.B. and Ohi,M.D. (2020) Structural analysis of the *Legionella pneumophila* dot/icm type IV secretion system core complex. *Elife*, **9**. 10.7554/eLife.59530
44. Moore,D., Maneewannakul,K., Maneewannakul,S.,Wu,J.H., Ippen-Ihler,K. and Bradley,D.E. (1990) Characterization of the F-plasmid conjugative transfer gene *traU*. *J. Bacteriol.*, **172**, 4263–4270.
45. Chlebek,J.L., Hughes,H.Q., Ratkiewicz,A.S., Rayyan,R.,Wang,J.C., Herrin,B.E., Dalia,T.N., Biais,N. and Dalia,A.B. (2019) PilT and PilU are homohexameric atpases that coordinate to retract type iva pili. *PLoS Genet.*, **15**, e1008448. 10.1371/journal.pgen.1008448
46. Aguilar,J., Cameron,T.A., Zupan,J. and Zambryski,P. (2011) Membrane and core periplasmic *agrobacterium tumefaciens* virulence type IV secretion system components localize to multiple sites around the bacterial perimeter during lateral attachment to plant cells. *Mbio*, **2**, e00218–e00211.
47. Delavat,F., Mitri,S., Pelet,S. and van der Meer,J.R. (2016) Highly variable individual donor cell fates characterize robust horizontal gene transfer of an integrative and conjugative element. *Proc. Natl. Acad. Sci. U.S.A.*, **113**, E3375–E3383.
48. Christie,P.J., Atmakuri,K., Krishnamoorthy,V., Jakubowski,S. and Cascales,E. (2005) Biogenesis, architecture, and function of bacterial type IV secretion systems. *Annu. Rev. Microbiol.*, **59**, 451–485.
49. Kubori,T. and Nagai,H. (2016) The type IVB secretion system: an enigmatic chimera. *Curr. Opin. Microbiol.*, **29**, 22–29.
50. Chetrit,D., Hu,B., Christie,P.J., Roy,C.R. and Liu,J. (2018) A unique cytoplasmic atpase complex defines the *Legionella pneumophila* type IV secretion channel. *Nat Microbiol*, **3**, 678–686.
51. Ward,D.V., Draper,O., Zupan,J.R. and Zambryski,P.C. (2002) Peptide linkage mapping of the *Agrobacterium tumefaciens* vir-encoded type IV secretion system reveals protein subassemblies. *Proc. Natl. Acad. Sci. U.S.A.*, **99**, 11493–11500.

52. Yuan,Q., Carle,A., Gao,C., Sivanesan,D., Aly,K.A., Hoppner,C., Krall,L., Domke,N. and Baron,C. (2005) Identification of the VirB4-VirB8-VirB5-VirB2 pilus assembly sequence of type IV secretion systems. *J. Biol. Chem.*, **280**, 26349–26359.
53. Mossey,P., Hudacek,A. and Das,A. (2010) *Agrobacterium tumefaciens* type IV secretion protein VirB3 is an inner membrane protein and requires VirB4, VirB7, and VirB8 for stabilization. *J. Bacteriol.*, **192**, 2830–2838.
54. Jones,A.L., Shirasu,K. and Kado,C.I. (1994) The product of the virB4 gene of *Agrobacterium tumefaciens* promotes accumulation of VirB3 protein. *J. Bacteriol.*, **176**, 5255–5261.
55. Jakubowski,S.J., Krishnamoorthy,V., Cascales,E. and Christie,P.J. (2004) *Agrobacterium tumefaciens* VirB6 domains direct the ordered export of a DNA substrate through a type IV secretion system. *J. Mol. Biol.*, **341**, 961–977.
56. Casu,B., Mary,C., Sverzhinsky,A., Fouillen,A., Nanci,A. and Baron,C. (2018) VirB8 homolog TraE from plasmid pKM101 forms a hexameric ring structure and interacts with the VirB6 homolog TraD. *Proc. Natl. Acad. Sci. U.S.A.*, **115**, 5950–5955.
57. Matilla,I., Alfonso,C., Rivas,G., Bolt,E.L., de la Cruz,F. And Cabezón,E. (2010) The conjugative DNA translocase TrwB is a structure-specific DNA-binding protein. *J. Biol. Chem.*, **285**, 17537–17544.
58. Redzej,A., Ukleja,M., Connery,S., Trokter,M., Felisberto-Rodrigues,C., Cryar,A., Thalassinos,K., Hayward,R.D., Orlova,E.V. and Waksman,G. (2017) Structure of a VirD4 coupling protein bound to a VirB type IV secretion machinery. *EMBO J.*, **36**, 3080–3095.
59. Cascales,E. and Christie,P.J. (2004) *Agrobacterium* VirB10, an ATP energy sensor required for type IV secretion. *Proc. Natl. Acad. Sci. U.S.A.*, **101**, 17228–17233.
60. Craig,L., Forest,K.T. and Maier,B. (2019) Type IV pili: dynamics, biophysics and functional consequences. *Nat. Rev. Microbiol.*, **17**, 429–440.
61. Hoppner,C., Liu,Z., Domke,N., Binns,A.N. and Baron,C. (2004) VirB1 orthologs from *Brucella suis* and pKM101 complement defects of the lytic transglycosylase required for efficient type IV secretion from *Agrobacterium tumefaciens*. *J. Bacteriol.*, **186**, 1415–1422.
62. Mushegian,A.R., Fullner,K.J., Koonin,E.V. and Nester,E.W. (1996) A family of lysozyme-like virulence factors in bacterial pathogens of plants and animals. *Proc. Natl. Acad. Sci. U.S.A.*, **93**, 7321–7326.
63. Elton,T.C., Holland,S.J., Frost,L.S. and Hazes,B. (2005) F-like type IV secretion systems encode proteins with thioredoxin folds that are putative DsbC homologues. *J. Bacteriol.*, **187**, 8267–8277.
64. Saveson,C.J. and Lovett,S.T. (1999) Tandem repeat recombination induced by replication fork defects in *Escherichia coli* requires a novel factor, RadC. *Genetics*, **152**, 5–13.
65. Redfield,R.J., Cameron,A.D., Qian,Q., Hinds,J., Ali,T.R., Kroll,J.S. and Langford,P.R. (2005) A novel CRP-dependent regulon controls expression of competence genes in *Haemophilus influenzae*. *J. Mol. Biol.*, **347**, 735–747.
66. Berka,R.M., Hahn,J., Albano,M., Draskovic,I., Persuh,M., Cui,X., Sloma,A., Widner,W. and Dubnau,D.. (2002) Microarray analysis of the *Bacillus subtilis* K-state: genome-wide expression changes dependent on ComK. *Mol. Microbiol.*, **43**, 1331–1345.
67. Rimini,R., Jansson,B., Feger,G., Roberts,T.C., de Francesco,M., Gozzi,A., Faggioni,F., Domenici,E., Wallace,D.M., Frandsen,N. *et al.* (2000) Global analysis of transcription kinetics during competence development in *Streptococcus pneumoniae* using high density DNA arrays. *Mol. Microbiol.*, **36**, 1279–1292.
68. Ogura,M., Yamaguchi,H., Kobayashi,K., Ogasawara,N., Fujita,Y. and Tanaka,T. (2002) Whole-genome analysis of genes regulated by the *Bacillus subtilis* competence transcription factor ComK. *J. Bacteriol.*, **184**, 2344–2351.

69. Attaiech,L., Granadel,C., Claverys,J.P. and Martin,B. (2008) RadC, a misleading name?*J. Bacteriol.*, **190**, 5729–5732.
70. Hong,J.S., Yoon,E.J., Lee,H., Jeong,S.H. and Lee,K. (2016) Clonal dissemination of *Pseudomonas aeruginosa* sequence type 235 isolates carrying blaIMP-6 and emergence of blaGES-24 and blaIMP-10 on novel genomic islands PAGI-15 and -16 in South Korea. *Antimicrob. Agents Chemother.*, **60**, 7216–7223.
71. Roy Chowdhury,P., Scott,M., Worden,P., Huntington,P., Hudson,B., Karagiannis,T., Charles,I.G. and Djordjevic,S.P. (2016) Genomic islands 1 and 2 play key roles in the evolution of extensively drug-resistant ST235 isolates of *Pseudomonas aeruginosa*. *Open Biol*, **6**. 10.1098/rsob.150175

Supplementary data

Supplementary table 1: Characteristics of strains used in the study.

Strains	Strain Number	Description	Reference
<i>E. coli</i> DH5 α - λ pir	1854	λ pir lysogen	(Platt, Drescher, Park, & Phillips, 2000)
<i>P. putida</i> UWC1	1291	Plasmid-free derivative of <i>P. putida</i> KT2440, rifampicin resistant.	(McClure, Weightman, & Fry, 1989)
UWC1 Tn7-P _{tac} - <i>mcherry</i>	2744	<i>P. putida</i> UWC1 carrying Tn7-P _{tac} - <i>mCherry</i> (used as ICE clc recipient)	(Miyazaki & van der Meer, 2011)
UWC1 Tn7- <i>lacI-cfp</i>	6429	Derivative of strain 1291 with a mini-Tn7 <i>araC</i> -P _{BAD} - <i>lacI-cfp</i> insertion (used as ICE clc recipient)	This study
UWC1- <i>clc5</i> , <i>lacO</i> _{array}	5214	Derivative of strain 1291 with one ICE clc copy integrated into <i>tRNA</i> _{Gly-5} and a <i>lacO</i> array	(Delavat, Moritz, & van der Meer, 2019)
UWC1- <i>clc3</i> , <i>lacO</i> _{array} , Δ <i>orf59888</i>	5512	<i>P. putida</i> UWC1- <i>clc3</i> with a deletion of <i>orf59888</i> (<i>iceB4</i>) in the ICE clc .	This study
UWC1- <i>clc3</i> , <i>lacO</i> _{array} , Δ <i>virB4</i> , Tn5 P _{67231-<i>orf59888</i>}	5571-74	Derivative of strain 5512 with a mini Tn5 P _{67231-<i>orf59888</i>} insertion. Three independent clones were stored at -80 °C.	This study
UWC1- <i>clc5</i> , <i>lacO</i> _{array} , Δ <i>orf68987</i>	6660	Derivative of strain 5214 with a deletion of <i>orf68987</i> (<i>iceD4</i>) in the ICE clc .	This study
UWC1- <i>clc5</i> , <i>lacO</i> _{array} , Δ <i>orf68987</i> , Tn5 P _{67231-<i>orf68987</i>}	7023-25	Derivative of strain 6660 with a mini Tn5 P _{67231-<i>orf68987</i>} (<i>iceD4</i>) insertion. Three independent clones were stored at -80 °C.	This study
UWC1- <i>clc5</i> , <i>lacO</i> _{array} , Δ <i>orf53587</i>	6678	Derivative of strain 5214 with a deletion of <i>orf53587</i> in the ICE clc .	This study
UWC1- <i>clc5</i> , <i>lacO</i> _{array} , Δ <i>orf53587</i> , Tn5 P _{67231-<i>orf53587</i>}	7019-21	Derivative of strain 6678 with a mini Tn5 P _{67231-<i>orf53587</i>} insertion. Three independent clones were stored at -80 °C.	This study
UWC1- <i>clc5</i> , <i>lacO</i> _{array} , Δ <i>orf63176</i>	6842	Derivative of strain 5214 with a deletion of <i>orf63176</i> (<i>iceB10</i>) in the ICE clc .	This study
UWC1- <i>clc5</i> , <i>lacO</i> _{array} , Δ <i>orf63176</i> , Tn5 P _{67231-<i>orf63176</i>}	6916-18	Derivative of strain 6842 with a mini Tn5 P _{67231-<i>orf63176</i>} insertion. Three independent clones were stored at -80 °C.	This study
UWC1- <i>clc5</i> , <i>lacO</i> _{array} , Δ <i>orf56883</i>	6853	Derivative of strain 5214 with a deletion of <i>orf56883</i> (<i>iceU</i>) in the ICE clc .	This study
UWC1- <i>clc5</i> , <i>lacO</i> _{array} , Δ <i>orf56883</i> , Tn5 P _{67231-<i>orf56883</i>}	7032-34	Derivative of strain 6853 with a mini Tn5 P _{67231-<i>orf56883</i>} insertion. Three independent clones were stored at -80 °C.	This study
UWC1- <i>clc5</i> , <i>lacO</i> _{array} , Δ <i>orf55476</i>	6854	Derivative of strain 5214 with a deletion of <i>orf55476</i> in the ICE clc .	This study
UWC1- <i>clc5</i> , <i>lacO</i> _{array} , Δ <i>orf55476</i> , Tn5 P _{67231-<i>orf55476</i>}	7338- 7340	Derivative of strain 6854 with a mini Tn5 P _{67231-<i>orf55476</i>} insertion. Three independent clones were stored at -80 °C.	This study
UWC1- <i>clc5</i> , <i>lacO</i> _{array} , Δ <i>orf71723</i>	6855	Derivative of strain 5214 with a deletion of <i>orf71723</i> (<i>iceB1</i>) in the ICE clc .	This study

UWC1- <i>clc5</i> , <i>lacO</i> _{array} , Δ <i>orf71723</i> , <i>Tn5</i> <i>P</i> _{67231-<i>orf71723</i>}	6943-45	Derivative of strain 6855 with a mini <i>Tn5</i> <i>P</i> _{67231-<i>orf71723</i>} insertion. Three independent clones were stored at -80 °C.	This study
UWC1- <i>clc5</i> , <i>lacO</i> _{array} , Δ <i>orf58432</i>	6906	Derivative of strain 5214 with a deletion of <i>orf58432</i> (<i>radC</i>) in the ICE <i>clc</i> .	This study
UWC1- <i>clc5</i> , <i>lacO</i> _{array} , Δ <i>orf58432</i> , <i>Tn5</i> <i>P</i> _{67231-<i>orf58432</i>}	6925-27	Derivative of strain 6906 with a mini <i>Tn5</i> <i>P</i> _{67231-<i>orf58432</i>} (<i>radC</i>) insertion. Three independent clones were stored at -80 °C.	This study
UWC1- <i>clc5</i> , <i>lacO</i> _{array} , Δ <i>orf64584</i>	6910	Derivative of strain 5214 with a deletion of <i>orf64584</i> (<i>iceB9</i>) in the ICE <i>clc</i> .	This study
UWC1- <i>clc5</i> , <i>lacO</i> _{array} , Δ <i>orf64584</i> , <i>Tn5</i> <i>P</i> _{67231-<i>orf64584</i>}	6940-42	Derivative of strain 6910 with a mini <i>Tn5</i> <i>P</i> _{67231-<i>orf64584</i>} (<i>iceB9</i>) insertion. Three independent clones were stored at -80 °C.	This study
UWC1- <i>clc5</i> , <i>lacO</i> _{array} , Δ <i>orf73676</i>	6933	Derivative of strain 5214 with a deletion of <i>orf73676</i> (<i>iceB7</i>) in the ICE <i>clc</i> .	This study
UWC1- <i>clc5</i> , <i>lacO</i> _{array} , Δ <i>orf73676</i> , <i>Tn5</i> <i>P</i> _{67231-<i>orf73676</i>}	7029-31	Derivative of strain 6933 with a mini <i>Tn5</i> <i>P</i> _{67231-<i>orf73676</i>} (<i>iceB7</i>) insertion. Three independent clones were stored at -80 °C.	This study
UWC1- <i>clc5</i> , <i>lacO</i> _{array} , Δ <i>orf59110</i>	6937	Derivative of strain 5214 with a deletion of <i>orf59110</i> (<i>dsbA</i>) in the ICE <i>clc</i> .	This study
UWC1- <i>clc5</i> , <i>lacO</i> _{array} , Δ <i>orf59110</i> , <i>Tn5</i> <i>P</i> _{67231-<i>orf59110</i>}	7777-79	Derivative of strain 6937 with a mini <i>Tn5</i> <i>P</i> _{67231-<i>orf59110</i>} insertion. Three independent clones were stored at -80 °C.	This study
UWC1- <i>clc5</i> , <i>lacO</i> _{array} , Δ <i>orf62755</i>	6938	Derivative of strain 5214 with a deletion of <i>orf62755</i> in the ICE <i>clc</i> .	This study
UWC1- <i>clc5</i> , <i>lacO</i> _{array} , Δ <i>orf62755</i> , <i>Tn5</i> <i>P</i> _{67231-<i>orf62755</i>}	7137-39	Derivative of strain 6938 with a mini <i>Tn5</i> <i>P</i> _{67231-<i>orf62755</i>} insertion. Three independent clones were stored at -80 °C.	This study
UWC1- <i>clc5</i> , <i>lacO</i> _{array} , Δ <i>orf68241</i>	6939	Derivative of strain 5214 with a deletion of <i>orf68241</i> in the ICE <i>clc</i> .	This study
UWC1- <i>clc5</i> , <i>lacO</i> _{array} , Δ <i>orf68241</i> , <i>Tn5</i> <i>P</i> _{67231-<i>orf68241</i>}	7026-28	Derivative of strain 6938 with a mini <i>Tn5</i> <i>P</i> _{67231-<i>orf68241</i>} insertion. Three independent clones were stored at -80 °C.	This study
UWC1- <i>clc5</i> , <i>lacO</i> _{array} , Δ <i>orf66625</i> , <i>67001</i> , <i>67231</i>	6995	Derivative of strain 5214 with a deletion of <i>orf67231-67001-66625</i> (<i>iceB2</i>) in the ICE <i>clc</i> .	This study
UWC1- <i>clc5</i> , <i>lacO</i> _{array} , Δ <i>orf66625</i> , <i>67001</i> , <i>67231</i> , <i>Tn5</i> <i>P</i> _{67231-<i>orf67231-67001-66625</i>}	7061-63	Derivative of strain 6995 with a mini <i>Tn5</i> <i>P</i> _{67231-<i>orf67231-67001-66625</i>} (<i>iceB2</i>) insertion. Three independent clones were stored at -80 °C.	This study
UWC1- <i>clc5</i> , <i>lacO</i> _{array} , Δ <i>orf66625</i> , <i>67001</i> , <i>67231</i> , <i>Tn5</i> <i>P</i> _{67231-<i>orf66625</i>}	7002-03	Derivative of strain 6995 with a mini <i>Tn5</i> <i>P</i> _{67231-<i>orf66625</i>} (<i>iceB2</i>) insertion. Two independent clones were stored at -80 °C.	This study

UWC1- <i>clc5</i> , <i>lacO</i> _{array} , Δ <i>orf66625</i> , <i>67001</i> , <i>67231</i> , <i>Tn5</i> P ₆₇₂₃₁ - <i>orf67231</i>	7004-06	Derivative of strain 6995 with a mini <i>Tn5</i> P ₆₇₂₃₁ - <i>orf67231</i> insertion. Three independent clones were stored at -80 °C.	This study
UWC1- <i>clc5</i> , <i>lacO</i> _{array} , Δ <i>orf66625</i> , <i>67001</i> , <i>67231</i> , <i>Tn5</i> P ₆₇₂₃₁ - <i>orf67001</i>	7058-60	Derivative of strain 6995 with a mini <i>Tn5</i> P ₆₇₂₃₁ - <i>orf67001</i> insertion. Three independent clones were stored at -80 °C.	This study
UWC1- <i>clc5</i> , <i>lacO</i> _{array} , Δ <i>orf66625</i> , <i>67001</i> , <i>67231</i> , <i>Tn5</i> P ₆₇₂₃₁ - <i>orf67231-67001</i>	7533-35	Derivative of strain 6995 with a mini <i>Tn5</i> P ₆₇₂₃₁ - <i>orf67231-67001</i> insertion. Three independent clones were stored at - 80 °C.	This study
UWC1- <i>clc5</i> , <i>lacO</i> _{array} , Δ <i>orf66625</i> , <i>67001</i> , <i>67231</i> , <i>Tn5</i> P ₆₇₂₃₁ - <i>orf67231-66625</i>	7536-38	Derivative of strain 6995 with a mini <i>Tn5</i> P ₆₇₂₃₁ - <i>orf67231-66625</i> insertion. Three independent clones were stored at - 80 °C.	This study
UWC1- <i>clc5</i> , <i>lacO</i> _{array} , Δ <i>orf66625</i> , <i>67001</i> , <i>67231</i> , <i>Tn5</i> P ₆₇₂₃₁ - <i>orf67001-66625</i>	7543-45	Derivative of strain 6995 with a mini <i>Tn5</i> P ₆₇₂₃₁ - <i>orf67001-66625</i> insertion. Three independent clones were stored at - 80 °C.	This study
UWC1- <i>clc5</i> , <i>lacO</i> _{array} , Δ <i>orf65513</i>	7122	Derivative of strain 5214 with a deletion of <i>orf65513</i> (<i>iceB8</i>) in the ICE <i>clc</i> .	This study
UWC1- <i>clc5</i> , <i>lacO</i> _{array} , Δ <i>orf65513</i> , <i>Tn5</i> P ₆₇₂₃₁ - <i>orf65513</i>	7123-25	Derivative of strain 7122 with a mini <i>Tn5</i> P ₆₇₂₃₁ - <i>orf65513</i> (<i>iceB8</i>) insertion. Three independent clones were stored at - 80 °C.	This study
UWC1- <i>clc5</i> , <i>lacO</i> _{array} , Δ <i>orf73029</i>	7134	Derivative of strain 5214 with a deletion of <i>orf73029</i> in the ICE <i>clc</i> .	This study
UWC1- <i>clc5</i> , <i>lacO</i> _{array} , Δ <i>orf73029</i> , <i>Tn5</i> P ₆₇₂₃₁ - <i>orf73029</i>	7140-42	Derivative of strain 7134 with a mini <i>Tn5</i> P ₆₇₂₃₁ - <i>orf73029</i> insertion. Three independent clones were stored at -80 °C.	This study
UWC1- <i>clc5</i> , <i>lacO</i> _{array} , Δ <i>orf66202</i>	7303	Derivative of strain 5214 with a deletion of <i>orf66202</i> in the ICE <i>clc</i> .	This study
UWC1- <i>clc5</i> , <i>lacO</i> _{array} , Δ <i>orf66202</i> , <i>Tn5</i> P ₆₇₂₃₁ - <i>orf66202</i>	7341-43	Derivative of strain 7303 with a mini <i>Tn5</i> P ₆₇₂₃₁ - <i>orf66202</i> insertion. Three independent clones were stored at -80 °C.	This study
UWC1- <i>clc5</i> , <i>lacO</i> _{array} , Δ <i>orf67800</i>	7305	Derivative of strain 5214 with a deletion of <i>orf67800</i> in the ICE <i>clc</i> .	This study
UWC1- <i>clc5</i> , <i>lacO</i> _{array} , Δ <i>orf67800</i> , <i>Tn5</i> P ₆₇₂₃₁ - <i>orf67800</i>	7351-53	Derivative of strain 7305 with a mini <i>Tn5</i> P ₆₇₂₃₁ - <i>orf67800</i> insertion. Three independent clones were stored at -80 °C.	This study
UWC1- <i>clc5</i> , <i>lacO</i> _{array} , Δ <i>orf71178</i>	7319	Derivative of strain 5214 with a deletion of <i>orf71178</i> in the ICE <i>clc</i> .	This study
UWC1- <i>clc5</i> , <i>lacO</i> _{array} , Δ <i>orf71178</i> , <i>Tn5</i> P ₆₇₂₃₁ - <i>orf71178</i>	7354-56	Derivative of strain 7319 with a mini <i>Tn5</i> P ₆₇₂₃₁ - <i>orf71178</i> insertion. Three independent clones were stored at -80 °C.	This study

UWC1- <i>clc5</i> , <i>lacO</i> _{array} , Δ <i>orf57827</i>	7491	Derivative of strain 5214 with a deletion of <i>orf57827</i> in the ICE <i>clc</i> .	This study
UWC1- <i>clc5</i> , <i>lacO</i> _{array} , Δ <i>orf57827</i> , <i>Tn5</i> <i>P</i> _{67231-<i>orf57827</i>}	7780-82	Derivative of strain 7491 with a mini <i>Tn5</i> <i>P</i> _{67231-<i>orf57827</i>} insertion. Three independent clones were stored at -80 °C.	This study
UWC1- <i>clc5</i> , <i>lacO</i> _{array} , <i>sfgfp::orf65513</i>	7436	Derivative of strain 5214 with <i>sfgfp</i> insertion upstream of <i>orf65513</i> (<i>iceB8</i>).	This study
UWC1- <i>clc5</i> , <i>lacO</i> _{array} , Δ <i>orf53587</i> , <i>sfgfp::orf65513</i>	7448	Derivative of strain 6678 with <i>sfgfp</i> insertion upstream of <i>orf65513</i> (<i>iceB8</i>).	This study
UWC1- <i>clc5</i> , <i>lacO</i> _{array} , Δ <i>orf68241</i> , <i>sfgfp::orf65513</i>	7459	Derivative of strain 6939 with <i>sfgfp</i> insertion upstream of <i>orf65513</i> (<i>iceB8</i>).	This study
UWC1- <i>clc5</i> , <i>lacO</i> _{array} , <i>orf68987::sfgfp</i>	7440	Derivative of strain 5214 with <i>sfgfp</i> insertion downstream of <i>orf68987</i> (<i>iceD4</i>).	This study
UWC1- <i>clc5</i> , <i>lacO</i> _{array} , Δ <i>orf59888</i> , <i>orf68987::sfgfp</i>	7482	Derivative of strain 5512 with <i>sfgfp</i> insertion upstream of <i>orf68987</i> (<i>iceD4</i>).	This study
UWC1- <i>clc5</i> , <i>lacO</i> _{array} , Δ <i>orf63176</i> , <i>orf68987::sfgfp</i>	7483	Derivative of strain 6842 with <i>sfgfp</i> insertion upstream of <i>orf68987</i> (<i>iceD4</i>).	This study
UWC1- <i>clc5</i> , <i>lacO</i> _{array} , <i>orf59888::sfgfp</i>	7461	Derivative of strain 5214 with <i>sfgfp</i> insertion downstream of <i>orf59888</i> (<i>iceB4</i>).	This study
UWC1- <i>clc5</i> , <i>lacO</i> _{array} , Δ <i>orf68241</i> , <i>orf59888::sfgfp</i>	7462	Derivative of strain 6939 with <i>sfgfp</i> insertion upstream of <i>orf59888</i> (<i>iceB4</i>).	This study
UWC1- <i>clc5</i> , <i>lacO</i> _{array} , Δ <i>orf65513</i> , <i>orf59888::sfgfp</i>	7463	Derivative of strain 7122 with <i>sfgfp</i> insertion upstream of <i>orf59888</i> (<i>iceB4</i>).	This study
UWC1- <i>clc5</i> , <i>lacO</i> _{array} , Δ <i>orf66202</i> , <i>orf59888::sfgfp</i>	7464	Derivative of strain 7303 with <i>sfgfp</i> insertion upstream of <i>orf59888</i> (<i>iceB4</i>).	This study
UWC1- <i>clc5</i> , <i>lacO</i> _{array} , Δ <i>orf53587</i> , <i>orf59888::sfgfp</i>	7466	Derivative of strain 6678 with <i>sfgfp</i> insertion upstream of <i>orf59888</i> (<i>iceB4</i>).	This study
UWC1- <i>clc5</i> , <i>lacO</i> _{array} , Δ <i>orf63176</i> , <i>orf59888::sfgfp</i>	7488	Derivative of strain 6842 with <i>sfgfp</i> insertion upstream of <i>orf59888</i> (<i>iceB4</i>).	This study
UWC1- <i>clc5</i> , <i>lacO</i> _{array} , <i>orf66202::sfgfp</i>	7500	Derivative of strain 5214 with <i>sfgfp</i> insertion downstream of <i>orf66202</i> .	This study

UWC1- <i>clc5</i> , <i>lacO</i> _{array} , <i>orf56883::mcherry</i>	7489	Derivative of strain 5214 with <i>mcherry</i> insertion downstream of <i>orf56883</i> (<i>iceU</i>).	This study
UWC1- <i>clc5</i> , <i>lacO</i> _{array} , <i>orf55476::mcherry</i>	7492	Derivative of strain 5214 with <i>mcherry</i> insertion downstream of <i>orf55476</i> .	This study
UWC1- <i>clc3</i> , <i>lacO</i> _{array} , Δ <i>orf59888</i> , <i>orf55476::mcherry</i>	7549	Derivative of strain 5512 with <i>mcherry</i> insertion downstream of <i>orf55476</i> .	This study
UWC1- <i>clc5</i> , <i>lacO</i> _{array} ,	7550	Derivative of strain 6939 with <i>mcherry</i> insertion downstream of <i>orf55476</i> .	This study
<hr/>			
Δ <i>orf68241</i> , <i>orf55476::mcherry</i>			
UWC1- <i>clc5</i> , <i>lacO</i> _{array} , <i>mcherry::orf62755</i>	7501	Derivative of strain 5214 with <i>mcherry</i> insertion upstream of <i>orf62755</i> .	This study
UWC1- <i>clc5</i> , <i>lacO</i> _{array} , Δ <i>orf73676</i> , <i>mcherry::orf62755</i>	7542	Derivative of strain 6933 with <i>mcherry</i> insertion upstream of <i>orf62755</i> .	This study
UWC1- <i>clc5</i> , <i>lacO</i> _{array} , <i>orf71178::mcherry</i>	7521	Derivative of strain 5214 with <i>mcherry</i> insertion downstream of <i>orf71178</i> .	This study
UWC1- <i>clc5</i> , <i>lacO</i> _{array} , <i>orf73676::mcherry</i>	7539	Derivative of strain 5214 with <i>mcherry</i> insertion downstream of <i>orf73676</i> (<i>iceB7</i>).	This study
UWC1- <i>clc5</i> , <i>lacO</i> _{array} , Δ <i>orf64584</i> , <i>orf73676::mcherry</i>	7540	Derivative of strain 6910 with <i>mcherry</i> insertion downstream of <i>orf73676</i> (<i>iceB7</i>).	This study
UWC1- <i>clc5</i> , <i>lacO</i> _{array} , Δ <i>orf62755</i> , <i>orf73676::mcherry</i>	7541	Derivative of strain 6938 with <i>mcherry</i> insertion downstream of <i>orf73676</i> (<i>iceB7</i>).	This study
UWC1- <i>clc5 lacO</i> <i>array</i> , <i>Tn5::P</i> ₆₇₂₃₁ - <i>sfgfp</i> , pME <i>bisR</i>	7143-44	Derivative of strain 5214 with a <i>Tn5::P</i> ₆₇₂₃₁ - <i>sfgfp</i> , carrying the plasmid pME for inducible expression of <i>bisR</i> . Two independent clones were stored at -80 °C	This study
UWC1, <i>Tn5::P</i> ₆₇₂₃₁ - <i>orf59888-sfgfp</i> , pME <i>bisDC</i>	7502-05	Derivative of strain 1291 with a <i>Tn5 P</i> ₆₇₂₃₁ - <i>orf59888-sfgfp</i> insertion and carrying pME <i>bisDC</i> . Four independent clones were stored at -80 °C.	This study
UWC1, <i>Tn7::P</i> ₆₇₂₃₁ - <i>sfgfp-orf65513</i> , pME <i>bisDC</i>	7506-07	Derivative of strain 1291 with a <i>Tn7 P</i> ₆₇₂₃₁ - <i>sfgfp-orf65513</i> insertion and carrying pME <i>bisDC</i> . Two independent clones were stored at -80 °C.	This study
UWC1, <i>Tn5::P</i> ₆₇₂₃₁ - <i>orf68987-sfgfp</i> , pME <i>bisDC</i>	7516-19	Derivative of strain 1291 with a <i>Tn5 P</i> ₆₇₂₃₁ - <i>orf68987-sfgfp</i> insertion and carrying pME <i>bisDC</i> . Four independent clones were stored at -80 °C.	This study
UWC1, <i>Tn5::P</i> ₆₇₂₃₁ - <i>orf71178-mcherry</i> , pME <i>bisDC</i>	7551-52	Derivative of strain 1291 with a <i>Tn5 P</i> ₆₇₂₃₁ - <i>orf71178-mcherry</i> insertion and carrying pME <i>bisDC</i> . Two independent clones were stored at -80 °C.	This study
UWC1- <i>clc5</i> , <i>lacO</i> _{array} ,	7606	Derivative of strain 5214 with <i>mcherry</i> insertion downstream of <i>orf73676</i> (<i>iceB7</i>) and <i>sfgfp</i> insertion downstream of	This study

<i>orf59888::sfgfp,</i> <i>orf73676::mcherry</i>		<i>orf59888 (iceB4).</i>	
UWC1- <i>clc5,</i> <i>lacO</i> _{array} , <i>orf59888::sfgfp,</i> <i>Tn5::P_{inR}-echerry</i>	7612-13	Derivative of strain 7461 with a <i>Tn5::P_{inR}-echerry</i> insertion.	This study
UWC1- <i>clc5,</i> <i>lacO</i> _{array} , Δ <i>orf63176,</i> <i>orf73676::mcherry</i>	7614	Derivative of strain 6842 with <i>mcherry</i> insertion downstream of <i>orf73676 (iceB7).</i>	This study
UWC1- <i>clc5,</i> <i>lacO</i> _{array} ,	7615	Derivative of strain 6933 with <i>sfgfp</i> insertion downstream of <i>orf59888 (iceB4).</i>	This study
Δ <i>orf73676,</i> <i>orf59888::sfgfp</i>			
UWC1- <i>clc5,</i> <i>lacO</i> _{array} , <i>orf59888::sfgfp,</i> <i>orf55476::mcherry</i>	7654	Derivative of strain 5214 with <i>mcherry</i> insertion downstream of <i>orf55476</i> and <i>sfgfp</i> insertion downstream of <i>orf59888 (iceB4).</i>	This study

Delavat, F., Moritz, R., & van der Meer, J. R. (2019). Transient Replication in Specialized Cells Favors Transfer of an Integrative and Conjugative Element. *mBio*, 10(3). doi:10.1128/mBio.01133-19

McClure, N. C., Weightman, A. J., & Fry, J. C. (1989). Survival of *Pseudomonas putida* UWC1 containing cloned catabolic genes in a model activated-sludge unit. *Appl Environ Microbiol*, 55(10), 2627-2634. doi:10.1128/aem.55.10.2627-2634.1989

Miyazaki, R., & van der Meer, J. R. (2011). A dual functional origin of transfer in the ICE_{clc} genomic island of *Pseudomonas knackmussii* B13. *Mol Microbiol*, 79(3), 743-758. doi:10.1111/j.1365-2958.2010.07484.x

Platt, R., Drescher, C., Park, S. K., & Phillips, G. J. (2000). Genetic system for reversible integration of DNA constructs and *lacZ* gene fusions into the *Escherichia coli* chromosome. *Plasmid*, 43(1), 12-23. doi:10.1006/plas.1999.1433

Supplementary table 2: List of all plasmids used in the study.

Plasmid	Description	Reference
pEMG	Km ^R , <i>oriR6K</i> , P _{tac} - <i>lacZ</i> _a , I-SceI sites	(Martinez-Garcia & de Lorenzo, 2011)
pSW	Amp ^R , <i>oriRK2</i> , P _m -I-SceI	(Martinez-Garcia & de Lorenzo, 2011)
pBAM	Km ^R , Amp ^R , <i>ori6K</i> , mini <i>Tn5</i> system	(Martinez-Garcia, Calles, Arevalo-Rodriguez, & de Lorenzo, 2011)
pUC_Tn7	Gm ^R , Amp ^R , mini Tn7 system	(Choi et al., 2005)
pUX-BF13	Helper plasmid for Tn7 integration	(Choi et al., 2005)
pME6032; pME	Tc ^R , P _{tac} , ORI pVS1	(Heeb, Blumer, & Haas, 2002)
pEMG-HR- <i>orf53587</i>	pEMG derivative allowing the deletion of <i>orf53587</i> in the ICE <i>clc</i> element.	This study
pEMG-HR- <i>orf55476</i>	pEMG derivative allowing the deletion of <i>orf55476</i> in the ICE <i>clc</i> element.	This study
pEMG-HR- <i>orf56883</i>	pEMG derivative allowing the deletion of <i>orf56883</i> in the ICE <i>clc</i> element.	This study
pEMG-HR- <i>orf57827</i>	pEMG derivative allowing the deletion of <i>orf57827</i> in the ICE <i>clc</i> element.	This study
pEMG-HR- <i>orf58432</i>	pEMG derivative allowing the deletion of <i>orf58432</i> in the ICE <i>clc</i> element.	This study
pEMG-HR- <i>orf59110</i>	pEMG derivative allowing the deletion of <i>orf59110</i> in the ICE <i>clc</i> element.	This study
pEMG-HR- <i>orf59888</i>	pEMG derivative allowing the deletion of <i>orf59888</i> in the ICE <i>clc</i> element.	This study
pEMG-HR- <i>orf62755</i>	pEMG derivative allowing the deletion of <i>orf62755</i> in the ICE <i>clc</i> element.	This study
pEMG-HR- <i>orf63176</i>	pEMG derivative allowing the deletion of <i>orf63176</i> in the ICE <i>clc</i> element.	This study
pEMG-HR- <i>orf64584</i>	pEMG derivative allowing the deletion of <i>orf64584</i> in the ICE <i>clc</i> element.	This study
pEMG-HR- <i>orf65513</i>	pEMG derivative allowing the deletion of <i>orf64584</i> in the ICE <i>clc</i> element.	This study
pEMG-HR- <i>orf66202</i>	pEMG derivative allowing the deletion of <i>orf64584</i> in the ICE <i>clc</i> element.	This study
pEMG-HR- <i>orf66625-67001-67231</i>	pEMG derivative allowing the deletion of <i>orf67231-67001-66625</i> in the ICE <i>clc</i> element.	This study
pEMG-HR- <i>orf67800</i>	pEMG derivative allowing the deletion of <i>orf67800</i> in the ICE <i>clc</i> element.	This study
pEMG-HR- <i>orf68241</i>	pEMG derivative allowing the deletion of <i>orf68241</i> in the ICE <i>clc</i> element.	This study
pEMG-HR- <i>orf68987</i>	pEMG derivative allowing the deletion of <i>orf68987</i> in the ICE <i>clc</i> element.	This study
pEMG-HR- <i>orf71178</i>	pEMG derivative allowing the deletion of <i>orf71178</i> in the ICE <i>clc</i> element.	This study
pEMG-HR- <i>orf71723</i>	pEMG derivative allowing the deletion of <i>orf71723</i> in the ICE <i>clc</i> element.	This study
pEMG-HR- <i>orf73029</i>	pEMG derivative allowing the deletion of <i>orf73029</i> in the ICE <i>clc</i> element.	This study
pEMG-HR- <i>orf73676</i>	pEMG derivative allowing the deletion of <i>orf73676</i> in the ICE <i>clc</i> element.	This study
pBAM-P ₆₇₂₃₁ - <i>orf53587</i>	pBAM derivative carrying P ₆₇₂₃₁ - <i>orf53587</i> . Used for the complementation of the respective deletion.	This study

pBAM-P ₆₇₂₃₁ - <i>orf55476</i>	pBAM derivative carrying P ₆₇₂₃₁ - <i>orf55476</i> . Used for the complementation of the respective deletion.	This study
pBAM-P ₆₇₂₃₁ - <i>orf56883</i>	pBAM derivative carrying P ₆₇₂₃₁ - <i>orf56883</i> . Used for the complementation of the respective deletion.	This study
pBAM-P ₆₇₂₃₁ - <i>orf57827</i>	pBAM derivative carrying P ₆₇₂₃₁ - <i>orf57827</i> . Used for the complementation of the respective deletion.	This study
pBAM-P ₆₇₂₃₁ - <i>orf58432</i>	pBAM derivative carrying P ₆₇₂₃₁ - <i>orf58432</i> . Used for the complementation of the respective deletion.	This study
pBAM-P ₆₇₂₃₁ - <i>orf59110</i>	pBAM derivative carrying P ₆₇₂₃₁ - <i>orf59110</i> . Used for the complementation of the respective deletion.	This study
pBAM-P ₆₇₂₃₁ - <i>orf59888</i>	pBAM derivative carrying P ₆₇₂₃₁ - <i>orf59888</i> . Used for the complementation of the respective deletion.	This study
pBAM-P ₆₇₂₃₁ - <i>orf62755</i>	pBAM derivative carrying P ₆₇₂₃₁ - <i>orf62755</i> . Used for the complementation of the respective deletion.	This study
pBAM-P ₆₇₂₃₁ - <i>orf63176</i>	pBAM derivative carrying P ₆₇₂₃₁ - <i>orf63176</i> . Used for the complementation of the respective deletion.	This study
pBAM-P ₆₇₂₃₁ - <i>orf64584</i>	pBAM derivative carrying P ₆₇₂₃₁ - <i>orf64584</i> . Used for the complementation of the respective deletion.	This study
pBAM-P ₆₇₂₃₁ - <i>orf65513</i>	pBAM derivative carrying P ₆₇₂₃₁ - <i>orf65513</i> . Used for the complementation of the respective deletion.	This study
pBAM-P ₆₇₂₃₁ - <i>orf66202</i>	pBAM derivative carrying P ₆₇₂₃₁ - <i>orf66202</i> . Used for the complementation of the respective deletion.	This study
pBAM-P ₆₇₂₃₁ - <i>orf67231-67001-66625</i>	pBAM derivative carrying P ₆₇₂₃₁ - <i>orf67231-67001-66625</i> . Used for the complementation of the respective deletion.	This study
pBAM-P ₆₇₂₃₁ - <i>orf67231</i>	pBAM derivative carrying P ₆₇₂₃₁ - <i>orf67231</i> . Used for the complementation of the respective deletion.	This study
pBAM-P ₆₇₂₃₁ - <i>orf67001</i>	pBAM derivative carrying P ₆₇₂₃₁ - <i>orf67001</i> . Used for the complementation of the respective deletion.	This study
pBAM-P ₆₇₂₃₁ - <i>orf66625</i>	pBAM derivative carrying P ₆₇₂₃₁ - <i>orf66625</i> . Used for the complementation of the respective deletion.	This study
pBAM-P ₆₇₂₃₁ - <i>orf67231-67001</i>	pBAM derivative carrying P ₆₇₂₃₁ - <i>orf67231-67001</i> . Used for the complementation of the respective deletion.	This study
pBAM-P ₆₇₂₃₁ - <i>orf67231-66625</i>	pBAM derivative carrying P ₆₇₂₃₁ - <i>orf67231-66625</i> . Used for the complementation of the respective deletion.	This study
pBAM-P ₆₇₂₃₁ - <i>orf67001-66625</i>	pBAM derivative carrying P ₆₇₂₃₁ - <i>orf67001-66625</i> . Used for the complementation of the respective deletion.	This study
pBAM-P ₆₇₂₃₁ - <i>orf67800</i>	pBAM derivative carrying P ₆₇₂₃₁ - <i>orf67800</i> . Used for the complementation of the respective deletion.	This study
pBAM-P ₆₇₂₃₁ - <i>orf68241</i>	pBAM derivative carrying P ₆₇₂₃₁ - <i>orf68241</i> . Used for the complementation of the respective deletion.	This study
pBAM-P ₆₇₂₃₁ - <i>orf68987</i>	pBAM derivative carrying P ₆₇₂₃₁ - <i>orf68987</i> . Used for the complementation of the respective deletion.	This study
pBAM-P ₆₇₂₃₁ - <i>orf71178</i>	pBAM derivative carrying P ₆₇₂₃₁ - <i>orf71178</i> . Used for the complementation of the respective deletion.	This study
pBAM-P ₆₇₂₃₁ - <i>orf71723</i>	pBAM derivative carrying P ₆₇₂₃₁ - <i>orf71723</i> . Used for the complementation of the respective deletion.	This study
pBAM-P ₆₇₂₃₁ - <i>orf73029</i>	pBAM derivative carrying P ₆₇₂₃₁ - <i>orf73029</i> . Used for the complementation of the respective deletion.	This study
pBAM-P ₆₇₂₃₁ - <i>orf73676</i>	pBAM derivative carrying P ₆₇₂₃₁ - <i>orf73676</i> . Used for the complementation of the respective deletion.	This study
pBAM-P ₆₇₂₃₁ - <i>orf59888-sfgfp</i>	pBAM derivative carrying P ₆₇₂₃₁ - <i>orf59888-sfgfp</i> .	This study
pBAM-P ₆₇₂₃₁ - <i>orf68987-sfgfp</i>	pBAM derivative carrying P ₆₇₂₃₁ - <i>orf68987-sfgfp</i> .	This study
pUC_Tn7-araC-P _{BAD} - <i>lacI-cfp</i>	pUC_Tn7 derivative allowing arabinose-inducible expression of LacI-CFP	(Delavat, Moritz, & van der Meer, 2019)

pME <i>bisDC</i>	pME6032 derivative allowing IPTG-controlled expression of <i>bisCD</i>	(Carraro et al., 2020)
pME <i>bisR</i>	pME6032 derivative allowing IPTG-controlled expression of <i>bisR</i>	(Carraro et al., 2020)
pEMG-HR- <i>orf59888-sfgfp</i>	pEMG derivative allowing chromosomal insertion of <i>sfgfp</i> downstream of <i>orf59888 (iceB4)</i>	This study
pEMG-HR- <i>orf68987-sfgfp</i>	pEMG derivative allowing chromosomal insertion of <i>sfgfp</i> downstream of <i>orf68987 (iceD4)</i>	This study
pEMG-HR- <i>orf66202-sfgfp</i>	pEMG derivative allowing chromosomal insertion of <i>sfgfp</i> downstream of <i>orf66202</i>	This study
pEMG-HR- <i>sfgfp-orf65513</i>	pEMG derivative allowing chromosomal insertion of <i>sfgfp</i> upstream of <i>orf65513 (iceB8)</i>	This study
pEMG-HR- <i>orf55476-mCherry</i>	pEMG derivative allowing chromosomal insertion of <i>mCherry</i> downstream of <i>orf55476</i>	This study
pEMG-HR- <i>orf71178-mCherry</i>	pEMG derivative allowing chromosomal insertion of <i>mCherry</i> downstream of <i>orf71178</i>	This study
pEMG-HR- <i>orf56883-mCherry</i>	pEMG derivative allowing chromosomal insertion of <i>mCherry</i> downstream of <i>orf56883 (iceU)</i>	This study
pEMG-HR- <i>orf73676-mCherry</i>	pEMG derivative allowing chromosomal insertion of <i>mCherry</i> downstream of <i>orf73676 (iceB7)</i>	This study
pEMG-HR- <i>mCherry-orf62755</i>	pEMG derivative allowing chromosomal insertion of <i>mCherry</i> upstream of <i>orf62755</i>	This study

Carraro, N., Richard, X., Sulser, S., Delavat, F., Mazza, C., & van der Meer, J. R. (2020). An analog to digital converter controls bistable transfer competence development of a widespread bacterial integrative and conjugative element. *Elife*, *9*. doi:10.7554/eLife.57915

Choi, K. H., Gaynor, J. B., White, K. G., Lopez, C., Bosio, C. M., Karkhoff-Schweizer, R. R., & Schweizer, H. P. (2005). A Tn7-based broad-range bacterial cloning and expression system. *Nat Methods*, *2*(6), 443-448. doi:10.1038/nmeth765

Delavat, F., Moritz, R., & van der Meer, J. R. (2019). Transient Replication in Specialized Cells Favors Transfer of an Integrative and Conjugative Element. *mBio*, *10*(3). doi:10.1128/mBio.01133-19

Heeb, S., Blumer, C., & Haas, D. (2002). Regulatory RNA as mediator in GacA/RsmA-dependent global control of exoproduct formation in *Pseudomonas fluorescens* CHA0. *J Bacteriol*, *184*(4), 1046-1056. doi:10.1128/jb.184.4.1046-1056.2002

Martinez-Garcia, E., Calles, B., Arevalo-Rodriguez, M., & de Lorenzo, V. (2011). pBAM1: an all-synthetic genetic tool for analysis and construction of complex bacterial phenotypes. *BMC Microbiol*, *11*, 38. doi:10.1186/1471-2180-11-38

Martinez-Garcia, E., & de Lorenzo, V. (2011). Engineering multiple genomic deletions in Gram-negative bacteria: analysis of the multi-resistant antibiotic profile of *Pseudomonas putida* KT2440. *Environ Microbiol*, *13*(10), 2702-2716. doi:10.1111/j.1462-2920.2011.02538.x

Supplementary table 3: List of the used primers and their targets.

Primer Number	Sequence 5'-3' ^a	Target
130315	CGATGGATCAGCTAGAATTCGGCCGTTACACCACTTTTC	Amplification of upstream and downstream flanking regions for <i>orf59888</i> deletion
130316	GCTGGAAACTCCCCTGGCGCCCTGGAAGTGTCTGTAA	
130317	GCCAGGGGAGTTTCCAGC	
130318	GTGACATTAGCATCTCTAGACGCTCGCCATCGATTTTCG	
190408	AATTCGAGCTCGGTACCCGGGGATCCGCTCTACGCCGTGGCCTT	Amplification of upstream and downstream flanking regions for <i>orf68987</i> deletion
190409	GGCTTCATTGCTCGATGCCG	
190410	GGCATCGAGCAATGAAGCCATGAAGGATGCCGCCTCGA	
190411	AGAAGCTTGCATGCCTGCAGGTTCGACGGACCACAACCACGCGCTA	
190519	AATTCGAGCTCGGTACCCGGGGATCCACACGGCTGCAACTGC	Amplification of upstream and downstream flanking regions for <i>orf63176</i> deletion
190520	CGGCGTGAGCTTGGCG	
190521	CCGGCGCCAAGCTCACGCCGTCCCGAAGGCCGCAAG	
190522	AGAAGCTTGCATGCCTGCAGGTTCGACGCCAGCCGGGTTCCC	
190523	AATTCGAGCTCGGTACCCGGGGATCCGAGAACCTGCGCGAAGC	Amplification of upstream and downstream flanking regions for <i>orf53587</i> deletion
190524	GGCCTCGATCTCCCCTC	
190525	CTTGAGGGGAGATCGAGGCCTCGGTGCGCCATTTTCAGT	
190526	AGAAGCTTGCATGCCTGCAGGTTCGACGCGCGCAAGAGAAC	
190901	ATTCGAGCTCGGTACCCGGGGATCCGTATTAGAGCTGAAAGCCGCC	Amplification of upstream and downstream flanking regions for <i>orf56883</i> deletion
190902	TCACGGCTGAGCCCT	
190903	ACCGGAGGGCTCAGCCGTGAGAGGTGGTGCCATGAAG	
190904	GAAGCTTGCATGCCTGCAGGTTCGACCGAGGTCCAGGTCTGG	
190905	AATTCGAGCTCGGTACCCGGGGATCCGGATCTGCTACTGGCTCTACT	Amplification of upstream and downstream flanking regions for <i>orf55476</i> deletion
190906	TCAGAGGAAATCGACGCTGC	
190907	CGGCAGCGTCGATTTCTCTGAGGGAGGCAACCCATGAG	
190908	AGAAGCTTGCATGCCTGCAGGTTCGACGCGTGCATGAACGCC	
190909	AATTCGAGCTCGGTACCCGGGGATCCGCGGTTCGAGGGAAACAC	Amplification of upstream and downstream flanking regions for <i>orf71723</i> deletion
190910	TCAGGGTTGGCGCTGC	
190911	AATGGCAGCGCCAACCCTGAAGGAGACCTCCCCATGA	
190912	AGAAGCTTGCATGCCTGCAGGTTCGACTTGCTGGTCATCACGTAGC	
191011	AATTCGAGCTCGGTACCCGGGGATCCGCCATGTACTGATCTCACG	Amplification of upstream and downstream flanking regions for <i>orf64584</i> deletion
191012	CTTGAATACAGGGTGCTTCATG	
191013	TGAAGCACCTGTATTCAAGGCCAGCAAGGAGTCC	
191014	AGAAGCTTGCATGCCTGCAGGTTCGACTTGACCGTGCCGTCAAT	
191015	AATTCGAGCTCGGTACCCGGGGATCCGGAAGCCGAGATCGCC	Amplification of upstream and downstream flanking regions for <i>orf73676</i> deletion
191016	CTCGGCGTCTGAAACAT	
191017	CGATGTTTCAGGACGCCGAGTCTGTTTCGGGAGGCCA	
191018	AGAAGCTTGCATGCCTGCAGGTTCGACCTCTGGCTCTGCGCATT	
191105	TAGGGATAACAGGGTAATCTGAATTCAGATGGGCAACCCGGA	Amplification of upstream and downstream flanking regions for <i>orf58432</i> deletion
191106	CATGCAGGAGTCATTGACGA	
191107	TCAATGACTCCTGCATGTATTCTTCGCTGAGCACG	
191108	AGAAGCTTGCATGCCTGCAGGTTCGACAGTAGAGCCAGTAGCAGATCC	
191109	TAGGGATAACAGGGTAATCTGAATTCGACACTGCCCGAGAT	Amplification of upstream and downstream flanking
191110	TATCGGAATGGAAGGACGTT	
191111	GTCCTTCCATTCCGATAGCCGACGTTGTCGGC	

191112	AGAAGCTTGCATGCCTGCAGGTCGACAATGCGCATCACGGACA	regions for <i>orf59110</i> deletion
200113	TAGGGATAACAGGGTAATCTGAATTCCACGGCGAAAACCGTG	Amplification of upstream and downstream flanking regions for <i>orf62755</i> deletion
200114	CGCCAGGCCCTTATTCAA	
200115	ACTTGAATAAGGGCCTGGCGCGCGTGGAGGACTACTG	
200116	AGAAGCTTGCATGCCTGCAGGTCGACGCGCGGGTTGAACCA	
200117	TAGGGATAACAGGGTAATCTGAATTCCAACCTCGATGTTTCAGCGATCT	Amplification of upstream and downstream flanking regions for <i>orf68241</i> deletion
200118	CGAGGCGGCATCCTTC	
200119	CCATGAAGGATGCCGCCTCGGCGGGGAGCTTCAAAAAGT	
200120	AGAAGCTTGCATGCCTGCAGGTCGACGTCGAGCTGGCGCAG	
200125	TAGGGATAACAGGGTAATCTGAATTCCGACGCTGATGCCATA	Amplification of upstream and downstream flanking regions for <i>orf66625</i> , <i>67001</i> and <i>67231</i> deletion
200126	GCGCAGCCAGGTTAAAGC	
200127	TGGCTTTAACCTGGCTGCGCCTGCTCACCGAAGCCAC	
200128	AGAAGCTTGCATGCCTGCAGGTCGACGAGCGGCGGTAGTCGTA	
200701	TAGGGATAACAGGGTAATCTGAATTCCGCATCCTCAATCCCG	Amplification of upstream and downstream flanking regions for <i>orf65513</i> deletion
200702	ATGGGTGATCTCGTTCTTG	
200703	TTCAAGAACGAGATCACCCATCCACAAGCGCCCCAA	
200704	AGAAGCTTGCATGCCTGCAGGTCGACTTCGTGCTGGAAGGTGG	
200714	TAGGGATAACAGGGTAATCTGAATTCCGCTCGATGTGCGTTTTCA	Amplification of upstream and downstream flanking regions for <i>orf73029</i> deletion
200715	CACCACCACCGCAGC	
200716	CGGCCGCTGCGGTGGTGGTGGCGATTCCCTGACC	
200717	AGAAGCTTGCATGCCTGCAGGTCGACGCGAGACGAGAGGCCA	
201113	TAGGGATAACAGGGTAATCTGAATTCTGGCCGCGAACAATC	Amplification of upstream and downstream flanking regions for <i>orf57827</i> deletion
201114	CGAGAACCTGGAAAAAGAAG	
201115	CTTCTTTTTCCAGGTTCTCGGTTCCAGCAGCACCGGA	
201116	AGAAGCTTGCATGCCTGCAGGTCGACTTGCCTGTCGAGGCAT	
201117	TAGGGATAACAGGGTAATCTGAATTCCGGCTGCTGGCTGATCTA	Amplification of upstream and downstream flanking regions for <i>orf66202</i> deletion
201118	ACGGACGTGCTGCTG	
201119	CCGAGCAGCAGCACGTCCGTAGGTCTGCAGCAAGGG	
201120	AGAAGCTTGCATGCCTGCAGGTCGACGGATTTCCACCGCCTG	
201121	TAGGGATAACAGGGTAATCTGAATTCCAGGACGAGGTACATCGC	Amplification of upstream and downstream flanking regions for <i>orf67800</i> deletion
201122	GAAAGAGTACCCCAACTCCA	
201123	TGGAGTTGGGGTACTCTTTCGTGTACGCACGGTTGAA	
201124	AGAAGCTTGCATGCCTGCAGGTCGACATGAAGGATGCCGCCT	
201209	TAGGGATAACAGGGTAATCTGAATTCTGACCTGTACATGGTC	Amplification of upstream and downstream flanking regions for <i>orf71178</i> deletion
201210	GAGATGGGCCAGATGGG	
201211	AATCCCATCTGGCCATCTCACCGGCATCGAGCAAT	
201212	AGAAGCTTGCATGCCTGCAGGTCGACCCAAATGGAAGACATAGAACTCG	
191023	AATTCGAGCTCGGTACCCGGGGATCCACATAGACCACTCAACGAGA	Forward and reverse primer for amplification of P ₆₇₂₃₁ .
200202	CAGTAGTCCTCCACGC	
200508	GAGCGCGTGGAGGACTACTGATGTCGGGAAACAGCC	Amplification of <i>orf68987</i> for K.O. complementation
191104	AGCATAACTAGTGCGGCCGAAGCTTTCATGGCGAGGCCTC	
191028	GTGCCCACTTTTCTCGTGATCGCCAGCAAGGAGTCC	Amplification of

191029	AGCATAACTAGTGC GGCCGCAAGCTTTTATTCAAGTTCGAGAGCATGGC	orf63176 for K.O. complementation
200203	GAGCGCGTGGAGGACTACTGATGACGCTTTTCACGACCG	Amplification of orf53587 for K.O. complementation
191004	AGCATAACTAGTGC GGCCGCAAGCTTTCAAAGCACCTTGCCGGT	
200510	GAGCGCGTGGAGGACTACTGGTGACTCGTGCATTTCGACCT	Amplification of orf56883 for K.O. complementation
191022	AGCATAACTAGTGC GGCCGCAAGCTTTTCAGAGGAAATCGACGCTGC	
200509	GAGCGCGTGGAGGACTACTGATGAAGTTTCGTCCTGCATTCAA	Amplification of orf55476 for K.O. complementation
191006	AGCATAACTAGTGC GGCCGCAAGCTTTTCATGGGTTGCCTCCCG	
200123	GTGCCCACTTTTCTCGTGATATCTCCAGCGGTCGT	Amplification of orf71723 for K.O. complementation
191102	AGCATAACTAGTGC GGCCGCAAGCTTTTCATGGGGAGGTCTCCTG	
191030	GTGCCCACTTTTCTCGTGATACAAGCGCCCCAAGGAG	Amplification of orf64584 for K.O. complementation
191031	AGCATAACTAGTGC GGCCGCAAGCTTTTACTGCGCATGGCGGG	
200503	GAGCGCGTGGAGGACTACTGATGTTTCAGGACGCCGAGC	Amplification of orf73676 for K.O. complementation
191035	AGCATAACTAGTGC GGCCGCAAGCTTTTCATGGCTGGCCTCCC	
191001	ATTCGAGCTCGGTACCCGGGGATCCCGATGCCTTGCTGTCG	Amplification of P ₅₈₄₃₂ and orf58432 for K.O. complementation
191119	AGCATAACTAGTGC GGCCGCAAGCTTTCTACAGCAGGCCGTG	
191120	GTGCCCACTTTTCTCGTGATCCAGCCCTGGAAGTGC	Amplification of orf59110 for K.O. complementation
191121	AGCATAACTAGTGC GGCCGCAAGCTTTCTACCTGGGCATGTGCG	
200506	GAGCGCGTGGAGGACTACTGATGCTCTCGAAGTTGAATAAG	Amplification of orf62755 for K.O. complementation
200507	AGCATAACTAGTGC GGCCGCAAGCTTTTCAGTAGTCCTCCACG	
200504	GAGCGCGTGGAGGACTACTGATGAAGGATGCCGCCTC	Amplification of orf68241 for K.O. complementation
200505	AGCATAACTAGTGC GGCCGCAAGCTTTTCACAGGTACTTTTTGAAGCTCC	
200601	GAGCGCGTGGAGGACTACTGATGGTGGCTTTAACCTGG	Amplification of orf66625-67001-67231 for K.O. complementation
200602	AGCATAACTAGTGC GGCCGCAAGCTTTTACAGGATGCCGGTG	
200603	GAGCGCGTGGAGGACTACTGATGAACGGCGCCAG	Amplification of orf67001 for K.O. complementation
200604	AGCATAACTAGTGC GGCCGCAAGCTTTCAAAGAGAGGAGGAAGAACTCA	
191023	AATTCGAGCTCGGTACCCGGGGATCCACATAGACCACTCAACGAGA	Amplification of orf67231 for K.O. complementation
191024	AGCATAACTAGTGC GGCCGCAAGCTTTTCATGGCTTGTCTCCAC	
191026	GTGCCCACTTTTCTCGTGATACCTGAAAGGCATGACCAT	Amplification of orf66625 for K.O. complementation
191027	AGCATAACTAGTGC GGCCGCAAGCTTTTACAGGATGCCGGTGG	
200705	GAGCGCGTGGAGGACTACTGATGAGCCGTTTCAAGAACG	Amplification of orf65513 for K.O. complementation
200706	AGCATAACTAGTGC GGCCGCAAGCTTTTCATGGGGTGCTTCCTC	
200801	GAGCGCGTGGAGGACTACTGATGACCGCCCCGAG	Amplification of orf73029 for K.O. complementation
200802	AGCATAACTAGTGC GGCCGCAAGCTTTTCAGGGAATCGCCACGC	
201203	GAGCGCGTGGAGGACTACTGATGCCAGCTTCTTTTCCAGG	Amplification of orf57827 for K.O. complementation
201204	AGCATAACTAGTGC GGCCGCAAGCTTTTCACGGCTGAGCCCT	
201205	GAGCGCGTGGAGGACTACTGATGTCCGAGCAGCAGCA	Amplification of orf66202

201206	AGCATAACTAGTGCGGCCGCAAGCTTTCATCGTGACCCCCTTGC	for K.O. complementation
201207	GAGCGCGTGGAGGACTACTGATGGAGTTGGGGTACTCTT	
201208	AGCATAACTAGTGCGGCCGCAAGCTTTCAGACCTTCAACCGTGC	Amplification of orf67800 for K.O. complementation
210101	GAGCGCGTGGAGGACTACTGATGACGAAATCCCATCTGG	Amplification of orf71178 for K.O. complementation
210102	AGCATAACTAGTGCGGCCGCAAGCTTTCATTGCTCGATGCCG	
221005	GAGCGCGTGGAGGACTACTGATGGAACAGAAACGTCCTT	Amplification of orf59110 for K.O. complementation
221006	AGCATAACTAGTGCGGCCGCAAGCTTCTACCTGGGCATGTCCG	
210201	TAGGGATAACAGGGTAATCTGAATTCCTACGCTCGTGAGGGCTA	Amplification of upstream and downstream flanking regions for insertion of <i>sfgfp</i> at the C-terminal of <i>orf59888</i>
210202	CGACAGTTCCAGGGCTG	
210203	GCCGGAGAACGCCAT	
210204	AGAAGCTTGCATGCCTGCAGGTCGACCGTTACACCACTTTTCGTGG	
210205	CGCCAGCCCTGGAAGTGTGAAAGCTTCCGGAAAATTCG	Amplification of linker- <i>sfgfp</i> for C-terminal tag of <i>orf59888</i>
210206	GTTCCATGGCGTTCTCCGGCTTACTTGTACAGTTCGTCCAT	
210301	TAGGGATAACAGGGTAATCTGAATTCGTGGCATTGCTGGTTGT	Amplification of upstream and downstream flanking regions for insertion of <i>sfgfp</i> at the N-terminal of <i>orf65513</i>
210302	GCTCATCGTGACCCC	
210303	CGTTTCAAGAACGAGATCACCC	
210304	AGAAGCTTGCATGCCTGCAGGTCGACTTGGCTCCGGCGTAC	
210305	GCAAGGGGGTCACGATGAGCATGTGCAAGGGCGAAGAAGT	Amplification of <i>sfgfp</i> -linker for N-terminal tag of <i>orf65513</i>
210306	GTGATCTCGTTCTTGAAACGAAGCTTGGTGCCGAC	
210307	TAGGGATAACAGGGTAATCTGAATTCAGCACGGGATCGACGAT	Amplification of upstream and downstream flanking regions for insertion of <i>sfgfp</i> at the C-terminal of <i>orf68987</i>
210308	GCCGGCGCTGTCGT	
210309	AACGAGGCCTCGCCAT	
210310	AGAAGCTTGCATGCCTGCAGGTCGACGGCAAGAGGATCAGTAATGGG	
210311	ACCGACGACAGCGCCGGCAAGCTTCCGGAAAATTCG	Amplification of linker- <i>sfgfp</i> for C-terminal tag of <i>orf68987</i>
210312	CTTCATGGCGAGGCCTCGTTCCTGTACAGTTCGTCCATG	
210426	TAGGGATAACAGGGTAATCTGAATTCCTCGGCCATCGAGCA	Amplification of upstream and downstream flanking regions for insertion of <i>mCherry</i> at the C-terminal of <i>orf55476</i>
210427	ATTGCCCTTCTGGAGCC	
210428	CCGGGAGGCAACCCA	
210429	AGAAGCTTGCATGCCTGCAGGTCGACAAAGCGCGTGCATGAACG	
210511	ACCGGCTCCAGAAGGGCAATAAGCTTCCGGAAAATTCGAA	Amplification of linker- <i>mCherry</i> for C-terminal tag of <i>orf55476</i>
210512	GTCATGGGTTGCCTCCCGGTTTGTACAGCTCATCCATGC	
210515	TAGGGATAACAGGGTAATCTGAATTCACCATCGTCGGCTCG	Amplification of upstream and downstream flanking regions for insertion of <i>mCherry</i> at the C-terminal of <i>orf56883</i>
210516	GAGGAAATCGACGCTGC	
210517	TGAGGTGGTGCCATGAA	
210518	AGAAGCTTGCATGCCTGCAGGTCGACTTCTTCTCGCCGAGTAC	
210519	TCGGCAGCGTCGATTCCTCAAGCTTCCGGAAAATTC	Amplification of linker-

210520	<i>ACTTCATGGCACACCTCATTGTACAGCTCATCCAT</i>	<i>mCherry</i> for C-terminal tag of <i>orf56883</i>
210533	<i>TAGGGATAACAGGGTAATCTGAATTCAAACCGTGGCGAACGCG</i>	Amplification of upstream and downstream flanking regions for insertion of <i>mCherry</i> at the N-terminal of <i>orf62755</i>
210534	<i>GCCGCCGAGCACCG</i>	
210535	<i>TGCGCCACCAGTAAGGAAAA</i>	
210536	<i>AGAAGCTTGCATGCCTGCAGGTCGACAAGCTGGGCTCGTCCTG</i>	
210537	<i>CCGTCGCGGTGCTCGGCGGCATGGTTTCCAAGGGCGAG</i>	Amplification of <i>mCherry</i> -linker for N-terminal tag of <i>orf62755</i>
210538	<i>TTTTCTTACTGGTGGCGCAAAGCTTGGTGGCCGAC</i>	
210551	<i>TAGGGATAACAGGGTAATCTGAATTCTTCGTGCGCTGCTGGT</i>	Amplification of upstream and downstream flanking regions for insertion of <i>mCherry</i> at the C-terminal of <i>orf73676</i>
210552	<i>AACAGAAGGCTCCAGCGG</i>	
210553	<i>TCGGGAGGCCAGCCAT</i>	
210554	<i>AGAAGCTTGCATGCCTGCAGGTCGACTTCGGGGTTCGGGCG</i>	
210555	<i>CCCGCTGGAGCCTTCTGTTAAGCTTCCGGAAAATTCG</i>	Amplification of linker- <i>mCherry</i> for C-terminal tag of <i>orf73676</i>
210556	<i>GTCATGGCTGGCCTCCCGATTTGTACAGCTCATCCATG</i>	
210557	<i>TAGGGATAACAGGGTAATCTGAATTCAACGGCCTACGTGGG</i>	Amplification of upstream and downstream flanking regions for insertion of <i>sfGFP</i> at the C-terminal of <i>orf66202</i>
210558	<i>TGCAGACCTTCGGGTG</i>	
210559	<i>GCAAGGGGGTCACGAT</i>	
210560	<i>AGAAGCTTGCATGCCTGCAGGTCGACTTCGCTGACGCCAGC</i>	
210561	<i>GACCACCCGAAGGTCTGCAAAGCTCCGGAAAATTCG</i>	Amplification of linker- <i>sfGFP</i> for C-terminal tag of <i>orf66202</i>
210562	<i>CTCATCGTGACCCCTTGCCTTGTACAGTTCGTCCATG</i>	

a) Restriction enzymes are underlined, primer overhangs are represented in italic

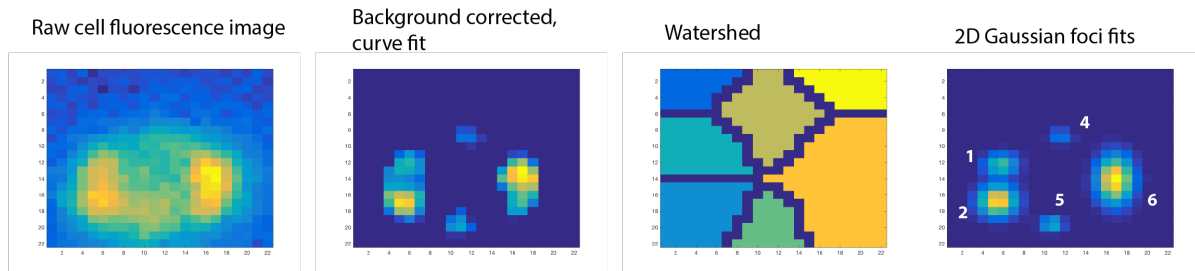
Supplementary table S4: Overview of measured foci parameters in wild-type and mutant strains.

Strain	Genotype	Mutation	Tc cell foci intensity distr	Gaussian fit score	Gaussian fit sigma	Airyscan (aspect)	EFM (aspect)	EFM (median top5)	EFM (prop zero foci among tc cells)	EFM envelope (low20)	EFM envelope (high 95)	EFM envelope (std)
7436	sfGFP-IceB8	–	Distinct			Crisp, some cell envelope						
7459	sfGFP-IceB8	Δ orf68241	Similar	Similar	Similar	Not tested	Similar	nd	nd			
7448	sfGFP-IceB8	Δ orf53587	Less distinct	Higher	Higher	More fuzzy	More accentuated cell envelope	nd	Higher			
7440	IceD4-sfGFP	–	Distinct			Mostly crisp						
7482	IceD4-sfGFP	Δ IceB4	Less distinct	Similar	Lower	fuzzy	Less bright	Lower	nd			
7483	IceD4-sfGFP	Δ IceB10	Less distinct	Higher	Lower	Fuzzy	Less bright	Lower	nd			
7461	IceB4-sfGFP	–	Distinct			Crisp foci – little envelope						
7462	IceB4-sfGFP	Δ orf68241	Similar	Similar	Similar	Not tested	Similar	nd	nd			
7463	IceB4-sfGFP	Δ IceB8	less distinct	Lower	Higher	Fuzzy	Lower	Lower	Higher			
7464	IceB4-sfGFP	Δ orf66202	Less distinct	Lower	Higher	Fuzzy	Fuzzy	Lower	Higher			
7466	IceB4-sfGFP	Δ orf53587	Similar	Higher	Similar	Fuzzy	Less bright	Lower	Higher			
7488	IceB4-sfGFP	Δ IceB10	Less distinct	Lower	More variable	Fuzzy	Less crisp	nd	Higher			
7615	IceB4-sfGFP	Δ IceB7	Similar	Similar	Similar	nd	Less bright	Lower	Higher			
7492	Orf55476-mChe	–	Distinct			Crisp foci with visible cell envelope						
7459	Orf55476-mChe	Δ IceB4		Higher	Lower	Similar	Similar			nd	Higher	Higher
7550	Orf55476-mChe	Δ orf68241		Similar	Higher	Cell envelope more accentuated	fuzzy			Lower	Lower	nd
7539	IceB7-mCherry	–	Distinct			Few crisp foci and envelope ‘patches’						
7540	IceB7-mCherry	Δ IceB9		Higher	Lower	Envelope more accentuated	Single clear foci	Lower	Higher	Higher	Not tested	Lower
7541	IceB7-mCherry	Δ orf62755		Similar	Similar	More patches	Less bright	Lower	Higher	Higher	Not tested	Lower
7614	IceB7-mCherry	Δ IceB10		Lower (n.s.)	Similar	Similar	More patchy	Lower (n.s.)	Higher (n.s.)	Higher	Not tested	nd

Supplementary Table S5: Median cell fluorescence for IceD4- and IceB4-labeled wild-type and mutant strains, and corresponding tc cell proportions

Strain	Protein fusion	ICE gene deletion	Proportion tc cells					Tc cell median cytoplasmic fluorescence				
			Mean	Rep1	Rep2	Rep3	TTEST	Mean	Rep1	Rep2	Rep3	TTEST
7461	IceB4-sfGFP	–	0.0462	0.0193	0.0939	0.0254	-	836.46	644.05	606.86	1258.46	-
7462	IceB4-sfGFP	Δ orf68241	0.0235	0.0346	0.0177	0.0183	0.4084	688.73	877.57	634.59	554.03	0.5598
7463	IceB4-sfGFP	Δ iceB8	0.0383	0.0791	0.0115	0.0243	0.8159	628.59	682.44	601.12	602.21	0.3843
7464	IceB4-sfGFP	Δ orf66202	0.0886	0.0951	0.0840	0.0868	0.1536	652.38	713.01	636.56	607.57	0.4374
7466	IceB4-sfGFP	Δ orf53587	0.0665	0.0597	0.0630	0.0769	0.4527	608.61	620.42	598.39	607.03	0.3417
7488	IceB4-sfGFP	Δ iceB10	0.0137	0.0075	0.0265	0.0070	0.2596	718.83	754.00	706.50	696.00	0.6085
7615	IceB4-sfGFP	Δ iceB7	0.0747	0.0594	0.0581	0.1064	0.3776	463.00	448.00	402.00	540.00	0.1580
7440	IceD4-sfGFP	–	0.0254	0.0231	0.0085	0.0447	-	817.16	712.50	996.50	742.50	-
7482	IceD4-sfGFP	Δ iceB4	0.0416	0.0632	0.0195	0.0423	0.3798	551.64	490.00	451.00	490.25	0.0202
7483	IceD4-sfGFP	Δ iceB10	0.0249	0.0220	0.0167	0.0359	0.9643	530.33	453.00	463.00	534.25	0.0235

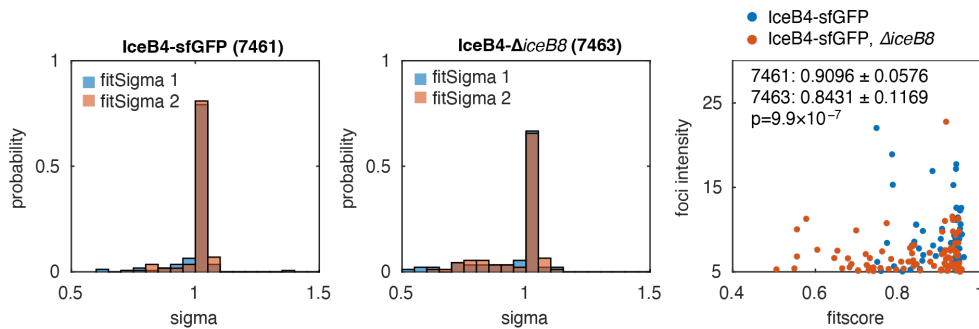
A Example: strain 7461-IceB4-sfgfp
 Replicate 1
 technical replicate: xy01
 cell000073.mat



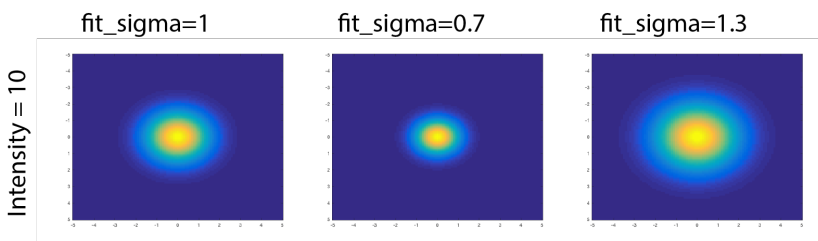
B

Fields	r	score	intensity	shortaxis	longaxis	fitSigma1	fitSigma2	fitScore
1	[316.764...	11.7340	13.1045	-0.9709	-4.7722	0.9639	1.1220	0.9339
2	[316.431...	25.2390	22.9431	2.6304	-7.3912	0.8581	0.8144	0.9199
3	[315,1563]	NaN	0	-8.9598	-1.9050	1	1	NaN
4	[322.552...	3.2813	5.5763	-0.9372	2.0130	1.3608	1.6607	0.8890
5	[321.711...	6.4258	11.4090	7.8397	-4.4046	1.3809	1.6732	0.8600
6	[327.839...	30.0702	23.9085	6.4196	3.6789	0.9051	0.5332	0.9045
7	[327,1562]	NaN	0	-3.4978	8.8266	1	1	NaN

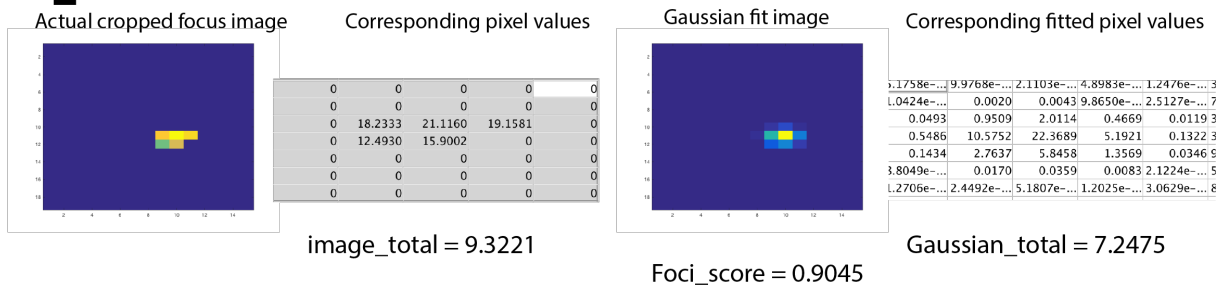
C



D



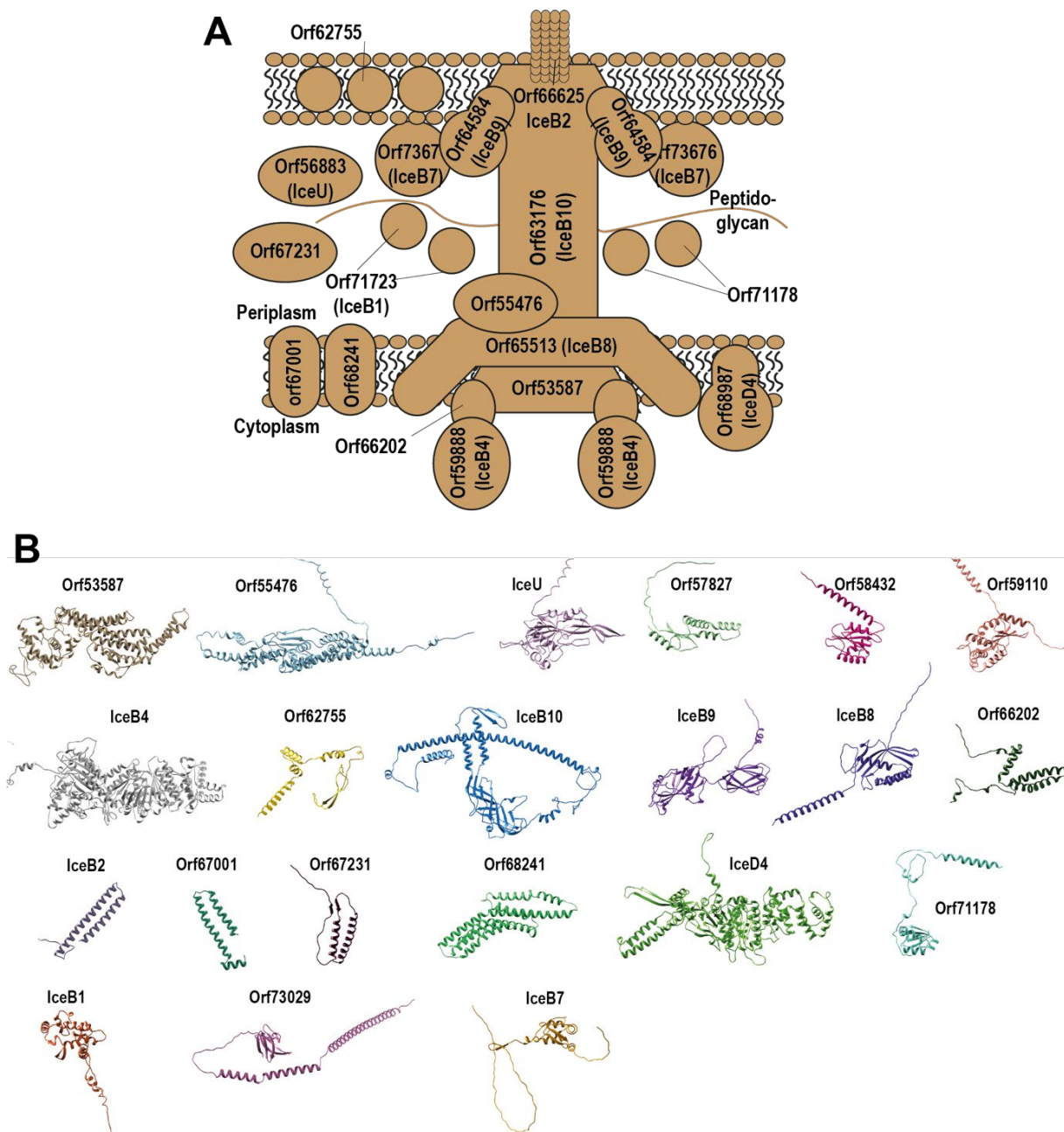
E



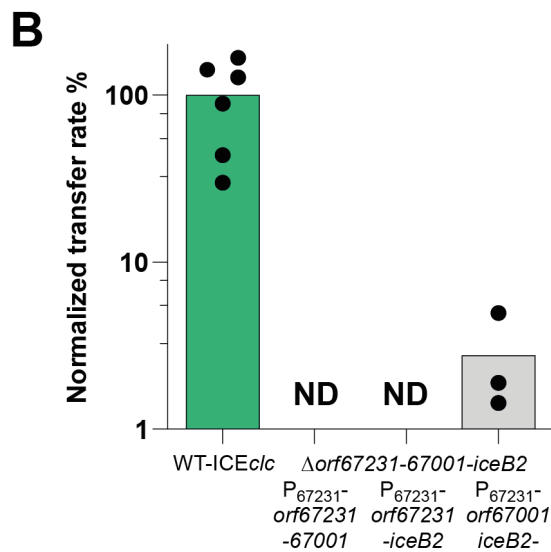
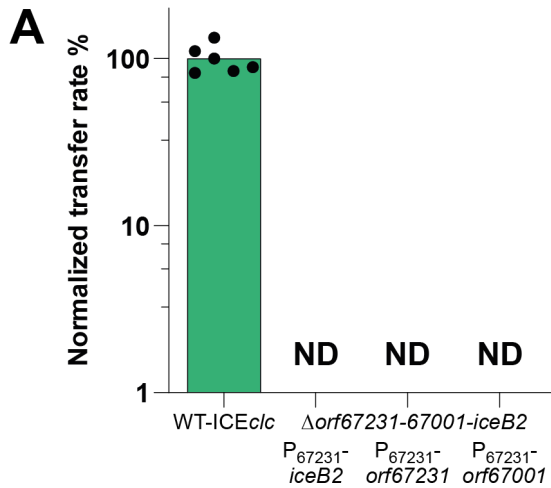
Supplementary figure S1. Procedure and examples of Gaussian foci detection and fitting.

A) Example of raw cell fluorescence image, the background corrected foci image, the watershed imposed sectioning for the individual foci quantification, and the resulting 2D

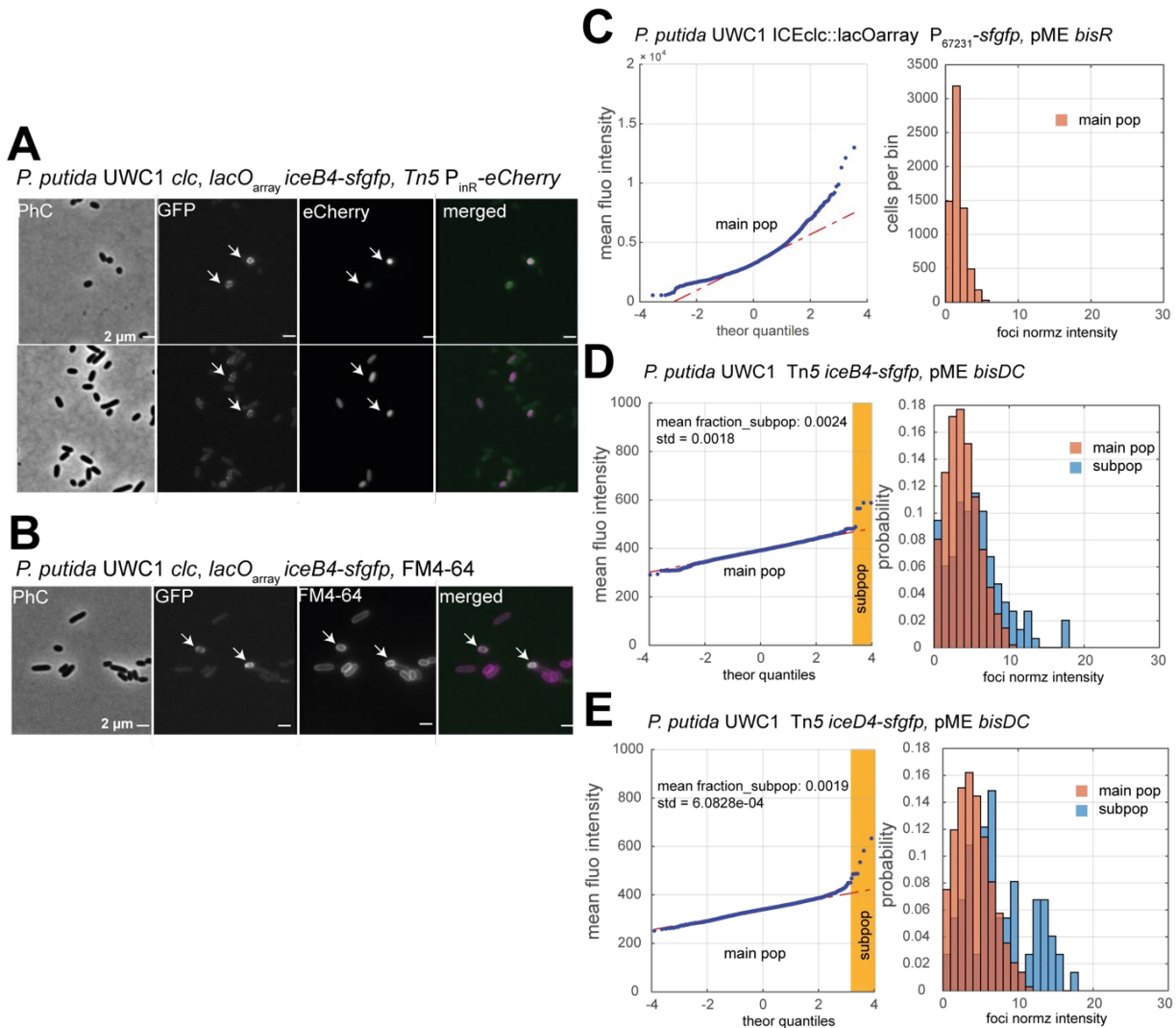
Gaussian fits. **B)** Corresponding data table for the foci in the cell image of **A**. **C)** Example of distribution of foci fitSigma values for *P. putida* UWC1-ICE*clc* expressing IceB4-sfGFP and its corresponding Δ *iceB8* mutation, and a plot of the measured fitScores and foci intensities. **D)** Effect of fitSigma on value on foci appearance at the same foci intensity. **E)** Explanation of the calculation of the fitScore from the square roots of the difference between the sum of the actual pixel and the fitted pixel values.



Supplementary figure S2. Predicted assembly and structures of ICEcIc conjugative transfer proteins. A) Schematic positioning of the ICEcIc T4SS and its components in the cell envelope (cytoplasmic membrane, periplasmic space and outer membrane), deduced from protein structure homologies and domain predictions (see Table 1). **B)** Individual AlphaFold2 predicted structures for ICEcIc proteins in the conjugation gene region of Fig. 1; scaled to the same size.



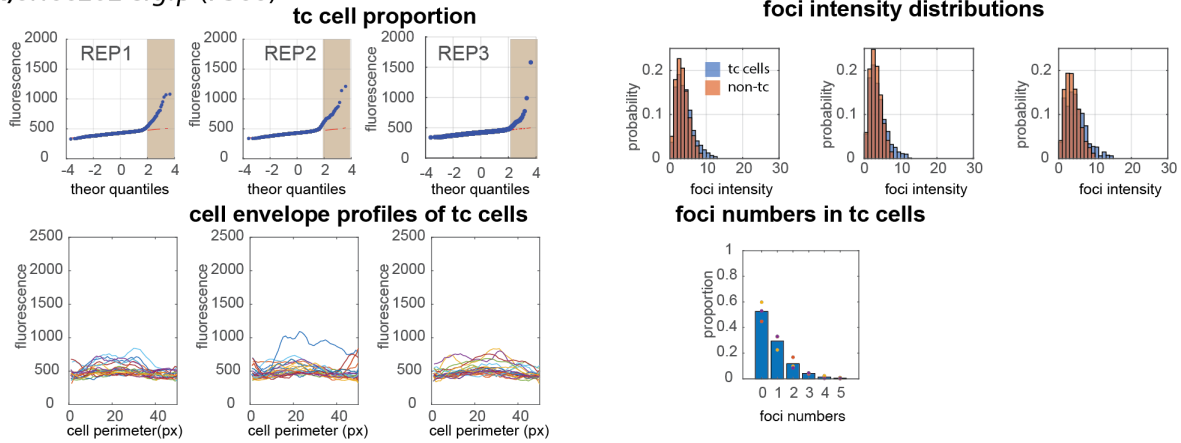
Supplementary figure S3. Effects of individual and dual gene complementation in the *orf67231-67001-iceB2* region on ICE*clc* transfer. A) Normalized transfer rate of ICE*clc* deleted for the *orf67231-67001-iceB2* region, complemented with single copy individual ICE*clc* genes under expression of the transfer competence promoter P_{67231} . B) As A, but complemented with single copy insertions of gene pairs. Bars represent the mean normalized transfer rates as percentage of that of wild-type ICE*clc* (green) in *P. putida* UWC1 isogenic matings, each individually quantified as the frequency of transconjugant colony forming units (CFU) on 3- CBA medium per donor CFU. Dots show the individual replicate values. *Orf* and gene names indicated below. ND, below detection limit (< 1%). WT, unmodified ICE*clc* wild-type.



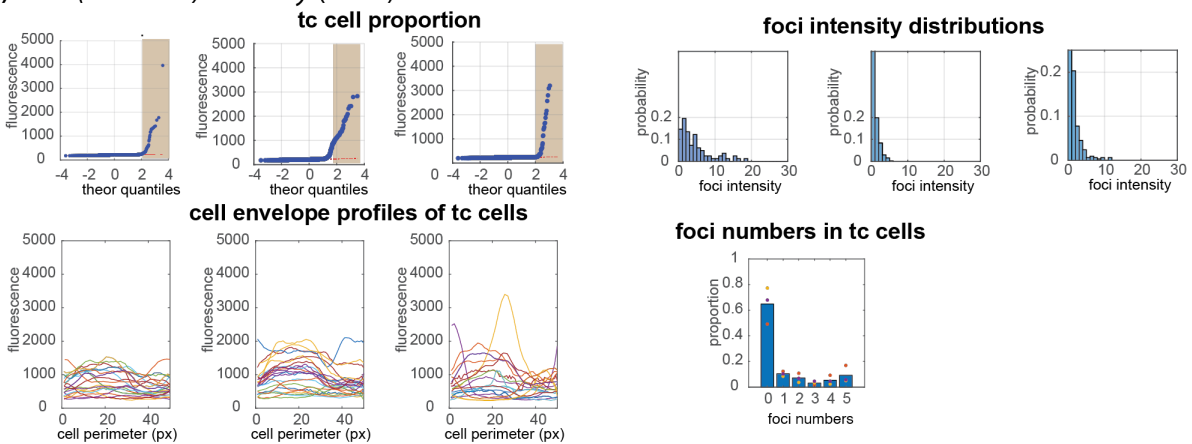
Supplementary figure S4. Fluorescence foci control experiments in *P. putida*.

- A)** IceB4-sGFP foci express only in transfer competent cells. Micrographs show stationary phase *P. putida* ICEclc-*lacOarray* with native fusion of *iceB4* to *sfgfp*, and further carrying a single copy mini-Tn5 insertion of the *mcherry* gene transcriptionally fused to the *P*_{inR}-promoter active only in tc cells. Images show two different regions with cells expressing both markers simultaneously (examples indicated by arrows).
- B)** Fluorescent IceB4-sGFP foci localize to the cell envelope. Micrographs show stationary phase *P. putida* ICEclc-*lacOarray* with native fusion of *iceB4* to *sfgfp* simultaneously stained with the membrane dye FM4-64. Arrows point to tc cells with fluorescent foci, amidst non-tc cells with solely cell envelope outlines visible.
- C) –E)** Normalized foci intensity distributions among the main (salmon) and the subpopulation (blue) of cells, the threshold determined by quantile-quantile plotting as shown in the left panel of each, for the three different *P. putida* control strains – as indicated on the top of each panel. Mean subpopulation fractions calculated from three independently grown cultures determined in stationary phase, and induced with 0.5 mM IPTG to force expression of the fluorescent protein fusion in all cells by the intermediate of BisR or BisDC (explained in ref. 7 of the main manuscript, Carraro *et al.*, 2020).

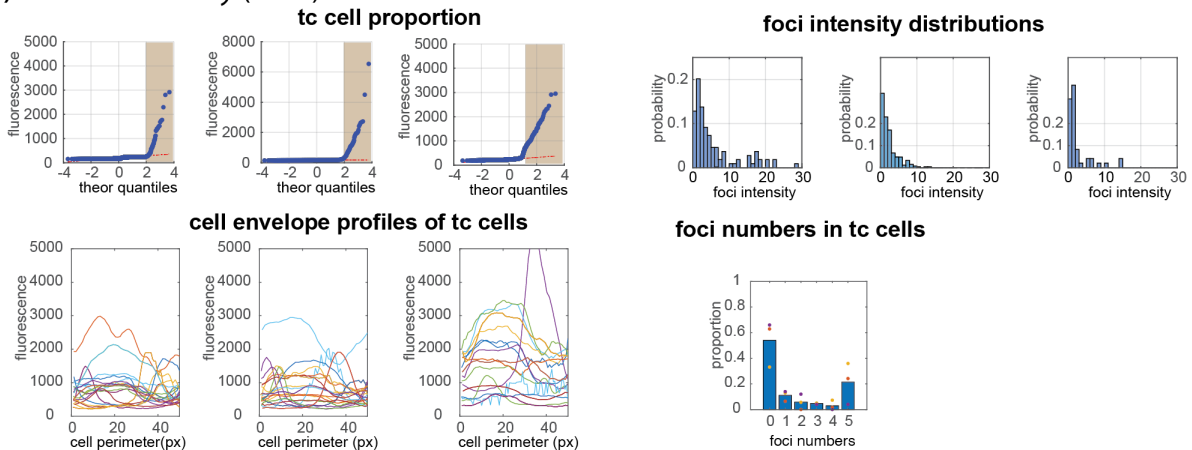
A) *orf66202-sfgfp* (7500)



B) *iceU-(orf56883)-mcherry* (7489)



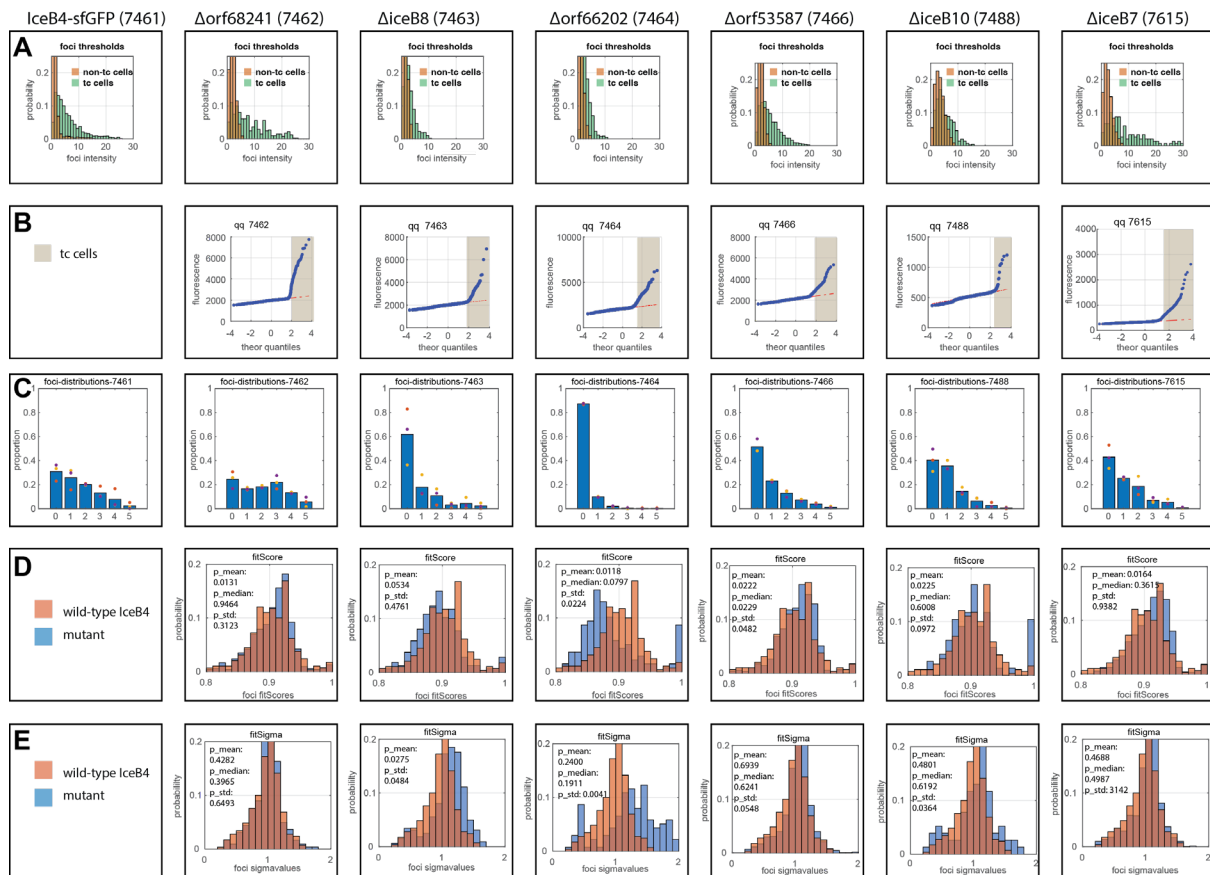
C) *orf71178-mcherry* (7521)



Supplementary figure 5: Proportions of, foci numbers and intensity distributions in tc cells of *P. putida* ICE clc expressing Orf66202-sfGFP, IceU-mCherry or Orf71178-mCherry fusions.

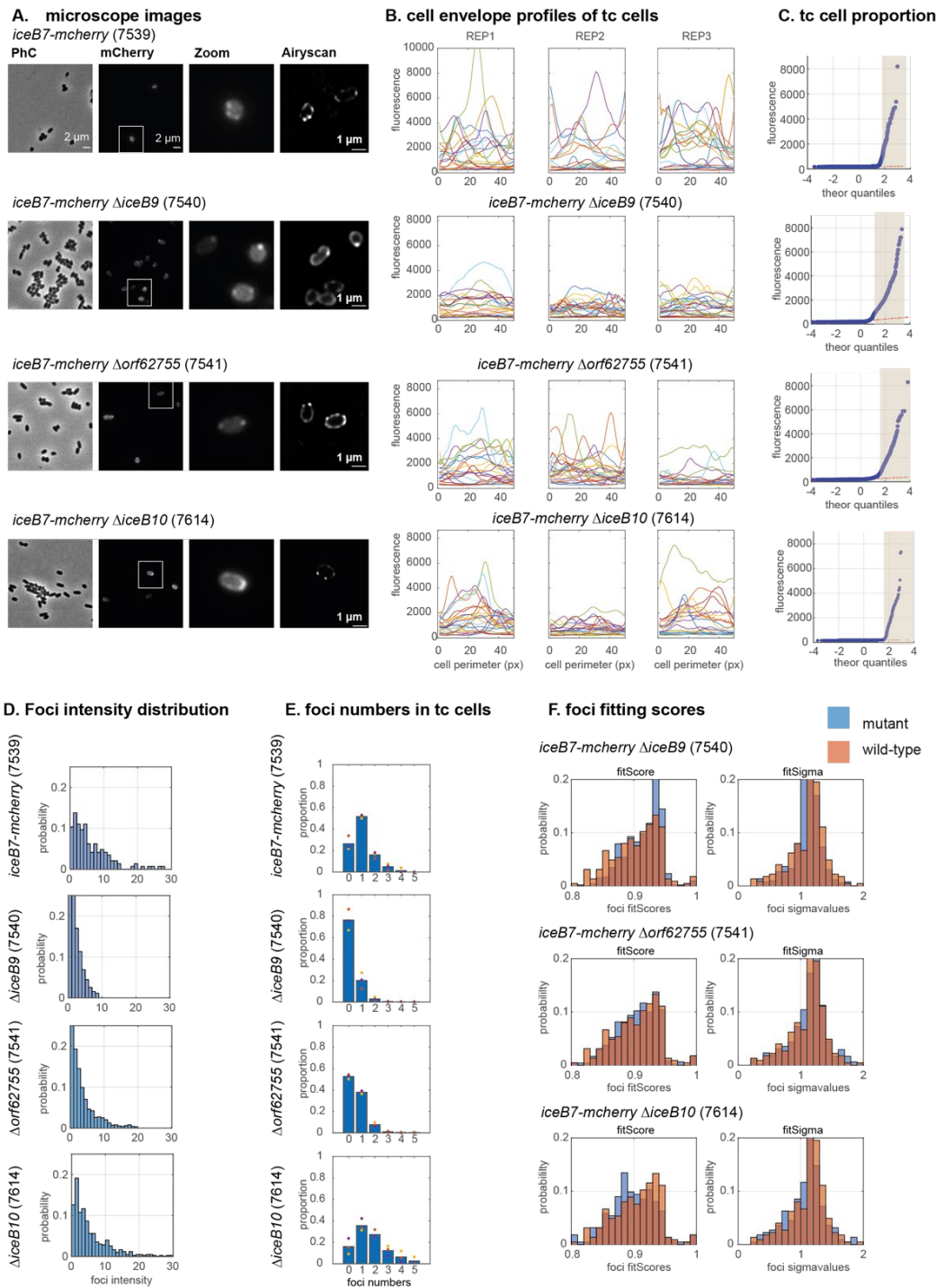
A) *Pseudomonas putida* ICE clc expressing Orf66202-sfGFP fusion from its native location (strain 7500), imaged and analyzed in stationary phase after growth on 3-chlorobenzoate by epifluorescence microscopy for mean cell fluorescence and foci intensities. Three independent biological replicates (REP1, REP2, REP3) – all cells plotted for their observed versus expected quantile fluorescence distribution to identify the proportion of transfer competent (tc) cells (highlighted in brown shading); the extracted 1 px fluorescent signal of the cell envelopes of tc cells (shown for 25 randomly selected tc cells per replicate);

differences of the probability normalized distributions of attributed foci intensity scores for the tc and non-tc cell populations per replicate; and the mean (bars) attributed foci numbers per cell across the identified tc cell population (dots are individual replicate means). **B**) as for *P. putida* ICE*clc* expressing the *iceU*-mCherry fusion (strain 7489). **C**) as for *P. putida* ICE*clc* expressing Orf71178-mCherry (strain 7521). For the mCherry fusions no foci were detectable in non-tc cells because of its lower fluorescence background in *P. putida* than sfGFP fusions.



Supplementary figure 6: Proportions of, foci numbers and intensity distributions, Gaussian foci score and calculated sigma value distributions in tc cells of wild-type or mutant *P. putida* ICElc expressing IceB4-sfGFP.

Foci analysis data for *Pseudomonas putida* ICElc expressing IceB4-sfGFP fusion from its native location (strain 7461), in wild-type or mutant backgrounds (as indicated on the top of panels A). **A)** Differences of the probability normalized distributions of attributed foci intensity scores for the tc and non-tc cell populations for one the replicate samples (threshold placed at a value of 6). **B)** Identified tc cell subpopulations (highlighted in brown shading) in one of the three independent biological replicates by quantile plotting of the observed versus expected mean cell fluorescence. **C)** Extracted mean (bars) attributed foci numbers per cell across the identified tc cell populations across three independent replicates (dots are individual replicate means). **D)** Extracted distribution of Gaussian fitting scores of detected foci in tc cells of mutants (blue) compared to wild-type (red), and **E)** of the extracted sigma values of the foci fitting (explanations of both parameters in Supplementary figure S1). P-values correspond to t-test comparisons of triplicate mutant versus triplicate wild-type values of mean, median or standard deviations of the foci-score and sigma value distributions.

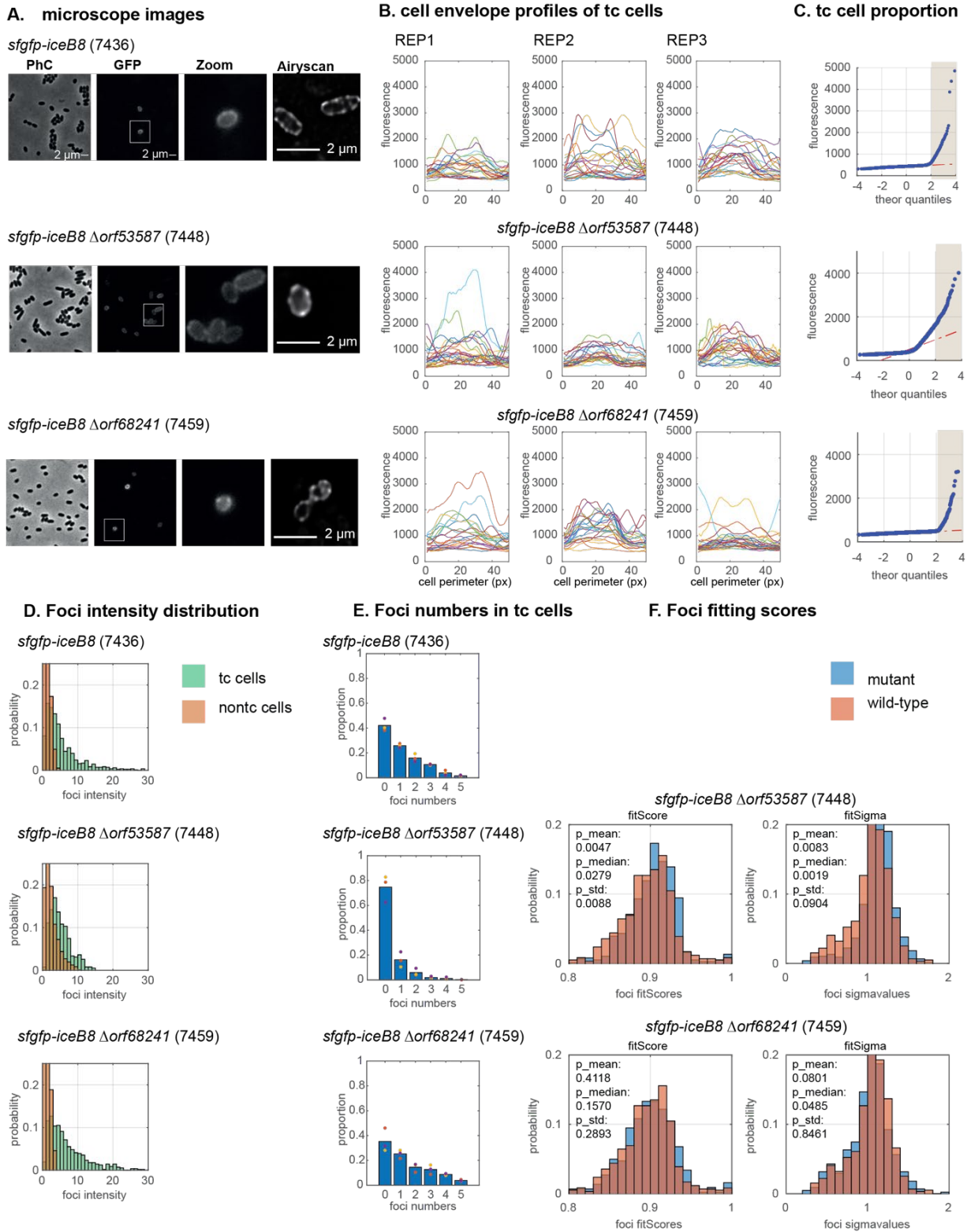


Supplementary figure 7: Dependencies of tc cell foci formation of *P. putida* ICElcIc expressing IceB7-mCherry on additional gene deletions of *iceB9*, *iceB10* or *orf62755*.

A) Visible aspect of IceB7-mCherry foci formation in *P. putida* in stationary phase after growth on 3-chlorobenzoate with a single integrated copy of (otherwise) wild-type ICElcIc::lacOarray, in comparison to additional deletions of *iceB9*, *orf62755* or *iceB10*. Micrographs as in Fig. 4 with a highlighted cell area (Zoom) from the mCherry image and a high-resolution Airyscan image (single 170-nm slice). Images are scaled to the same maximum and minimum intensities. **B)** mCherry fluorescence traces of the perimeter of 25 randomly selected individual tc cells (1-pixel outer ‘shell’) of the indicated constructs in

panel (A) on their absolute fluorescent scales. 'Peaks' correspond to foci in the cell micrographs. **C)** Identified tc cell subpopulations (highlighted in brown shading) in one of the three independent biological replicates by quantile plotting of the observed versus expected mean cell fluorescence. **D)** Differences of the probability normalized distributions of attributed foci intensity scores for the tc cell populations (shown for a single of three replicates). No foci were detectable in non-tc cells because of the low mCherry fluorescence background. **E)** Extracted mean (bars) attributed foci numbers per cell across the identified tc cell populations across three independent replicates (dots are individual replicate means).

F) Extracted distribution of Gaussian fitting scores and of the fitting sigma values of foci in tc cells of mutants (blue) compared to wild-type (red; explanations of both parameters in Supplementary figure S1).

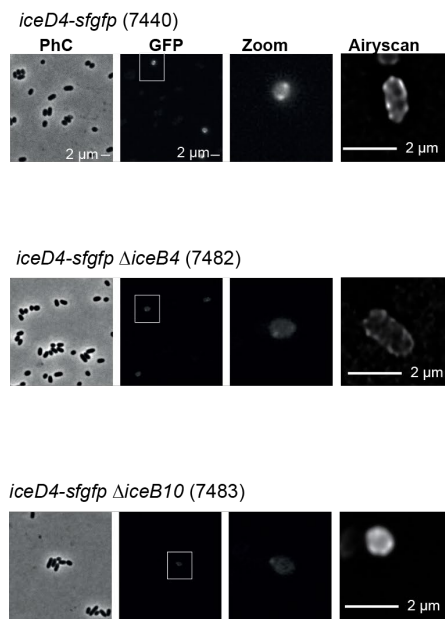


Supplementary figure 8: Dependencies of tc cell foci formation of *P. putida* ICEIcIc expressing sfGFP-IceB8 on additional gene deletions of *orf53587* or *orf68241*.

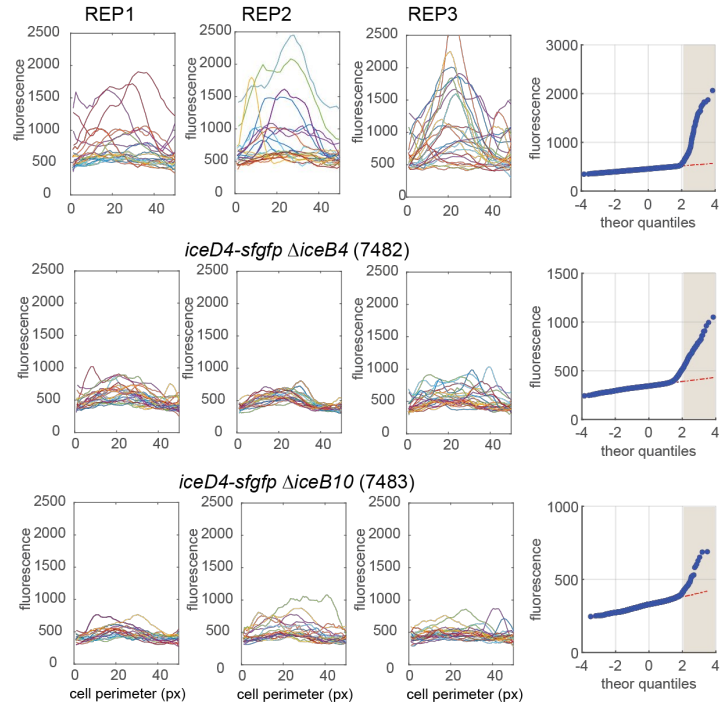
A) Visible aspect of sfGFP-IceB8 foci formation in *P. putida* in stationary phase after growth on 3-chlorobenzoate with a single integrated copy of (otherwise) wild-type ICEIcIc::lacOarray, in comparison to additional deletions of *orf53587* or *orf68241*. Micrographs as in Fig. 4 with

a highlighted cell area (Zoom) from the GFP image and a high-resolution Airyscan image (single 170-nm slice). Images are scaled to the same maximum and minimum intensities. **B)** sfGFP fluorescence traces of the perimeter of 25 randomly selected individual tc cells (1- pixel outer 'shell') of the indicated constructs in panel (A) on their absolute fluorescent scales. 'Peaks' correspond to foci in the cell micrographs. **C)** Identified tc cell subpopulations (highlighted in brown shading) in one of the three independent biological replicates by quantile plotting of the observed versus expected mean cell fluorescence. **D)** Differences of the probability normalized distributions of attributed foci intensity scores for the tc and non-tc cell populations (shown for a single of three replicates). **E)** Extracted mean (bars) attributed foci numbers per cell across the identified tc cell populations across three independent replicates (dots are individual replicate means). **F)** Extracted distribution of Gaussian fitting scores and of the fitting sigma values of foci in tc cells of mutants (blue) compared to wild-type (red; explanations of both parameters in Supplementary figure S1). P-values correspond to t-test comparisons of triplicate mutant versus triplicate wild-type values of mean, median or standard deviations of the foci-score and sigma value distributions.

A. microscope images

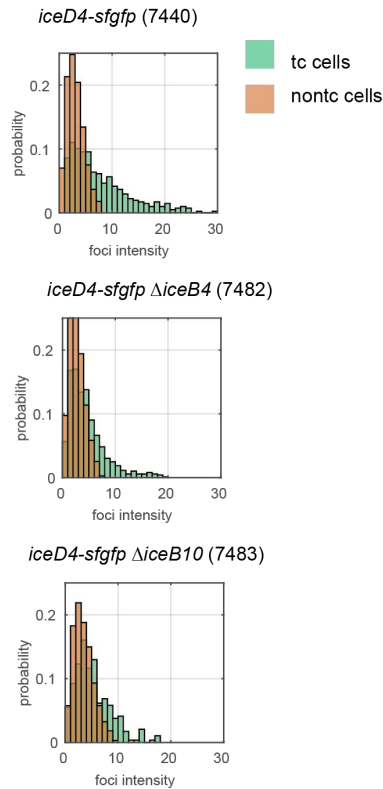


B. cell envelope profiles of tc cells

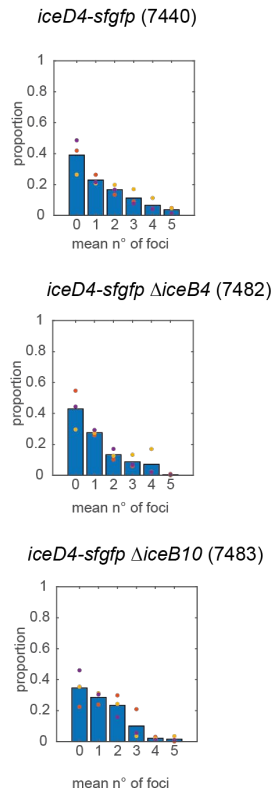


C. tc cell proportion

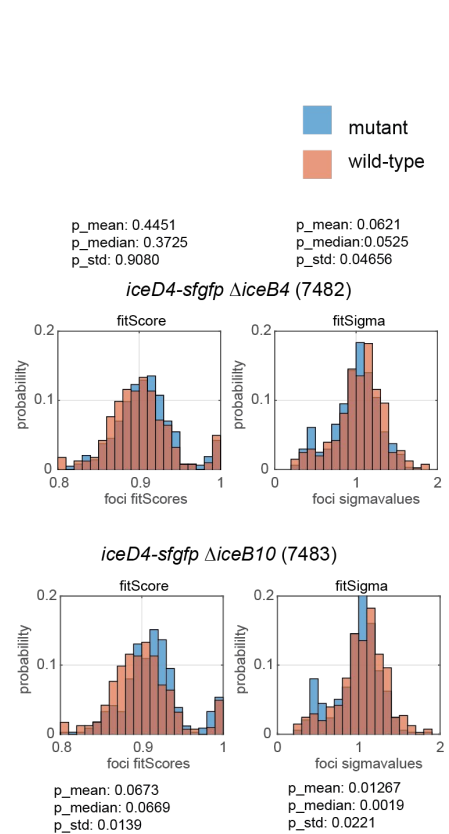
D. Foci intensity distribution



E. Foci numbers in tc cells



F. Foci fitting scores

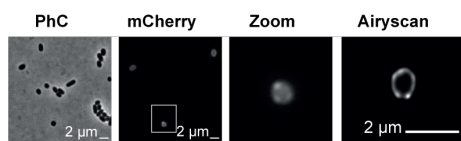


Supplementary figure 9: Dependencies of tc cell foci formation of *P. putida* ICE*cl* expressing IceD4-sfGFP on additional gene deletions of *iceB4* or *iceB10*.

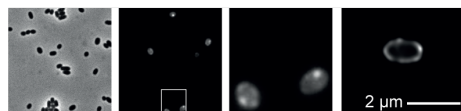
A) Visible aspect of IceD4-sfGFP foci formation in *P. putida* in stationary phase after growth on 3-chlorobenzoate with a single integrated copy of (otherwise) wild-type ICE $_{clc}::lacO_{array}$, in comparison to additional deletions of *iceB4* or *iceB10*. Micrographs as in Fig. 4 with a highlighted cell area (Zoom) from the GFP image and a high-resolution Airyscan image (single 170-nm slice). Images are scaled to the same maximum and minimum intensities. **B)** sfGFP fluorescence traces of the perimeter of 25 randomly selected individual tc cells (1- pixel outer 'shell') of the indicated constructs in panel (A) on their absolute fluorescent scales. 'Peaks' correspond to foci in the cell micrographs. **C)** Identified tc cell subpopulations (highlighted in brown shading) in one of the three independent biological replicates by quantile plotting of the observed versus expected mean cell fluorescence. **D)** Differences of the probability normalized distributions of attributed foci intensity scores for the tc and non-tc cell populations (shown for a single of three replicates). **E)** Extracted mean (bars) attributed foci numbers per cell across the identified tc cell populations across three independent replicates (dots are individual replicate means). **F)** Extracted distribution of Gaussian fitting scores and of the fitting sigma values of foci in tc cells of mutants (blue) compared to wild-type (red; explanations of both parameters in Supplementary figure S1). P-values correspond to t-test comparisons of triplicate mutant versus triplicate wild-type values of mean, median or standard deviations of the foci-score and sigma value distributions.

A. microscope images

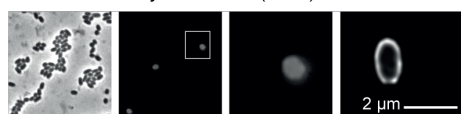
orf55476-mcherry (7492)



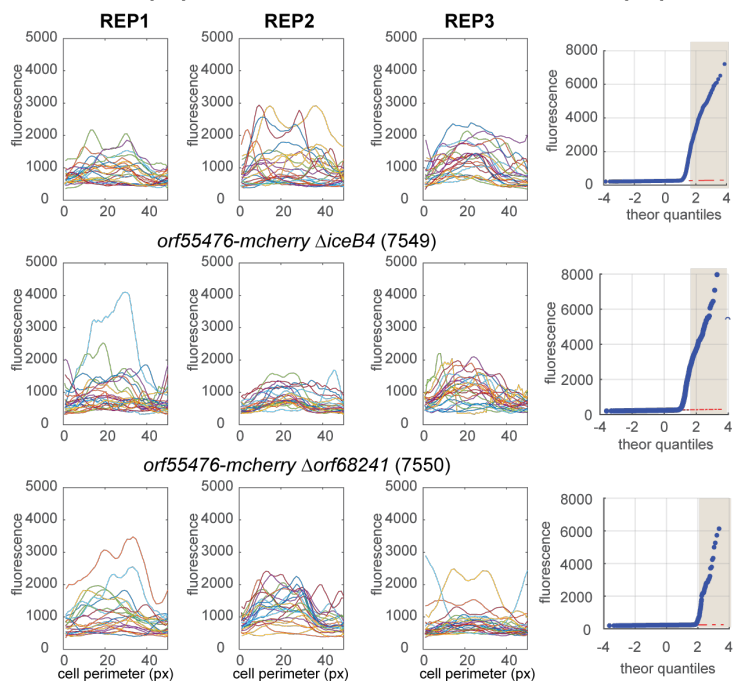
orf55476-mcherry ΔiceB4 (7549)



orf55476-mcherry Δorf68241 (7550)

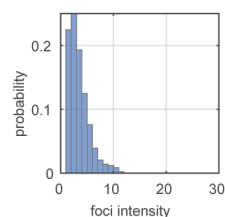


B. cell envelope profiles of tc cells

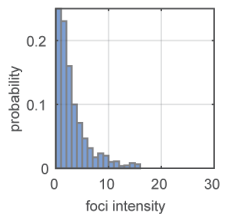


D. Foci intensity distribution in tc cells

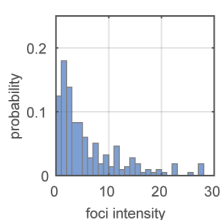
orf55476-mcherry (7492)



orf55476-mcherry ΔiceB4 (7549)

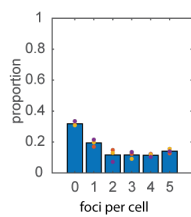


orf55476-mcherry Δorf68241 (7550)

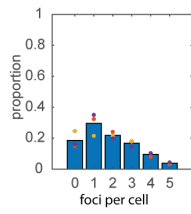


E. foci numbers in tc cells

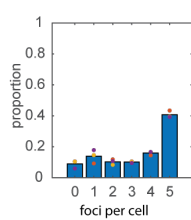
orf55476-mcherry (7492)



orf55476-mcherry ΔiceB4 (7549)

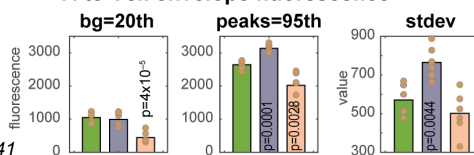


orf55476-mcherry Δorf68241 (7550)

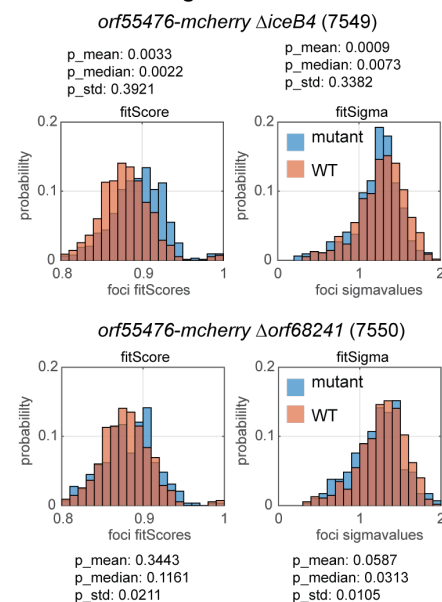


■ WT
■ $\Delta iceB4$
■ $\Delta orf68241$

F. tc Cell envelope fluorescence



G. foci fitting scores



Supplementary figure 10: Dependencies of tc cell foci formation of *P. putida* ICE clc expressing Orf55476-mCherry on additional gene deletions of *iceB4* or *orf68241*.

A) Visible aspect of Orf55476-mCherry foci formation in *P. putida* in stationary phase after growth on 3-chlorobenzoate with a single integrated copy of (otherwise) wild-type

ICE $clc::lacO_{array}$, in comparison to additional deletions of *iceB4* or *orf68241*. Micrographs as in Fig. 4 with a highlighted cell area (Zoom) from the mCherry image and a high-resolution Airyscan image (single 170-nm slice). Images are scaled to the same maximum and minimum intensities. **B)** mCherry fluorescence traces of the perimeter of 25 randomly selected individual tc cells (1-pixel outer 'shell') of the indicated constructs in panel (A) on their absolute fluorescent scales. 'Peaks' correspond to foci in the cell micrographs. **C)** Identified tc cell subpopulations (highlighted in brown shading) in one of the three independent biological replicates by quantile plotting of the observed versus expected mean cell fluorescence. **D)** Differences of the probability normalized distributions of attributed foci intensity scores for the tc cell populations (shown for a single of three replicates). **E)** Extracted mean (bars) attributed foci numbers per cell across the identified tc cell populations across three independent replicates (dots are individual replicate means). **F)** Quantified cell envelope fluorescence features. Mean bg, mean of median 20th percentile cell envelope fluorescence values from biological replicates (n=3, two 1-px outer shells). Peaks, mean of the 95th percentiles. Stdev, mean of the calculated standard deviations. Values within bars report the calculated p-value in one-tailed t-test to wild-type with the means driving the direction of the alternative hypothesis. **G)** Extracted distribution of Gaussian fitting scores and of the fitting sigma values of foci in tc cells of mutants (blue) compared to wild-type (red; explanations of both parameters in Supplementary figure S1). P-values correspond to t-test comparisons of triplicate mutant versus triplicate wild-type values of mean, median or standard deviations of the foci-score and sigma value distributions.

Chapter 3

Identification of the ICEc/c conjugative pilus and *in vivo* visualization

Andrea Daveri, Valentina Benigno, Jan Roelof van der Meer

Abstract

Horizontal gene transfer by conjugation relies on a multiprotein complex to transfer the (DNA) substrate from a donor to a recipient cell. One of the requirements for successful conjugation is cell to cell contact. Conjugative pili play an important role in this process. By extending into the extracellular environment, they can scan for recipient cells. Once a contact is established, the pilus can depolymerise and bring the cells closer until their membranes touch. A small number of plasmid conjugative pili have been characterized, but none so far from ICE systems. Previous studies suggested two ICE*clc* essential transfer genes to be involved in pilin formation, namely *orf66625* and *orf67231*. By 3D protein structure prediction, fluorescent and cryo-tomography cell imaging, we now provide evidence for the major pilin of ICE*clc* to be encoded by *orf66625*. In contrast, Orf67231-fluorescent protein fusions presented multiple foci around the perimeter of *Pseudomonas putida* ICE*clc* transfer competent cells, the large majority of which did not overlap with IceD4-fluorescent protein fusions. The ICE*clc* conjugative pilus is thus most likely build-up of Orf66625 subunits, whereas *orf67231* likely codes for a periplasmic protein that associates to the T4SS structure.

Introduction

Conjugation is one of the three main mechanisms of horizontal gene transfer and plays a major role in bacterial evolution (1), by spreading gene functions with potential adaptive benefit, such as antimicrobial resistance determinants or catabolic pathways (2). Conjugation is mostly known from plasmids, but is also carried out by integrative and conjugative elements (ICE), which encode all the necessary parts for transfer of their own DNA (3). Conjugative transfer between two bacterial cells requires a macromolecular protein complex known as the Type IV Secretion System (T4SS), which is typically composed of 12-20 different subunits; each present in multiple copies (depending on the type of element) (4,5). The T4SS macromolecular complex in gram-negative bacteria can be divided into four subassemblies: (i) the cytoplasmic ATPase complex, usually composed of three subunits including the DNA coupling protein; (ii) the inner membrane complex (IMC); (iii) the outer membrane complex (OMC); and (iv) a conjugative pilus. The pilus is a multimer composed of a major pilin subunit and possibly a minor pilin subunit located at the pilus tip (6). Conjugative pili play a key role in conjugation. They are thought to scan for the presence of recipient cells and enable the formation of the mating junction (7). This process would occur by retraction (depolymerization) of the pilus until contact between the donor-recipient cell envelopes is established. An alternative hypothesis, whereby single stranded DNA (ssDNA) is transferred by the F-pili to recipient cells not in direct contact with donors, has also been reported, but at lower frequencies (8).

In this work, we focused on the characterization of the pilin of the ICE*clc*, a mobile element integrated in one (*Pseudomonas putida*) or two copies (*Pseudomonas knackmussii* B13) in the chromosome. We recently described the genes encoding the T4SS of ICE*clc*, located in a 20 kb conserved region between its *orf53587* and *orf73676* (9,10). Fourteen out of 24 genes in this region were essential for ICE*clc* transfer, some of which showed low but discernable homologies to other known T4SS conjugation systems, whereas others appeared unique. A previous comparative study for the classification of T4SS in bacterial genomes (11), suggested two small ICE*clc*-open readings frames named *orf67231* and *orf66625* to constitute potential pilin candidates. In order to confirm their roles in ICE*clc* pilin formation, we followed an approach of dynamic fluorescent imaging, similar as was conducted for other pili systems (12,13), complemented by cryo-tomography of *P. putida* ICE*clc* transfer competent cells. To enable cysteine-maleimide-conjugated fluorescent staining (14,15) we identified potential solvent accessible residues in both Orf67231 and Orf66625 and mutated those to cysteine. In addition, we produced variants with single or double Cys-residues at the C-terminal end of Orf66625. All mutants in *P. putida* were tested for ICE*clc* transfer rates, and

single transfer competent cells were imaged for fluorescently stained cell appendices. These experiments were conducted in presence or absence of recipient cells, to determine whether pilin dynamics would be different when donors could potentially establish cell-cell contacts for ICE conjugation. Studies were complemented by imaging of cells with (viable, transfer-neutral) translational fusion of *orf67231* to a fluorescent protein to study localisation of subcellular labeled complexes and in colocalisation with another labeled T4SS subunit. Finally, we used cryo correlated fluorescence microscopy and cryo-tomography to find evidence for pili appendices on *P. putida* transfer competent cells.

Materials and Methods

Strains and culture conditions

Escherichia coli DH5 α λ pir was used for cloning of ICE*clc* genes and plasmid amplification, and was grown at 37 °C on Luria-Bertani (LB) liquid or agar-solidified broth. *P. putida* UWC1-ICE*clc*::*lacO*_{array} was used as host of the ICE, carrying a single copy ICE*clc* integrated at the *tRNA^{Gly}-5* gene (16). The *lacO*_{array} modification was introduced in the *amnB* gene of the ICE with the purpose to follow single-copy ICE-DNA transfer, if needed (16). *P. putida* UWC1 Tn7 P_{tac}-*mcherry* was used as recipient for conjugation experiments. *P. putida* was cultured at 30 °C either on LB, or nutrient agar (NA, Oxoid) or on minimal medium (MM, type 21C (17)). MM was supplemented with either 5 mM succinate or 3 mM 3-chlorobenzoate (3-CBA) as sole carbon source. Both *E. coli* and *P. putida* were cultured aerobically in shaking flasks. Where necessary for plasmid maintenance or for selection of genomic constructs, antibiotics were added at the following concentrations: kanamycin (Km, 50 μ g mL⁻¹), ampicillin (Amp, 100 μ g mL⁻¹ for *E. coli*, 500 μ g mL⁻¹ for *P. putida*), tetracycline (Tc, 20 μ g mL⁻¹ for *E. coli*, 50 μ g mL⁻¹ for *P. putida*), or gentamycin (Gm, 20 μ g mL⁻¹, 10 μ g mL⁻¹ in MM). The following supplements were added for insert screening or promoter induction (see below): 5-bromo-4-chloro-3-indolyl- β -D-galactopyranoside (X-Gal; 20 μ g mL⁻¹), isopropyl- β -D-1-thiogalactopyranoside (IPTG, 0.5 mM), or m-toluate (15 mM). All produced strains are listed in Supplementary table S1.

DNA manipulations

DNA manipulations followed standard procedures as indicated by the reagent supplier. Plasmids were purified from *E. coli* DH5 α λ pir using NucleoSpin Plasmid kits (Macherey-Nagel, Duren, Germany). Oligonucleotide primers were purchased from SigmaAldrich. PCR amplicons and digested fragments were purified using NucleoSpin Gel and PCR Clean-up kits (Macherey-Nagel). Clones were

initially screened by PCR on resuspended individual colonies in a GoTaq® G2 green master mix (20 µL, Promega, Madison, United States). Plasmid fragments were assembled using the ClonExpress II One Step Cloning Kit (Vazyme, Nanjing, China), digesting the plasmid backbone with appropriate restriction enzymes (New England Biolabs, Ipswich, United States), and mixing with insert-DNA. DNA fragments were ligated overnight at 16 °C using T4 DNA Ligase (New England Biolabs). All constructed plasmid inserts were sequenced prior to further use in *P. putida*, to verify their correctness, using the ICE*clc* sequence as a reference (18) (GenBank AJ617740.2). Plasmids are listed in Supplementary table S2.

Protein homology assignments.

The Alphafold 2 platform was used to produce 3D models of both Orf66625 and Orf67231 based on their primary structure (deploying default settings on the web server platform https://colab.research.google.com/github/sokrypton/ColabFold/blob/main/beta/AlphaFold2_advanced.ipynb). The two models were then compared against the PDB database to find potential structural similarities with known proteins, either using PDBeFold (19) or Dali (20). Both database comparisons were run with default parameters. Amino acids on the structures potentially exposed to the 'outside' solvents were predicted with NetSurfP-2.0 (21).

Site-directed mutagenesis for cysteine replacements

To introduce cysteine mutations in *orf66625* and *orf67231* we used double recombination with marker counterselection (22) combined with PCR site-directed mutagenesis. We specifically targeted here amino acids that were solvent exposed (predicted with NetSurfP-2.0), and exclusively consisting of serine, threonine or alanine residues, as the success of staining was reported to be higher for these residues (14). We first PCR-amplified the *orf66625* and *orf67231* reading frames including 1 kb up- and downstream regions from ICE*clc*, and cloned each fragment into plasmid pEMG (22). In order to introduce the site-specific mutation, we designed appropriate overlapping reverse complementary primers, which included the mutated codon (now coding for a cysteine) and were 5' phosphorylated. Subsequently, we PCR-amplified the full length plasmid using Q5 high-fidelity polymerase, digested the product with DpnI to selectively degrade the parental (non-methylated) DNA (23), purified the remaining DNA, ligated overnight and transformed the mixture into *E. coli* DH5α λ*pir*. Recovered plasmids from between 8 and 16 *E. coli* transformants were then sequenced to confirm the presence of the mutation. Successful plasmids were subsequently electroporated into relevant *P. putida* UWC1 ICE*clc* backgrounds (Table S1). Single recombinants

(from pEMG insertion) were selected on plates with Km^R, and colonies were verified by PCR for integration of the suicide vector. Positive clones were then transformed with 50 ng of plasmid pSW (22), and transformants were induced for 16 h in 10 mL LB, Amp⁵⁰⁰ by adding 15 mM *m*-toluate. This leads to expression of the I-SceI nuclease encoded on pSW, cutting the unique site on pEMG, and forcing chromosomal repair. After induction, the cultures were diluted and spread on LB agar plates without antibiotics. Individual colonies were verified by PCR for double recombination and sequenced to verify the exactness of the mutation. Mutated clones were subsequently cultured in absence of antibiotics to cure the pSW vector and were finally stored at –80 °C with 15% v/v glycerol. Primers used for mutations are listed in supplementary table S3.

Fluorescent protein fusions

A similar strategy as described above was PCR and double recombination followed by marker exchange were used to translationally fuse the *mcherry* reading frame at the 3'-terminal region of *orf67231* (directly at its native position on ICE*clc*). In this case we cloned into the pEMG suicide vector the up- and downstream flanking regions interspersed by the *mcherry* open reading frame. To avoid folding difficulties, a short linker peptide was introduced between the two genes as described in ref. (24). The fluorescent protein was inserted before the stop codon of the target gene, without disturbing the ribosome binding site of the downstream-located gene on ICE*clc*. Primers used for the amplification of the homology regions and fluorescent proteins are listed in Supplementary table S3. A *P. putida* codon-optimized coding sequence for mCherry was designed by Jcat (25) and synthesized by ThermoFisher (Waltham, USA). Fluorescently labelled *P. putida* strains were grown to stationary phase in liquid MM supplemented with 3 mM 3-CBA to induce ICE*clc* transfer competence as described before (26).

Maleimide-conjugated dye staining

Alexa Fluor™ 488 C5 Maleimide (ThermoFisher Scientific) was dissolved in dimethylsulfoxide (DMSO; 1 mg mL⁻¹) and stored at –20 °C, protected from light. Strains used for staining were grown at 30 °C in MM with 3 mM 3-CBA for 72 h in shaking flasks to induce ICE*clc* transfer competence. A volume of 80 µL of cell suspension was mixed with the dye to a final concentration of 25 µg mL⁻¹ according to Ref (14), and left in the dark for 15 minutes at room temperature. To avoid shearing of pili from the cell surface, the excess of dye was removed by pipetting 50 µL stained cells on top of a 0.2-µm cellulose acetate filter (25 mm, Ø) (HUBERLAB, Aesch, Switzerland), previously sterilized and posed on a 1.5% MM agarose plate (without carbon source). Once the excess of staining solution

drained through the filter, the cells on the filter were rinsed by pipetting a droplet of 30 μL of MM (without carbon source), and letting this being absorbed by the agarose. When the filter surface seemed visually dry, filters were removed from the surface and placed upside down on an 1% ultra-pure agarose (ThermoFisher Scientific) patch (10 mm, \emptyset), to gently transfer cells from the filter to the agarose surface. Agarose patches were then subsequently turned upside down and mounted between glass cover slips for imaging (see below).

Fluorescence microscopy

Five μL of cell suspension for imaging were deposited and gently spread on top of a 1-mm thick 1%-agarose in MM “patch” (\emptyset 1 cm), which was enclosed in an imaging chamber (Perfusion Chamber, H. Saur Laborbedarf, Germany) as described in ref. (27). Patches were amended with 1 mM 3-CBA. A Nikon Eclipse Ti inverted microscope, installed in a controlled temperature room (22 °C), was used for standard snapshot and time-lapse epifluorescence imaging. The microscope was equipped with a perfect focus system (PFS), pE-100 CoolLED, a Plan Apo λ 100 \times 1.45 oil objective (Nikon) and a Hamamatsu ORCA-Flash4.0 V2 C11440-22CU camera (Hamamatsu, Hamamatsu City, Japan). GFP and mCherry channels were imaged with exposure times of 500 ms.

For higher resolution imaging, we used a Nikon AX/AX R NSPARC confocal scanning microscope equipped with a NIS 5.42.03 software, installed in a temperature (22 °C) controlled room. Samples were prepared as described above. Bacterial cells were located on the patches using brightfield, after which Z-stacks ($Z=0.17$ nm, 14 layers) were acquired on an area of 78.14 μm^2 in both GFP and/or mCherry channels. Exposure time was set to 2s per channel and layer in case of Z-stacks and reduced to 500 ms in case of time-lapse. Maleimide-stained samples were also imaged in time-lapse modes on the Nikon NSPARC for a duration of 10 minutes with 30-s intervals between frames. Images were cropped and maximum-minimum fluorescent intensities were set to the same values in Fiji (28). After which the resolution was set to 350 ppi in Photoshop and saved as 8 bit Tiff files.

Cell culture and preparation for cryo-EM

P. putida UWC1 ICE clc , *iceB7-mcherry*, *iceB4-sfgfp* donor strain and recipients were precultured overnight in 10 mL of LB. After measuring the culture turbidity, the two cell types were mixed in a 1:2 ratio and 8 μL drops were placed on top of a regular 80-mm diameter agarose (1.5% w/v) plate with 1 mM 3CBA, which was incubated at 30 °C for 72 h to ensure formation of tc donor cells. Cells were recovered after three days of incubation by using a plastic loop, and were gently resuspended

in 50 μ L of MM without carbon source, into which were further mixed a 10-nm gold beads suspension at 1:8 dilution from the stock (Aurion, Ede, Netherlands).

Four μ L of cell suspension was then pipetted on top of glow-discharged 3 mm copper grids (Quantifoil 200 mesh Copper, 2 μ m holes). Excess liquid was removed after 6 s by blotting to a filter paper at the bottom side, after which bacteria on the grids were plunge-frozen in liquid ethane. For sample freezing we used a Leica automatic plunge freezer EM GP2 machine cooled down to -180°C with liquid nitrogen. Grids were then stored in liquid nitrogen until further imaging.

Cryo-fluorescent correlation microscopy and cryo-tomography

In order to detect *P. putida* tc cells on the grids, the stored grids were c-clipped and transferred into an appropriate sample holder (Leica Cartridge for Autogrids) for fluorescent imaging; all steps being carried out at -180°C . The microscope we used was the Leica THUNDER Imager EM Cryo equipped with a 50X objective, Leica DFC9000 GT camera and Leica LED3 light source. Z-stacks were acquired in 3 different channels: reflected light, GFP and RFP (4 ms, 100 ms, 100 ms exposure, respectively). The Z-step was set to 1 μ m and images were stitched together as a mosaic to cover most of the surface of the grid. tc Cells were identified on the basis of their stronger mCherry fluorescence expressed from the ICE clc T4SS subunit *iceB7-mcherry*, as previously explained (9). Positions of identified tc cells were recorded and used to reposition cryo-tomogram imaging in a Titan Krios G4 Cryo-TEM (ThermoFisher). The power of the electron beam was set to 300 kV, the tilt angle was set from $+60^{\circ}$ to -60° and images were acquired at steps of 2 degrees. The magnification was set to 33000 X for a resolution of 0.371 nm per pixel, and we used a range of defocus angles between -5° to -8° . Tomograms were reconstructed using IMOD 4.11 software (etomo) (29).

ICE clc conjugation experiments

ICE clc conjugation frequencies from different *P. putida* donors were quantified from isogenic mating experiments, by dividing the number of transconjugant colonies by the number of donor colonies. As donors we used *P. putida* UWC1 with a single copy ICE clc , wild-type for positive controls or with the specified modifications. As recipient we used isogenic *P. putida* UWC1 devoid of ICE clc , with a chromosomally integrated Gm resistance (Table S1). Donors and recipients were freshly plated on LB agar (with antibiotics, if necessary) from -80°C glycerol stocks and grown overnight (O/N). Three biological replicates (donors) and a single clone (recipient) were inoculated in 10 mL LB with antibiotics. The pre-cultures were grown O/N in a shaking incubator. The next day, 40 μ L of these

pre-cultures were transferred in 8 mL of MM supplemented with 3 mM of 3-CBA (donors) or 5 mM of succinate (recipient) as the unique carbon sources. After 48 h (donors on 3-CBA) or 24 h (recipients) of growth, the optical density (OD₆₀₀) of all cultures was measured, and recipient and donor suspensions were mixed in sterile vials in a 2:1 ratio (OD/OD) respectively, to a final volume of 1 mL. Donor and recipient cultures alone served as controls for the appearance of background growth on selective plates. Donor-recipient cell mixtures were centrifuged at 13,000 rpm (Thermo Scientific Fresco™ 21 Microcentrifuge) for 1 min, after which the supernatant was discarded and the cell pellet was resuspended in 1 mL of sterile MM (without carbon source). The suspension was centrifuged as before and cell pellets were now resuspended in 20 µL of MM. The suspension was transferred on top of a 0.2-µm, 25 mm ø cellulose acetate filter (Huberlab), that had been placed on a MM agar plate with 0.5 mM 3-CBA. Matings were incubated at 30 °C for 48 h, after which cells were washed from the filters with 1 mL MM. Cell suspensions were tenfold serially diluted and 5 µL aliquots of every dilution were dropped and dried on MM-agar with 3 mM 3-CBA to select for the donor alone, on MM-agar with 5 mM succinate and Gm to select for the recipient, and on MM-agar with 3 mM 3-CBA and Gm to select for the transconjugants. Plates were incubated at 30 °C until colonies appeared. ICEc/c transfer rates were then calculated as the ratio of the number of transconjugant colonies per filter and that of the donor.

Results

Identification of the ICE*clc* pilin protein

Previous work by Guglielmini et al. provided a novel classification of T4SS in bacteria (Guglielmini et al. 2014). Among others, their analysis predicted low homology between the *virB2* gene, which encodes for the major pilin of the *Agrobacterium tumefaciens* Ti plasmid T4SS, and two genes, *tfc9* and *tfc10*, found in the ICE*Hin10810* of *Haemophilus influenzae* (Fig. 1A). This suggested that both could be pilins. ICE*Hin10810* is similar to ICE*Hin1065*, whose gene products Tfc9 and Tfc10 were previously shown to display 28-33% amino acid similarity to Orf67231 and Orf66625 of ICE*clc* (10). Consequently, we considered these two genes as potential candidates to encode pilins of the ICE*clc* T4SS (Fig. 1B). Further sequence comparison and structure prediction suggested that *orf66625* may be the most likely candidate for a conjugative pilus (Fig. 1C). For this reason, we renamed *orf66625* to *iceB2*, following the *virB*- nomenclature of the *A. tumefaciens* pTi plasmid T4SS (*virB2*, being the major pilin of the system). The *orf67231* gene product did not show any predicted structural homology to known conjugative pili, but only to a viral major capsid protein (Fig. 1D). Its deletion had resulted in a 40-fold decrease in ICE*clc* transfer efficiency (9). For this reason, we presumed that Orf67231 plays an important role in ICE transfer and, given the close vicinity of its gene to *iceB2*, potentially in pili formation. We decided to include it in the investigations described below.

IceB2 cysteine modification for chemical labelling

In order to potentially visualize the localization of both IceB2 and Orf67231 *in vivo* at single cell level, we attempted both fluorescent protein translational fusions and maleimide-staining. Maleimide staining was developed by Ellison and collaborators (14) and is based on chemical labelling of extracellular cysteines with a maleimide-conjugated fluorophore (15). IceB2 already contains a Cys at position 74 (Fig. 2A). However, its predicted relative solvent accessibility (RSA) value is 0.27; suggesting it is poorly accessible for the chemical staining. Therefore, we considered replacing five different residues for targeted replacement to Cys. Three of these were Thr-residues (T39, T42 and T116) and two were Ala-residues (A99 and A115). Of these, we only managed to recover substitutions of T39C and T42C (Table 1, Fig. 2A, Table S4), suggesting the other impair viability of the host.

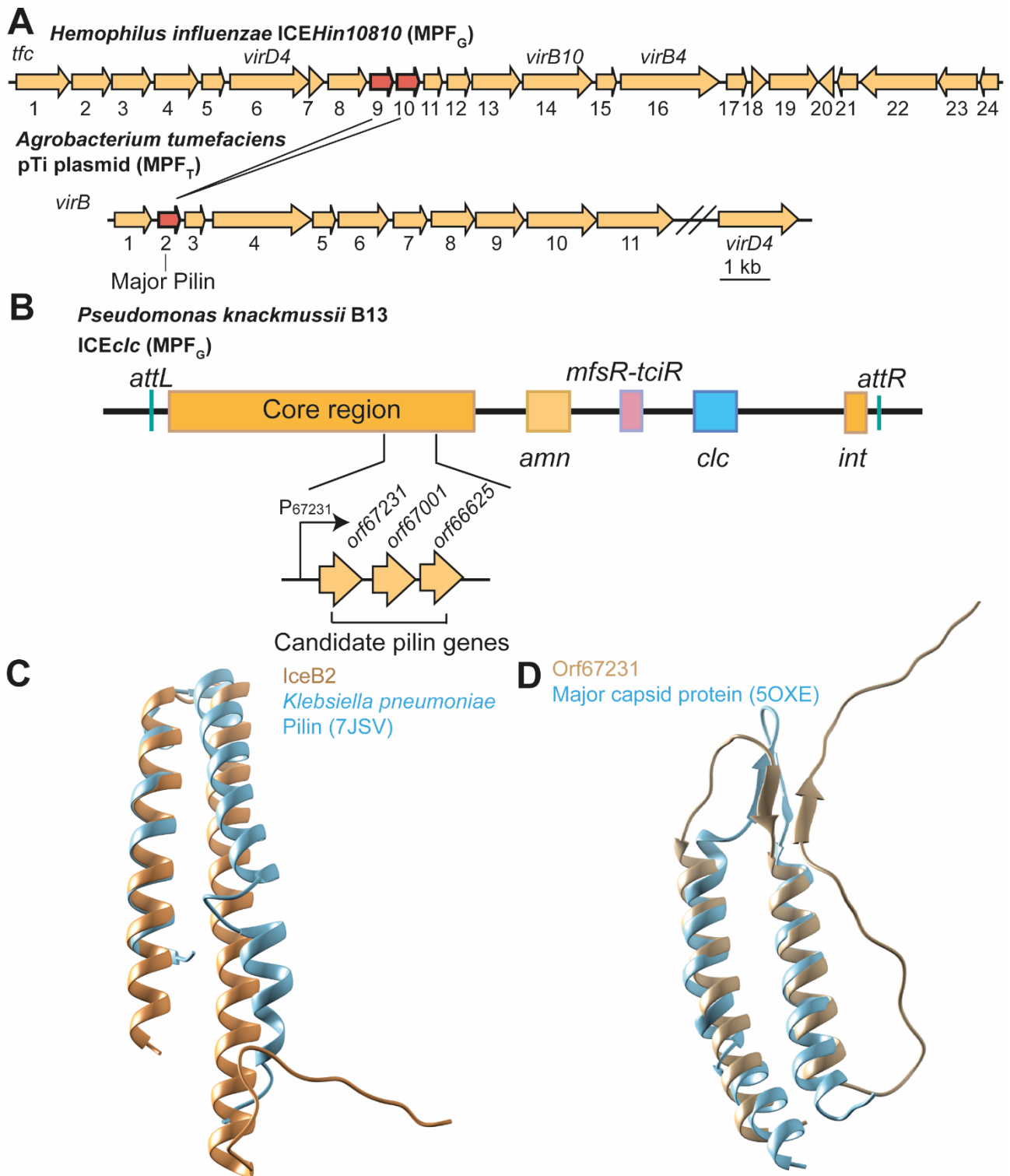


Figure 1 Schematic representation of T4SS pilin loci in different mobile elements. **A)** Comparison between the T4SS pilin locus of the *A. tumefaciens* Ti plasmid and the the ICEHin10810 element of *H. influenzae*. Low homologies between *virB2* of the pTi plasmid and *tfc9* and *tfc10* of ICEHin10810 are colored in red. **B)** Schematic representation of ICEclc element, with a detail of the region containing the two candidate pilin genes *orf67231* and *orf66625*. **C)** 3D structure overlap of IceB2 (Gold, AlphaFold2 prediction) and the *Klebsiella pneumoniae* conjugative pilin subunit (Light blue, PDB: 7JSV). The signal peptide of IceB2 was removed from the 3D model. **D)** 3D structure overlap of Orf67231 (Beige, AlphaFold2 prediction) and the *Aeropyrum pernix* virus 1 APBV1 conjugative pilin subunit (Light blue, PDB: 50XE). The signal peptide of Orf67231 was removed from the 3D model.

Table 1 List of the obtained cysteine modifications on Orf67231 and IceB2, showing their Relative Solvent Availability and their effect on ICE*cl*c transfer.

Protein	Mutation/Insertion	Relative Solvent Availability (RSA)	Effect on transfer
IceB2 (<i>orf66625</i>)	T39C	0.60	Abolished
	T42C	0.75	Abolished
	CYS insertion at the C-terminal (Cys1)	-	10 ⁴ fold reduction
	CYS-CYS insertion at the C-terminal (Cys2)	-	10 fold reduction
Orf67231	S63C	0.76	No effect
	A86C	0.47	No effect
	S95C	0.78	No effect

Unfortunately, also both IceB2-T39C and -T42C mutations completely abolished ICE*cl*c transfer from *P. putida* donors (Fig. 2B), which suggests their pili to be non-functional and perhaps causing misassembly of the T4SS itself. We then made two further mutations at the IceB2 C-terminal end, which seemed to contain a non-structured loop that we thought might be permissive for extension. Two extensions were made, adding either a single C-terminal Cys (IceB2-Cys1) or a tandem Cys-Cys (IceB2-Cys2; Table 1). Both strains carrying the Cys-extensions were viable, although ICE*cl*c transfer was affected – but less so than with the T39C or T42C mutations. Transfer of ICE*cl*c with IceB2-Cys1 was reduced by 10,000-fold, whereas that of IceB2-Cys2 decreased by 10-fold (Fig. 2C). Despite the transfer decrease, this would bring the IceB2-Cys2 mutant into the range to show potential stained structures on tc cells by epifluorescence microscopy.

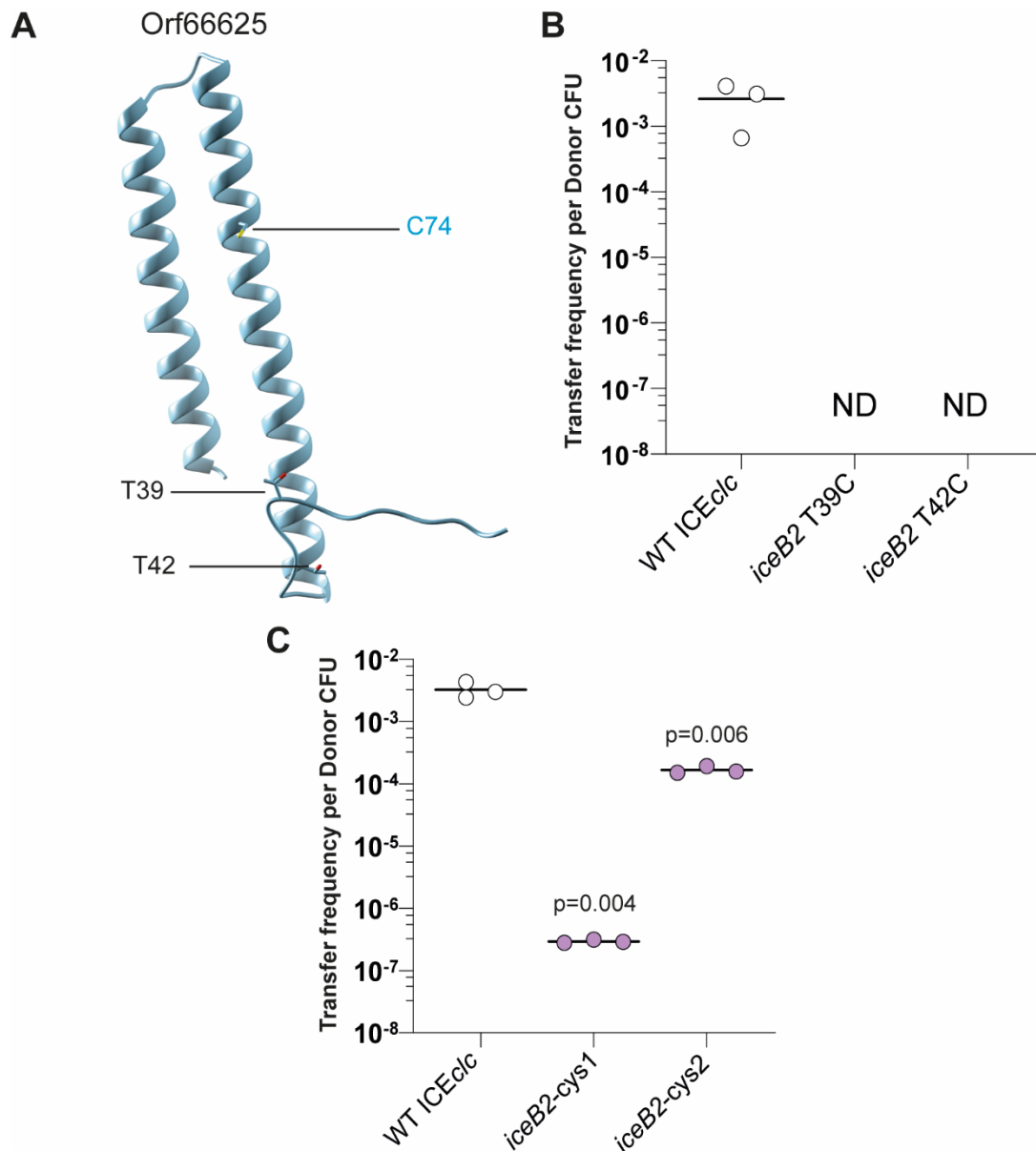


Figure 2 Effect of mutated *iceB2* on ICEclc transfer efficiency. **A)** AlphaFold2 predicted 3D model of IceB2. The positions of the targeted residues and of CYS74 (highlighted in blue) are shown. **B-C)** Effects of Cys-substitutions in IceB2 of ICEclc transfer frequencies in comparison to wild-type (WT). Black lines represent the average of three biological replicates, with individual values shown as open (WT) or filled circles (mutants). ND (below detection limit). p-Values were calculated with a two-tailed t-test between wild-type (WT) and mutant transfer rates.

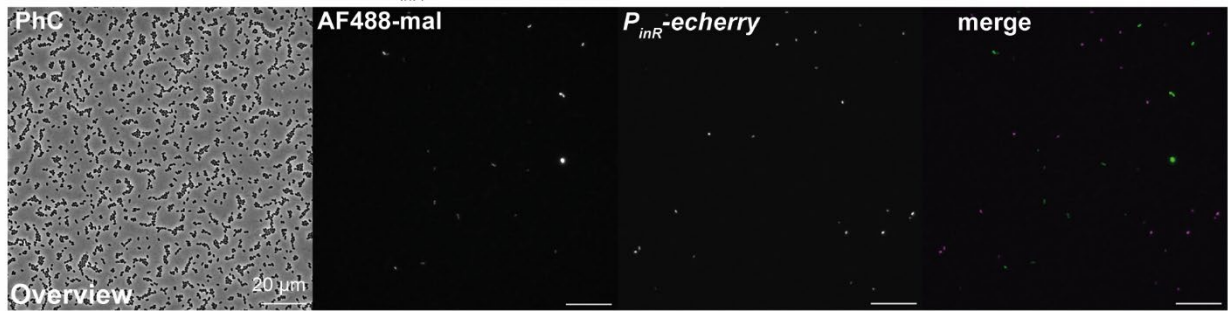
Detection and visualization of chemically fluorescently labelled IceB2 pilin

Staining of a variety of *P. putida* UWC1 strains with AF488-maleimide (AF488-mal) grown to stationary phase showed incidental presence of intracellular fluorescent foci (Fig. S1). Such foci were found in *P. putida* UWC1 itself (without ICEclc), or *P. putida* with integrated *clc* genes but without the ICE, but also in *P. putida* UWC1 ICEclc with mutations that should prevent pilus polymerization, like *iceB4* deletion, or deletion of the presumed pilin locus (*iceB2-orf67001-orf67231*); all showing a similar staining aspect (i.e., 1–3 fluorescent foci inside cells; Fig. S1). Given that AF488-mal should

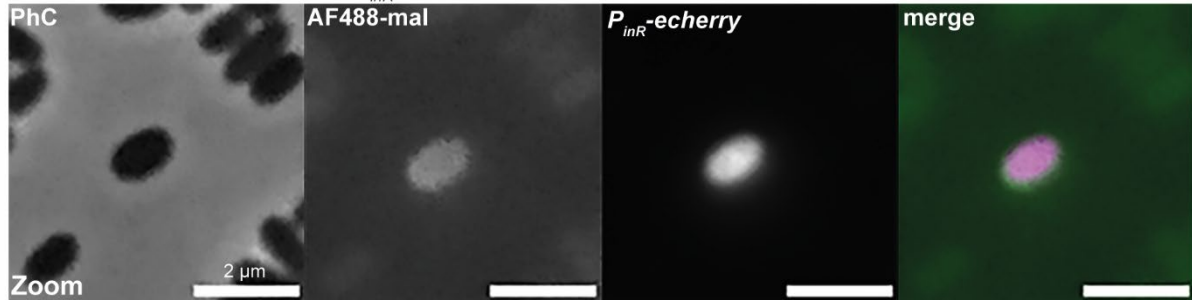
not penetrate intact cells, we assume that such incidental intracellular fluorescent foci are the result of damaged cells.

Next, we focused specifically on the AF488-mal staining of tc cells, which would be the ones where ICE lc is activated and which build the T4SS complexes (9). To enable this, we included a genetically encoded marker for tc cell formation in form of a single integrated copy of the mini-Tn5 P_{inR} -*echerry* fusion (30). *P. putida* UWC1 ICE lc cells (carrying the wild-type IceB2-Cys74 allele) were grown to stationary phase on 3CBA-medium to induce formation of tc cells (identified by their eCherry fluorescence; Fig. S2A). Only 0.36 % of 563 tc cells stained with the maleimide dye, and with little overlap (Fig. 3A-B), which was probably the result of spurious labelling of cells, perhaps those with membrane damage and penetration of the maleimide conjugate, rather than staining of extracellular protein complexes (Fig. 3B). Staining of *P. putida* UWC1 ICE lc strains with the T39C, T42C or the Cys1 substitutions was not attempted, because they showed very low to no ICE lc transfer (Table 1, Fig 2B & C). We thus turned our attention to *P. putida* UWC1 ICE lc with the *iceB2-cys2* modification, which still showed transfer, albeit at only 10% of wild-type rates. To increase the proportion of formed tc cells in stationary phase, we additionally deleted the master regulator *mfsR* (31), and tagged the resulting strain with a translational fusion between *iceB7* and *mcherry* to simultaneously identify tc cells with T4SS foci (9). Maleimide staining of the resulting *P. putida* ICE lc ::*iceB2-cys2*, *iceB7-mcherry*, Δ *mfsR* cells grown on 3CBA to stationary phase indeed showed a number of AF488-mal-specific protuberances, and exclusively on tc cells, but only on very few (Fig. 3C). Some cells displayed multiple extensions (Fig. 3C Panel 1, 3, 4), suggestive for multiple pili to be formed simultaneously. In contrast, no such structures were observed on tc cells from *P. putida* ICE lc strains with either P_{inR} -*echerry* or *iceB7-mcherry* but without IceB2-Cys2 (Fig. S2 A, B). Despite repeated attempts in time-lapse microscopy (covering 1–10 minutes, or 1–60 minutes duration), we could not observe any dynamics of protruding or retreating individual stained protuberances, as has been seen before in other systems (7,32). Although the detected AF488-mal protuberances were extremely rare in the IceB2-Cys2 strain (likely as a consequence of the reduced transfer rates), their aspect on exclusively tc cells and their absence in control strains suggest they could represent the actual (stained) ICE lc pili. Multiple simultaneous pili would then be in agreement with the multiple observed T4SS complexes with fluorescent protein translational fusions (as in (9)).

A *P. putida* UWC1 ICE $_{clc}$, Tn5 P_{inR} -mcherry (strain 7573)



B *P. putida* UWC1 ICE $_{clc}$, Tn5 P_{inR} -echerry (strain 7573)



0.36 % of tc cells stained with maleimide dye (n=563)

C *P. putida* UWC1 ICE $_{clc}$, *iceB2-cys2*, *iceB7-mcherry*, $\Delta mfsR$

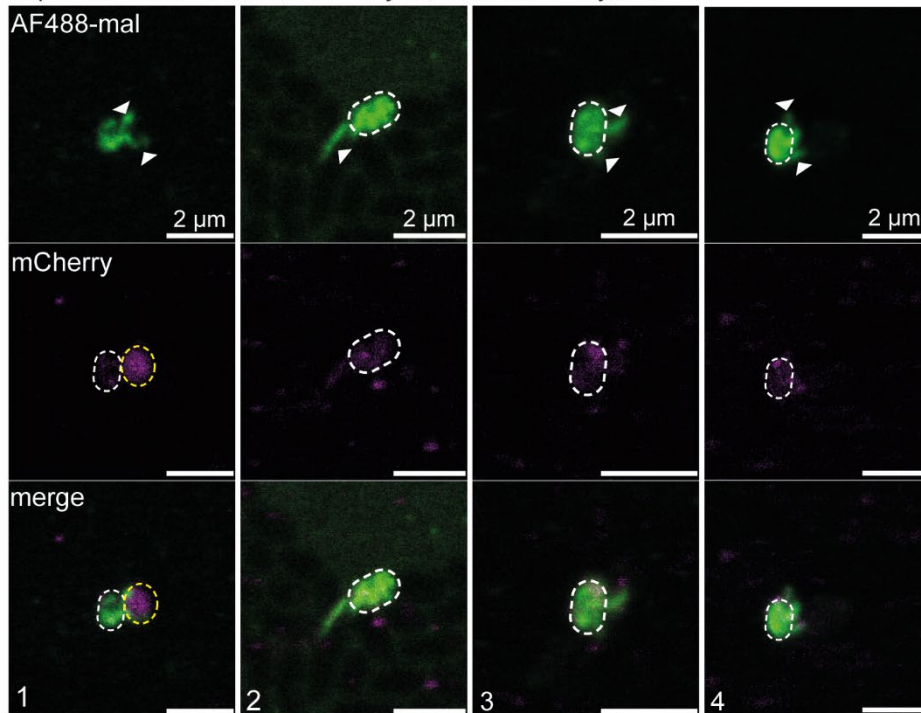


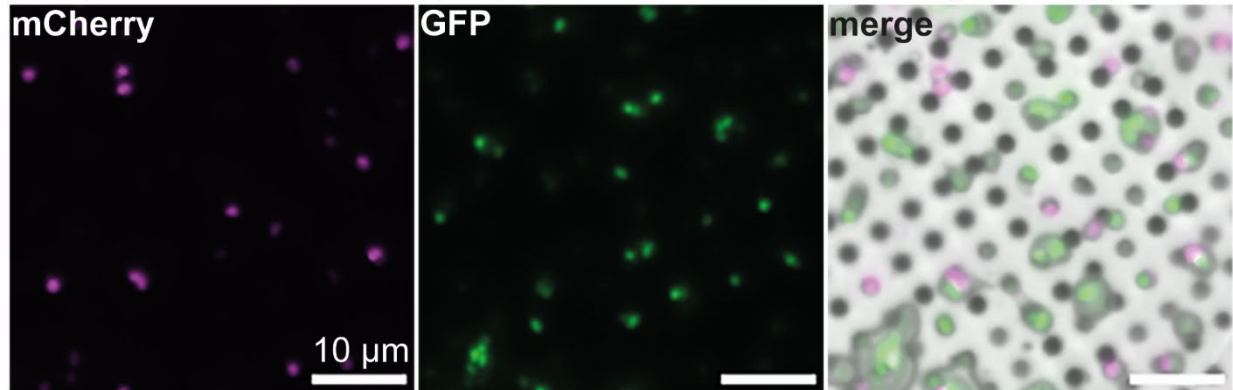
Figure 3 Examples of *P. putida* cells with AF488-mal-stained surface protuberances. **A)** Overview of a microscopy snapshot of AF488-maleimide stained *P. putida* cells grown to stationary phase in 3-CBA. Phase Contrast (PhC), AF488-mal, P_{inR} -echerry, merge. **B)** Detail of a microscopy snapshot of AF488-maleimide stained *P. putida* cells. Phase Contrast (PhC), AF488-mal, P_{inR} -mcherry, merge. **C)** Images show individual tc cells of *P. putida* UWC1 ICE $_{clc}::iceB2-cys2$, *iceB7-mcherry*, $\Delta mfsR$ sampled from stationary phase after growth on 3-CBA (white dotted line), stained with AF488-mal and exposed in mCherry wavelengths to detect tc status (merge is an overlay of both). The images in the respective fluorescent channels are scaled to the same maximum and minimum intensities. White arrows in each panel indicate fluorescent protuberances that could represent ICE-pili. The scale bar indicates 2 μ m. Note that in this imaging technique

no simultaneous phase-contrast image can be taken. Dotted cell outlines are added manually for clarity. In panel 1 recipient cells shining in mcherry channel were added to the mixture (yellow dotted line).

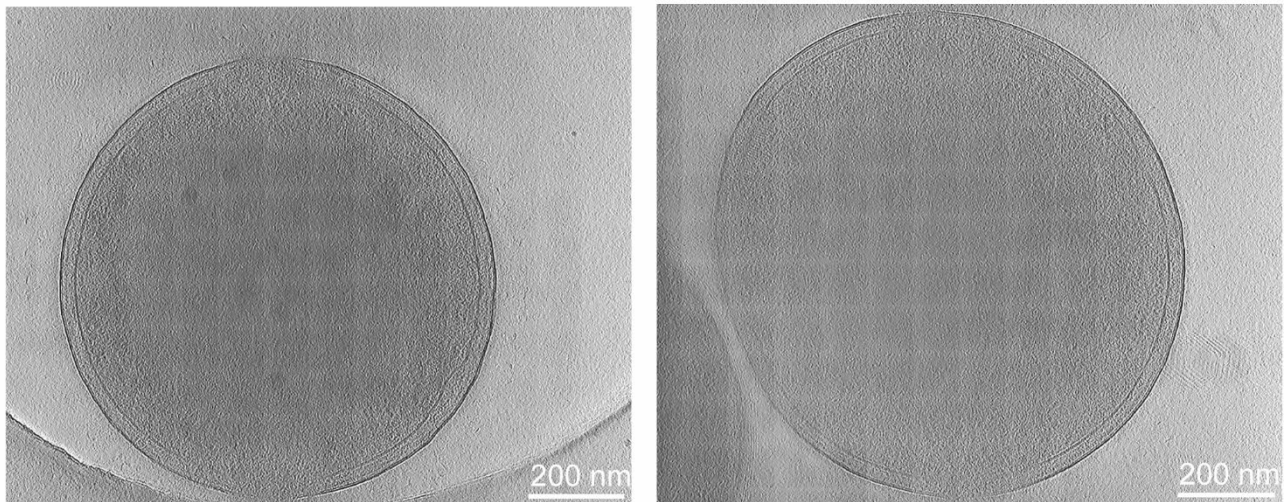
ICE clc conjugative pilus visualization in EM

In order to acquire more evidence on the pilus formation in tc cells we employed cryo electron microscopy tomography techniques. To discriminate tc cells from others, we again deployed the *P. putida* ICE clc strains with *iceB7-mcherry* or *iceB4-sfgfp* native loci replacements, and used cryo-CLEM to identify and locate tc cells on the EM-grids by epifluorescence microscopy (Fig. 4A). The same cell positions were then imaged with cryo-EM. In total we imaged 103 tc cells, some of which did not show any cell extensions in the imaged cell plane (e.g., Fig. 4B), but in some cases did (e.g., Fig. 4C overview and detail). These structures had an average width of 8 nm (Fig. 4C), which contrasted to other structures that were also sometimes captured in cryo-tomograms but that we consider represent a flagellum (15 nm average width; Fig. S3), given their very peculiar morphology. The thinner structure might thus correspond to the ICE clc conjugative pilus.

A Cryo-Fluorescence Microscopy: *P. putida* UWC1 ICE_{clc}, *iceB7-mcherry*, *iceB4-sfgfp*, $\Delta mfsR$



B Cryo-EM Tomography: *P. putida* UWC1 ICE_{clc}, *iceB7-mcherry*, *iceB4-sfgfp*, $\Delta mfsR$



C Cryo-EM Tomography: *P. putida* UWC1 ICE_{clc}, *iceB7-mcherry*, *iceB4-sfgfp*, $\Delta mfsR$

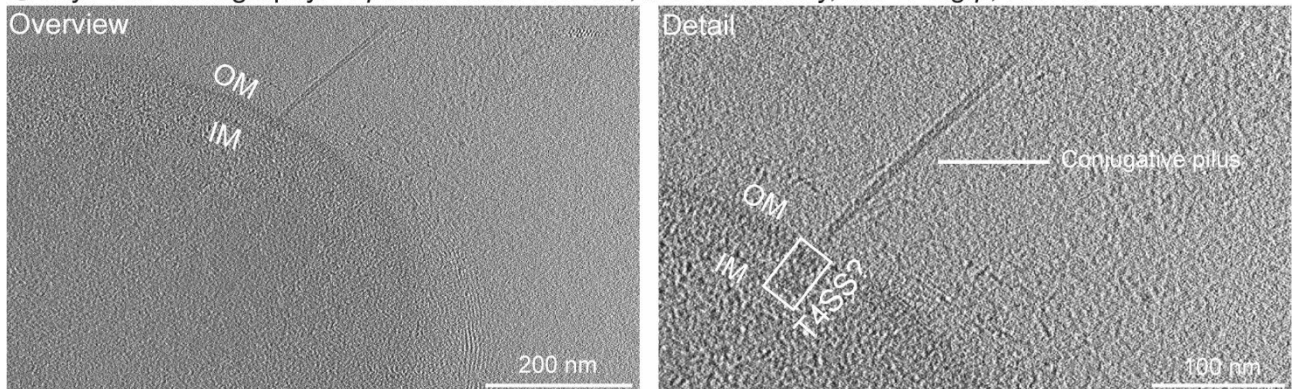


Figure 4 Cryo-EM tomography of transfer competent cells. **A)** Micrographs of cryo-preserved *P. putida* UWC1 strains with indicated fluorescent tags. mCherry, GFP and merged. **B)** Micrographs of tc cells of the indicated *P. putida* UWC1 strain imaged with cryo-EM. The single images represent a single slice of the reconstructed tomogram. The two single cells show absence of filamentous structures. **C)** Micrograph of tc cells of the indicated *P. putida* UWC1 strain. The images represent a single slice of the reconstructed tomogram. Overview and detail. OM: outer membrane, IM: inner membrane, T4SS?: possible location of the conjugative machinery. The predicted conjugative pilus is indicated in the Detail panel.

Characterisation of the potential role of Orf67231

To clarify the potential role of the second small open reading frame we identified from the homologies listed above, we again used a combination of AF488-mal staining, transfer experiments, but also fluorescent protein fusions.

In contrast to IceB2, Orf67231 does not contain any cysteine-residues. We mutated three existing Ser-, Thr-, or Ala-residues into cysteine, focusing only on those with a relative solvent availability (RSA) >0.4 predicted by NestSurfP 2.0 (21) (Fig. 5A, Table 1). In contrast to most site-directed mutants of IceB2, the produced Cys-replacements in Orf67231 did not cause a significantly different ICE clc transfer rates compared to the wild-type controls (although Ala85Cys was on average five-fold lower; Table 1, Fig 5B). This suggested that Orf67231 indeed could not be the major pilin for ICE clc transfer but had some secondary role, and therefore, may be more permissive to mutations. AF488-mal staining of *P. putida* ICE clc variants with the Orf67231 Cys-replacements additionally equipped with a single copy insertion of the *P_{inR}-echerry* to identify tc cells, showed a small number of cells with overlapping fluorescent signals (Fig. 5C). In contrast to the fluorescent protuberances seen in IceB2-Cys2 imaging, AF488-mal staining of Orf67231 showed individual membrane-located foci and stained membrane outlines, similar as had been detected for other T4SS subunit fluorescent protein fusions (Fig. 5C, 9). The proportion of tc cells co-stained with AF488-mal was 8.8% for *P. putida* with the Ser63Cys substitution, but only 3.1% and 1.4% in the Ala86Cys and Ser95Cys variants, respectively (Fig. 5D). This indicated that it is unlikely that Orf67231 forms part of an extracellular extension such as expected from a conjugative pilus. In contrast, the low occurrence AF488-mal staining among tc cells suggests surface-exposed Orf67231 protein, unless we assume that this low proportion again constitutes damaged cells.

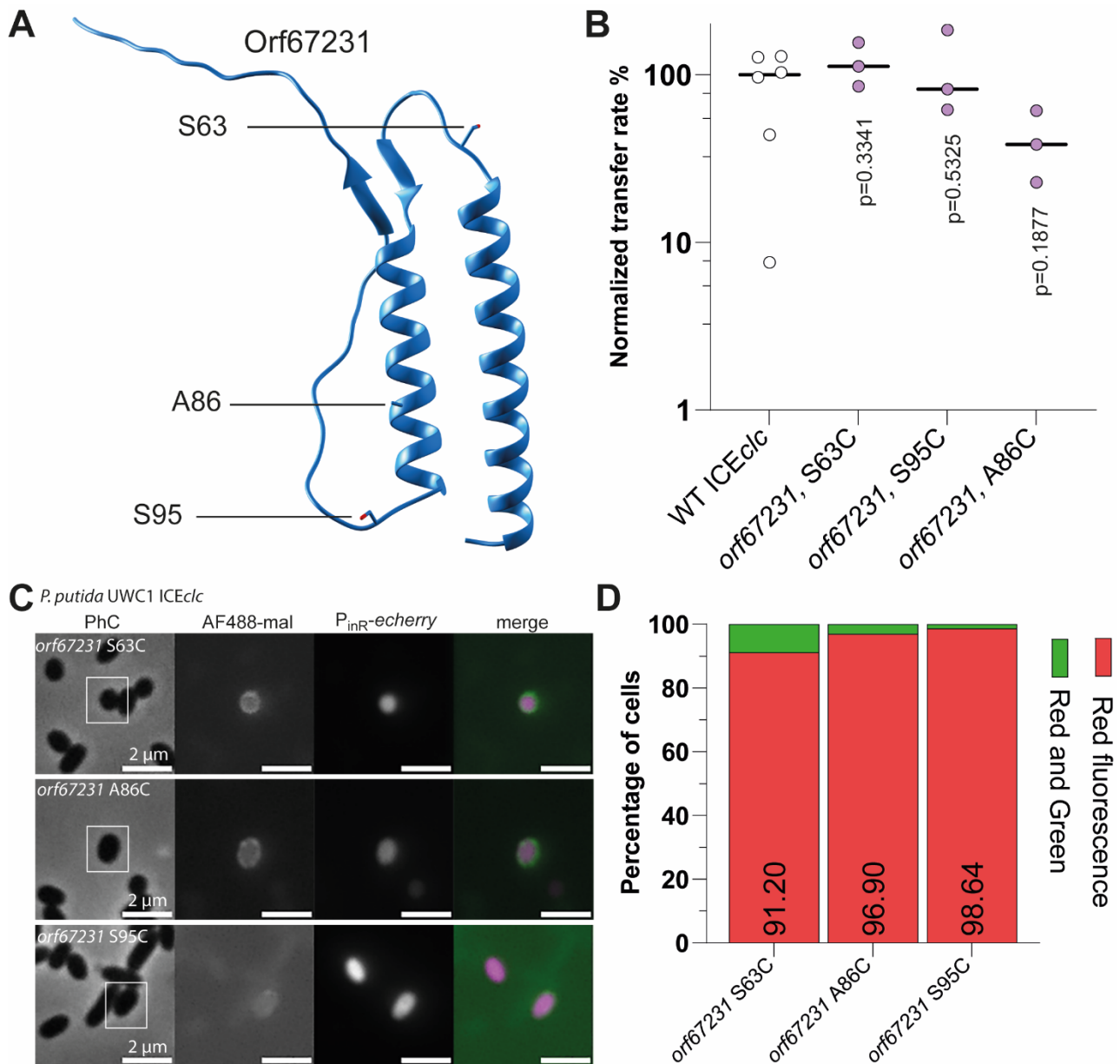


Figure 5 AF488-mal labeling of Orf67231 variants in *P. putida* ICEclc. **A)** AlphaFold2 predicted 3D model of Orf67231. The side chains of the targeted residues for cys-replacements are indicated. **B)** Normalized transfer frequency from *orf67231*-modified *P. putida* ICEclc donor strains in comparison to wild-type ICEclc (set to 100%). Black lines represent the average of biological triplicates; individual values are shown as open (WT) or filled circles (mutants). p-Values from two-tailed t-test between wild-type (WT) and mutant transfer rates. **C)** Micrographs of *P. putida* UWC1 ICEclc, P_{inR} -eCherry, *orf67231*-cys variant strains in stationary phase after growth on 3CBA, labelled with AF488-maleimide, in comparison to eCherry to identify tc cells. PhC, Phase-contrast; Merge, merged AF488/eCherry fluorescence. Scale bar 2 μ m. **D)** Percentage of tc cells with overlapping AF488 (green) and eCherry (red) fluorescent signals.

To study this question on Orf67231 localisation more clearly, we produced a variant in which *mcherry* was fused to the *orf67231* C-terminal end on its native locus, separated by a short linker peptide as in (9, 24) to avoid folding problems. Interestingly, this mutant was viable and its ICEclc transfer rate was not affected (Fig. 6A). Epifluorescence imaging of stationary phase *P. putida* ICEclc::*orf67231-mcherry* cells after growth on 3CBA showed an average of 6% fluorescent cells, as

expected for the subpopulation of tc cells (Fig. 6B). Individual tc cells showed accentuated fluorescent outlines, with a number of clear ‘embedded’ fluorescent foci (Fig 6C & D), and an occasional very strong focus (Fig. 6E). This would be in agreement with the predicted localization of Orf67231 in the periplasm (Fig. 6D). Orf67231-mCherry fusions thus displayed a similar fluorescent cell phenotype as previously investigated T4SS fluorescent protein fusions (9).

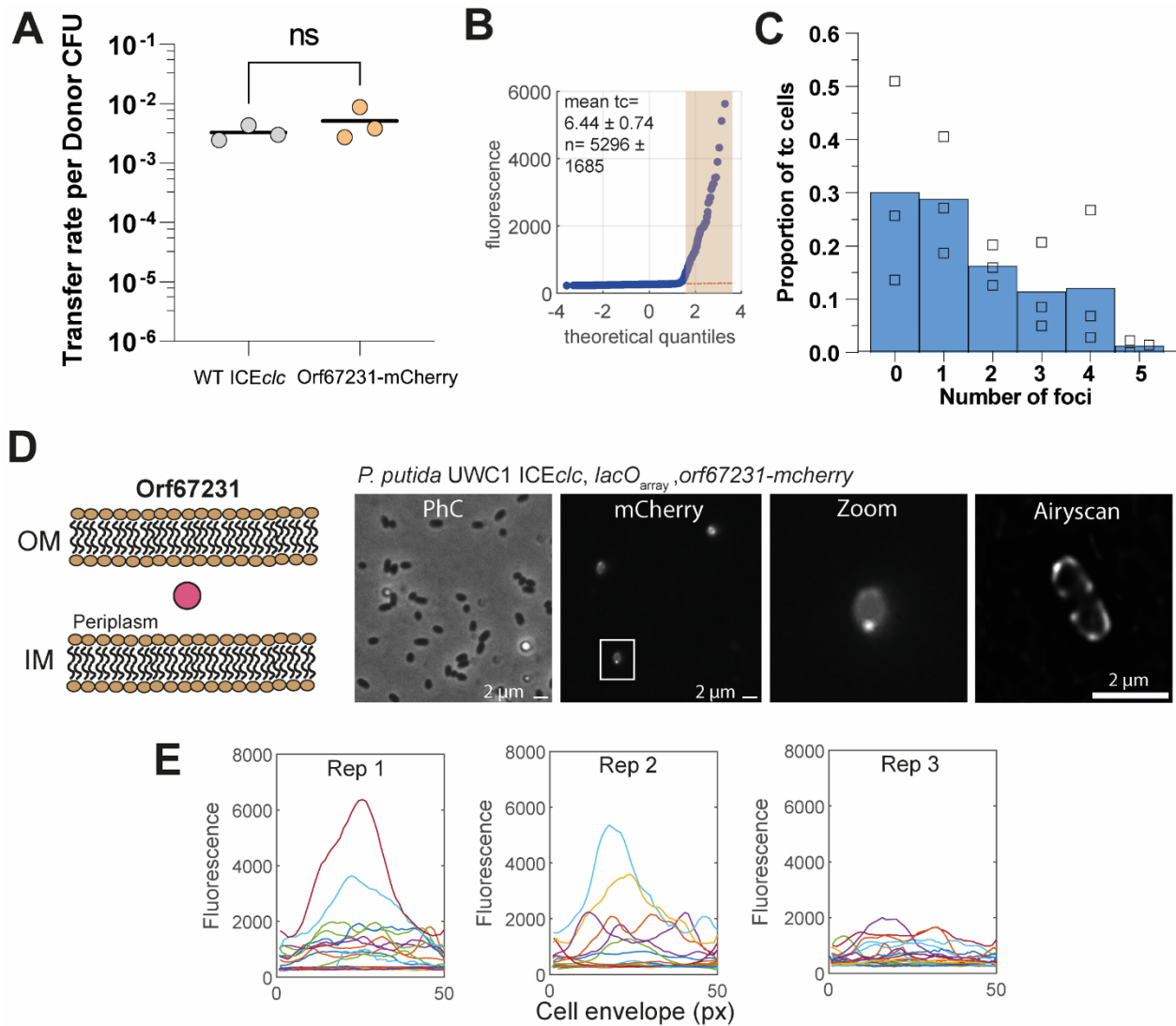


Figure 6 Subcellular localization of Orf67231-mCherry fusion proteins in *P. putida* ICEclc. **A)** Mean ICEclc transfer rates (black line) from *P. putida* with wild-type ICEclc or with the *orf67231-mcherry* fusion on the ICE. Filled circles represent values from biological triplicates. Statistical significance was assigned with a two-tailed T-test (ns, p-value >0.05). **B)** Quantile-quantile plot of median fluorescence per cell measured on a single replicate set of images and showing the derived tc cell subpopulation size (highlighted in light brown; average of tc cells per replicate \pm SD and n, the number of cells per biological replicate). **C)** Average proportion of tc cells with 0-5 detected fluorescent foci (open squares represent individual replicates). **D)** Micrographs of *P. putida* ICEclc cells carrying a native locus replacement of *orf67231-mcherry*, imaged in stationary phase after growth on 3-CBA. Panel on the left indicates the bioinformatic prediction of Orf67231 localization with respect to inner membrane (IM), periplasmic space, or outer membrane (OM); magenta, mCherry-signal. PhC, Phase contrast; Zoom, zoomed in detail of boxed cell in mCherry image. Airyscan, high-resolution deconvoluted 170-nm image slice. **E)** mCherry fluorescence profiles of the perimeter of 25 randomly chosen tc cells (1-

pixel outer 'shell'), from three biological replicates, of the relevant construct on their absolute fluorescent scales. 'Peaks' correspond to foci in the cell micrographs.

In order to confirm whether Orf67231-mCherry foci could be part of the T4SS protein complex, we quantified its fluorescent colocalization with a native-expressed IceD4-sfGFP marker in the same cell (IceD4 being the coupling ATPase of conjugation system). Indeed, both markers expressed in the same cells, confirming that they only appear in *P. putida* ICE*clc* tc cells (Fig. 7A). However, IceD4-sfGFP and Orf67231-mCherry foci overlapped only in ca. 30% of cases (Fig. 7B; overlap scored when foci geometric distances were inferior than 165 nm = 2.5 pixels). In 70% of the observed cells, no overlap occurred between the two fluorescent signals (Fig. 7B), suggesting they occur as independent protein complexes.

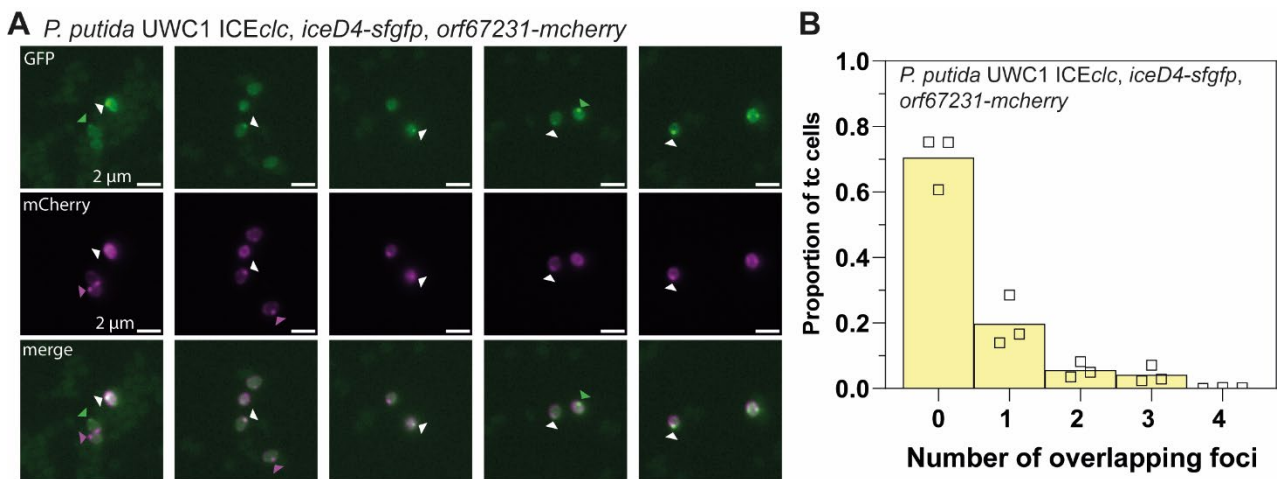


Figure 7 Colocalization of Orf67231-mCherry and IceD4-sfGFP in *P. putida* ICE*clc* cells. **A)** Micrographs of cells of *P. putida* UWC1 ICE*clc*::*iceD4-sfgfp*, *orf67231-mcherry* (fusions at their native loci) imaged in stationary phase after growth on 3-CBA. Merge; overlay of GFP (green) and mCherry (magenta) signals. White triangles point to overlapping sfGFP and mCherry foci (i.e., less than 165 nm or 2 pixels of the fitted foci geometric centres), whereas green and magenta triangles indicate non-overlapping foci. **B)** Mean proportion of tc cells with 0 to 4 overlapping foci. Values of individual biological replicates are represented by open squares.

Discussion

In this work we attempted to characterize the ICE*clc* T4SS conjugative pilin by a combination of cysteine-exposed fluorescent labeling, fluorescent protein fusion, transfer studies and electron tomography imaging. From two candidate pilin genes in the ICE*clc* T4SS identified by low homologies to the ICE*Hin10810* system, our results indicate the major pilin most likely to be encoded by *iceB2* (previously *orf66625*), with the other gene (*orf67231*) coding for a periplasmic protein, associated partly to other T4SS subsystem components. Our evidence is based on fluorescent cell protuberances seen with AF488-mal staining exclusively in case of IceB2 labeling and not in case of Orf67231, and incidental pili-structures observed by cryo-tomography on *P. putida* ICE*clc* tc cells.

Labelling of the conjugative pilus was based on chemical bonding between a maleimide-conjugated fluorophore (AF488) and the S-H group of a cysteine residue (14,15). Since primarily solvent-exposed Cys-residues can be targeted with the maleimide dye conjugate, we mutated several residues in both Orf67231 and IceB2 to cysteine. In the case of Orf67231, the addition of cysteine at three different positions did not affect ICE transfer, while all modifications in IceB2 either completely abolished or significantly decreased transfer rates. This might be expected as the lateral group of cysteine has a very important role in redox reactions and it is fundamental for the process known as oxidative protein folding (33,34), thus adding such residue in the sequence may hinder protein functionality. AF488-mal staining of Orf67231-cys variants did not show any fluorescent cell surface extensions, whereas staining of the IceB2-Cys2 mutant resulted in fluorescent pili-like structures. Cells with both one and two fluorescent pili-structures were observed, which would be in agreement with previous findings showing the presence of multiple T4SS assembled per cell (9,35). Unfortunately, the number of cells with fluorescent protuberances was extremely low. There may be several reasons for this low occurrence. First of all, the IceB2-Cys2 variant resulted in a ten-fold reduction of ICE $_{c/c}$ transfer. Even in the background of a 'constitutively' active ICE $_{c/c}$ (caused by the *mfsR* deletion) tc cells appear at a frequency of ca. 20% in the stationary phase population after growth on 3CBA (36), but this would still only translate in one in every tenth identified tc cell to potentially produce a surface structure (assuming a wild-type transfer rate of 10^{-3} with ca. 3% tc cells, Fig. 2). Secondly, the two added cysteines may form disulphide bonds between themselves or with C74 of IceB2, thus not allowing chemical bond with the maleimide dye. In addition, the window and duration of maleimide staining may not be congruent to the period of actual dynamic formation of the pili, since stationary phase cells are exposed to the chemical only for 15 minutes, and tc cell activation can arise more or less stochastically within a period of 12 h after entry into stationary phase (30). Finally, we observed that pili are easily sheared from the surface and, even though we adapted a filter-staining procedure to treat the cells as gently as possible, it is not unlikely that some fraction of pili were lost for visualization. Low frequencies of pili labelling have been observed before in other species using the same technique (37), and, thus, our evidence may be as good as it can get without finding any additional mutants that could alt pili retraction as shown in previous studies (38,39).

The second piece of evidence to conclude that *iceB2* must encode the ICE $_{c/c}$ pilin comes from cryo-tomography imaging. By combining fluorescent imaging to identify and locate tc cells on EM-grids, which were subsequently imaged by cryo-tomography, we also showed rare incidences of

filamentous structures protruding from tc cells. The thickness of these structures (8 nm) would be in agreement with what has been observed before for conjugative pili (diameter between 7.4 and 8.7 nm; (40-42)). These filamentous structures on tc cell surfaces were different from flagella, which we also observed, but which had a diameter of 15 nm, similar to the typical value of 13 and 17 nm found for other species (43-45). The small number of filaments (~7 among 100 imaged cells) is not sufficient to reconstruct a good 3D model (which could also support IceB2 being its major subunit), but it presented the best evidence we have so far for the ICE*clc* conjugative pilus.

In contrast to IceB2, we conclude that Orf67231 does not code for the major pilin but rather an accessory protein localised in the periplasmic space. AF488-maleimide labelling of *P. putida* expressing cys-modified Orf67231 (S63C, A86C, S95C) from its native ICE*clc* locus did not show any pili-like extrusions from tc cells, but rather fluorescent foci within stained cell envelopes on a small proportion of tc cells. This small proportion could mean that the cells are damaged, but if we assume they are not, the AF488-mal staining would indicate Orf67231 to be accessible for the dye from the extracellular space. We tried to confirm this further by fusing Orf67231 with mCherry, again expressed from its native ICE*clc* locus. The translational fusion did not impair ICE transfer, therefore, the observed phenotype could indicate the true Orf67231 localization. In this strain, Orf67231-mCherry fluorescence appeared as multiple foci around the cell within the region of the cell envelope, consistent with the bioinformatic predicted localization of Orf67231. This phenotype (of multiple fluorescent foci) was very similar to what we had observed for other ICE*clc* labeled T4SS subunits (particularly *iceB7*), suggesting that, despite not being essential for transfer, Orf67231 (9) associates to the T4SS in the periplasm forming multisubunit assemblages of some kind. These multisubunit assemblages only partly (ca. 30%) colocalize with labeled IceD4-sfGFP in the same cell. In comparison to IceB4 and IceB7 (9), the number of cells without colocalization to IceD4-sfGFP is 2.3 folds higher. This suggests Orf67231-mCherry to be more transiently associated to the core of the T4SS complexes in tc cells, perhaps only in combination of an existing or developing pilus. The partial colocalization is in line with the idea that T4SS are dynamic protein complexes with different structural configurations that are not all simultaneously functional in terms of readiness for conjugation (35,46).

Acknowledgments

We thank Manuela Hospenthal and Dianhong Wang, for providing crucial advice in cryo-EM sample preparation and image processing. We thank Christel Genoud and Jean Daraspe from the electron

microscopy facility of the University of Lausanne, and the Dubochet Center of Imaging (DCI) where cryo-EM images were acquired.

References

1. Arnold, B.J., Huang, I.T. and Hanage, W.P. (2022) Horizontal gene transfer and adaptive evolution in bacteria. *Nat Rev Microbiol*, **20**, 206-218.
2. Juhas, M., van der Meer, J.R., Gaillard, M., Harding, R.M., Hood, D.W. and Crook, D.W. (2009) Genomic islands: tools of bacterial horizontal gene transfer and evolution. *FEMS Microbiol Rev*, **33**, 376-393.
3. Delavat, F., Miyazaki, R., Carraro, N., Pradervand, N. and van der Meer, J.R. (2017) The hidden life of integrative and conjugative elements. *FEMS Microbiol Rev*, **41**, 512-537.
4. Mace, K., Vadakkepat, A.K., Redzej, A., Lukoyanova, N., Oomen, C., Braun, N., Ukleja, M., Lu, F., Costa, T.R.D., Orlova, E.V. *et al.* (2022) Cryo-EM structure of a type IV secretion system. *Nature*, **607**, 191-196.
5. Sheedlo, M.J., Durie, C.L., Chung, J.M., Chang, L., Roberts, J., Swanson, M., Lacy, D.B. and Ohi, M.D. (2021) Cryo-EM reveals new species-specific proteins and symmetry elements in the *Legionella pneumophila* Dot/Icm T4SS. *Elife*, **10**.
6. Christie, P.J. (2016) The Mosaic Type IV Secretion Systems. *EcoSal Plus*, **7**.
7. Clarke, M., Maddera, L., Harris, R.L. and Silverman, P.M. (2008) F-pili dynamics by live-cell imaging. *Proc Natl Acad Sci U S A*, **105**, 17978-17981.
8. Babic, A., Lindner, A.B., Vulic, M., Stewart, E.J. and Radman, M. (2008) Direct visualization of horizontal gene transfer. *Science*, **319**, 1533-1536.
9. Daveri, A., Benigno, V. and van der Meer, J.R. (2023) Characterization of an atypical but widespread type IV secretion system for transfer of the integrative and conjugative element (ICEclc) in *Pseudomonas putida*. *Nucleic Acids Res*, **51**, 2345-2362.
10. Gaillard, M., Pradervand, N., Minoia, M., Sentchilo, V., Johnson, D.R. and van der Meer, J.R. (2010) Transcriptome analysis of the mobile genome ICEclc in *Pseudomonas knackmussii* B13. *BMC Microbiol*, **10**, 153.
11. Guglielmini, J., Neron, B., Abby, S.S., Garcillan-Barcia, M.P., de la Cruz, F. and Rocha, E.P. (2014) Key components of the eight classes of type IV secretion systems involved in bacterial conjugation or protein secretion. *Nucleic Acids Res*, **42**, 5715-5727.
12. Vesel, N. and Blokesch, M. (2021) Pilus Production in *Acinetobacter baumannii* Is Growth Phase Dependent and Essential for Natural Transformation. *J Bacteriol*, **203**.
13. Ellison, C.K., Dalia, T.N., Vidal Ceballos, A., Wang, J.C., Biais, N., Brun, Y.V. and Dalia, A.B. (2018) Retraction of DNA-bound type IV competence pili initiates DNA uptake during natural transformation in *Vibrio cholerae*. *Nat Microbiol*, **3**, 773-780.
14. Ellison, C.K., Dalia, T.N., Dalia, A.B. and Brun, Y.V. (2019) Real-time microscopy and physical perturbation of bacterial pili using maleimide-conjugated molecules. *Nat Protoc*, **14**, 1803-1819.
15. Ellison, C.K., Kan, J., Dillard, R.S., Kysela, D.T., Ducret, A., Berne, C., Hampton, C.M., Ke, Z., Wright, E.R., Biais, N. *et al.* (2017) Obstruction of pilus retraction stimulates bacterial surface sensing. *Science*, **358**, 535-538.
16. Delavat, F., Moritz, R. and van der Meer, J.R. (2019) Transient Replication in Specialized Cells Favors Transfer of an Integrative and Conjugative Element. *mBio*, **10**.
17. Gerhardt, P., Murray, R., Costilow, R., Nester, E.W., Wood, W.A., Krieg, N.R. and Phillips, G.B. (1981) *Manual of methods for general bacteriology*. American Society for Microbiology Washington, DC.
18. Gaillard, M., Vallaey, T., Vorholter, F.J., Minoia, M., Werlen, C., Sentchilo, V., Puhler, A. and van der Meer, J.R. (2006) The *clc* element of *Pseudomonas* sp. strain B13, a genomic island with various catabolic properties. *J Bacteriol*, **188**, 1999-2013.
19. Krissinel, E. and Henrick, K. (2004) Secondary-structure matching (SSM), a new tool for fast protein structure alignment in three dimensions. *Acta Crystallogr D Biol Crystallogr*, **60**, 2256-2268.

20. Holm, L. (2022) Dali server: structural unification of protein families. *Nucleic Acids Res*, **50**, W210-W215.
21. Klausen, M.S., Jespersen, M.C., Nielsen, H., Jensen, K.K., Jurtz, V.I., Sonderby, C.K., Sommer, M.O.A., Winther, O., Nielsen, M., Petersen, B. *et al.* (2019) NetSurfP-2.0: Improved prediction of protein structural features by integrated deep learning. *Proteins*, **87**, 520-527.
22. Martinez-Garcia, E. and de Lorenzo, V. (2011) Engineering multiple genomic deletions in Gram-negative bacteria: analysis of the multi-resistant antibiotic profile of *Pseudomonas putida* KT2440. *Environ Microbiol*, **13**, 2702-2716.
23. Li, S. and Wilkinson, M.F. (1997) Site-directed mutagenesis: a two-step method using PCR and DpnI. *Biotechniques*, **23**, 588-590.
24. Miyazaki, R., Minoia, M., Pradervand, N., Sulser, S., Reinhard, F. and van der Meer, J.R. (2012) Cellular variability of RpoS expression underlies subpopulation activation of an integrative and conjugative element. *PLoS Genet*, **8**, e1002818.
25. Grote, A., Hiller, K., Scheer, M., Munch, R., Nortemann, B., Hempel, D.C. and Jahn, D. (2005) JCat: a novel tool to adapt codon usage of a target gene to its potential expression host. *Nucleic Acids Res*, **33**, W526-531.
26. Minoia, M., Gaillard, M., Reinhard, F., Stojanov, M., Sentchilo, V. and van der Meer, J.R. (2008) Stochasticity and bistability in horizontal transfer control of a genomic island in *Pseudomonas*. *Proc Natl Acad Sci U S A*, **105**, 20792-20797.
27. Reinhard, F., Miyazaki, R., Pradervand, N. and van der Meer, J.R. (2013) Cell differentiation to "mating bodies" induced by an integrating and conjugative element in free-living bacteria. *Curr Biol*, **23**, 255-259.
28. Schindelin, J., Arganda-Carreras, I., Frise, E., Kaynig, V., Longair, M., Pietzsch, T., Preibisch, S., Rueden, C., Saalfeld, S., Schmid, B. *et al.* (2012) Fiji: an open-source platform for biological-image analysis. *Nat Methods*, **9**, 676-682.
29. Kremer, J.R., Mastrorade, D.N. and McIntosh, J.R. (1996) Computer visualization of three-dimensional image data using IMOD. *J Struct Biol*, **116**, 71-76.
30. Sulser, S., Vucicevic, A., Bellini, V., Moritz, R., Delavat, F., Sentchilo, V., Carraro, N. and van der Meer, J.R. (2022) A bistable prokaryotic differentiation system underlying development of conjugative transfer competence. *PLoS Genet*, **18**, e1010286.
31. Pradervand, N., Delavat, F., Sulser, S., Miyazaki, R. and van der Meer, J.R. (2014) The TetR-type MfsR protein of the integrative and conjugative element (ICE) ICEclc controls both a putative efflux system and initiation of ICE transfer. *J Bacteriol*, **196**, 3971-3979.
32. Adams, D.W., Stutzmann, S., Stoudmann, C. and Blokesch, M. (2019) DNA-uptake pili of *Vibrio cholerae* are required for chitin colonization and capable of kin recognition via sequence-specific self-interaction. *Nat Microbiol*, **4**, 1545-1557.
33. Collet, J.F. and Bardwell, J.C. (2002) Oxidative protein folding in bacteria. *Mol Microbiol*, **44**, 1-8.
34. Welker, E., Narayan, M., Wedemeyer, W.J. and Scheraga, H.A. (2001) Structural determinants of oxidative folding in proteins. *Proc Natl Acad Sci U S A*, **98**, 2312-2316.
35. Park, D., Chetrit, D., Hu, B., Roy, C.R. and Liu, J. (2020) Analysis of Dot/Icm Type IVB Secretion System Subassemblies by Cryoelectron Tomography Reveals Conformational Changes Induced by DotB Binding. *mBio*, **11**.
36. Pradervand, N., Sulser, S., Delavat, F., Miyazaki, R., Lamas, I. and van der Meer, J.R. (2014) An operon of three transcriptional regulators controls horizontal gene transfer of the integrative and conjugative element ICEclc in *Pseudomonas knackmussii* B13. *PLoS Genet*, **10**, e1004441.
37. Zuke, J.D., Erickson, R., Hummels, K.R. and Burton, B.M. (2023) Visualizing dynamic competence pili and DNA capture throughout the long axis of *Bacillus subtilis*. *J Bacteriol*, **205**, e0015623.
38. Chlebek, J.L., Hughes, H.Q., Ratkiewicz, A.S., Rayyan, R., Wang, J.C., Herrin, B.E., Dalia, T.N., Biais, N. and Dalia, A.B. (2019) PilT and PilU are homohexameric ATPases that coordinate to retract type IVa pili. *PLoS Genet*, **15**, e1008448.
39. Adams, D.W., Pereira, J.M., Stoudmann, C., Stutzmann, S. and Blokesch, M. (2019) The type IV pilus protein PilU functions as a PilT-dependent retraction ATPase. *PLoS Genet*, **15**, e1008393.

40. Beltran, L.C., Cvirkaite-Krupovic, V., Miller, J., Wang, F., Kreutzberger, M.A.B., Patkowski, J.B., Costa, T.R.D., Schouten, S., Levental, I., Conticello, V.P. *et al.* (2023) Archaeal DNA-import apparatus is homologous to bacterial conjugation machinery. *Nat Commun*, **14**, 666.
41. Zheng, W., Pena, A., Low, W.W., Wong, J.L.C., Frankel, G. and Egelman, E.H. (2020) Cryoelectron-Microscopic Structure of the pKpQIL Conjugative Pili from Carbapenem-Resistant *Klebsiella pneumoniae*. *Structure*, **28**, 1321-1328 e1322.
42. Costa, T.R.D., Ilangovan, A., Ukleja, M., Redzej, A., Santini, J.M., Smith, T.K., Egelman, E.H. and Waksman, G. (2016) Structure of the Bacterial Sex F Pilus Reveals an Assembly of a Stoichiometric Protein-Phospholipid Complex. *Cell*, **166**, 1436-1444 e1410.
43. Sanchez, J.C., Montemayor, E.J., Ploscariu, N.T., Parrell, D., Baumgardt, J.K., Yang, J.E., Sibert, B., Cai, K. and Wright, E.R. (2023) Atomic-level architecture of *Caulobacter crescentus* flagellar filaments provide evidence for multi-flagellin filament stabilization. *bioRxiv*.
44. Nedeljkovic, M., Sastre, D.E. and Sundberg, E.J. (2021) Bacterial Flagellar Filament: A Supramolecular Multifunctional Nanostructure. *Int J Mol Sci*, **22**.
45. Yamaguchi, T., Makino, F., Miyata, T., Minamino, T., Kato, T. and Namba, K. (2021) Structure of the molecular bushing of the bacterial flagellar motor. *Nat Commun*, **12**, 4469.
46. Hu, B., Khara, P. and Christie, P.J. (2019) Structural bases for F plasmid conjugation and F pilus biogenesis in *Escherichia coli*. *Proc Natl Acad Sci U S A*, **116**, 14222-14227.

Supplementary Information.

Supplementary table 1: Characteristics of strains used in the study.

Strains	Strain Number	Description	Reference
<i>E. coli</i> DH5 α - λ pir	1854	λ pir lysogen	(Platt et al., 2000)
<i>P. putida</i> UWC1	1291	Plasmid-free derivative of <i>P. putida</i> KT2440, rifampicin resistant.	(McClure et al., 1989)
<i>P. putida</i> UWC1, ICE <i>clc</i>	2737	Derivative of strain 1291, with ICE <i>clc</i> insertion downstream of the tRNA ^{Gly} 5 gene.	(Miyazaki and van der Meer, 2011)
UWC1 <i>Tn7-P_{tac}-mcherry</i>	2744	<i>P. putida</i> UWC1 carrying <i>Tn7-P_{tac}-mCherry</i> (used as ICE <i>clc</i> recipient)	(Miyazaki and van der Meer, 2011)
UWC1, <i>clc</i> operon	3227	Derivative of strain 1291 carrying the <i>clc</i> (A, B, D, E, R) operon from the ICE <i>clc</i> element.	Unpublished
UWC1 <i>clc</i> , <i>lacO</i> _{array}	5214	Derivative of strain 1291 with one ICE <i>clc</i> copy integrated into <i>tRNA^{Gly}-5</i> and a <i>lacO</i> array	(Delavat et al., 2019)
UWC1 <i>clc</i> , <i>lacO</i> _{array} Δ <i>iceB4</i>	5512	Derivative of strain 5214 with a deletion of <i>orf59888</i> (<i>iceB4</i>) in the ICE <i>clc</i> .	(Daveri et al., 2023)
UWC1- <i>clc</i> , <i>lacO</i> _{array} , Δ <i>orf66625</i> , <i>67001</i> , <i>67231</i>	6995	Derivative of strain 5214 with a deletion of <i>orf67231-67001-66625</i> (<i>iceB2</i>) in the ICE <i>clc</i> .	(Daveri et al., 2023)
UWC1 <i>clc5</i> , <i>lacO</i> _{array} <i>orf67231</i> , S63C	7510	Derivative of strain 5214 with S63C mutation of <i>orf67231</i> in the ICE <i>clc</i> element.	This study
UWC1 <i>clc5</i> , <i>lacO</i> _{array} <i>orf67231</i> , S63C, <i>Tn5 P_{inR}-echerry</i>	7546-47	Derivative of strain 7510 with a <i>Tn5 P_{inR}-echerry</i> insertion. Two independent clones were stored at -80 °C.	This study
UWC1 <i>clc5</i> , <i>lacO</i> _{array} <i>orf67231</i> , A86C	7553	Derivative of strain 5214 with A86C mutation of <i>orf67231</i> in the ICE <i>clc</i> element.	This study
UWC1 <i>clc5</i> , <i>lacO</i> _{array} <i>orf67231</i> , A86C, <i>Tn5 P_{inR}-echerry</i>	7561-63	Derivative of strain 7553 with a <i>Tn5 P_{inR}-echerry</i> insertion. Three independent clones were stored at -80 °C.	This study
UWC1 <i>clc5</i> , <i>lacO</i> _{array} <i>orf67231</i> , S95C	7554	Derivative of strain 5214 with S95C mutation of <i>orf67231</i> in the ICE <i>clc</i> element.	This study
UWC1 <i>clc5</i> , <i>lacO</i> _{array} <i>orf67231</i> , S95C, <i>Tn5 P_{inR}-echerry</i>	7564-66	Derivative of strain 7554 with a <i>Tn5 P_{inR}-echerry</i> insertion. Three independent clones were stored at -80 °C.	This study
UWC1 ICE <i>clc</i> , <i>lacO</i> _{array} , <i>Tn5 P_{inR}-echerry</i>		Derivative of strain 5214 carrying the <i>Tn5 P_{inR}-echerry</i> construct	This study
UWC1 <i>clc5</i> , <i>lacO</i> _{array} <i>Orf66625</i> , T39C	7626	Derivative of strain 5214 with T39C mutation of <i>orf66625</i> (<i>iceB2</i>) in the ICE <i>clc</i> element.	This study
UWC1 <i>clc5</i> , <i>lacO</i> _{array} <i>Orf66625</i> , T42C, <i>iceB7-mcherry</i>	7648	Derivative of strain 5214 with T42C mutation of <i>orf66625</i> (<i>iceB2</i>) in the ICE <i>clc</i> element and a <i>mcherry</i> insertion at the C-terminal of <i>iceB7</i> .	This study
UWC1 <i>clc</i> , <i>iceB2-cys1</i>	7704	Derivative of strain 2737 with a single cysteine insertion at the C-terminal of <i>orf66625</i> (<i>iceB2</i>).	This study
UWC1 <i>clc5</i> , <i>lacO</i> _{array} <i>orf67231-mcherry</i> , <i>iceD4-sfgfp</i>	7708	Derivative of strain 5214 with <i>mcherry</i> insertion at the C-terminal of <i>orf67231</i> , and <i>sfgfp</i> insertion at the C-terminal of <i>iceD4</i> .	This study

UWC1 <i>clc</i> , <i>iceB2-cys2</i> , <i>iceB7-mcherry</i>	7710	Derivative of strain 2737 with a double cysteine insertion at the C-terminal of <i>orf66625</i> (<i>iceB2</i>) and <i>mcherry</i> insertion at the C-terminal of <i>iceB7</i> .	This study
UWC1 <i>clc5</i> , <i>lacO_{array}</i> <i>orf67231-mcherry</i>	7713	Derivative of strain 5214 with <i>sfgfp</i> insertion at the C-terminal of <i>iceD4</i> and <i>mcherry</i> insertion at the C-terminal of <i>orf67231</i> .	This study
UWC1 <i>clc</i> , <i>iceB2-cys2</i> , <i>iceB7-mcherry</i> , Δ <i>mfsR</i>	7845	Derivative of strain 7710 with a deletion of the <i>mfsR</i> gene in the ICE <i>clc</i> element.	This study

Supplementary table 2: List of all plasmids used in the study.

Plasmid	Description	Reference
pEMG	Km ^R , <i>oriR6K</i> , P _{tac} - <i>lacZa</i> , I-SceI sites	(Martinez-Garcia and de Lorenzo, 2011)
pSW	Amp ^R , <i>oriRK2</i> , P _m -I-SceI	(Martinez-Garcia and de Lorenzo, 2011)
pBAM	Km ^R , Amp ^R , <i>ori6K</i> , mini <i>Tn5</i> system	(Martinez-Garcia et al., 2011)
pBAM <i>P_{inR}-echerry</i>	pBAM derivative carrying the <i>P_{inR}-echerry</i> construct.	(Minoia et al., 2008)
pEMG-HR- <i>orf66625</i>	pEMG derivative including <i>orf66625</i> flanked by two 1 kb long homology regions. The plasmid was further modified with targeted mutagenesis.	This study
pEMG-HR- <i>orf67231</i>	pEMG derivative including <i>orf67231</i> flanked by two 1 kb long homology regions. The plasmid was further modified with targeted mutagenesis.	This study
pEMG-HR- <i>orf67231-S63C</i>	pEMG-HR- <i>orf67231</i> derivative with a point mutation at position S63, allowing for cysteine substitution of the targeted residue in the chromosome.	This study
pEMG-HR- <i>orf67231-A86C</i>	pEMG-HR- <i>orf67231</i> derivative with a point mutation at position A86, allowing for cysteine substitution of the targeted residue.	This study
pEMG-HR- <i>orf67231-S95C</i>	pEMG-HR- <i>orf67231</i> derivative with a point mutation at position S95, allowing for cysteine substitution of the targeted residue.	This study
pEMG-HR- <i>orf66625-T39C</i>	pEMG-HR- <i>orf66625</i> derivative with a point mutation at position T39, allowing for cysteine substitution of the targeted residue.	This study
pEMG-HR- <i>orf66625-T42C</i>	pEMG-HR- <i>orf66625</i> derivative with a point mutation at position T42, allowing for cysteine substitution of the targeted residue.	This study
pEMG-HR- <i>orf66625-CYS</i>	pEMG-HR- <i>orf66625</i> derivative with an insertion of a single cysteine at the C-terminal of <i>orf66625</i> .	This study
pEMG-HR- <i>orf66625-CYS-CYS</i>	pEMG-HR- <i>orf66625</i> derivative allowing double cysteine insertion at the C-terminal of <i>orf66625</i> .	This study
pEMG-HR- <i>orf67231-mcherry</i>	pEMG derivative allowing the chromosomal insertion of <i>mcherry</i> downstream of <i>orf67231</i> in the ICE <i>clc</i> .	This study
pEMG-HR- <i>orf73676-mcherry</i>	pEMG derivative allowing the chromosomal insertion of <i>mcherry</i> downstream of <i>orf73676</i> (<i>iceB7</i>) in the ICE <i>clc</i> .	(Daveri et al., 2023)
pEMG-HR- <i>orf68987-sfgfp</i>	pEMG derivative allowing the chromosomal insertion of <i>sfgfp</i> downstream of <i>orf68987</i> (<i>iceD4</i>) in the ICE <i>clc</i> .	(Daveri et al., 2023)
pEMG-HR- <i>mfsR</i>	pEMG derivative allowing the chromosomal deletion of <i>mfsR</i> from the ICE <i>clc</i> element	This study

Supplementary Table 3. List of primers used in the study.

Primer Number	Sequence 5'-3' ^a	Target
210521	<i>TAGGGATAACAGGGTAATCTGAATTCATAGACCACTCAACGAGACT</i>	Amplification of <i>orf66625</i> plus the upstream and downstream flanking regions.
210522	<i>AGAAGCTTGCATGCCTGCAGGT<u>CGACT</u>AGTACTCGTCGGCGGT</i>	
210525	<i>TAGGGATAACAGGGTAATCTGAATTCCTTGCTCACGTTGCCG</i>	Amplification of <i>orf67231</i> plus the upstream and downstream flanking regions.
210526	<i>AGAAGCTTGCATGCCTGCAGGT<u>CGAC</u>ATACAGCCAGGTGTCGG</i>	
210527	<i>TGCATCCAGCCGGGCGAACG^b</i>	Primers for S63C substitution on <i>orf67231</i> .
210528	<i>GGCATGCGCGGCGCT^b</i>	
210803	<i>TGCGGCATCCAGGCCAC^b</i>	Primers for A86C substitution on <i>orf67231</i> .
210804	<i>GCGCATACGCGCTAGATC^b</i>	
210807	<i>CTTACCCCGTGCCTGCCCCAGCC^b</i>	Primers for S95C substitution on <i>orf67231</i> .
210808	<i>GTGGGCCTGGATGCCAGC^b</i>	
220203	<i>TGCCGTGGCACCGGCAAC^b</i>	Primers for T39C substitution on <i>orf66625</i> .
220204	<i>CGGGTTCTCCAAGTGC^b</i>	
220205	<i>TGCGGCAACGGCATCATGGAG^b</i>	Primers for T42C substitution on <i>orf66625</i> .
220206	<i>GCCACGGGTCGGGT^b</i>	
220501	<i>TGCTGCTAAGGCGAGGCTGGTATGTC^b</i>	Primers for the insertion of single (220503) and double cysteine (220501) at the C-terminal of <i>orf66625</i> .
220502	<i>CAGGATGCCGGTGGCT^b</i>	
220503	<i>TGCTAAGGCGAGGCTGGTATGTC^b</i>	
220504	<i>TAGGGATAACAGGGTAATCTGAATTCATCTCGTGCCTCTCGC</i>	Amplification of upstream and downstream flanking regions for insertion of <i>mcherry</i> at the C-terminal of <i>orf67231</i> .
220505	<i>AGTCGTCGGCAGCGAT</i>	
220506	<i>GTGGAGAACAAGCCATGAAC</i>	
220507	<i>AGAAGCTTGCATGCCTGCAGGT<u>CGACA</u>AAGCGGATCGTGCG</i>	
220508	<i>GGGATCGCTGCCGACGACTAAGCTTCCGGAAAATTCG</i>	Amplification of <i>linker-mcherry</i> for C-terminal tag of <i>orf67231</i> .
220509	<i>GTTTATGGCTTGTCTCCACTTTGTACAGCTCATCCATG</i>	
221001	<i>TAGGGATAACAGGGTAATCTGAATTCGCAAGACTTTTCTATGGGTG</i>	Amplification of upstream and downstream flanking regions for deletion of <i>mfsR</i> from ICE <i>clc</i> .
221002	<i>TTGGTTAGTGCCTTGCAT</i>	
221003	<i>AGATGCAACGCACTAACCAAGAAGCGTCCAGTAAACGC</i>	
221004	<i>AGAAGCTTGCATGCCTGCAGGT<u>CGACT</u>CCTTGCTTGCTCCAGGA</i>	

a) Restriction enzymes are underlined, primer overhangs are represented in italic, cysteine codon for targeted mutagenesis are highlighted in blue.

b) 5' Phosphorilated primers.

Table S4. List of targeted residues for cysteine substitution in IceB2

Protein	Targeted Residues	Relative Solvent Availability (RSA)	Success
IceB2	THR 39	0.59	Successful
	THR 42	0.75	Successful
	THR 116	0.56	Unsuccessful
	ALA 99	0.55	Unsuccessful
	ALA 115	0.46	Unsuccessful

Daveri, A., Benigno, V., and van der Meer, J.R. (2023). Characterization of an atypical but widespread type IV secretion system for transfer of the integrative and conjugative element (ICEclc) in *Pseudomonas putida*. *Nucleic Acids Res* *51*, 2345-2362.

Delavat, F., Moritz, R., and van der Meer, J.R. (2019). Transient Replication in Specialized Cells Favors Transfer of an Integrative and Conjugative Element. *mBio* *10*.

Martinez-Garcia, E., Calles, B., Arevalo-Rodriguez, M., and de Lorenzo, V. (2011). pBAM1: an all-synthetic genetic tool for analysis and construction of complex bacterial phenotypes. *BMC Microbiol* *11*, 38.

Martinez-Garcia, E., and de Lorenzo, V. (2011). Engineering multiple genomic deletions in Gram-negative bacteria: analysis of the multi-resistant antibiotic profile of *Pseudomonas putida* KT2440. *Environ Microbiol* *13*, 2702-2716.

McClure, N.C., Weightman, A.J., and Fry, J.C. (1989). Survival of *Pseudomonas putida* UWC1 containing cloned catabolic genes in a model activated-sludge unit. *Appl Environ Microbiol* *55*, 2627-2634.

Minoia, M., Gaillard, M., Reinhard, F., Stojanov, M., Sentschilo, V., and van der Meer, J.R. (2008).

Stochasticity and bistability in horizontal transfer control of a genomic island in *Pseudomonas*. *Proc Natl Acad Sci U S A* *105*, 20792-20797.

Miyazaki, R., and van der Meer, J.R. (2011). A dual functional origin of transfer in the ICEclc genomic island of *Pseudomonas knackmussii* B13. *Mol Microbiol* *79*, 743-758.

Platt, R., Drescher, C., Park, S.K., and Phillips, G.J. (2000). Genetic system for reversible integration of DNA constructs and lacZ gene fusions into the *Escherichia coli* chromosome. *Plasmid* *43*, 12-23.

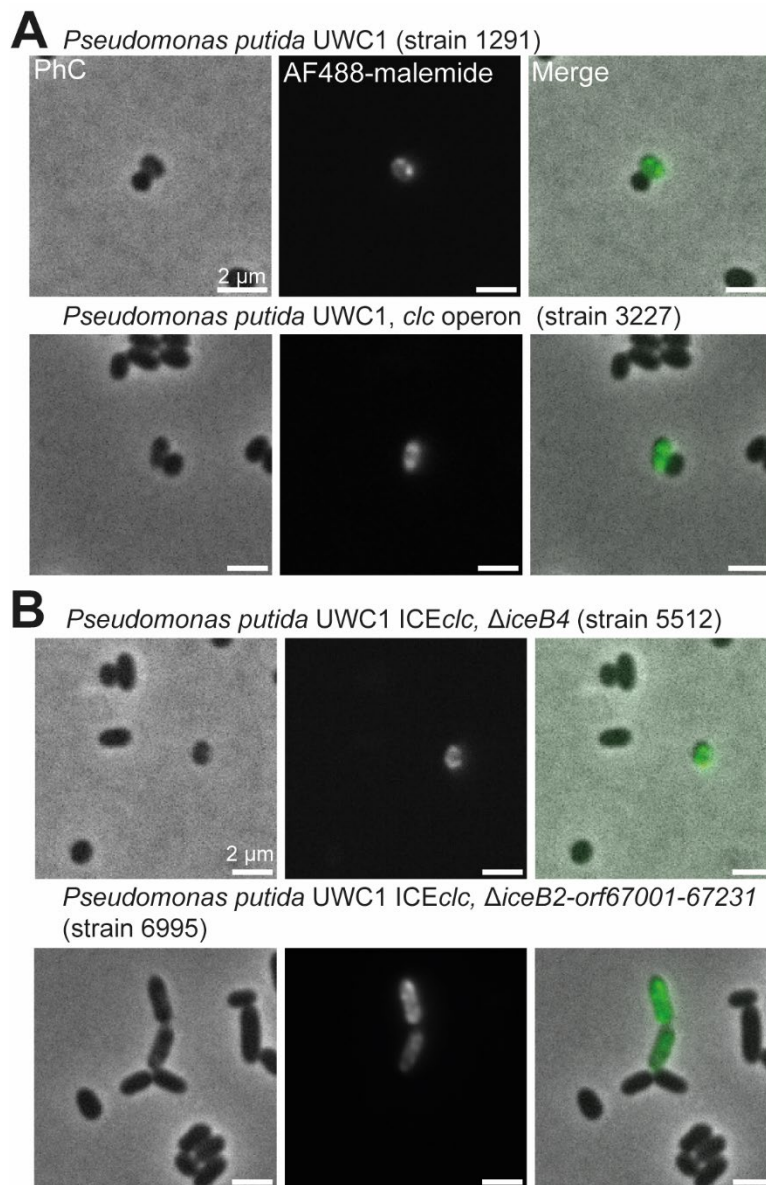


Figure S1 Maleimide staining of control strains. A) Micrographs of AF488-maleimide stained *P. putida* strains devoid of ICE*clc*. Phase Contrast (PhC), AF488-maleimide, Merge. B) Micrographs of AF488-maleimide stained *P. putida* with deletions of different T4SS components. Phase Contrast (PhC), AF488-maleimide, Merge.

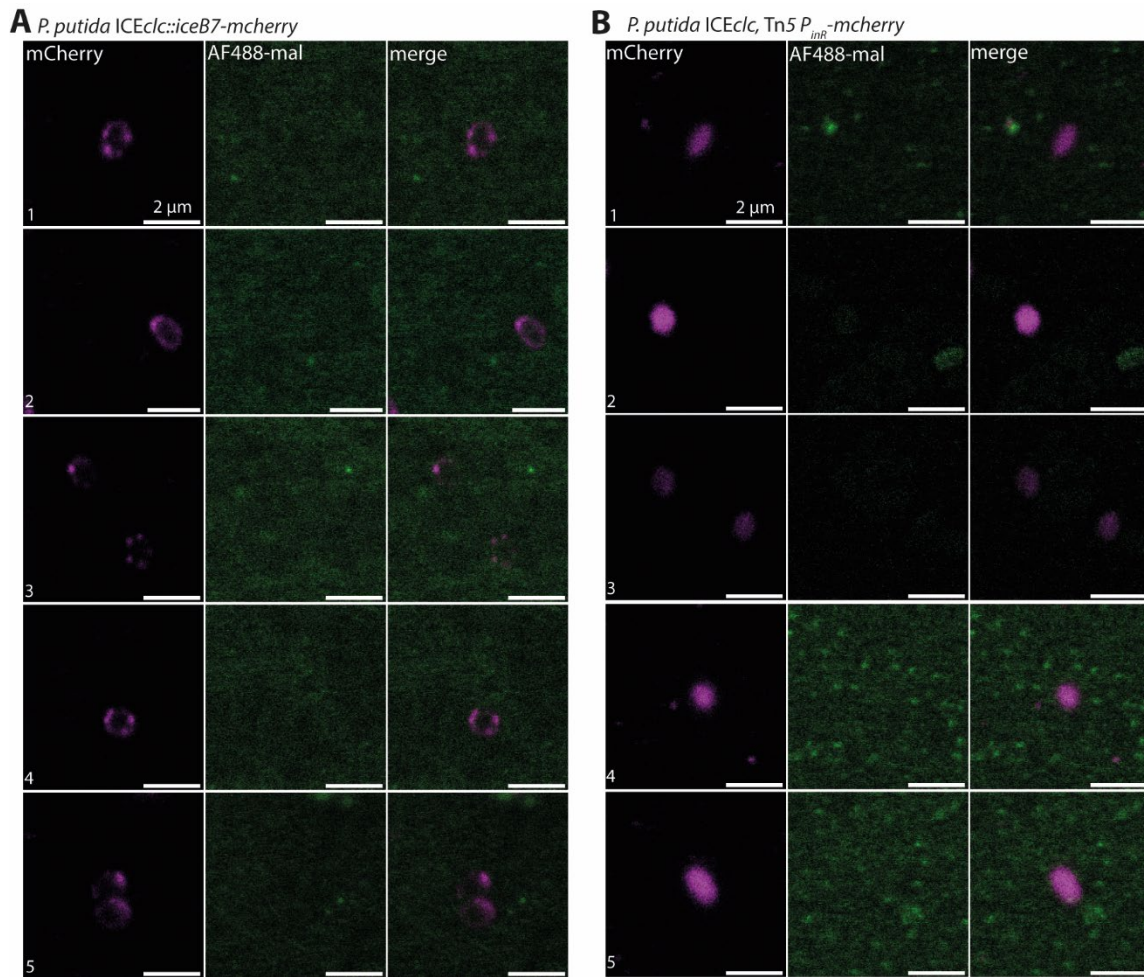
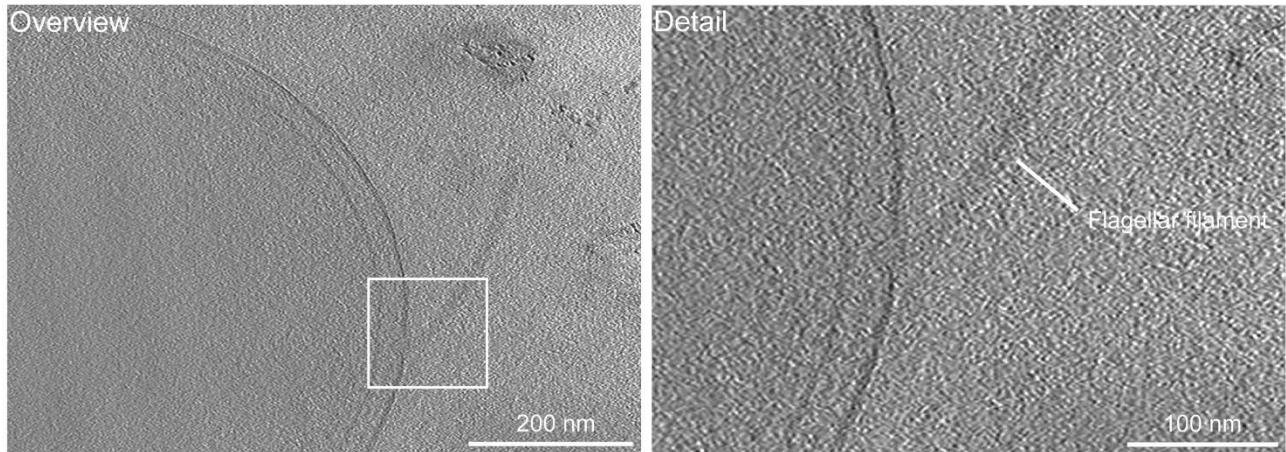


Figure S2 Maleimide staining of *P. putida* ICEclc cells with wild-type iceB2. A) Micrographs of *P. putida* tc cells stained with AF488-maleimide. mCherry, AF488-mal, merge. The tc cell marker is *iceB7-mcherry*. **B)** Micrographs of *P. putida* tc cells stained with AF488-maleimide. mCherry, AF488-mal, merge. The tc cell marker is P_{inR} -mcherry.

A *P. putida* UWC1, ICE*clc*, *iceB4-sfgfp*, *iceB7-mcherry*, Δ *mfsR*



B *P. putida* UWC1, ICE*clc*, *iceB4-sfgfp*, *iceB7-mcherry*, Δ *mfsR*

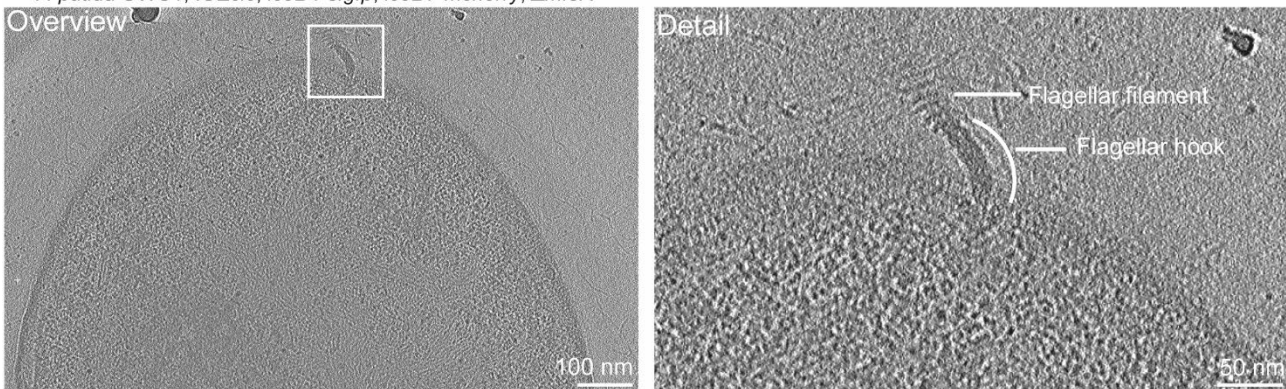


Figure S3 Cryo-EM images of *P. putida* tc cells showing different morphological detail. A) Micrographs of *P. putida* tc cells showing no filamentous structures. **B)** Micrographs of *P. putida* tc cells showing a filamentous structure, resembling the bacterial flagellum. The two distinct sections of the flagellum (hook, filament) are indicated. Overview and Detail. The white rectangle on the left panel indicates the area of interest shown in the Detail panel. **C)** Micrographs of *P. putida* tc cells showing a filamentous structure, resembling the conjugative pilus, indicated with a white line. Overview and Detail. The white rectangle on the left panel indicates the area of interest as in section B.

Chapter 4

Dynamic behaviour of an inner and outer membrane subunit of the T4SS encoded by *ICEclc* in *Pseudomonas putida*

Andrea Daveri, Jan Roelof van der Meer

Abstract

The Type IV Secretion System (T4SS) is a versatile molecular machinery widespread in bacteria, which facilitates the transfer of macromolecules (DNA or proteins) across cell membranes. Conjugative systems are usually made of multiple subunits, from a minimum of 12 to more than 20, which co-ordinately assemble and operate to convey the substrate to a recipient. The common conception underlying the process of conjugation is that the cell assembles one or more complete T4SSs, which can then transfer the substrate. However, recent cryo-EM studies have shown that T4SS can occur in different configurations, suggesting they are not all complete and functional, and perhaps more dynamic than assumed. Here we tried to obtain evidence for dynamic T4SS formation, using two distinct subunits of the ICE c -encoded T4SS. We targeted fluorescent protein fusions to either IceB4 or IceB7, the labeling of which did not measurably change ICE transfer rates. IceB4 is the ATPase that associates to the inner-membrane complex, whereas IceB7 is a core component of the outer membrane complex. With high-resolution time-lapse microscopy, we discovered that IceB7 fluorescent protein foci are very stable at the cell membrane, but IceB4 foci have higher radial movement. Addition of a recipient to the donor cell population increased IceB7 stability, while it did not change the dynamics that we first observed for IceB4, meaning that some other regulatory mechanisms come into play towards the assembly of a complete T4SS and conjugative transfer. Given the difficulty of studying protein molecular dynamics in live cells, our study provides a first evidence on the dynamic nature of the conjugative machinery, distinguishing between outer and inner membrane complexes as two independent units.

Introduction

Type IV secretion systems (T4SS) are macromolecular protein assemblies occurring widely among prokaryotes (1). Depending on the bacterial species and/or the mobile element encoding them, T4SS can have different functions, mainly: DNA conjugation, targeted protein secretion or DNA uptake from the environment (2-4). Despite the differences in function and in the number of subunits forming the complex, e.g., 12 in the VirB system of *Agrobacterium tumefaciens* (5), and more than 20 in the Dot/Icm system of *Legionella pneumophila* (6), their global structural organization is conserved. Four main protein subassemblies can be distinguished: I) a set of cytoplasmic ATPases, usually three, but only two for the F-plasmid T4SS (7); II) an inner membrane complex (IMC), made of several lipophilic multimeric subunits that form the mating channel in the inner membrane (IM); III) an outer membrane complex (OMC), also made of a number of multimeric subunits, which form the pore in the outer membrane (OM); and IV) the conjugative pilus, formed by hundreds of pilin subunits, which extends into the extracellular space and is crucial for recipient recognition and cell-cell contact (8,9). Conjugative transfer can only be achieved when cytoplasmic ATPases, IMC and OMC are connected together. However, recent cryo-EM experiments revealed that T4SSs can exist in different assembly states (10) and that the vast majority of conjugative complexes *in vivo* are incomplete (11), lacking either the OMC or the IMC (12). This suggests a dynamic nature of T4SS assembly with IMC and OMC possibly occurring in the cell envelope independently, that need to connect to form an active conjugation complex.

As conjugation requires a recipient cell, it could be actually a contact signal or other that facilitates the formation of the full T4SS. Within the recipient cell, the newly acquired single-stranded (ss) DNA is recircularized and converted into a double-stranded (ds) DNA molecule. Subsequently, the expression of horizontally acquired genes establishes the mobile element and converts recipient into a transconjugant cell. Eventually, a transconjugant cell can act as a new donor. This sequence of events is well documented (13,14). However, we still lack a detailed understanding of the molecular mechanisms, particularly for the reactions occurring within the recipient cell between DNA entry and the eventual establishment of a transconjugant cell. A recent study highlighted the importance of the helicase UvrD, which is directly involved in the replication of the second strand of the mobile element in the recipient. Indeed, deletion of this protein in *E. coli* recipients significantly decreased F plasmid transfer efficiency (15).

In this work we aimed at understanding the dynamic behaviour of two distinct subunits of the T4SS encoded by ICE*clc* of *Pseudomonas putida*. As a representative of the IMC we chose IceB4 (analog of VirB4), and IceB7 (analog of VirB7) for the OMC (12). We have shown before that both IceB4 and IceB7 can be fused with a fluorescent protein without losing transfer efficiency. In addition, we previously showed that IceB4- and IceB7-fluorescent foci only partly colocalize, suggesting independent dynamic movement. Consequently, we focused on detecting the potential movement of labelled IceB4- and IceB7 in live cells of *P. putida* with ICE*clc* by high-resolution fluorescence microscopy, under conditions that trigger the formation of transfer competent cells. Labelled donor strains were also incubated in the presence of *P. putida* recipient cells, in order to quantify any changes in dynamic localization of both ICE*clc* encoded T4SS subunits as a consequence of recipient cell vicinity. Our results show different dynamic behaviour between both subunits, supporting the hypothesis of multiple independently circulating OMC and IMC.

Material and Methods

Strains, reagents and growth conditions

Escherichia coli DH5 α λ pir was used for cloning of ICE*clc* genes and plasmid amplification, and was grown at 37°C on Luria-Bertani (LB) liquid or agar-solidified broth. *P. putida* UWC1-ICE*clc*::*lacO*_{array} was used as host of the ICE, carrying a single copy ICE*clc* integrated at the tRNAGly-5 gene (16). The *lacO*_{array} modification was introduced in the *amnB* gene of the ICE with the purpose to follow single-copy ICE-DNA transfer, if needed (16). *P. putida* UWC1 Tn7 sGFP2 or UWC1 Tn7 P_{tac}-*mcherry* were used as recipient strains for mating experiments. *P. putida* was cultured at 30°C either on LB, on nutrient agar (Oxoid) or on minimal medium (MM, type 21C (17)). MM was supplemented with either 5 mM succinate or 3 mM 3-chlorobenzoate (3-CBA) as sole carbon source. Both *E. coli* and *P. putida* were cultured aerobically in shaking flasks. Where necessary for plasmid maintenance or for selection of genomic constructs, antibiotics were added at the following concentrations: kanamycin (Km, 50 μ g ml⁻¹), ampicillin (Amp, 100 μ g ml⁻¹ for *E. coli*, 500 μ g ml⁻¹ for *P. putida*), tetracycline (Tc, 20 μ g ml⁻¹ for *E. coli*, 50 μ g ml⁻¹ for *P. putida*), or gentamycin (Gm, 20 μ g ml⁻¹, 10 μ g ml⁻¹ in MM). The following supplements were added for screening or promoter induction (see below): 5-bromo-4-chloro-3-indolyl- β -D-galactopyranoside (X-Gal; 20 μ g ml⁻¹), or m-toluate (15 mM). All produced strains are listed in Supplementary table S1.

DNA manipulations

The different DNA manipulations followed standard procedures as suggested by the providers. Plasmids were purified from *E. coli* DH5 α λ pir using NucleoSpin Plasmid kits (Macherey-Nagel, Duren, Germany). Oligonucleotides for PCR amplification were purchased from SigmaAldrich. PCR products were purified with NucleoSpin Gel and PCR clean up kits (Macherey-Nagel). Clones were verified with colony PCR using a GoTaq[®] G2 green master mix (20 μ l, Promega, Madison, United States). PCR amplicons were assembled into plasmids using the ClonExpress II One Step Cloning Kit (Vazyme, Nanjing, China), after appropriate enzymatic digestion. Restriction enzymes were purchased from NEB (New England Biolabs, Ipswich, United States). All the newly constructed plasmids (Table S2) were sequenced before further use, to verify the correctness of the inserts.

Single gene knockout

Seamless in-frame deletions of ICE*clc* genes were created using double recombination with marker counterselection (18). We targeted specifically a deletion in the major global repressor of ICE*clc* activity, *mfsR*, which results in fractions of 20-30 % of transfer competent cells (19). Up- and downstream regions of the *mfsR* gene were PCR amplified with Q5 high fidelity polymerase (New England Biolabs) and assembled into pEMG suicide vector (18). The newly constructed plasmid was transformed (300-500 ng) into the relevant *P. putida* UWC1 strain using the procedure as described in reference (20). Transformants were selected on LB agar plates added with Km, verifying the chromosomal insertion of the suicide vector by colony PCR using appropriate primers (Table S3). Positive clones were next transformed with 50 ng of the pSW vector (18) and selected on Amp and Km LB agar plates. One positive colony was then inoculated in 10 mL of LB added with Amp (500 μ g mL⁻¹) and 15 mM of m-toluate (Honeywell Fluka[™]) to induce the expression of the I-SceI and force chromosomal repair, after which culture dilutions were spread on LB plates. Candidate colonies were again verified by PCR for the success of the double recombination and the deletion genotype. Positive clones were further cultured without antibiotics to cure the pSW plasmid, after which they were stored at -80[°]C in 15% v/v glycerol. Primers are listed in Table S3.

Cell preparation for microscopy and experimental setup

Fluorescently labelled *P. putida* ICE*clc* (*iceB7-mcherry*, *iceB4-sfgfp*) donor strains were grown for 96 h in liquid MM supplemented with 3 mM 3-CBA to induce ICE*clc* transfer competence (Nico Paper 2020). In case of experiments with recipients, the *P. putida* UWC1 recipients were grown for 24 h in

liquid MM supplemented with 5 mM succinate as the sole carbon source and mixed with donors at a 1:1 (OD/OD) ratio, to a final volume of 500 μ L. The donor-recipient mixture was washed with 500 μ L of MM (with no carbon source) prior to further use. An aliquot of 5 μ L of donor suspension alone or of donor-recipient mixtures was then spread on the surface of a 1-mm thick 1% MM-agarose patches (\varnothing 1 cm) supplemented with 1 mM 3-CBA placed, which was then placed upside down on a round microscope slide and enclosed in an imaging chamber (Perfusion Chamber, H. Saur Laborbedarf, Germany) as described in ref. (21). Cells were imaged with a ZEISS LSM 980 Airyscan 2 microscope equipped with ZEN 3.3 software, installed in a controlled temperature room (22°C). sfGFP and mCherry fluorescence were imaged in Z-stacks covering 2.2 μ m, with exposure times of 250 ms each and exported as 16-bit .TIF files. In case of time-lapse imaging we tested periods of 15 s (with 0.8 s interval between images), or 1 h with intervals of two minutes. Images for display were cropped in Fiji (22) to the same dimensions and rendered in Adobe Photoshop at 350 dpi resolution (v. 2022, Adobe Inc.), downsampled to 8-bit and saved as .tiff files.

Image analysis pipeline

In absence of phase-contrast, the tc cells on each frame (only one slice of the full z-stack was included in the final analysis) were manually segmented based on their fluorescence. This mask was then projected across all image data in time series (Fig. 1A). Foci within each cell mask were detected by Gaussian fitting, adapting part of the SuperSegger script (23), recovering foci positions, intensity scores and fitting values. The fluorescent values of the outer most shell of 10 pixels of the masked cells was extracted, transformed into a linear representation and plotted over time to visualize dynamic foci positioning (Fig. 1B, kymographs). From the foci coordinates in the segmented cells we then calculated the pair-wise Euclidean distances to foci at subsequent time points. This list of distances was then used to find the 'shortest' path for each fluorescent focus over time, starting from the highest to lowest intensity foci at time 0, from which we calculated its median distance. The median distance was taken as a quantitative value for the dynamic movement of each focus. Prior to statistical analysis, we imposed a threshold based on fluorescence intensity to filter the foci, in order to exclude false positives.

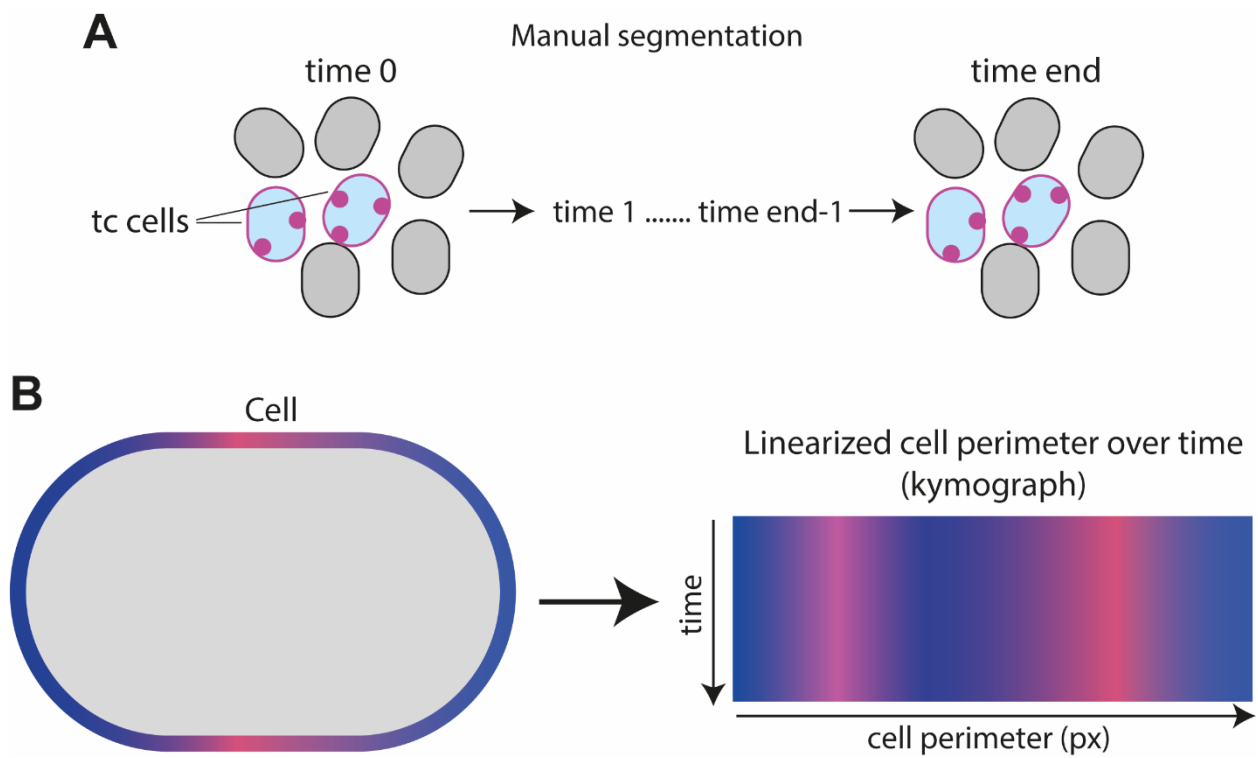


Figure 1 Schematic picture of the image analysis pipeline. A) Tc cell (magenta outline) of the relevant fluorescently labelled *P. putida* ICEclc strains (magenta dots represent fluorescent foci formed by the T4SS subunit) are manually identified at the starting image frame of the time lapse, and used to derive a mask that is placed across all subsequent images of the series. **B)** The fluorescence intensity of a 10 pixel wide cellular outline is linearized for each time point and stacked to build a kymograph (magenta shaded region corresponds to the area with highest fluorescent intensity (foci)).

Results

The inner membrane subunit IceB4 shows more intracellular movement than the OMC component IceB7

Based on our previous studies, where we observed only partial colocalization between IceB4 and IceB7, we decided to follow their localization over time in individual cells to understand whether absence of colocalization would be due to differences in independent ‘circulation’ of the IMC (IceB4) and OMC (IceB7) complexes (Fig. 2A). For the time lapse experiments we used *P. putida* strains carrying the ICE*clc* with native replacements of either *iceB4-sfGFP* or *iceB7-mcherry*. Both expressed IceB7-mCherry or IceB4-sfGFP formed visible foci in tc cells, with appreciable differences in intensities. Time-lapse imaging over a duration of 1 h suggested IceB4-sfGFP foci to be more mobile than IceB7-mCherry within individual cells (Fig. 2B). Kymographs with fluorescence intensity on a linearized cell perimeter scale confirm this visual impression, indicating that whereas IceB4-sfGFP foci intensity changes drastically over time and position, IceB7-mCherry foci remained essentially at a single spot (Fig 2C). To further corroborate this visual impression, we quantified foci movement in multiple tc cells over time as the shortest geometric distance ‘path’ of the same foci across multiple images in time. Even though here we group all foci per cell, irrespective of their individual intensity, this comparison showed that on average, IceB4-sfGFP foci have ca. twofold higher distances between consecutive time points (here 2 min) than IceB7-mCherry foci (Fig. 2D). Similar results were obtained in two more independent experiments (Fig. S1 A-B), proving that our observation is not a false positive, but rather describes the intrinsic properties of the two proteins.

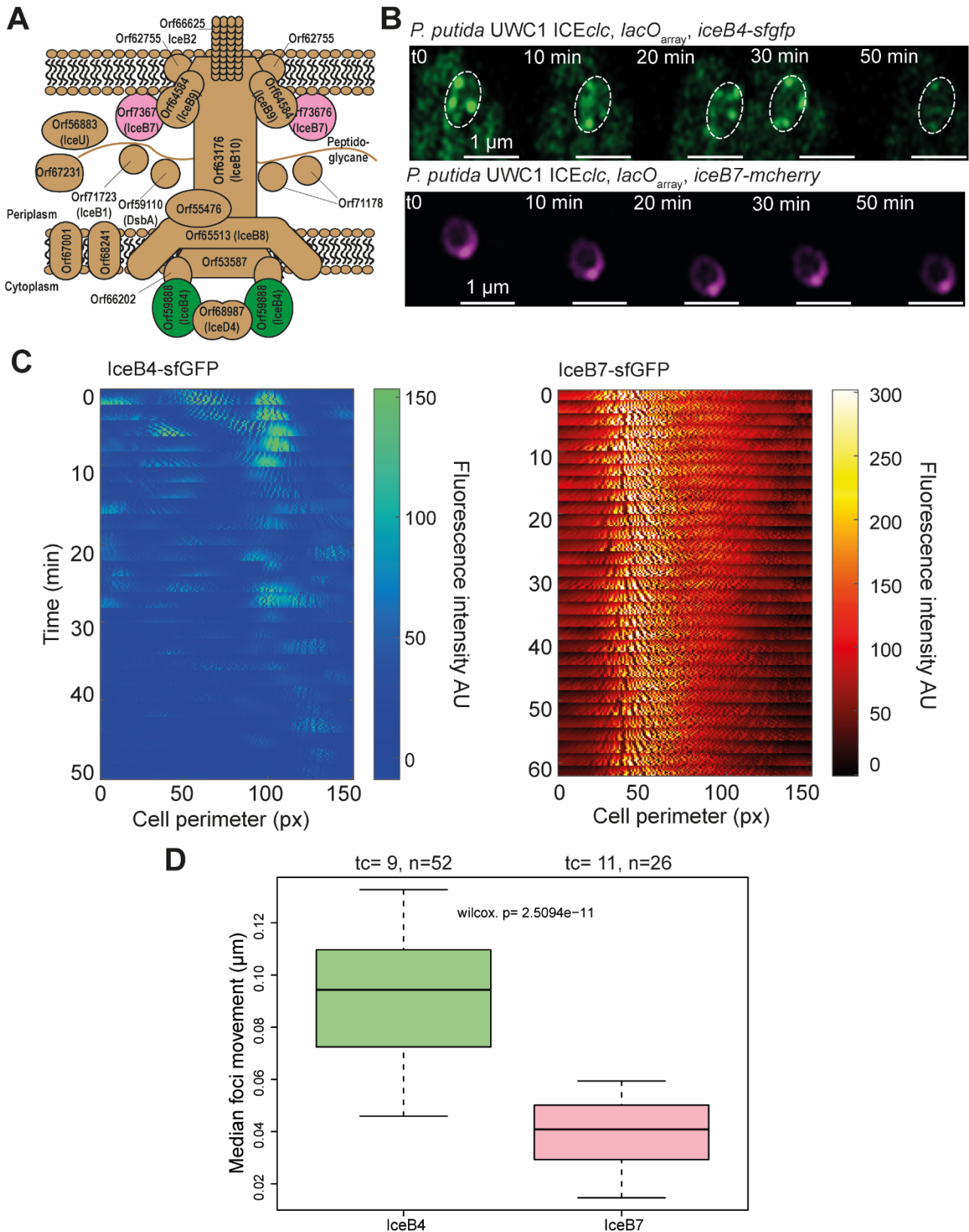


Figure 2 Dynamic behaviour of of IceB4 and IceB7 subunits. A) Schematic view of the ICE*clc* encoded T4SS. Two fluorescently tagged subunits IceB4 and IceB7 are highlighted in green and pink respectively. **B)** Micrographs of time-lapse experiments (0 to 50 minutes, interval between snapshots 2 minutes) of fluorescently labelled *P. putida* UWC1 with ICE*clc* and either of *iceB4* or *iceB7* replaced at its native locus by the tagged variant. The white dotted line in the upper panel indicates the cell outline. Images show a single 170-nm slice of the Airyscan stack. Scales on images represent 1 μm . **C)** Kymographs represent linearized fluorescence intensity profiles of the 10 outer pixels of the cell

envelope stacked over time. **D)** Median averaged paired shortest distances of IceB4-sfgfp and IceB7-mcherry foci across all consecutive time points. Statistical significance between the datasets was assessed with a two-sided Wilcoxon test (p = p-value, tc = number of tc cells in the experiment, n = number of single foci).

Brighter IceB7 foci show higher stability at the membrane

We noticed that the majority of tc cells carried more than one fluorescent focus, which displayed differences in fluorescent intensity within the same cell. Since the fluorescent proteins are expressed from a 3' end fusion to the native gene, it is unlikely that the intensity differences originate from expression differences. Rather, this suggests that the fluorescence signal that we quantify is a consequence of the number of subunits of the respective proteins. Some loss of foci brightness is the result of 2D projection, but this is less than the differences observed among foci (Fig. S2). Although we have no calibration for the relation between foci intensity and monomer numbers in individual cells, this would still indicate that brighter foci are an accumulation of a higher number of IceB4/IceB7 monomers than those with lower fluorescence intensity. This might be due to, incidentally, two or more full T4SS complexes being very close together in the cell beyond our image resolution, or might represent cases where weaker foci correspond to incomplete OMC or IMC. In order to understand whether foci with different intensities also have different average movement in cells, we separated the median foci movement of the brightest and least bright focus per tc cell. Results, from 1h long time-lapse experiments, indicated that bright IceB7-mCherry foci move twofold less compared to the least bright ones (Fig. 3A, $p=0.0034$), whereas for IceB4-sfGFP there was no significant difference (Fig. 3B, $p=0.5479$). To further corroborate these results, we plotted a map of the foci localization over the duration of the time lapse within individual tc cells. The cells displayed in Figure S3 A-B have one or two bright IceB7-mCherry foci that remain stable over time, among a background of lower intensity foci that move at the position of the periplasm. In contrast, the cell in Fig. S3C shows IceB4-sfGFP foci all around the cell with only rare stable foci appearing (Fig. S3D). In addition to that, we also observed that bright IceB7-mCherry foci on rare occasions split into two separate (bright) foci (Fig. S4A-B). This may imply that bright IceB7 foci represent instances of more than one assembled T4SS complex. In conclusion, IceB7 bright foci may represent fully assembled OMC subassemblies that remain stable at the membrane. On the other hand, IceB4 fully assembled units (brightest foci) still show a strong dynamic behaviour.

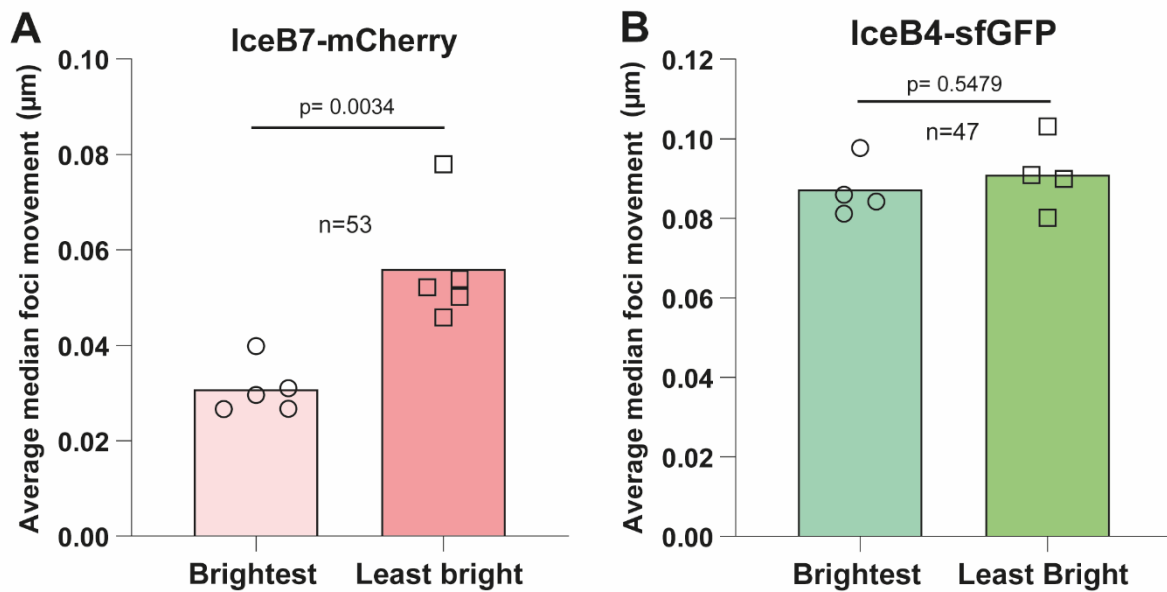


Figure 3 Comparison of the average movement of foci with the highest and lowest fluorescent intensities in tc cells. **A-B)** Average movement of IceB7-mCherry and IceB4-sfGFP foci with highest and lowest fluorescent intensities. Open circles and open squares indicate the individual value of biological replicates coming from independent experiments. Statistical significance was assessed with a two-tailed t-test, p-value is indicated. n represents the number of tc cells considered in the quantification. Only tc cells with at least two detected fluorescent foci were included in the data analysis.

Effect of recipients on T4SS subunit dynamics

Next, we tried to find out whether the presence of a recipient cell would influence and/or reduce the mobility of T4SS subunits expressed in donor cells. To study this, we tagged *P. putida* recipients with a constitutively expressed fluorescent protein to distinguish them from donors as indicated in Fig 4A. From visual inspection of time-lapse experiments, no clear differences could be observed compared to experiments without recipients (Fig. 4A). Similarly, kymographs of tc cells resembled the ones obtained previously, with IceB7-mcherry forming stable bright foci and IceB4-sfGFP showing a more dynamic behaviour (Fig. 4B). Quantification of foci dynamics between different biological replicates showed that the presence of recipient cells does have an influence in the localization of T4SS. In 3 out of 4 biological replicates IceB7-mCherry units are significantly less mobile in presence of a recipient cell, compared to donor cells alone (Fig. 4C). In contrast, IceB4 foci movement was not significantly different in presence or absence of recipient (Fig. 4D). This suggests that OMC and IMC subunit react differently to the presence of recipients. Here we gained an overview of whether the presence of recipient can affect foci movement in donor cells. To be more precise, we next tried to identify foci close to the direct contact point of donor and recipient cells, and whether foci at contact sites would show different movement than those not in obvious contact.

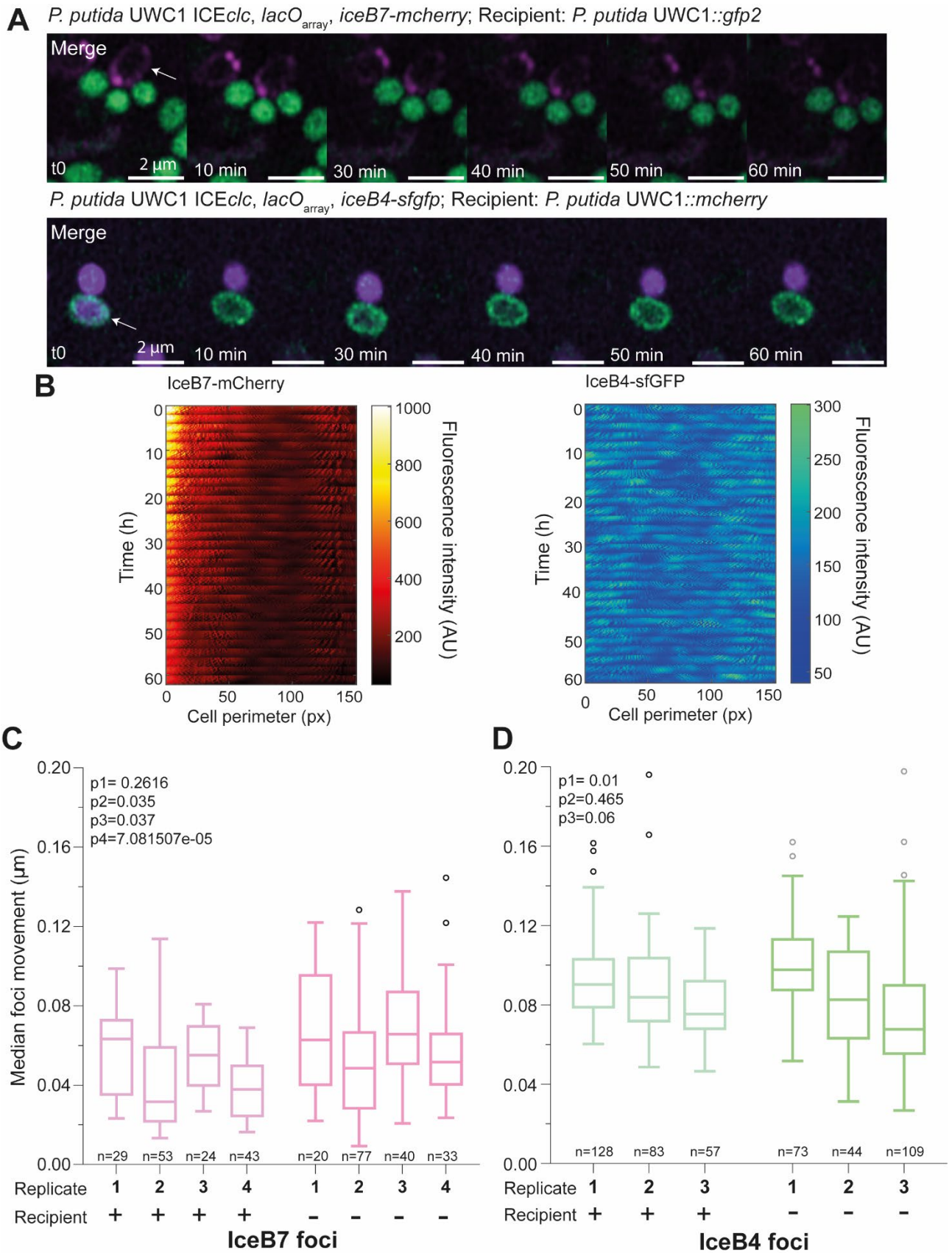


Figure 4 Recipients influence the stability of T4SS subunits in donor cells. A) Micrographs of the indicated *P. putida* UWC1 strains imaged for 60 minutes in presence of recipients (interval between snapshots 2 minutes). Airyscan high-resolution images, 170 nm slices. The white arrow indicates the tc cells represented kymographs in the next section. **B)** Kymographs representing the fluorescence profile of the two indicated tc cells. The 10 outmost pixels of each tc cell are linearly projected for each time point. **C-D)** Median foci movement of IceB4-sfGFP and IceB7-mCherry foci between two

time points, in presence (+) or absence (-) of recipients, calculated from the foci coordinates in tc cells. Statistical significance between the datasets was assessed with a two sided Wilcoxon test ($p_{1...n} = p\text{-value}$, $n = \text{number of single foci}$).

In order to do this, we manually identified donor cells in contact with recipients, and identified in an interactive script the visual closest points of cell-cell contacts. The script would then automatically find the nearest identified focus to the indicated contact point. We then distinguished all the foci nearest to the recipient cell contact (Fig. 5, Contact) and those not in direct contact with the recipient (Fig. 5, No Contact). Here we only consider a subset of foci not in contact, because they widely outnumber the ones in contact (note that tc cells only have one or two contact points with recipients) and this would bias the statistical analysis due to sample size disparity. The obtained results did not show any significant difference in median foci movement of 'contact' and 'no contact' foci, neither for IceB4 nor for IceB7 fusions (Fig. 5 A&B). This thus suggests that direct contact with recipient cells does not influence the dynamics of OMC or IMC foci (Fig. 5 A-B), which indicates that there must be other underlying factors explaining the generally lower IceB7 foci movement in presence of recipients (Fig. 4).

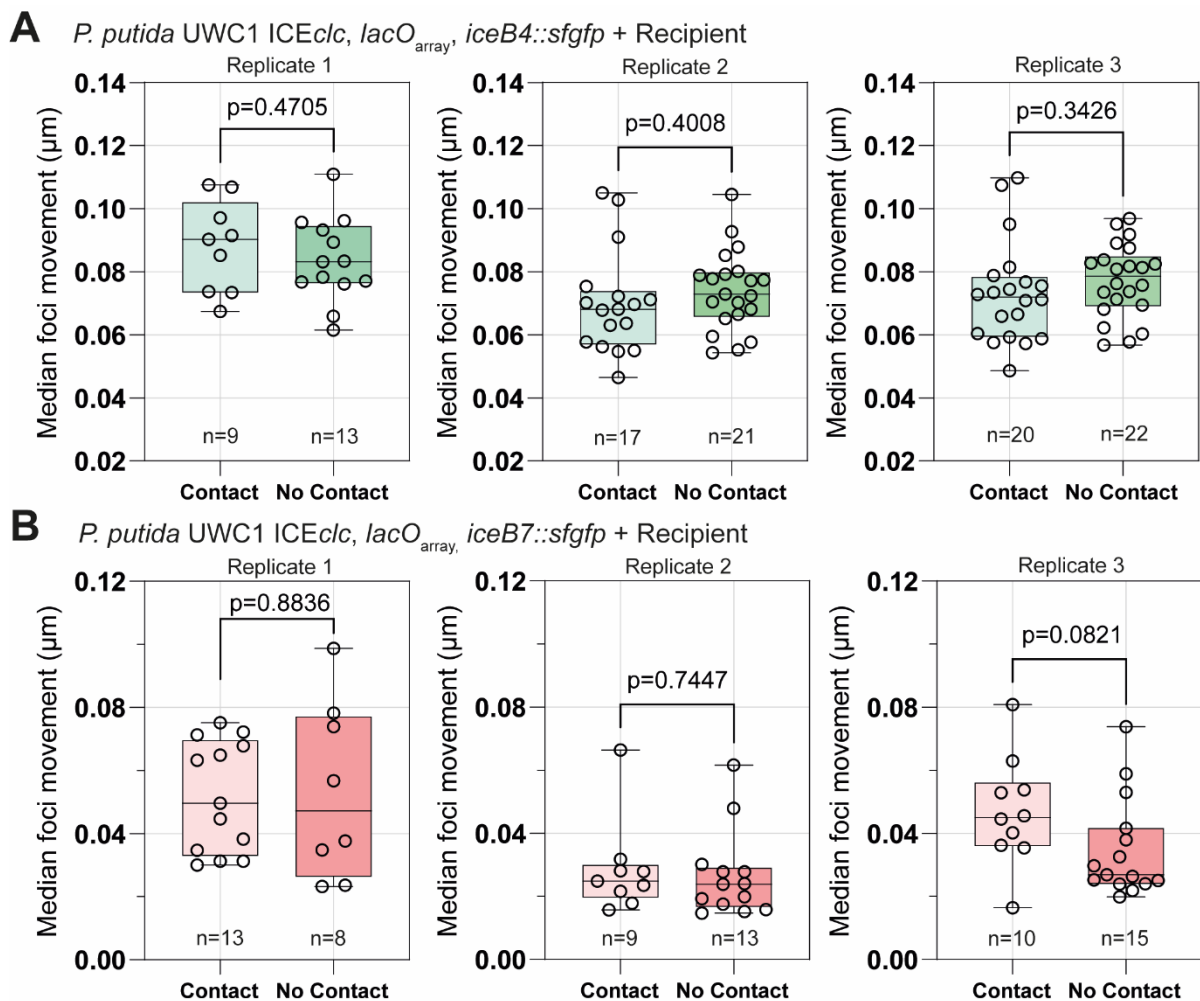


Figure 5 Dynamics of foci in direct contact with the recipient. A) Comparison of the median movement of IceB4-sfGFP foci in direct contact and not in contact with recipient cells. Open circles represent individual foci movement values. Statistical significance between the datasets was assessed with a two tailed t-test, p-value indicated (n= number of single foci). **B)** Comparison of the median movement of IceB7-mCherry foci in direct contact and not in contact with recipient cells. Open circles represent individual foci movement values. Statistical significance between the datasets was assessed with a two tailed t-test, p-value indicated (n= number of single foci).

IceB4 foci are stable at lower time scales

The evidence that we collected until now, suggests that IceB4 would be more mobile than IceB7. We next wondered if this 'motility' would be different at shorter time periods, and, therefore we repeated the time-lapse imaging but at smaller intervals (0.8 s). From visual observation of the time-lapse we can already notice differences compared to the 1 hour long experiments. Indeed, the position of bright IceB4 foci within tc cells seem stable on a 15 s-period (Fig. 6A), and in translated kymograph fluorescent profiles (Fig. 6B). This trend was confirmed by quantitative analysis of a larger number of IceB4 foci (n=38 across 8 tc cells), which showed that the median foci movement of IceB4 in the short period (15 s) on average was 2.5-fold lower than in the long period (1 h, Fig. 6C). This would indicate either that IceB4 stably localizes at the membrane in a shorter periods of time (but moves in between longer periods), or is moving very slowly such that its movement is not detected within 15 s but is over longer periods. The temporary stability could offer the potential for a stable complete T4SS complex (OMC + IMC) to form, which could then allow ICEc/c transfer.

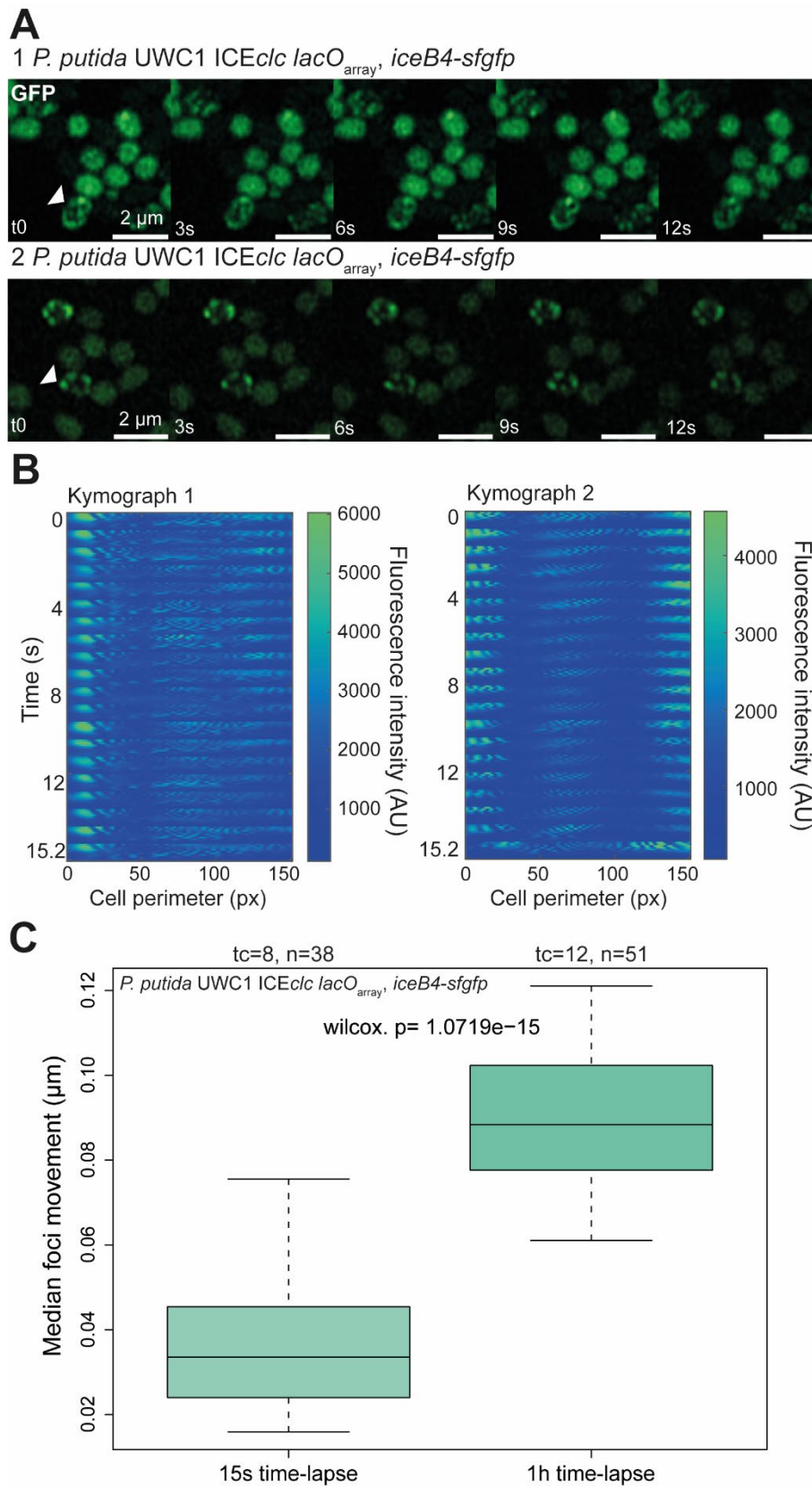


Figure 6 IceB4 stably locates at the membrane in the seconds time scale. **A)** Micrographs of the indicated *P. putida* strains imaged over a 15s time span (interval between snapshots 0.8s). Airyscan high-resolution images. The white triangle indicates the tc cells represented as kymographs in section B. **B)** Kymographs representing the fluorescence profile of a single tc-cell (indicated with white triangle in section A). The 10 outmost pixels of a tc cells are linearly projected for each time point. **C)** Median foci movement of IceB4-sfGFP foci in 15s and 1h long time-lapses, calculated

from the foci coordinates in tc cells. Statistical significance between the datasets was assessed with a two sided Wilcoxon test ($p = p\text{-value}$, $tc = \text{number of tc cells in the experiment}$, $n = \text{number of single foci}$).

Discussion

In this work we attempted to study the kinetics of T4SS subunit movement inside individual tc cells, in order to better understand the role of dynamic protein behaviour in ICE*clc* conjugation. Our first goal was to demonstrate whether there is any dynamic repositioning at all, and secondly, we aimed to show whether T4SS subunit parts would move independently of each other. To study this, we focused on the IMC and OMC complexes, which were represented in our study by the proteins IceB4 and IceB7, respectively. We had determined previously (12), that both IceB4 and IceB7 are essential for ICE*clc* transfer but can be tagged with fluorescent protein fusions without disturbing ICE*clc* conjugation frequencies. We had also previously shown that both proteins form multiple fluorescent foci in tc cells, which we considered to represent individual T4SS complexes, but that IceB4 foci only partly colocalized to IceB7 foci. This had suggested that complete T4SS are perhaps dynamically reconstituted from their independent IMC (represented by the labeled IceB4) and OMC subassemblies (represented by the labeled IceB7). Our study here focused in more depth on tracing the subcellular localization of the two subunits over-time in live tc cells by high-resolution time-lapse microscopy. Our results suggest that the IceB7 and IceB4 subunits indeed behave as distinct entities, showing foci with different properties (brightness), differences in relative movement with respect to the cell envelope (more or less 'stable'), and effects of presence of recipient cell. Notably, IceB4-foci were generally less stable than IceB7-foci, bright IceB7-foci were less dynamic than dim IceB7-foci, and the bright foci seemed to move even less in presence of recipient cell.

Several studies have suggested that T4SS are not static protein machineries (with a singular structure), but undergo a series of conformational and structural modifications during the different phases of conjugation (24). These studies had been accomplished using different conjugation systems, but indicated that their T4SS can exist in multiple structural conformations in the same cell (10) and that not all assembled T4SS in bacterial cells are complete with all their subunits (11). More recently, Macé and collaborators (25) resolved a high resolution structure of the R388 plasmid-encoded T4SS, which captured the T4SS in a conformation which is not able to transfer DNA, since the channel in the IMC was occupied by VirB6. In their current hypothesis, this conformation serves to assemble the pilus and not to transfer DNA. If this is true, it would indicate that the actual T4SS-DNA-transferring configuration is different. From this it would also follow that the T4SS is a dynamic machine undergoing multiple structural transitions. In our experiments we find that the IMC subunit

(IceB4) had significantly higher dynamics in terms of foci movement across the cell envelope than the OMC (IceB7). This may, firstly, be the result of some intrinsic property of the IM in gram-negative bacteria. For example, Rassam and collaborators (26) showed how IM protein diffusion is higher than that of OM proteins throughout the cell cycle. In addition, IceB4 is one of the two ATPases that we identified in the ICEc/c T4SS (12). A reasonable hypothesis is that not all IceB4 subassemblies interact at all times with the IMC of the T4SS, but only when required, for example, for pilus elongation/retraction and/or during conjugative transfer. Pilus elongation/retraction is a process that can last for 1-5 minutes (27). Although we do not know exactly how long it takes for ICE DNA to be transferred, it is reasonable to think that it could be a matter of seconds, as was observed for F plasmid conjugation (28). The observed IceB4 dynamic behaviour would fit with this idea. For example, IceB4 foci tended to be stable at short time intervals and more mobile at longer (1 h), but with occasional stable foci over the longer periods as well. Short term stable foci could represent IceB4 associated to a pilus assembling T4SS or conjugation building activity, whereas more mobile foci could represent isolated IceB4-complexes moving around the IM or in between T4SS dynamic states. Contrary to IceB4-foci, those of IceB7 were less dynamic, which is perhaps a reflection of its structural role in OMC assembly. IceB7 is a structural component of the ICEc/c T4SS, thought to interact with IceB9 and IceB10 in the OM forming the so called core complex of the machinery (12,29). For the same reasons as mentioned above, perhaps the OMC is simply less mobile than the IMC because of the generally lower fluidity of the OM than the IM.

During conjugation donor and recipient are in close contact, with their membranes fusing at the mating junction (30). Therefore, there must be a complex molecular mechanism allowing the formation of a temporary 'hole' in the recipient's cell envelope to facilitate DNA transfer, which as of today is completely unknown. With our experiments we tried to infer whether the mere presence of a recipient in close proximity to the donor is sufficient to influence T4SS localization or assembly. Our results suggested that IceB7-foci in donor cells indeed become more stable in presence of recipients than in their absence, whereas this was not the case for IceB4 foci. Although we could not demonstrate that the increased stability of IceB7-foci in presence of recipients is directly dependent on contact between the two cells (at least with our experimental settings, and analysis pipeline), this type of behaviour, though (a macromolecular cell-envelope located machine reacting to recipient cells) is reminiscent to the results observed with the type VI secretion system (T6SS) of *Acinetobacter baylyi* (31). That study showed how the T6SS assembles in presence of target cells with equal efficiency at the surface of contact with the target cell and in parts that are not in direct

contact with it. Notably, also additional periplasmic and OM proteins (e.g., OmpA) were required for contact-dependent assembly of the T6SS. Those results would thus suggest that cells can sense the physical contact with target (or recipient) cells through a cascade dependent on the presence of specific proteins in the periplasm and OM, possibly interacting with their counterparts in the contacted cells. This could be explained with the fact that T6SS are used to specifically target and damage neighbouring cells (32,33), therefore, assembly at contact point is crucial. So far, we could not confirm that T4SS at the direct contact site with a recipient cell are more stable compared to elsewhere in the donor cell, which might be assumed to represent a characteristic of T4SS that engage in conjugation. However, for conjugation to occur, it might be rather the conjugative pilus that needs to contact recipient cells, which then only after pilus retraction leads to establishment of a conjugative pore between donor and recipient (34). We assume that this is the scenario for ICE*clc*, although recent evidence from the F-plasmid shows that there can be DNA transfer directly through the pilus to a physically distant cell (35), suggesting that direct contact may not always be a deciding factor in bacterial conjugation.

The only protein known to date to have a role in mating pair stabilization during conjugation is TraN, which is encoded on different conjugative plasmids (36,37). The idea with TraN is that it interacts with Omp proteins on the OM of the recipient cell, to stabilize the mating junction and allow DNA transfer. Interestingly, some elements encode different TraN isoforms, which seem to allow different conjugation efficiencies depending on the recipient species (34,38), implying an important role for TraN in the spread of those elements. However, we have not been able to identify a TraN-homolog on ICE*clc* (12), therefore, it is difficult to say if a similar mechanism exists which would stabilize mating pairs in ICE*clc* transfer. Previous data in our lab showed that individual tc cells can transfer the ICE to multiple contacted recipient cells simultaneously (16), suggesting that ICE*clc* also has evolved efficient mechanisms to stabilize mating pairs, which so far remain elusive.

In conclusion, we characterize the dynamic movement of two ICE*clc* T4SS subunits as representatives of two distinct subassemblies of the conjugation machine in individual *P. putida* transfer competent donor cells. All our evidence points to multiple complexes per cell with different assembly 'states', and independently circulating IMC and OMC. Our data suggest that the presence of recipient cells influences the dynamic movement of the OMC-'part', pointing at some mechanism to stabilize the T4SS at a mating pair contact site (although we could not detect this specifically).

Our work represents one of the first studies in which a systematic analysis on conjugation dynamics was performed.

References

1. Sheedlo, M.J., Ohi, M.D., Lacy, D.B. and Cover, T.L. (2022) Molecular architecture of bacterial type IV secretion systems. *PLoS Pathog*, **18**, e1010720.
2. Cabezon, E., Ripoll-Rozada, J., Pena, A., de la Cruz, F. and Arechaga, I. (2015) Towards an integrated model of bacterial conjugation. *FEMS Microbiol Rev*, **39**, 81-95.
3. Qiu, J. and Luo, Z.Q. (2013) Effector translocation by the Legionella Dot/Icm type IV secretion system. *Curr Top Microbiol Immunol*, **376**, 103-115.
4. Hofreuter, D., Odenbreit, S. and Haas, R. (2001) Natural transformation competence in *Helicobacter pylori* is mediated by the basic components of a type IV secretion system. *Mol Microbiol*, **41**, 379-391.
5. Christie, P.J., Atmakuri, K., Krishnamoorthy, V., Jakubowski, S. and Cascales, E. (2005) Biogenesis, architecture, and function of bacterial type IV secretion systems. *Annu Rev Microbiol*, **59**, 451-485.
6. Kubori, T. and Nagai, H. (2016) The Type IVB secretion system: an enigmatic chimera. *Curr Opin Microbiol*, **29**, 22-29.
7. Koraimann, G. (2018) Spread and Persistence of Virulence and Antibiotic Resistance Genes: A Ride on the F Plasmid Conjugation Module. *EcoSal Plus*, **8**.
8. Christie, P.J. (2016) The Mosaic Type IV Secretion Systems. *EcoSal Plus*, **7**.
9. Anthony, K.G., Sherburne, C., Sherburne, R. and Frost, L.S. (1994) The role of the pilus in recipient cell recognition during bacterial conjugation mediated by F-like plasmids. *Mol Microbiol*, **13**, 939-953.
10. Hu, B., Khara, P. and Christie, P.J. (2019) Structural bases for F plasmid conjugation and F pilus biogenesis in *Escherichia coli*. *Proc Natl Acad Sci U S A*, **116**, 14222-14227.
11. Park, D., Chetrit, D., Hu, B., Roy, C.R. and Liu, J. (2020) Analysis of Dot/Icm Type IVB Secretion System Subassemblies by Cryoelectron Tomography Reveals Conformational Changes Induced by DotB Binding. *mBio*, **11**.
12. Daveri, A., Benigno, V. and van der Meer, J.R. (2023) Characterization of an atypical but widespread type IV secretion system for transfer of the integrative and conjugative element (ICE_{lc}) in *Pseudomonas putida*. *Nucleic Acids Res*, **51**, 2345-2362.
13. Virolle, C., Goldlust, K., Djermoun, S., Bigot, S. and Lesterlin, C. (2020) Plasmid Transfer by Conjugation in Gram-Negative Bacteria: From the Cellular to the Community Level. *Genes (Basel)*, **11**.
14. Delavat, F., Miyazaki, R., Carraro, N., Pradervand, N. and van der Meer, J.R. (2017) The hidden life of integrative and conjugative elements. *FEMS Microbiol Rev*, **41**, 512-537.
15. Shen, M., Goldlust, K., Daniel, S., Lesterlin, C. and Yamaichi, Y. (2023) Recipient UvrD helicase is involved in single- to double-stranded DNA conversion during conjugative plasmid transfer. *Nucleic Acids Res*, **51**, 2790-2799.
16. Delavat, F., Moritz, R. and van der Meer, J.R. (2019) Transient Replication in Specialized Cells Favors Transfer of an Integrative and Conjugative Element. *mBio*, **10**.
17. Gerhardt, P., Murray, R., Costilow, R., Nester, E.W., Wood, W.A., Krieg, N.R. and Phillips, G.B. (1981) *Manual of methods for general bacteriology*. American Society for Microbiology Washington, DC.
18. Martinez-Garcia, E. and de Lorenzo, V. (2011) Engineering multiple genomic deletions in Gram-negative bacteria: analysis of the multi-resistant antibiotic profile of *Pseudomonas putida* KT2440. *Environ Microbiol*, **13**, 2702-2716.
19. Pradervand, N., Sulser, S., Delavat, F., Miyazaki, R., Lamas, I. and van der Meer, J.R. (2014) An operon of three transcriptional regulators controls horizontal gene transfer of the integrative and conjugative element ICE_{lc} in *Pseudomonas knackmussii* B13. *PLoS Genet*, **10**, e1004441.
20. Miyazaki, R. and van der Meer, J.R. (2011) A dual functional origin of transfer in the ICE_{lc} genomic island of *Pseudomonas knackmussii* B13. *Mol Microbiol*, **79**, 743-758.
21. Reinhard, F., Miyazaki, R., Pradervand, N. and van der Meer, J.R. (2013) Cell differentiation to "mating bodies" induced by an integrating and conjugative element in free-living bacteria. *Curr Biol*, **23**, 255-259.

22. Schindelin, J., Arganda-Carreras, I., Frise, E., Kaynig, V., Longair, M., Pietzsch, T., Preibisch, S., Rueden, C., Saalfeld, S., Schmid, B. *et al.* (2012) Fiji: an open-source platform for biological-image analysis. *Nat Methods*, **9**, 676-682.
23. Stylianidou, S., Brennan, C., Nissen, S.B., Kuwada, N.J. and Wiggins, P.A. (2016) SuperSegger: robust image segmentation, analysis and lineage tracking of bacterial cells. *Mol Microbiol*, **102**, 690-700.
24. Cascales, E. and Christie, P.J. (2004) Agrobacterium VirB10, an ATP energy sensor required for type IV secretion. *Proc Natl Acad Sci U S A*, **101**, 17228-17233.
25. Mace, K., Vadakkepat, A.K., Redzej, A., Lukoyanova, N., Oomen, C., Braun, N., Ukleja, M., Lu, F., Costa, T.R.D., Orlova, E.V. *et al.* (2022) Cryo-EM structure of a type IV secretion system. *Nature*, **607**, 191-196.
26. Rassam, P., Copeland, N.A., Birkholz, O., Toth, C., Chavent, M., Duncan, A.L., Cross, S.J., Housden, N.G., Kaminska, R., Seger, U. *et al.* (2015) Supramolecular assemblies underpin turnover of outer membrane proteins in bacteria. *Nature*, **523**, 333-336.
27. Clarke, M., Maddera, L., Harris, R.L. and Silverman, P.M. (2008) F-pili dynamics by live-cell imaging. *Proc Natl Acad Sci U S A*, **105**, 17978-17981.
28. Couturier, A., Virolle, C., Goldlust, K., Berne-Dedieu, A., Reuter, A., Nolivos, S., Yamaichi, Y., Bigot, S. and Lesterlin, C. (2023) Real-time visualisation of the intracellular dynamics of conjugative plasmid transfer. *Nat Commun*, **14**, 294.
29. Amin, H., Ilangovan, A. and Costa, T.R.D. (2021) Architecture of the outer-membrane core complex from a conjugative type IV secretion system. *Nat Commun*, **12**, 6834.
30. Samuels, A.L., Lanka, E. and Davies, J.E. (2000) Conjugative junctions in RP4-mediated mating of Escherichia coli. *J Bacteriol*, **182**, 2709-2715.
31. Lin, L., Capozzoli, R., Ferrand, A., Plum, M., Vettiger, A. and Basler, M. (2022) Subcellular localization of Type VI secretion system assembly in response to cell-cell contact. *EMBO J*, **41**, e108595.
32. Crisan, C.V. and Hammer, B.K. (2020) The Vibrio cholerae type VI secretion system: toxins, regulators and consequences. *Environ Microbiol*, **22**, 4112-4122.
33. Unterweger, D., Miyata, S.T., Bachmann, V., Brooks, T.M., Mullins, T., Kostiuik, B., Provenzano, D. and Pukatzki, S. (2014) The Vibrio cholerae type VI secretion system employs diverse effector modules for intraspecific competition. *Nat Commun*, **5**, 3549.
34. Low, W.W., Wong, J.L.C., Beltran, L.C., Seddon, C., David, S., Kwong, H.S., Bizeau, T., Wang, F., Pena, A., Costa, T.R.D. *et al.* (2022) Mating pair stabilization mediates bacterial conjugation species specificity. *Nat Microbiol*, **7**, 1016-1027.
35. Goldlust, K., Ducret, A., Halte, M., Dedieu-Berne, A., Erhardt, M. and Lesterlin, C. (2023) The F pilus serves as a conduit for the DNA during conjugation between physically distant bacteria. *Proc Natl Acad Sci U S A*, **120**, e2310842120.
36. Klimke, W.A., Rypien, C.D., Klinger, B., Kennedy, R.A., Rodriguez-Maillard, J.M. and Frost, L.S. (2005) The mating pair stabilization protein, TraN, of the F plasmid is an outer-membrane protein with two regions that are important for its function in conjugation. *Microbiology (Reading)*, **151**, 3527-3540.
37. Klimke, W.A. and Frost, L.S. (1998) Genetic analysis of the role of the transfer gene, traN, of the F and R100-1 plasmids in mating pair stabilization during conjugation. *J Bacteriol*, **180**, 4036-4043.
38. Low, W.W., Seddon, C., Beis, K. and Frankel, G. (2023) The Interaction of the F-Like Plasmid-Encoded TraN Isoforms with Their Cognate Outer Membrane Receptors. *J Bacteriol*, **205**, e0006123.

Supplementary information

Table S1 List and description of the strains used in this work

Strains	Strain number	Description	Reference
<i>E. coli</i> DH5 α - λ pir	1854	λ pir lysogen	(1)
<i>P. putida</i> UWC1 Tn7-P _{tac} -mcherry	2744	<i>P. putida</i> UWC1 carrying Tn7-P _{tac} -mCherry (used as ICEclc recipient)	(2)
<i>P. putida</i> UWC1 Tn7-sGFP2	7596	<i>P. putida</i> UWC1 carrying Tn7-sGFP2 expressing constitutive sGFP2 (used as ICEclc recipient)	This study
<i>P. putida</i> UWC1-clc5, lacO _{array} , iceB4::sfgfp	7461	<i>P. putida</i> UWC1 ICEclc lacO _{array} with sfgfp insertion downstream of orf59888 (iceB4) in the ICEclc element.	(3)
<i>P. putida</i> UWC1-clc5, lacO _{array} , iceB7::mcherry	7539	<i>P. putida</i> UWC1 ICEclc lacO _{array} with mcherry insertion downstream of orf73676 (iceB7) in the ICEclc element.	(3)
<i>P. putida</i> UWC1-clc5, lacO _{array} , iceB7::mcherry, iceB4::sfgfp, Δ mfsR	7776	Derivative of strain 7461, with an additional insertion of mcherry downstream of iceB7 in the ICEclc element and a deletion of the mfsR gene.	This study

Table S2 List of plasmids used in this study

Plasmid	Description	Reference
pEMG	Km ^R , oriR6K, P _{tac} -lacZ α , I-SceI sites	(4)
pSW	Amp ^R , oriRK2, P _m -I-SceI	(4)
pEMG-HR-mfsR	pEMG derivative allowing the deletion of mfsR in the ICEclc element.	This study
pMRE-Tn7-152	Mini Tn7 system used for the constitutive expression of sGFP2.	(5)

Table S3 List of primers used in this study

Primer number	Sequence 5'-3' ^a	Target
221001	<i>TAGGGATAACAGGGTAATCTGAATT</i> <u>CGCAAGACTTTTCTATGGGTG</u>	Amplification of upstream and downstream flanking regions for mfsR deletion
221002	TTGGTTAGTGCGTTGCAT	
221003	AGATGCAACGCACTAACCAAGAAGCGTCCAGTAAACGC	
221004	AGAAGCTTGCATGCCTGCAGGTCGACTTGTGCTTGCTCCAGGA	

a) Restriction enzyme sequences are underlined and primer overhangs are displayed in italic.

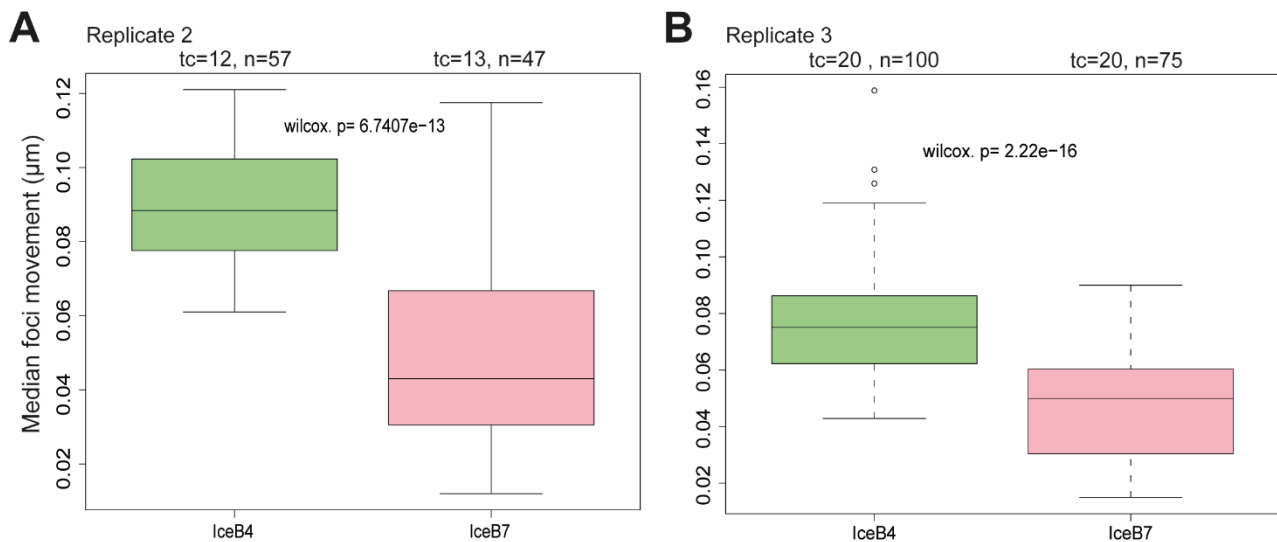


Figure S1 Dynamic behaviour of of IceB4 and IceB7 subunits. A-B) Median foci movement of IceB4-sfGFP and IceB7-mCherry foci between two time points, calculated from the foci coordinates in tc cells. Statistical significance between the datasets was assessed with a two sided Wilcoxon test ($p = p\text{-value}$, $tc =$ number of tc cells in the experiment, $n =$ number of single foci). The two datasets were obtained from two independent experiments.

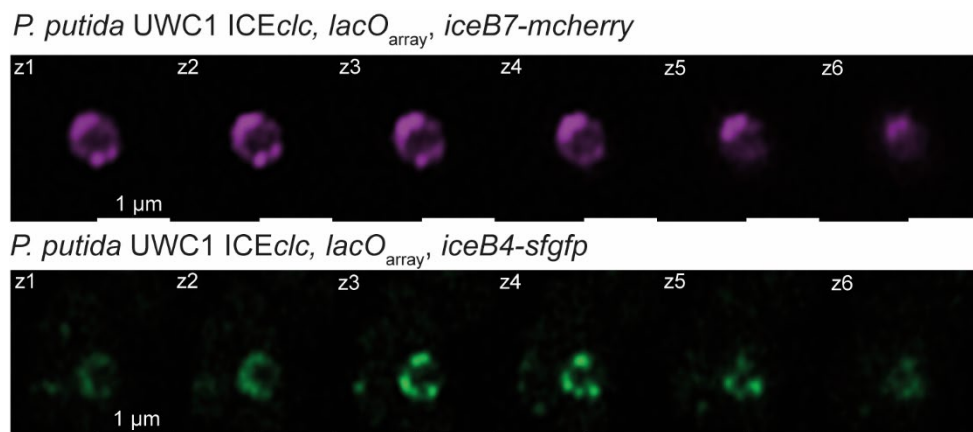


Figure S2 Z-stack of fluorescently labelled tc cells. Micrographs representing z-stacks of the indicated *P. putida* UWC1 (step between snapshots 0.17 μm). Ayriscan high-resolution images.

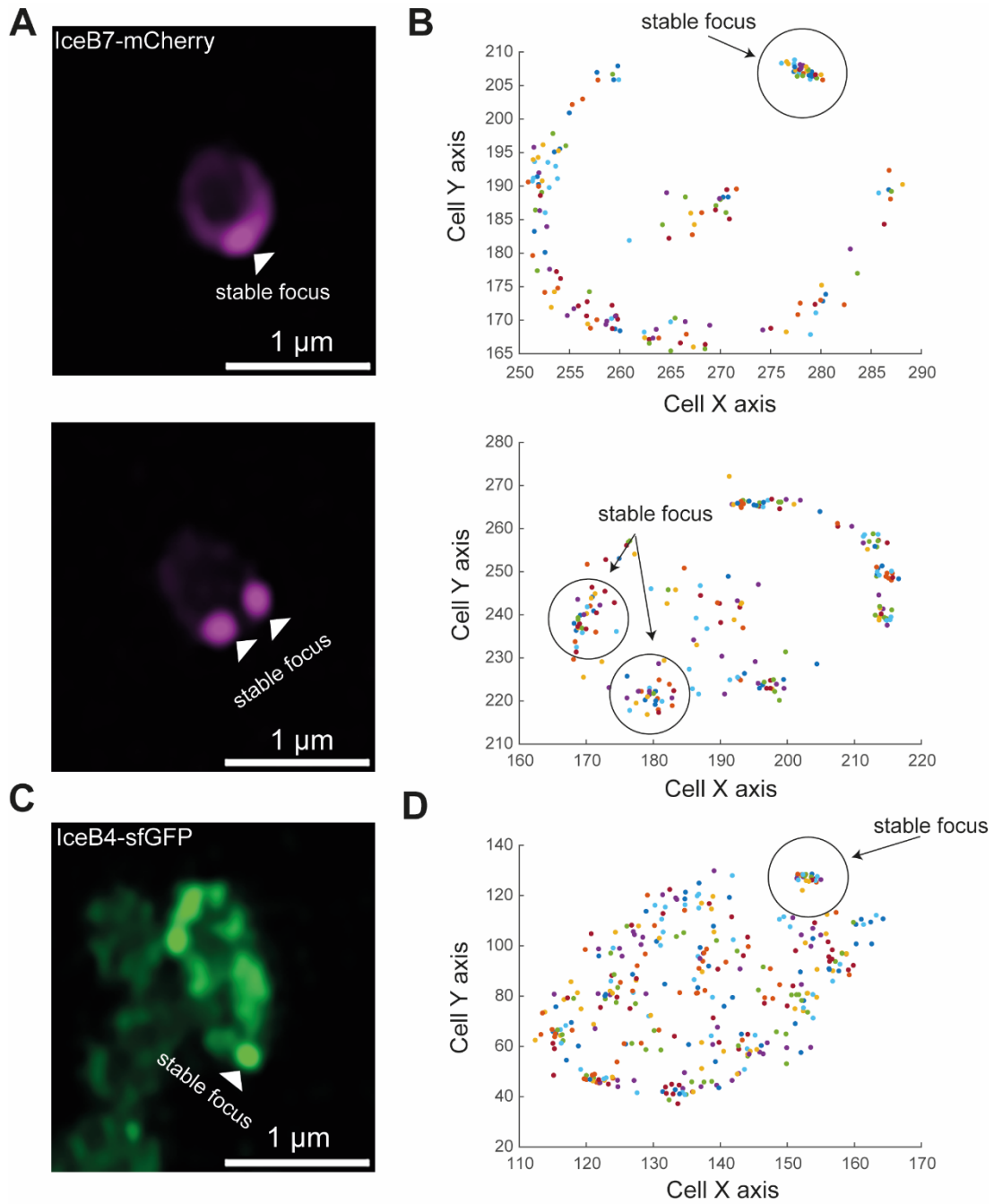


Figure S2 Foci map in tc cells. **A-C)** Microscopy images of *P. putida* UWC1 ICElc strain with the indicated fluorescent tag. Stable foci are indicated in the image with a white triangle. Ayriscan high-resolution images, 170 nm slices. **B-D)** Map of foci localization over the course of 60 minutes. Dots represent the coordinates of the IceB7-mCherry and IceB4-sfGFP foci centre at a given time point. Each color represent a single time point. Stable foci are indicated with a black circle.

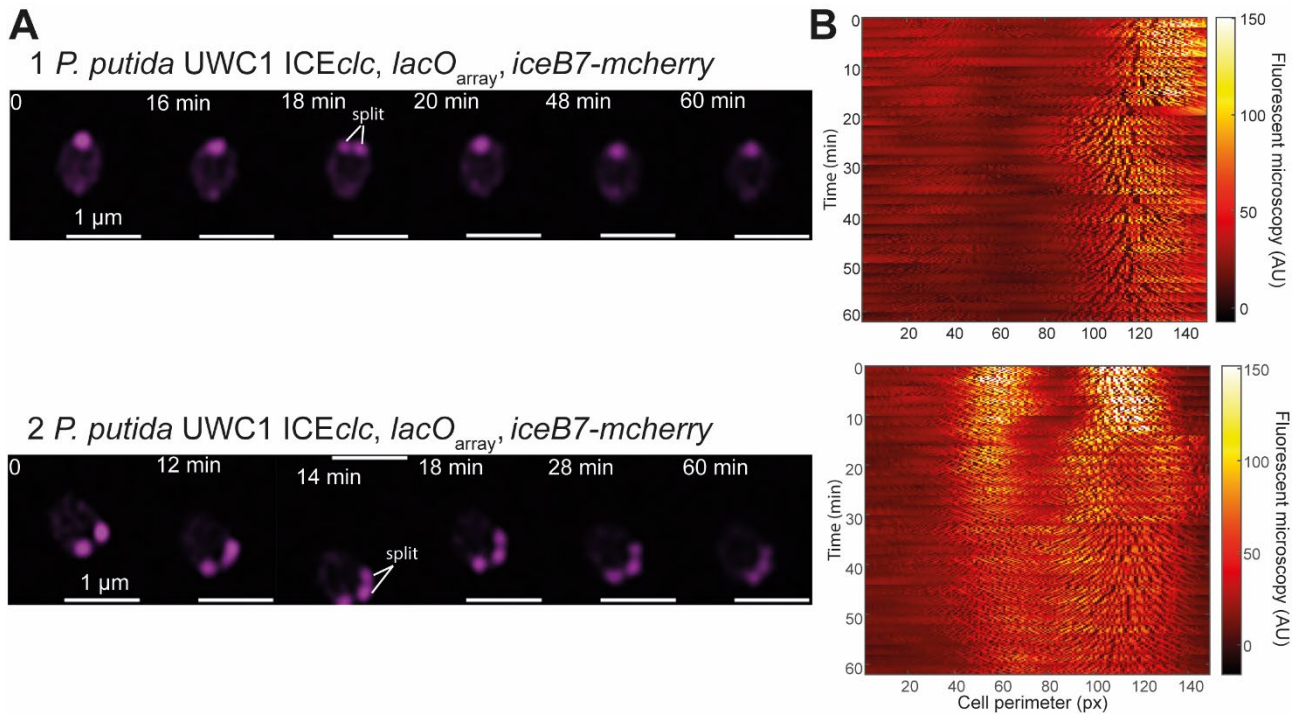


Figure S3 IceB7 foci split in rare occasions. A) Micrographs of the indicated *P. putida* strains imaged for 60 minutes (interval between snapshots 2 minutes). Ayriscan high-resolution images, 170 nm slices. Foci splitting events are indicated in the respective frame. **B)** Kymographs representing the fluorescence profile of the respective tc-cell. The 10 outmost pixels of a tc cells are linearly projected for each time point.

Reference

1. Platt, R., Drescher, C., Park, S.K. and Phillips, G.J. (2000) Genetic system for reversible integration of DNA constructs and *lacZ* gene fusions into the *Escherichia coli* chromosome. *Plasmid*, **43**, 12-23.
2. Miyazaki, R. and van der Meer, J.R. (2011) A dual functional origin of transfer in the ICE $_{clc}$ genomic island of *Pseudomonas knackmussii* B13. *Mol Microbiol*, **79**, 743-758.
3. Daveri, A., Benigno, V. and van der Meer, J.R. (2023) Characterization of an atypical but widespread type IV secretion system for transfer of the integrative and conjugative element (ICE $_{clc}$) in *Pseudomonas putida*. *Nucleic Acids Res*, **51**, 2345-2362.
4. Martinez-Garcia, E. and de Lorenzo, V. (2011) Engineering multiple genomic deletions in Gram-negative bacteria: analysis of the multi-resistant antibiotic profile of *Pseudomonas putida* KT2440. *Environ Microbiol*, **13**, 2702-2716.
5. Schlechter, R.O., Jun, H., Bernach, M., Oso, S., Boyd, E., Munoz-Lintz, D.A., Dobson, R.C.J., Remus, D.M. and Remus-Emsermann, M.N.P. (2018) Chromatic Bacteria - A Broad Host-Range Plasmid and Chromosomal Insertion Toolbox for Fluorescent Protein Expression in Bacteria. *Front Microbiol*, **9**, 3052.

Chapter 5

General Discussion and Outlook

The aim of this thesis was to characterize the genetic locus coding for the transfer of the ICE*clc* element, which serves as a representative for the poorly characterized **MPF_G** class of T4SS, mostly found in ICEs belonging to β and γ -Proteobacteria (1). With a combination of *in silico* and *in vivo* approaches we dissected the possible structural organization of the ICE-T4SS and the subunits that form the different subassemblies in the machinery. To gain more knowledge on ICE transfer at a single cell level, I fluorescently labelled several subunits of the T4SS and followed their localization with epifluorescence microscopy. High-resolution time-lapse microscopy helped in elucidating dynamics of two different T4SS subunits in the outer and inner membrane. With different electron microscopy techniques (EM) I was also able to visualize what is likely the ICE*clc* conjugative pilus.

Previous studies in our group on ICE*clc* mostly focused on the regulatory aspects of its activation and excision (2-5), and on the physiology of the resulting transfer competent (tc) cells (6-8). Here we centered our efforts on the conjugative transfer which was predicted to be encoded in a ~20 kb region going from *orf53587* to *orf73676* (9) (Figure 1).

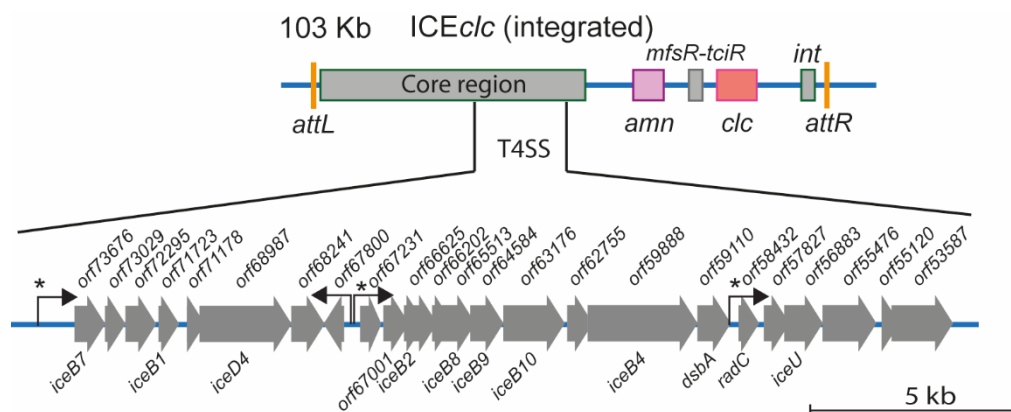


Figure 1 ICE*clc* conjugative transfer genetic locus. Detailed map of the conjugative gene region of ICE*clc*. Genes and their orientation are represented by gray arrows, with their original orf designation (as in GenBank AJ617740.2) described above and the deduced relevant gene names below (gene names follow analogous designation as in the vir system). Hooked arrows indicate known promoters; an asterisk pointing to those being active only in transfer competent cells as shown in Ref. (9).

In the main part of the project, we conducted a systematic analysis of the gene functions involved in ICE*clc* conjugation, which serves as a representative example of the poorly known MPF_G clade within T4SS conjugation systems (1). Our findings reveal that ICE*clc* encodes a conjugative system with both structural similarities to known T4SS systems and several unique components. These unique components are shared by a broader class of elements related to ICE*clc*. Our investigation also uncovered that the formation of the ICE*clc*-T4SS is limited to tc cells, which can carry multiple

such systems per cell, maybe each dedicated to a different copy of ICE*clc* for transfer to multiple recipients, as observed through microscopy imaging. The occurrence of multiple T4SS in *P. putida* tc cells resembles findings in *Agrobacterium tumefaciens* (10,11) and *Legionella pneumophila* Dot/Icm (12). Our functional analysis relied on detailed bioinformatic structural assessments, individual gene deletion and complementation studies, fluorescent fusion protein analysis, and their effects on ICE transfer on solid media. Within the ICE*clc* conjugative gene region, we identified 14 essential components. Although there were limited amino acid similarities and predicted structural homologies, we managed to classify analogs of archetypal T4SS structural components within the ICE*clc* system. These include IceB2 (analogous to VirB2, from *A. tumefaciens* VirB system), IceB4, IceB7, IceB8, IceB9, IceB10, and IceD4 (see Table 1, Chapter 2), which were all essential for ICE*clc* transfer. Single-copy complementation under the control of a transfer competence promoter partially or fully restored transfer in all cases except for *orf53587*, underscoring their gene-specific effects.

Microscopy imaging of strains expressing translational fluorescent protein fusions from their native ICE*clc* loci demonstrated that IceD4, IceB4, IceB8, and IceB7 fusions formed distinct localized fluorescent foci in the cell envelope. Of these, IceD4, IceB4, and IceB7 fusions retained wild-type transfer rates, confirming their functionality. Mutation studies, conducted in backgrounds of fluorescently-tagged ICE proteins, suggested that foci formation of IceB4-sfGFP was hindered by deletions of *iceB7*, *iceB8*, *iceB10*, *orf53587*, and *orf66202*; IceD4-sfGFP foci were affected by deletions of *iceB4* and *iceB10*, and IceB7-mCherry foci were influenced by *iceB9* or *orf62755*. This aligns with the hypothesis that IceB4, IceB7, IceB8, IceB9, IceB10, and IceD4 form a multicomponent structure similar to known plasmid-type T4SSs, in which components form a complex network of interactions between each other. Our study draws parallels between the ICE*clc* system and other T4SSs, supporting the notion of their shared structural resemblance. Fluorescent protein fusions to Orf66202 also formed multiple visible foci in the cell envelope of tc cells and remained functionally intact. Orf66202 is predicted to be an inner membrane protein with two transmembrane helices, potentially serving a role akin to VirB3 (13), although no detectable sequence or structural similarity exists between Orf66202 and VirB3. Furthermore, a colocalization experiment between IceB4 and IceB7 revealed a non-complete overlap of fluorescent foci, suggesting the existence of diverse assembly states of the T4SS, which would be in line with findings from cryo-electron microscopy of *E. coli* F-plasmid T4SS complexes, which revealed four distinct structural configurations of the machinery (14).

We fluorescently labelled two other proteins essential for transfer: Orf55476 and IceU (product of *orf56883*). Their exact role in conjugation is not clear, but colocalization studies and observation in mutant background revealed that Orf55476-mCherry foci largely co-localized with IceB4-sfGFP in individual cells. Moreover, Orf55476-mCherry foci formation was dependent on the presence of Orf68241, which is itself an essential transfer protein, suggesting its involvement in the inner membrane complex assembly. Our fluorescent reporter fusion to IceU was transfer-functional and localized to the cell envelope, producing occasional foci, which aligns with its predicted periplasmic location. This suggests a role for IceU in transfer, possibly involving transient interactions with T4SS complexes.

Some deletions within the ICE*clc* T4SS locus led to partial inhibition of transfer, while others had no significant effect. Several of these genes had well-defined predicted functions. For instance, *iceB1* (*orf71723*) encodes a lytic transglycosylase, which is commonly found in T4SS conjugative systems and are believed to play a role in locally degrading peptidoglycan to facilitate T4SS complex formation. Its deletion resulted in a substantial reduction in ICE transfer, down to approximately 3% compared to the wild type, similar to what is observed when the functional analog VirB1 is deleted in the *A. tumefaciens* system (15). Another gene *orf58432* belongs to the RadC family, its role in conjugation remains enigmatic, in our assay its deletion did not affect ICE*clc* transfer in tested conditions. Within the ICE*clc* T4SS locus, four genes were predicted to encode thioredoxin (*orf57827*, *orf59110*, *orf71178*, *orf72295*) homologs. Similar numbers of thioredoxins have been observed in other T4SS systems, such as those found in the F- and R27-plasmids of *E. coli* (16). These thioredoxins are thought to assist in the folding or stabilization of periplasmic, pilin, and outer membrane subunits of the T4SS. However, when deleted individually, they had only mild effects (a 10-fold reduction for *orf71178* and a 4-fold reduction for *orf57827*) or no impact on ICE*clc* transfer for *orf59110*, possibly due to functional redundancies.

Our study combined mutation analysis with the quantification of fluorescent foci, providing insights into the ICE*clc* conjugative system. However, the analysis of fluorescent foci in tc (transfer-competent) cells comes with limitations due to restricted resolution. Nevertheless, controls in isogenic *P. putida* cells lacking ICE*clc*, with overexpressed fluorescent proteins showed homogeneous signals, which demonstrates that foci were not the result of nonspecific fluorescent protein aggregation, but rather reflections of T4SS subunit multimerization.

In conclusion, our study offers a comprehensive characterization of the ICE*clc* conjugative system and its subcellular localization. While it shares similarities with known plasmid-type T4SSs, it also possesses distinct structural elements and previously unreported dependencies. The conservation of ICE*clc* gene loci in other β - and γ -proteobacteria, both in sequence and gene synteny, suggests that these T4SS gene regions may be part of other ICE*clc*-related elements.

In the second part of the thesis, we worked on the identification of the ICE*clc* conjugative pilin, visualization of the conjugative pilus in live cells, and we conducted a systematic investigation into the subcellular localization of *orf67231* using microscopy. Previous comparative studies suggested two possible candidate pilin genes: *orf66625* and *orf67231* (1). Tridimensional protein modelling pointed to *orf66625* as the gene encoding the pilin, which we renamed *iceB2*. In order to visualize the pilus, we adopted different microscopy techniques, one based on the chemical bonding between a maleimide-conjugated fluorophore and the S-H group of a cysteine residue, as previously described (17,18), the second is an electron microscopy technique named cryo-CLEM.

For successful maleimide staining, we introduced cysteine modifications at various positions in the two candidate pilin genes *orf67231* and *iceB2*. Introducing a cysteine at three different positions in *orf67231* did not affect the efficiency of ICE transfer. On the contrary, modifications attempted on *iceB2* either completely abolished ICE transfer or significantly reduced it. During our experiments, we observed a pilus-like structure in a restricted percentage of the entire cell population, which is even lower than the tc cell appearance. This observation can be justified by the fact that not all T4SS elongate the pilus at all times as proven by cryo-EM studies (14), thus not all tc cells produce pili. We observed similar phenotypes in our cryo-EM, indeed of the nearly 100 tc cells that we imaged, only 7 of them showed formation of pili like structures. Measurements of the width of these pili-like structures corresponds to examples found in literature (19-21). Interestingly though some tc cells formed a different filamentous structure, whose morphology and width highly resemble the one of flagella (22).

Maleimide labeling of modified *orf67231* did not yield conclusive results. Only a very small percentage of the transfer-competent population was stained with the dye, and no pilus-like structures were observed. This suggests that Orf67231 is not exposed to the extracellular space, thus confirms that is not a building block of the pilus. To further investigate the cellular localization of Orf67231, we fused it to a fluorescent protein. Both epifluorescent and higher-resolution Airyscan microscopy revealed the presence of multiple foci around the cell, with a periplasmic background.

This suggests that despite not being essential for transfer, Orf67231 associates with the T4SS in the periplasm and likely plays an important, albeit unclear, role in conjugation.

In the last chapter our aim was to study the localization of different T4SS subunits over time. Based on the evidence that we collected in previous experiments in which different subunits of the secretion system did not co-localize in a significant part of the tc cell population (23), our hypothesis was that different protein subassemblies (IMC, OMC) could exist as independent units and that T4SS can exist in several conformational states. Indeed, solved 3D structures of conjugative machineries from cryo-EM images showed the presence of both complete and incomplete T4SS (missing some subunits) as well as different conformational states (12,14). Here we focused exclusively on two T4SS subunits, one belonging to the outer membrane complex (OMC) namely IceB7 and the second is the cytoplasmic ATPase IceB4 that associates with the inner membrane complex (IMC). Our data showed that fluorescently labelled IceB4 moves around the membrane at higher speeds compared to IceB7, which on the other hand is highly stable for the duration of our experiments. We also gathered some evidence proving that the presence of recipient cells has an effect on IceB7 mobility. Overall, our data, together with other studies, prove that different T4SS protein subassemblies can exist as independent units and that, conjugation is a highly dynamic process, where the secreting machinery has to go through several structural rearrangements, leading to successful DNA transfer. Capturing all the details of such a complex biological mechanism is evidently extremely difficult, mostly due to technical limitations. Nevertheless, with the continuous development of cryo-EM, light microscopy and with the help of deep learning we can realistically think of solving this long lasting question. Below, we propose a model of how T4SS assembly states may look like in tc cells. In Figure 2 we present a *Pseudomonas* tc cell, with multiple copies of excised ICE l c molecules and its own T4SS assembled in the different structural configurations that we hypothesize: pilus assembling T4SS, DNA transferring T4SS, incomplete T4SS and isolated IceB4 subunits.

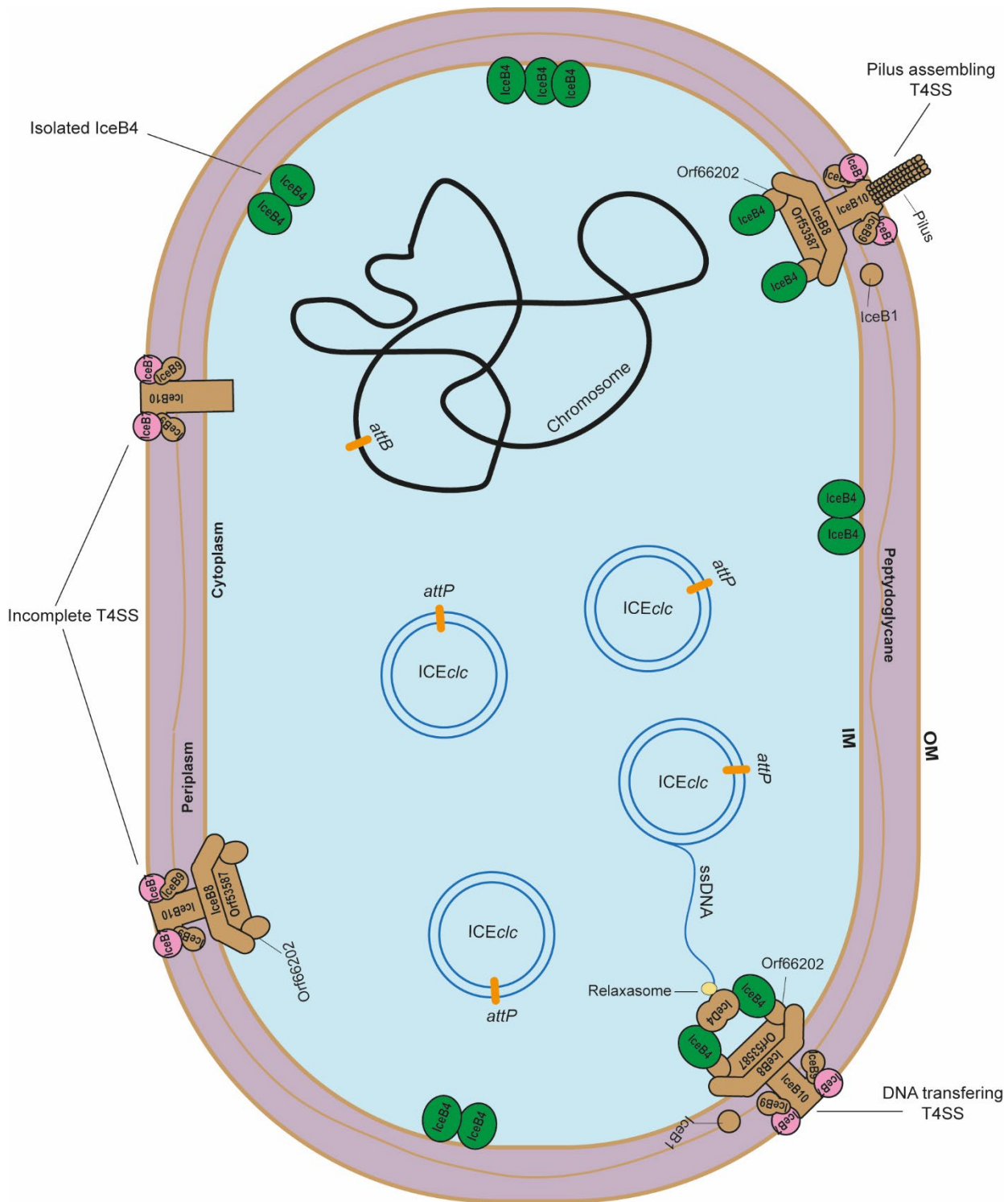


Figure 2 Schematic overview of ICEclc T4SS assembly states in tc cells. The figure represents a *P. putida* UWC1 ICEclc tc cell, in which ICEclc is excised (*attP*, *attB*, attachment sites) and the conjugative transfer genes are actively expressed (OM, outer membrane; IM, inner membrane). The two fluorescently labelled subunits IceB4 and IceB7 of the T4SS, on which we focused for our dynamics studies, are highlighted in green and pink respectively. Here we represent different structural configurations of the T4SS. Notably: DNA transferring T4SS (complete secretion system, including coupling protein IceD4), Pilus assembling T4SS (complete secretion system, without IceD4 and DNA substrate), Incomplete T4SS (partial or missing IMC), Isolated IceB4 (IceB4 subunits not attached to the secretion system). In the cytoplasmic compartment of the cell we find ICEclc circular molecules and the chromosome.

Outlook

Although we made important advancements on ICE*clc* conjugation, there are many aspects that remain unclear. Despite many attempts, we did not manage to obtain a structure of the ICE-T4SS in the cell, not of the 'complete' complex nor of parts of it, simply because the events are too rare and too difficult to spot even in cryo-CLEM and the subsequent cryo-EM images. Increasing tc cell formation frequencies like in the strains carrying the *mfsR* deletion, was not enough. Unfortunately, *P. putida* cells are slightly too thick (700 nm in stationary phase), which precludes direct complete imaging of T4SS complexes like was possible for *Legionella* (24). Having (a) better structure(s) would help to unravel which subunits of the genetic loci that we characterized actually have a structural role in the assembly of the system, specifically for those for which we could not find homologies to other known T4SS components. At the same time, this would allow to understand interactions between the different components, and therefore the mechanistic details underlying conjugation. Purification of the complete T4SS complexes from tc cells could be another avenue to pursue for structural analysis, but this is currently outside our competence.

Another aspect of conjugation which has barely been investigated is donor-recipient interaction. One of the assumed roles of the conjugative pilus is to scan the extracellular space in search of potential recipients. However, how pili recognize the recipient cell and bring it in contact with the donor is totally unknown. It is highly likely that there is either a set of outer membrane proteins or lipopolisaccharides on the recipient cell surface that are recognized by the pilus in order to confer specificity, and improve efficiency. Published works suggest Omp proteins on the recipient outer membrane to play an important function in mating pair stabilization. Therefore, knockout studies of *omp* genes in recipients might, at least partially, reveal details on donor-recipient interaction for ICE*clc* transfer. Secondly, in order for the DNA to be transferred a hole in both recipient membranes needs to be formed, again here there is close to no knowledge on the molecular and mechanistic processes that take place in the recipient cell. With the use of cryo-CLEM tomography, it might be possible to capture transfer events in live cells and possibly characterize the morphology of the mating junction.

Many other aspects of ICE*clc* conjugation could be investigated more in depth. For example, in our lab we recently discovered an ICE*clc*-encoded protein named BisD (3) with strong homology to ParB (25). This protein is thought to be important for ICE*clc* partition during cell division, to ensure its maintenance in the bacterial population. BisD specifically binds to the ICE DNA, therefore we could

potentially follow ICE*clc* localization in the cell by using fluorescent protein fusions to BisD. By combining BisD and one of the T4SS components fluorescent fusions, we could then follow even more closely the transfer dynamics of ICE*clc*. A modified strain of *P. putida* with a combination of *iceD4* and *bisD* fluorescent fusions has already been produced in our lab, but time was insufficient to carry out experiments to study the colocalization of the two proteins and possible ICE*clc* dynamics.

To conclude, it is important to invest time and resources towards better understanding of all aspects of bacterial conjugation, as it is one of the major players in the evolution of microorganisms, which shape our environment and influence our everyday life. As a prominent example we can think of the increasing appearance of antimicrobial-resistant bacteria, which is becoming one of the primary threats to human health. The main cause of this is in fact Horizontal Gene Transfer between bacteria. Actually, some ICE*clc* related elements confer antibiotic resistance in pathogenic *Pseudomonas aeruginosa* strains (23). Therefore, my data could provide important notions to fight against the dissemination of these elements, for example by developing drugs that would block the T4SS activity.

References

1. Guglielmini, J., Neron, B., Abby, S.S., Garcillan-Barcia, M.P., de la Cruz, F. and Rocha, E.P. (2014) Key components of the eight classes of type IV secretion systems involved in bacterial conjugation or protein secretion. *Nucleic Acids Res*, **42**, 5715-5727.
2. Sulser, S., Vucicevic, A., Bellini, V., Moritz, R., Delavat, F., Sentchilo, V., Carraro, N. and van der Meer, J.R. (2022) A bistable prokaryotic differentiation system underlying development of conjugative transfer competence. *PLoS Genet*, **18**, e1010286.
3. Carraro, N., Richard, X., Sulser, S., Delavat, F., Mazza, C. and van der Meer, J.R. (2020) An analog to digital converter controls bistable transfer competence development of a widespread bacterial integrative and conjugative element. *Elife*, **9**.
4. Pradervand, N., Delavat, F., Sulser, S., Miyazaki, R. and van der Meer, J.R. (2014) The TetR-type MfsR protein of the integrative and conjugative element (ICE) ICEclc controls both a putative efflux system and initiation of ICE transfer. *J Bacteriol*, **196**, 3971-3979.
5. Miyazaki, R., Minoia, M., Pradervand, N., Sulser, S., Reinhard, F. and van der Meer, J.R. (2012) Cellular variability of RpoS expression underlies subpopulation activation of an integrative and conjugative element. *PLoS Genet*, **8**, e1002818.
6. Delavat, F., Mitri, S., Pelet, S. and van der Meer, J.R. (2016) Highly variable individual donor cell fates characterize robust horizontal gene transfer of an integrative and conjugative element. *Proc Natl Acad Sci U S A*, **113**, E3375-3383.
7. Reinhard, F. and van der Meer, J.R. (2014) Life history analysis of integrative and conjugative element activation in growing microcolonies of *Pseudomonas*. *J Bacteriol*, **196**, 1425-1434.
8. Reinhard, F., Miyazaki, R., Pradervand, N. and van der Meer, J.R. (2013) Cell differentiation to "mating bodies" induced by an integrating and conjugative element in free-living bacteria. *Curr Biol*, **23**, 255-259.
9. Gaillard, M., Pradervand, N., Minoia, M., Sentchilo, V., Johnson, D.R. and van der Meer, J.R. (2010) Transcriptome analysis of the mobile genome ICEclc in *Pseudomonas knackmussii* B13. *BMC Microbiol*, **10**, 153.
10. Aguilar, J., Cameron, T.A., Zupan, J. and Zambryski, P. (2011) Membrane and core periplasmic *Agrobacterium tumefaciens* virulence Type IV secretion system components localize to multiple sites around the bacterial perimeter during lateral attachment to plant cells. *mBio*, **2**, e00218-00211.
11. Aguilar, J., Zupan, J., Cameron, T.A. and Zambryski, P.C. (2010) *Agrobacterium* type IV secretion system and its substrates form helical arrays around the circumference of virulence-induced cells. *Proc Natl Acad Sci U S A*, **107**, 3758-3763.
12. Park, D., Chetrit, D., Hu, B., Roy, C.R. and Liu, J. (2020) Analysis of Dot/Icm Type IVB Secretion System Subassemblies by Cryoelectron Tomography Reveals Conformational Changes Induced by DotB Binding. *mBio*, **11**.
13. Jones, A.L., Shirasu, K. and Kado, C.I. (1994) The product of the *virB4* gene of *Agrobacterium tumefaciens* promotes accumulation of VirB3 protein. *J Bacteriol*, **176**, 5255-5261.
14. Hu, B., Khara, P. and Christie, P.J. (2019) Structural bases for F plasmid conjugation and F pilus biogenesis in *Escherichia coli*. *Proc Natl Acad Sci U S A*, **116**, 14222-14227.
15. Mushegian, A.R., Fullner, K.J., Koonin, E.V. and Nester, E.W. (1996) A family of lysozyme-like virulence factors in bacterial pathogens of plants and animals. *Proc Natl Acad Sci U S A*, **93**, 7321-7326.
16. Elton, T.C., Holland, S.J., Frost, L.S. and Hazes, B. (2005) F-like type IV secretion systems encode proteins with thioredoxin folds that are putative DsbC homologues. *J Bacteriol*, **187**, 8267-8277.
17. Ellison, C.K., Dalia, T.N., Dalia, A.B. and Brun, Y.V. (2019) Real-time microscopy and physical perturbation of bacterial pili using maleimide-conjugated molecules. *Nat Protoc*, **14**, 1803-1819.
18. Ellison, C.K., Kan, J., Dillard, R.S., Kysela, D.T., Ducret, A., Berne, C., Hampton, C.M., Ke, Z., Wright, E.R., Biais, N. *et al.* (2017) Obstruction of pilus retraction stimulates bacterial surface sensing. *Science*, **358**, 535-538.

19. Kreida, S., Narita, A., Johnson, M.D., Tocheva, E.I., Das, A., Ghosal, D. and Jensen, G.J. (2023) Cryo-EM structure of the *Agrobacterium tumefaciens* T4SS-associated T-pilus reveals stoichiometric protein-phospholipid assembly. *Structure*, **31**, 385-394 e384.
20. Zheng, W., Pena, A., Low, W.W., Wong, J.L.C., Frankel, G. and Egelman, E.H. (2020) Cryoelectron-Microscopic Structure of the pKpQIL Conjugative Pili from Carbapenem-Resistant *Klebsiella pneumoniae*. *Structure*, **28**, 1321-1328 e1322.
21. Costa, T.R.D., Ilangoan, A., Ukleja, M., Redzej, A., Santini, J.M., Smith, T.K., Egelman, E.H. and Waksman, G. (2016) Structure of the Bacterial Sex F Pilus Reveals an Assembly of a Stoichiometric Protein-Phospholipid Complex. *Cell*, **166**, 1436-1444 e1410.
22. Tan, J., Zhang, X., Wang, X., Xu, C., Chang, S., Wu, H., Wang, T., Liang, H., Gao, H., Zhou, Y. *et al.* (2021) Structural basis of assembly and torque transmission of the bacterial flagellar motor. *Cell*, **184**, 2665-2679 e2619.
23. Daveri, A., Benigno, V. and van der Meer, J.R. (2023) Characterization of an atypical but widespread type IV secretion system for transfer of the integrative and conjugative element (ICEclc) in *Pseudomonas putida*. *Nucleic Acids Res*, **51**, 2345-2362.
24. Chetrit, D., Hu, B., Christie, P.J., Roy, C.R. and Liu, J. (2018) A unique cytoplasmic ATPase complex defines the *Legionella pneumophila* type IV secretion channel. *Nat Microbiol*, **3**, 678-686.
25. Soh, Y.M., Davidson, I.F., Zamuner, S., Basquin, J., Bock, F.P., Taschner, M., Veening, J.W., De Los Rios, P., Peters, J.M. and Gruber, S. (2019) Self-organization of parS centromeres by the ParB CTP hydrolase. *Science*, **366**, 1129-1133.

Acknowledgements

I want to spend the first words for my supervisor Jan. I want to thank him for giving me the opportunity to conduct research in his laboratory and for his attentive and passionate supervision. He never failed to give an advice when asked, and his help was crucial for the complicated image analysis that we performed in my project.

My appreciation extends to all EEM lab present and past members, you contributed to have a great working atmosphere and I will carry some great memories from my 5 years in the lab. Special thanks to Nico, Tania, Senka, Maxime, Roxane, Diogo, Valentina, Bouke, Anthony, Gaitan, Vladimir and Omar. You are all fantastic!!!

I want to thank the students that I had the pleasure to supervise during my project, Valentina, Samuel and Iris. In particular Valentina and Samuel who with their work majorly contributed to the project.

To all the people I met in DMF, who contribute to make this department a stimulating and pleasant place to work. I want to acknowledge all the administrative staff in DMF who helped me in several situations during the PhD. Thank you Aline, Nassim, Valeria and Nazife.

I want to thank the people at the Electron Microscopy Facility of UNIL, for training me and teaching me all the complicated techniques that I needed for my project. Special thanks to Christel, Jean, Damian and Antonio for their infinite patience.

I want to thank prof. Manuela Hospenthal for hosting me in her lab and Wang Dianhong for the crucial advices for the development of a cryo-EM protocol.

I also want to acknowledge my thesis committee: Melanie Blokesch, Stephan Gruber and Claus Wedekind.

I obviously want to thank all members of my family, who always supported me in all my choices. My parents, cousins, uncles, grandmothers thank you very much!

I want to thank my close friends, Enrico and Francesco. Although we are all scattered around Europe we never failed to hang out when possible, thank you guys!

Last but not least I want to thank my girlfriend Arianna. She was by my side during all these years, and without her presence and support it would have been much more difficult to successfully complete such a difficult challenge like the PhD. Thank you are amazing!!

CURRICULUM VITAE

Name	Andrea
Surname	Daveri
Date of Birth	May 24th, 1994
Citizenship	Italy
Residence Permit	Swiss B Permit
Contact	andrea.daveri@unil.ch; +41765792494

University of Lausanne

01.2019 to Present – Doctoral Research (PhD candidate)

Environmental and Evolutionary Microbiology laboratory | Supervisor: Prof. Jan Roelof van der Meer

Research project: The conjugative system encoded by the integrative conjugative element ICE_{clc} in *Pseudomonas putida*

Wageningen University (NL)

09.2016 to 10.2018 – MSc Cellular and Molecular Biotechnology, Final grade 8.0/10

MSc Thesis: "Engineering a thermophilic *Pseudomonas putida*" System and Synthetic Biology laboratory (6 months)

MSc Internship: "Isolation of new *Bilophila sp.* strains from the human gut" Microbial Physiology laboratory (4 months)

Università di Bologna (IT)

10.2013 to 07.2016 – BSc Biotechnology, Final grade 110/110

BSc Thesis: "Stabilization of G-quadruplex structures in human osteosarcoma cells" Cancer Genome Instability laboratory (4 months)

Languages

Italian (Native), English (C1), Spanish (B1), French (A2)

Publications

Daveri, Andrea, Valentina Benigno, and Jan Roelof van der Meer. "Characterization of an atypical but widespread type IV secretion system for transfer of the integrative and conjugative element (ICE clc) in *Pseudomonas putida*." *Nucleic Acids Research* 51.5 (2023): 2345-2362.

Conferences

SGM-SSM Annual meeting 2021 (online); Poster-presentation

ISME18 Conference 2022, Lausanne (CH); Poster-presentation

International Symposium on Plasmid Biology 2022, Toulouse (FR); Poster-presentation

SGM-SSM Annual meeting 2023, Lausanne (CH); Poster-presentation